Year : 2019

Lysosomes at the crossroads between CDK4 and mTOR pathway

Martínez Carreres Laia

Martínez Carreres Laia, 2019, Lysosomes at the crossroads between CDK4 and mTOR pathway

Originally published at : Thesis, University of Lausanne

Posted at the University of Lausanne Open Archive http://serval.unil.ch
Document URN : urn:nbn:ch:serval-BIB_56F16BEEB6626

UNIL | Université de Lausanne

Faculté de biologie et de médecine

Centre Intégratif de Génomique (CIG)

Lysosomes at the crossroads between CDK4 and mTOR pathway

Thèse de doctorat ès sciences de la vie (PhD)

présentée à la

Faculté de biologie et de médecine
de l'Université de Lausanne

par

Laia MARTÍNEZ CARRERES

Maîtrise universitaire en Médecine Translationnelle,
diplômée de l'Universitat de Barcelona

Jury

Dr. Murielle Bochud, Présidente (défense privée)
Dr. Ian Sanders, Président (défense publique)
Prof. Lluis Fajas, Directeur de thèse
Dr. Carles Cantó, Expert
Dr. Alejo Efeyan, Expert
Dr. Mario Pende, Expert

Lausanne
2019

UNIL | Université de Lausanne
Faculté de biologie
et de médecine

Ecole Doctorale
Doctorat ès sciences de la vie

Imprimatur

Vu le rapport présenté par le jury d'examen, composé de

Président·e	Monsieur	Prof. Ian **Sanders**
Directeur·rice de thèse	Monsieur	Prof. Lluis **Fajas Coll**
Expert·e·s	Monsieur	Dr Carles **Cantó**
	Monsieur	Dr Alejo **Efeyan**
	Monsieur	Dr Mario **Pende**

le Conseil de Faculté autorise l'impression de la thèse de

Madame Laia Martínez Carreres

Master in translational medicine, Universitat de Barcelona, Espagne

intitulée

Lysosomes at the crossroads between CDK4 and mTOR pathway

Lausanne, le 7 juin 2019

pour le Doyen
de la Faculté de biologie et de médecine

Prof. Ian Sanders
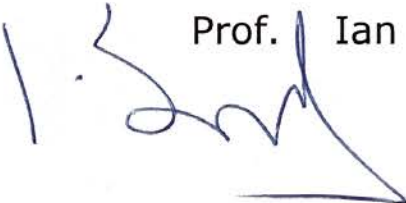
« There's a time when a man needs to fight
and a time when he needs to accept that his destiny's lost,
the ship has sailed and that only a fool will continue.
The truth is I've always been a fool. »
- Edward Bloom, *Big Fish*

In loving memory of Francesc Carreres.

To Ferran Fillat.

Acknowledgements

5 years ago I moved to Lausanne and started this project. It's been 5 intense years, full of learning and constant improvement. In these few lines, I would like to express my sincere gratitude towards all the people who have contributed to make this work possible.

Thanks a lot to Prof. Lluis Fajas, my thesis director, for letting me join your group, for giving me the opportunity to work in this challenging research project, and also for your guidance and support.

Thank you very much to the experts of my thesis and mid-thesis committee for your advices and follow-up: Dr. Carles Cantó, Dr. Mario Pende, Dr. Jean-Sebastien Annicotte and Dr. Alejo Efeyan. I also thank Dr. Murielle Bochud and Dr. Ian Sanders, for being the presidents of the private and public committee, respectively.

I would like to extend my sincerest gratitude to Dr. Julien Puyal. Thank you for your discussions and your collaboration. Your contribution has really busted this work.

Thanks a lot to the former and the current members of Fajas lab. Thank you for your help and time shared in the lab, the laughs, lunches and dinners… I really learned a lot from all of you having a wonderful time. We just became a big family. Specially, I would really like to thank the girls (Anita, Judit, and, adopted from BD's group, Tiziana) for your jokes, your support, your understanding and your friendship. I really care a lot about you guys and wish you all the best.

I also thank Meritxell, a super-supervisor, an example of strength and a good friend. In a short time you taught me a lot, in and outside the lab.

Thanks a lot also to the colleagues from both Department of Physiology and CIG, for creating such a nice work environment. In addition, I really appreciate the help of the people working in the platforms: M. Quadroni and P. Waridel, C. Moret, A. Paradis, etc.

Moltes gràcies a la meva família. Als que hi són, als que hi ha estat i als que han nascut. Moltes gràcies pel vostre suport, per ajudar-me a no rendir-me mai. Per ensenyar-me que voler és poder. Moltes gràcies M. Dolors. Mai t'estaré prou agraïda per haver-me obert aquest camí. I al Ferran. El meu company de vida i suport incondicional. Moltes gràcies per tot, TOT.

This stage comes to its end, but new challenges and experiences are waiting ahead.

Thanks. Gràcies.

Table of contents

Summary

Cancer is the name given to a group of related diseases characterized by uncontrolled cell growth and proliferation. In this project, we focused on the cell cycle regulator Cyclin-dependent kinase 4 (CDK4), which contributes to cell proliferation. Since this protein is commonly deregulated in cancer, CDK4 inhibitors have become a useful therapeutic tool for cancer treatment. The function of this protein is not limited to the control of the cell cycle; CDK4 also participates in the control of metabolism, always favoring anabolism and repressing catabolism. However, the exact mechanism by which CDK4 controls cell metabolism is not yet elucidated. It has been recently shown that CDK4 cross-talks with the master regulator of cell growth and metabolism, mammalian target of rapamycin (mTOR). This protein has also been effectively targeted in cancer treatments, since it is commonly hyperactive in cancer cells to maintain protein synthesis, cell growth and other anabolic processes. mTOR functions as two complexes: mTOR complex I (mTORC1) and mTOR complex II (mTORC2). Lysosomes, the main degradative organelles of the cell, are crucial for mTORC1 activation; mTORC1 is recruited to the surface of these organelles in response to extrinsic amino acids, or amino acids originated by the lysosomal degradation of macromolecules.

Here, we show that, on one hand, CDK4 phosphorylates FLCN, a regulator of mTORC1 translocation to the lysosomal surface, thus facilitating mTORC1 activation. On the other hand, we demonstrate that CDK4 promotes lysosomal degradation, which also results in mTORC1 activation. Finally, and most importantly for cancer therapy, we take advantage of this novel function of CDK4 to propose a new therapeutic strategy to treat triple-negative breast cancer (TNBC). We combined a CDK4 inhibitor, which impairs lysosomal function, with an inducer of autophagy (a degradative process in the cell in which lysosomal function is required) to trigger cancer cell death.

Overall, this project describes a novel role for CDK4 in the control of lysosomal biology and the mTOR pathway in cancer cells, and proposes a promising therapeutic strategy for cancer treatment.

Résumé

Le cancer comprend un ensemble de maladies caractérisées par une dérégulation de la croissance et de la prolifération cellulaires. Au cours de ce projet, nous nous sommes intéressés à un régulateur du cycle cellulaire, CDK4 (Cyclin-dependent kinase 4), qui contribue à la prolifération cellulaire. Cette protéine étant communément dérégulée au cours du cancer, les inhibiteurs de CDK4 sont utilisés comme traitements contre le cancer. De plus, les fonctions de CDK4 ne se limitent pas au contrôle du cycle cellulaire : il participe également au contrôle du métabolisme, à la fois en stimulant les voies anaboliques et inhibant les voies cataboliques. Cependant, le mécanisme exact par lequel CDK4 contrôle le métabolisme cellulaire n'a pas encore été élucidé. Récemment, il a été montré que CDK4 interagit avec mTOR (mammalian target of rapamycin), l'un des principaux régulateurs de la croissance cellulaire et du métabolisme. Cette protéine a également été utilisée comme cible de traitements contre le cancer puisqu'elle est hyperactive dans les cellules cancéreuses afin de maintenir la synthèse protéique, la croissance cellulaire et d'autres processus anaboliques. mTOR agit sous la forme de deux complexes, mTORC1 (mTOR complex 1) and mTORC2. Les lysosomes, qui sont les principaux organites en charge de la dégradation de macromolécules et de matériel cellulaire, sont essentiels à l'activation de mTORC1 : en effet, mTORC1 est recruté à la surface de ces organites en réponse aux acides aminés exogènes ou issus de la dégradation lysosomale de macromolécules.

Ici, nous montrons d'une part que CDK4 phosphoryle FLCN, un régulateur de la translocation de mTORC1 à la surface des lysosomes, facilitant ainsi l'activation de mTORC1. D'autre part, nous démontrons que CDK4 stimule la dégradation lysosomale, qui favorise également l'activation de mTORC1. Enfin, dans le but de développer une nouvelle approche thérapeutique contre le cancer, nous avons utilisé cette nouvelle fonction de CDK4 pour traiter le cancer du sein triple négatif. Nous avons combiné un inhibiteur de CDK4, qui altère la fonction lysosomale, avec un inducteur de l'autophagie, un processus qui requiert la dégradation lysosomale, pour induire la mort des cellules cancéreuses.

Dans l'ensemble, ce travail décrit un nouveau rôle de CDK4 dans le contrôle de la biologie lysosomale et de la voie mTOR dans les cellules cancéreuses, et propose une nouvelle stratégie thérapeutique prometteuse pour le traitement du cancer.

List of abbreviations

4E-PB1	4E binding protein 1
ACD	Autophagic cell death
AMBRA	Autophagy and beclin 1 regulator
AMPK	5' AMP-activated protein kinase
AMPKα2	alpha-2 subunit of AMPK
Atg	Autophagy-related genes
BNIP3	BCL2/adenovirus E1B 19 kDa protein-interacting protein 3
CAK	CDK-activating kinase
CDK	Cyclin-dependent kinase
CKIs	CDK inhibitors
DEPTOR	DEP-domain-containing mTOR-interacting protein
eIF4E	Eukaryotic translation initiation factor 4E
ER	Estrogen receptor
FDA	US Food and Drug Administration
FIP200	Focal adhesion kinase family interacting protein 200KDa
FLCN	Folliculin
FNIP1	Folliculin interacting protein 1
FRAP1	FK506-binding protein 12-rapamycin-associated protein 1
GAP	GTPase-activating protein
GCN5	General control non-derepressible 5
GEF	Guanine nucleotide exchange factor
HCQ	Hydroxychloroquine
HER2	Human epidermal growth factor receptor 2
HR	Hormone receptor
IGF	Insulin growth factor
IRS	Insulin receptor substrate
LAMP-1	Lysosome-associated membrane protein 1
LC3B	Microtubule-associated protein light chain 3
LMP	Lysosomal membrane permeabilization
LSDs	Lysosomal storage diseases

MAPK	Mitogen activated protein kinase
mLST8	Mammalian lethal with Sec13 protein 8
mSIN1	Mammalian stress-activated protein kinase interacting protein
mTOR	Mammalian/mechanistic target of rapamycin
mTORC1	Mammalian/mechanistic target of rapamycin complex 1
mTORC2	Mammalian/mechanistic target of rapamycin complex 2
PDK1	Phosphoinositide-dependent kinase 1
PGC1α	PPAR-γ coactivator 1α
PI3K	Phosphatidylinositol 3-kinase
PI3P	Phosphatidylinositol 3-phosphate (PI3P)
PKCα	Promoting protein kinase Cα
PML	Promyelocytic leukemia
PPARγ	Peroxisome proliferator-activated receptor gamma
PR	Progesterone receptor
PRAS40	Proline-rich AKT substrate 40 kDa
PROTOR-1	Protein observed with RICTOR-1
R24C	CDK4-Arg24Cys mutation
RAPTOR	Regulatory-associated protein of mTOR
RB	Retinoblastoma protein
REDD1	DNA damage response 1
RHEB	Ras homolog enriched in brain
RICTOR	Rapamycin-insensitive companion of mTOR
S6K1(p70S6K1)	p70 Ribosomal S6 kinase 1
SREBP	Sterol-responsive element-binding protein (SREBP)
TFEB	Transcription factor EB
TFIIH	Transcription factor II H
TNBC	Triple-negative breast cancer
TRAF6	TNF receptor associated factor 6
TSC	Tuberous sclerosis complex
ULK	Unc-51-like kinase
V-ATPase	vacuolar H^+-ATPase
YY1	Ying-Yang 1

Chapter 1. Introduction

I.   <u>CDK4 in cell cycle, metabolism and cancer</u>

1.   Cell cycle and Cyclin-dependent Kinases (CDKs)

The cell cycle is a highly ordered set of events, involving cellular growth and chromosome duplication that culminates in the division of a single cell into two daughter cells (Nurse, 2000). The cell cycle of most eukaryotic cells is divided into four phases: G_1, S, G_2 and M. In the G_1 phase, metabolic changes prepare the cell for division. If certain conditions are met, the cell is committed to division and moves to the S phase. The S phase is the period during which DNA replication occurs. In the G_2 phase, the cell undergoes more growth and checks the replicated DNA to ensure that the cell is safe to move on to cell division. A nuclear division (Mitosis) followed by a cell division (Cytokinesis) occurs in the M phase. The cell cycle can also be divided into two major stages: Interphase (which includes the G_1, S and G_2 phases), where the cells grow and prepare themselves for division, and Mitosis-Cytokinesis (M phase). The G_0 phase is a state outside of the replicative cell cycle in which cells rest in a quiescent state. Classically, it was thought that nutrient deprivation was the cause of G_0 phase entry. However, it has been shown that G_0 entry occurs for multiple reasons. For example, cells enter to this phase in the context of cell differentiation. The G_0 phase is reversible; cells can receive intrinsic or extrinsic signals to re-enter in the G_1 phase (Barnum & O'Connell, 2014).

The central machineries that drive cell cycle progression are some members of Cyclin-dependent Kinases (CDKs), which is a large family of serine/threonine protein kinases. CDK1, CDK2, CDK4 and CDK6 are the best-known members of this family that regulate the cell cycle progression. The expression of CDKs is constant, but they lack kinase activity until they bind to their corresponding Cyclin partners, which allow CDKs to adopt an active configuration (Lohka, Hayes, & Maller, 1988). Cyclins are tightly regulated at the levels of synthesis and ubiquitin-dependent proteolysis (Malumbres & Barbacid, 2005), and they are differently expressed at each

phase of the cell cycle. In that way, different CDKs/Cyclin complexes are formed in each phase of the cell cycle **(Figure 1)**. CDK4/Cyclin D and CDK6/Cyclin D are the main complexes of the G_1 phase (Matsushime et al., 1992; Meyerson & Harlow, 1994), CDK2/Cyclin E complex in the S phase (Koff et al., 1992; Ohtsubo, Theodoras, Schumacher, Roberts, & Pagano, 1995), and CDK1/Cyclin B complex during the transition G_2/M phases (Draetta & Beach, 1989; Pines & Hunter, 1992).
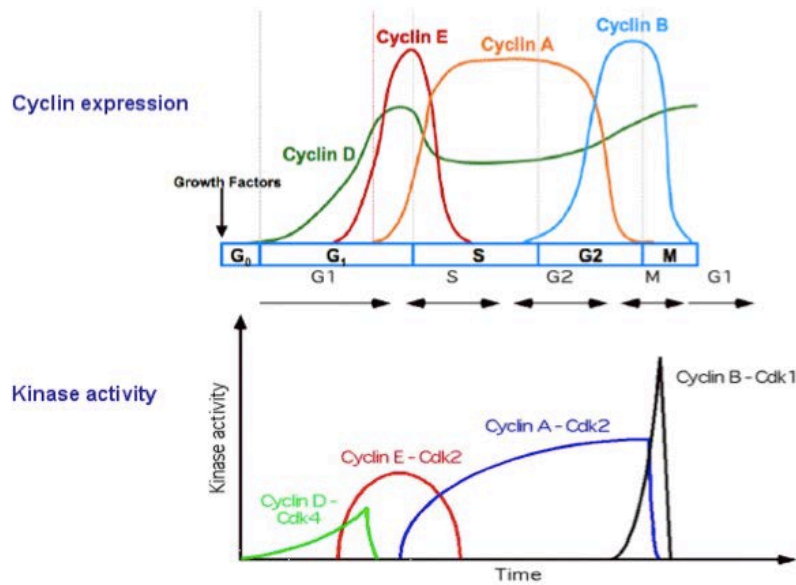
Figure 1. Cyclin expression and kinase activity of the differen types of Cyclins and CDK/Cyclin complexes.

Moreover, the binding of small inhibitory proteins, CDK inhibitors (CKIs), can modulate the activity of CDKs. Also, CDKs can be phosphorylated to activate or to block the phosphate transfer to substrates (Barnum & O'Connell, 2014).

Indeed, the large family of CDKs includes members whose function is not directly related to cell cycle regulation. CDK7 forms a trimeric complex with Cyclin H and MAT1, and functions as a CDK-activating kinase (CAK). In addition, CDK7 is an important component of the transcription factor II H (TFIIH), which is involved in transcription initiation and DNA repair. CDK8 and CDK9 are essentially implicated in the transcriptional machinery of RNA polymerase II. This protein is thought to serve as a direct link between the regulation of transcription and the cell cycle (Fisher, 2005). CDK11/Cyclin L complex interacts with a variety of elongation factors to facilitate transcription elongation (Trembley et al., 2005). It is additionally involved in RNA processing co-transcriptionally through its association with and

phosphorylation of factors responsible for pre-mRNA splicing (Dickinson, Edgar, Ehley, & Gottesfeld, 2002; Hu, Mayeda, Trembley, Lahti, & Kidd, 2003; Loyer et al., 2008). Little is known about the partners or the phosphorylation targets of CDK10. However, it has been studied that CDK10 plays a role in cancer progression (Leman et al., 2009; Yu et al., 2012; Zhong et al., 2012).

All CDKs have a conserved sequence in N-terminal which corresponds to the Cyclin-binding site: xGxPxxxxREx; (G, glycin; P, prolin; R, arginine; E, glutamic acid; and x, any amino acid). In addition, they phosphorylate substrates that contain the following motif: [S/T]-Px- [K/R] (S, serine; T, threonine; P, proline; K, lysine; R, arginine; and x, any amino acid). This phosphorylation confers conformational modifications to the target proteins, providing them with new properties.

2.   CDK4/Cyclin D-RB-E2F axis

In 1987, Hanks identified CDK4 by hybridizing a HeLa cell cDNA library with oligonucleotide probes homologous to known serine/threonine kinases. It was first named PSK-J3 (termed for putative serine/threonine kinase, filter J colony 3). During the Cold Spring Harbor Symposium on Cell Cycle in 1991, to unify the nomenclature for CDK family, PSK-J3 was renamed CDK4 (Hanks, 1987; Malumbres & Barbacid, 2005).

CDK4 controls the progression from the G_1 phase to the S phase of the cell cycle. The activation of CDK4 is due to a conformational change when it forms a complex with the D-type Cyclins in response to mitogenic signals. Cyclin D is one of the major cyclins produced in terms of its functional importance. Drosophila and many other organisms only have one cyclin D protein. In mice and humans, three types of D-type Cyclins have been identified: cyclin D1, D2 and D3. These three types of Cyclin D are expressed in most proliferating cells. However, their abundance differs in various cell types.

The activity of CDK4 also requires their activating phosphorylation on Thr172 by CDK7. Active CDK4/Cyclin D complexes are able to phosphorylate protein targets, such as the members of the retinoblastoma (RB) protein family (RB1, RBL1, and RBL2). Phosphorylated RB releases the transcription factor E2F1, which is then

able to activate its target genes, such as E-type Cyclins, which are thought to be necessary for CDK2 activation and for the proper completion of the G_1 phase (**Figure 2**). This process corresponds to the "restriction point": the stage during the G_1 in which cells no longer require mitogenic stimuli to undergo cell division.

Importantly, CDK6 also controls the transition from the G_1 to the S phase of the cell cycle through RB phosphorylation. Moreover, in the case of irreversible inactivation of CDK4 or CDK6, CDK2-Cyclin E is thought to phosphorylate RB (Bockstaele, Coulonval, Kooken, Paternot, & Roger, 2006; Neganova & Lako, 2008).
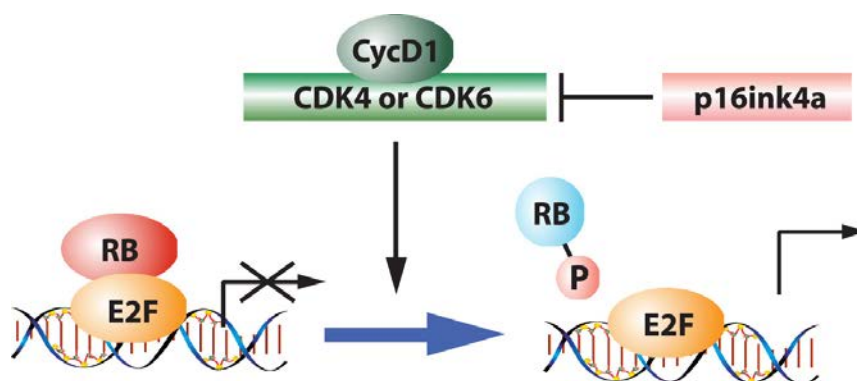
Figure 2. Cyclin D1/ CDK4 and CDK6/ Rb/ E2F pathway for G_t to S transition.

In addition, CDK4 activity is regulated by two families of proteins: 1) the INK4 family (p16^{ink4A}, p15^{INK4B}, p18^{INK4C}, p19^{INK4D}), which inhibit CDK4/Cyclin D activity by directly binding to the CDK and 2) the Cip and Kip family (particularly p21^{CIP1}, p27^{kip1}, and the less known p57^{kip2}) which have context-dependent positive (stabilizing) and negative (inhibiting) effects on CDK4/6 activity (Canepa et al., 2007).

The activity of CDK4 in the cell cycle is only required for the G_1 to S phase transition. Thus, after the phosphorylation of RB, CDK4/Cyclin D complex is translocated from the nucleus to cytoplasm, allowing the activity of other CDK/Cyclin complexes.

3.   Non-canonical roles of CDK4

The availability of knockout mouse models has uncovered the general and tissue-specific functions of CDKs and their partner Cyclins. Knockout mice of CDKs that regulate the transition from G_1 to S phase of cell cycle (not only CDK4 but also CDK2 and CDK6) demonstrated that they were individually dispensable for cell proliferation, but displayed additional tissue specific roles (Jayapal et al., 2015; Sherr & Roberts, 2004). CDK4 knockout mice are viable, although they are infertile and small. In addition, they present abnormalities in hypothalamic-pituitary axis, and develop diabetes (Mettus & Rane, 2003; Rane et al., 1999; Tsutsui et al., 1999). Indeed, these observations led to the initiation of research in the non-canonical roles of CDK4.

CDK4 has been shown to regulate insulin secretion in insulin-producing pancreatic β-cells through the CDK4-RB-E2F1 pathway. In response to high glucose, CDK4 kinase activity is increased through the insulin pathway, resulting in RB phosphorylation. Phosphorylated RB releases the E2F1-DP complex activating the transcription of the Kir6.2 gene, which codes for a key component of the KATP channel involved in insulin secretion (Annicotte et al., 2009).

In hepatocytes, and also through insulin signaling pathway, CDK4 has been found to regulate glucose uptake by phosphorylating the histone acetyltransferase general control non-derepressible 5 (GCN5). GCN5 subsequently acetylates the PPAR-γ coactivator 1α (PGC-1α), thereby inhibiting the expression of gluconeogenic genes. Thus, CDK4 is responsible for controlling glucose metabolism by suppressing hepatic glucose production in mice (Y. Lee et al., 2014).

Importantly, none of the above situations were proliferating conditions, suggesting that the effects of CDK4 in those cell types were cell cycle independent (Annicotte et al., 2009; Y. Lee et al., 2014).

In other cell types, CDK4 has been shown to play an essential role in cell differentiation, additionally to its role in cell proliferation. This is the case of hematopoiesis and adipogenesis. During hematopoiesis, CDK4 is regulated by GATA-1 and required for megakaryocyte growth and polyploidization (Muntean et al., 2007). CDK4 is also been found to play a role in lymphocyte adhesion and migration through endothelial cell matrix (Chow et al., 2010). On the other hand,

CDK4 deletion in 3T3-L1 cells blocks adipogenesis, while the hyperactive form of CDK4 (R24C) favors it; CDK4 regulates the nuclear receptor peroxisome proliferator-activated receptor gamma (PPARγ) and terminal differentiation and function of adipocytes (Abella et al., 2005).

Also in adipocytes, insulin activates the CDK4/Cyclin D3 complex, which subsequently phosphorylates the insulin receptor substrate 2 (IRS2). This generates a positive feedback loop maintaining insulin signaling pathway activated (Lagarrigue et al., 2016). CDK4-deficient mice display decreased lipogenesis and increased lipolysis in white adipose tissue, indicating that CDK4 is essential for promoting anabolic metabolism in adipocytes (Lagarrigue et al., 2016).

Furthermore, it has been recently shown that CDK4 is able to promote anabolism while directly repressing catabolism, by inhibiting the metabolic regulator 5' AMP-activated protein kinase (AMPK). Phosphorylation of the alpha-2 subunit of AMPK (AMPKα2) by CDK4 is associated with increased glycolysis and decreased fatty acid oxidation in mouse embryonic fibroblasts. In addition, CDK4 knockout mice increased their oxidative metabolism and exercise capacity in an AMPK-dependent manner (Lopez-Mejia et al., 2017).

In Drosophila, as in mammalian cells, CDK4 interacts genetically with the Drosophila RB family member RBF. However, CDK4 is not essential for progression through the cell cycle or for development to the adult stage. Nevertheless, CDK4 is clearly required for normal fertility and growth of cells and organisms (Meyer et al., 2000). Another study in the same model showed that CDK4/Cyclin D is able to activate TORC1 by phosphorylating one of its negative regulators, tuberous sclerosis complex 2 (TSC2) (Romero-Pozuelo, Demetriades, Schroeder, & Teleman, 2017). TORC1 is the homolog in drosophila of mammalian target of rapamycin complex 1 (mTORC1), as later on detailed, the master regulator of cell growth and metabolism.

Overall, these evidences highlight the importance of CDK4; a kinase that, on one hand regulates the G_1 to S phase transition of the cell cycle through phosphorylation of RB, and on the other hand, have many other phosphorylation targets for modulating metabolism in proliferating and differentiated cells, as well as at a whole body level.

4.   CDK4 and its inhibition in Cancer

Irregular entry into the cell cycle and uncontrolled cell proliferation are hallmarks of cancer. Hence, it is not surprising that the deregulation of CDKs plays a vital role in tumorigenesis. Specially, the hyperactivity of CDK4/Cyclin D-RB-E2F axis is known for being implicated in the abnormal proliferation of cancer cells (Malumbres & Barbacid, 2009). The retinoblastoma protein (RB) represents a checkpoint regulator in mammalian cells. When it is phosphorylated, RB enhances the expression of proteins that are essential for commitment to S phase and progression through the cell cycle. Normally, this step is tightly regulated, but in malignancy, this transition point can become less closely regulated, allowing for less controlled proliferation.

The importance of the CDK4 locus in human cancer first became evident following the identification of a germ line CDK4-Arg24Cys (R24C) mutation, which abolishes the ability of CDK4 to bind to its repressor $p16^{INK4a}$ (Rane, Cosenza, Mettus, & Reddy, 2002). Indeed, mice with R24C mutation develop endocrine, epithelial tumors and sarcomas (Malumbres & Barbacid, 2009). Later on, CDK4 had been found mutated in other forms of human cancer including glioma, sarcoma, breast, lung, ovary and oral cavity carcinomas (Mejia-Guerrero et al., 2010; Sabir, Baig, Mahjabeen, & Kayani, 2012; Wikman et al., 2005). Furthermore, Cyclin D1 mutations (mostly amplifications and overexpressions) have also been found in molecular analyses of many human cancers (Lantsov et al., 2005).

Given that the abnormal function of CDK4/Cyclin D complex might promote cell proliferation, CDK4 have become a genetically validated therapeutic target for cancer treatment (Salazar-Roa & Malumbres, 2017). First-generation of CDK inhibitors tended to be less specific, targeting other CDKs in a broad manner and were associated with chemotherapy-like toxicities and unacceptable safety profiles. A new generation of inhibitors of CDK4/Cyclin D complex, which also inhibit CDK6/Cyclin D due to their similarities, has been developed. Three drugs have been recently designed to bind to the ATP-binding pocket contained within the protein kinases, and thereby, block CDK4/6-mediated phosphorylation of RB: Palbociclib (PD0332991; Pfizer, USA), Ribociclib (LEE011; Novartis, Switzerland) and Abemaciclib (LY2835219; Eli Lilly, USA) (**Figure 3**).
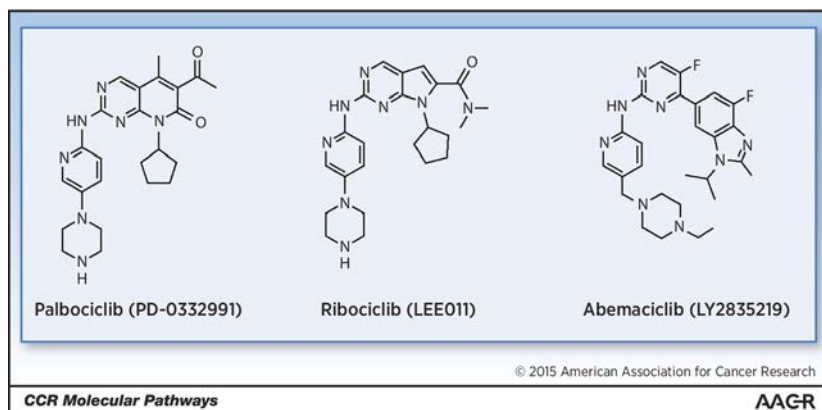
Figure 3. Chemical structures of selective CDK4/6 inhibitors in clinical development.

These three CDK4/6 inhibitors have shown to be effective especially for breast cancer, which often has aberrations throughout the Cyclin D-CDK4-RB pathway, particularly in Cyclin D1 gene or protein. Breast cancer is categorized into five distinct molecular subtypes including luminal A, luminal B, human epidermal growth factor receptor 2 (HER2)-enriched, basal-like, and claudin-low. Most types of breast cancers belong to luminal-type, and are characterized with the expression of estrogen receptor (ER) and/or progesterone receptor (PR), which can be effectively targeted with hormone therapy. By contrast, basal-like breast cancers, also known as triple-negative breast cancer (TNBC), due to the absent status of ER, PR and HER2, have comparatively aggressive phenotype and still lack efficient treatment strategy (Xu et al., 2017).

The administration of CDK4/6 inhibitors represents an important therapeutic advancement in breast oncology. All three CDK4/6 inhibitors have completed evaluation on randomized phase III studies and have received approval by the US Food and Drug Administration (FDA) for use in hormone receptor (HR)-positive breast cancers. Additionally, the drugs are being looked at preclinically and clinically in a variety of other tumor types as well, including melanoma, glioblastoma, pancreatic cancer, and colorectal cancer (Iams, Sosman, & Chandra, 2017; Knudsen et al., 2019; Olmez et al., 2018; J. Zhang, Zhou, Zhao, Dicker, & El-Deiry, 2017).

There is some evidence that manipulating metabolic pathways may be a useful addition of CDK4/6 inhibition. Ongoing studies include combinations of CDK4/6 inhibitors with other agents **(Table 1)**, such as phosphatidylinositol 3-kinase (PI3K) and mammalian target of rapamycin (mTOR) pathway inhibitors, and with selective

RAF and MEK inhibitors for tumors with alterations in the mitogen activated protein kinase (MAPK) pathway. Also some studies combined CDK4/6 inhibitors with immunotherapy and chemotherapy (Pernas, Tolaney, Winer, & Goel, 2018).

In addition, a number of non-RB targets for CDK4/6 have been identified in the metabolic machinery. Importantly, the use of CDK4/6 inhibitors for cancer treatment has shown that it suppresses the activity of the master regulator of cell growth and metabolism, mammalian target of rapamycin complex I (mTORC1), in HER2-positive breast cancer and glioblastoma (Goel et al., 2016; Olmez et al., 2017). The exact mechanism by which CDK4 regulates mTORC1 is not yet elucidated. However, the changes in metabolism after CDK4/6 inhibition may depend on the context and the oncogenic drivers, since opposite results were found in pancreatic ductal adenocarcinoma (Franco, Balaji, Freinkman, Witkiewicz, & Knudsen, 2016). This establishes new vulnerabilities in the use of CDK4/6 inhibitors and opens new venues for further investigation (Klein, Kovatcheva, Davis, Tap, & Koff, 2018).

Despite providing clear benefits, there are other challenges in the use and optimization of CDK4/6 inhibitors in clinical practice. For example, there is still a lack of predictive biomarkers to screen the appropriate population who can benefit the most from these treatments. Although several studies have implied some potential candidates for sensitivity prediction, such as the protein levels of RB and p16, further extensive clinical trials are needed to validate this finding (Polk, Kolmos, Kumler, & Nielsen, 2016; Xu et al., 2017).

Combination	Dosing Schedule	Disease	Phase	Identifier
Palbociclib				
Trastuzumab-DM1 (HER2 antibody)	palbociclib days 5–18 (21-day cycle) trastuzumab day 1	HER2⁺ breast cancer	Ib	NCT1976169
Tucatinib (HER2 inhibitor) + letrozole (aromatase inhibitor)	palbociclib days 1–21 (28-day cycle) letrozole and tucatinib days 1–28	HR⁺, HER2⁺ breast cancer	Ib/II	NCT03054363
Anastrozole (aromatase inhibitor) + trastuzumab + pertuzumab (HER2 inhibitor)	palbociclib days 1–21 (28-day cycle) anastrozole days 1–28 trastuzumab and pertuzumab once every 21 days	HR⁺, HER2⁺ breast cancer	I/II	NCT03304080
Baxedoxifene (ER modulator)	not stated	HR⁺ breast cancer	Ib/II	NCT02448771
SAR439859 (ER degrader)	palbociclib days 1–21 (28-day cycle) SAR439859 days 1–28	ER⁺ breast cancer	I/II	NCT03284957
GDC-0810 (ER downregulator)	palbociclib days 1–21 (28-day cycle) GDC-0810 days 1–28	ER⁺/HER2⁻ breast cancer	I/II	NCT01823835
Gedatolisib (PI3K/mTOR inhibitor) + fulvestrant (ER antagonist)	palbociclib days 1–21 (28-day cycle) gedatolisib days 1, 7, 14, 21; Fulvestrant day 1	ER⁺/HER2⁻ breast cancer	I	NCT02626507
Gedatolisib (PI3K/mTOR inhibitor)	palbociclib days 1–21 (28-day cycle) gedatolisib days 1, 7, 14, and 21	Solid tumors	I	NCT03065062
Copanlisib (PI3K inhibitor) + letrozole	palbociclib days 1–21 (28-day cycle) copanlisib days 1, 8, and 15; letrozole days 1–28	HR⁺, HER2⁻ breast cancer	Ib/II	NCT03128619
GDC-0077 (PI3K inhibitor) + letrozole	palbociclib days 1–21 (28-day cycle) GDC-0077 and Letrozole days 1–28	PIK3CA mutant, HR⁺, HER2⁻ breast cancer	I/II	NCT03006172
AZD2014 (mTORC1/2 inhibitor) + fulvestrant	not stated	ER⁺ breast cancer	I/II	NCT02599714
Everolimus (mTOR inhibitor) + exemestane (aromatase inhibitor)	palbociclib days 1–21 (28-day cycle) everolimus and exemestane days 1–28	ER⁺, HER2⁻ breast cancer	Ib/IIa	NCT02871791
PD-0325901 (MEK inhibitor)	palbociclib and PD-0325901 days 1–21 (28-day cycle)	KRAS mutant non-small cell lung cancer, solid tumors	I/II	NCT02022982
Binimetinib (MEK inhibitor)	palbociclib days 1–21 (28-day cycle) binimetinib days 1–28	KRAS mutant non-small cell lung cancer	I/II	NCT03170206
Neratinib (pan-ERBB inhibitor)	palbociclib and neratinib days 1–21 (28-day cycle)	EGFR, HER2/3/4 amplified/mutated advanced cancers	I	NCT03065387
Ibrutinib (BTK inhibitor)	palbociclib days 1–21 (28-day cycle) ibrutinib days 1–28	mantle cell lymphoma	I	NCT02159775
Erdafitinib (FGFR inhibitor) + fulvestrant	palbociclib days 1–21 (28-day cycle) erdafitinib days 1–28; fulvestrant day 1	ER⁺/HER2⁻/FGFR amplified breast cancer	I	NCT03238196
Cetuximab (EGFR inhibitor)	palbociclib days 1–21 (28-day cycle) cetuximab once weekly	squamous cell carcinoma of the head and neck	II	NCT02499120

Ribociclib				
Trastuzumab (HER2 antibody)	ribociclib days 5–18 (21-day cycle); trastuzumab day 1	HER2$^+$ breast cancer	I/II	NCT02657343
LSZ102 (ER degrader)	not stated	ER$^+$ breast cancer	I	NCT02734615
Everolimus (mTOR inhibitor)	ribociclib days 1–21 (28-day cycle) everolimus days 1–28	pancreatic adenocarcinoma	I/II	NCT02985125
Everolimus + letrozole	all drugs days 1–28 (28-day cycle)	endometrial cancer	II	NCT03008408
Everolimus	ribociclib days 1–21 (28-day cycle) everolimus days 1–28	dedifferentiated liposarcoma and leiomyosarcoma	II	NCT03114527
Everolimus	ribociclib days 1–21 (28-day cycle) everolimus days 1–28	neuroendocrine tumors	II	NCT03070301
Everolimus + exemestane (aromatase inhibitor)	ribociclib days 1–21 (28-day cycle) everolimus + exemestane days 1–28	HR$^+$, HER2$^-$ breast cancer	I	NCT01857193
BLY719 (PI3K inhibitor) + letrozole	ribociclib days 1–21 (28-day cycle) BLY719 + letrozole days 1–28	ER$^+$ breast cancer	I	NCT01872260
BLY719 $_{OR}$ BKM120 (pan-PI3K inhibitor) + fulvestrant	ribociclib days 1–21 (28-day cycle) BLY719 or BKM120 days 1–28; fulvestrant day 1	ER$^+$/HER2$^-$ breast cancer	I/II	NCT02088684
Trametinib (MEK inhibitor)	not stated	advanced solid tumors	I/II	NCT02703571
MEK162 (MEK inhibitor)	ribociclib days 1–21 (28-day cycle) MEK162 days 1–28	NRAS mutant melanoma	Ib/II	NCT01781572
LGX818 (RAF inhibitor) + MEK162	ribociclib days 1–21 (28-day cycle) LGX818 + MEK162 days 1–28	BRAF-dependent advanced solid tumors	I/II	NCT01543698
EGF816 (EGFR inhibitor)	not stated	EGFR mutant non-small cell lung cancer	I	NCT03333343
Ceritinib (ALK inhibitor)	not stated	ALK-positive non-small cell lung cancer	I	NCT02292550
Enzalutamide (anti-androgen)	ribociclib days 1–21 (28-day cycle); enzalutamide days 1–28	prostate cancer	I/II	NCT02555189
Bicalutamide (anti-androgen)	ribociclib days 1–21 (28-day cycle); bicalutamide days 1–28	AR$^+$ triple-negative breast cancer	I/II	NCT03090165
Carboplatin + paclitaxel (anti-mitotic)	ribociclib days 1–4, 8–11, 15–18 (28-day cycle) paclitaxel + carboplatin days 1, 8, 15	ovarian cancer	I	NCT03056833
Paclitaxel	not stated	advanced breast cancer	I	NCT02599363
Doxorubicin	ribociclib days 1–7 (21-day cycle) doxorubicin day 10	advanced soft tissue sarcoma	I	NCT03009201
Tamoxifen (anti-mitotic)	ribociclib days 1–21 (28-day cycle) tamoxifen days 1–28	ER$^+$, HER2$^-$ breast cancer	I	NCT02586675
Gemcitabine (nucleotide analog)	ribociclib days 8–14 (21-day cycle) gemcitabine days 1, 8	advanced solid tumors	I	NCT03237390
Docetaxel (anti-mitotic) + prednisone	ribociclib days 2–14 (21-day cycle) docetaxel and prednisone days 1–21	prostate cancer	I/II	NCT02494921
PDR001 (anti-PD1 antibody) ± fulvestrant	ribociclib days 1–21 (28-day cycle) PDR001 days 1–28	HR$^+$, HER2$^-$ breast and ovarian cancer	I	NCT03294694
Abemaciclib				
LY3023414 (PI3K/mTOR inhibitor)	not stated	pancreatic ductal adenocarcinoma	II	NCT02981342
LY3214996 (ERK1/2 inhibitor)	not stated	advanced solid tumors	I	NCT02857270
Ramucirumab (anti-VEGFR2)	abemaciclib days 1–28 (28-day cycle) ramucirumab days 1, 15	advanced solid tumors and lymphoma	I	NCT02745769
Xentuzumab (IGF1/2 inhibitor)	abemaciclib daily, xentuzumab once a week	advanced solid tumors, HR$^+$ breast cancer	I	NCT03099174
LY3039478 (Notchi)	both drugs daily	advanced solid tumors	Ib	NCT02787495
Exemestane (aromatase inhibitor) $_{OR}$ exemestane + everolimus $_{OR}$ LY3032414 + fulvestrant $_{OR}$ Letrozole (aromatase inhibitor) $_{OR}$ anastrozole (aromatase inhibitor) $_{OR}$ tamoxifen (anti-mitotic) $_{OR}$ trastuzumab (HER2 antibody)	all drugs daily	metastatic breast cancer	Ib	NCT02057133
Anastrozole $_{OR}$ letrozole	all drugs daily	HR$^+$, HER2$^-$ breast cancer	III	NCT02246621
Tamoxifen	both drugs daily	HR$^+$, HER2$^-$ breast cancer	II	NCT02747004
Premetrexed (anti-folate) $_{OR}$ gemcitabine $_{OR}$ Ramucirumab $_{OR}$ LY3023414 $_{OR}$ pembrolizumab (PD-1 inhibitor)	abemaciclib daily (21-day cycle) premetrexed day 1 gemcitabine days 1, 8 ramucirumab days 1, 8 pembrolizumab day 1	non-small cell lung cancer	I	NCT02079636
LY3300054 (anti-PD-L1)	abemaciclib daily (28-day cycle); LY3300054 days 1, 15	advanced solid tumors	I	NCT02791334

Table 1. List of clinical trials with CDK4/6 inhibitors in combination with other agents (Klein et al 2018).

II.   <u>mTOR, lysosomes and autophagy</u>

1. mTOR pathway

The mammalian target of rapamycin (mTOR), also known as the mechanistic target of rapamycin and FK506-binding protein 12-rapamycin-associated protein 1 (FRAP1), is a serine/threonine kinase belonging to the PI3K-related kinase family. It is conserved throughout evolution, and is encoded by the *MTOR* gene in humans. mTOR links with other proteins and serves as a core component (catalytic subunit) of two distinct protein complexes, mTOR complex 1 (mTORC1) and mTOR complex 2 (mTORC2) (Laplante and Sabatini, 2012).

As a core component of mTORC1, mTOR regulates cell growth, cell proliferation, cell motility, cell survival, protein synthesis, autophagy and transcription. mTORC1 is formed by mTOR, regulatory-associated protein of mTOR (RAPTOR) and mammalian lethal with Sec13 protein 8 (mLST8, also known as GβL). Proline-rich AKT substrate 40 kDa (PRAS40) and DEP-domain-containing mTOR-interacting protein (DEPTOR) are negative regulators of mTORC1 which are recruited to the complex for its inhibition (Peterson et al., 2009). mTORC1 responds to amino acids, stress, oxygen, energy, and growth factors, and is acutely sensitive to rapamycin (Laplante and Sabatini, 2012).

As a core component of mTORC2, mTOR participates in the activation of AKT via direct phosphorylation at Ser472/3; the full activation of AKT requires also another phosphorylation at Thr308 by phosphoinositide-dependent kinase 1 (PDK1), after the activation of insulin signaling pathway. Thus, since AKT is an important promoter of cell survival, metabolism and proliferation, mTORC2 is also stimulating these processes (Manning & Cantley, 2007). In addition, mTORC2 regulates actin cytoskeleton by promoting protein kinase Cα (PKCα) phosphorylation, phosphorylation of paxillin and its relocalization to focal adhesions, and GTP loading of RhoA and Rac1. However, the molecular mechanisms by which mTORC2 regulate these processes have not been determined yet (Jacinto et al., 2004). Like mTORC1, mTORC2 is a large complex. It is formed by mTOR, rapamycin-insensitive companion of mTOR (RICTOR), mammalian stress-activated protein kinase interacting protein (mSIN1), protein observed with RICTOR-1 (PROTOR-1) and

mLST8. Similar to mTORC1, DEPTOR negatively regulates the complex (Laplante and Sabatini, 2012). The signaling pathways that lead to mTORC2 activation are not well characterized. Since growth factors increase mTORC2 kinase activity and AKT phosphorylation at Ser473, they are considered to be a plausible signal for regulating this pathway (Guertin & Sabatini, 2007). mTORC2 is insensitive to acute rapamycin treatment but chronic exposure to the drug can disrupt its structure.

mTOR signaling pathway integrates both intracellular and extracellular signals, and serves as a central regulator of cell metabolism, growth, proliferation and survival. Due to its relevance in cancer models and its role in the regulation of lysosomal biology, in this project we focused mainly on mTORC1.

2. mTORC1: the master regulator of cell growth and metabolism

mTORC1 upstream signaling:

mTORC1 integrates four major signals (growth factors, amino acids, oxygen and energy status) to regulate many processes that are involved in the promotion of cell growth (**Figure 4A-B**).

Growth factors, such as insulin or insulin growth factors (IGFs), stimulate mTORC1 through the activation of the canonical insulin-signaling pathway. The binding of insulin or IGFs to their cell-surface receptor promotes the tyrosine kinase activity of the insulin receptor, the recruitment of insulin receptor substrate (IRS), the production of phosphatidylinositol 3-phosphate (PI3P) through the activation of PI3K, and followed by the activation of AKT. Once AKT is fully active, it can activate mTORC1 either by promoting the phosphorylation and dissociation of PRAS40 from mTORC1, or via the phosphorylation of tuberous sclerosis complex (TSC) (Laplante & Sabatini, 2012). TSC complex is a heterodimer comprised by TSC1 and TSC2. TSC1/2 functions as a GTPase-activating protein (GAP) for the small Ras-related GTPase RHEB (Ras homolog enriched in brain). As a RHEB-specific GAP, TSC1/2 negatively regulates mTORC1 signaling by converting RHEB into its inactive GDP-bound state. The active one, GTP-bound form of RHEB, directly interacts with mTORC1 to stimulate its activity (Inoki, Li, Xu, & Guan, 2003). mTORC1 can also be activated by the phosphorylation of TSC complex with RAS signaling pathway,

also promoted by growth factors. On the other hand, activation of mTORC1 negatively regulates the PI3K-AKT axis, given that p70 ribosomal S6 kinase 1 (S6K1) phosphorylates IRS1 and reduces its stability (Harrington, Findlay, & Lamb, 2005) **(Figure 4A-B)**.

Amino acids such as leucine, arginine, glutamine, and serine (Carroll et al., 2016; Fan et al., 2016; Jewell et al., 2015; Wang et al., 2015) are also crucial for mTORC1 activation. Precisely, the presence of amino acids promotes the relocalization of mTORC1 from discrete locations of the cell to the surface of the lysosomes, where is activated by RHEB. Amino acids, not only from the cytosol, but also the ones accumulated in the lysosomes (Sagne et al., 2001), activate Rag GTPases. Rag GTPases localize on the lysosomal surface and are essential for communicating amino acid availability to mTORC1 through their binding with RAPTOR (Sancak et al., 2008). In mammals, there are four members of the Rag subfamily: RagA, RagB, RagC and RagD, which function as heterodimers (Kim & Kim, 2016). RagA/B form heterodimeric pairs with RagC/D, suggesting the existence of four possible independent heterodimeric pairs. During amino acid starvation, RagA/B binds GDP and is quickly exchanged for GTP after amino acid restimulation, for recruiting mTORC1 to the lysosomal surface. The Rag GTPases are regulated by a complex signaling network, in which activators and inhibitors tightly modulate their nucleotide-bound state. Ragulator, GATOR1, GATOR2, FLCN-FNIP and KICSTOR are some of Rag GTPases regulators. In addition, the lysosomal membrane transporter SLC38A9, Sestrin2 and CASTOR1 have been recently identified as nutrient sensors, which modulate mTORC1 activation (Bar-Peled & Sabatini, 2014) **(Figure 4B)**.

In the present work, we focus on Folliculin (FLCN), a protein that in humans is associated with Birt-Hogg-Dubé syndrome and hereditary spontaneous pneumothorax, but also has been identified as a tumor suppressor. FLCN, together with its binding partner Folliculin interacting protein 1 (FNIP1), function as a GAP for RagC/D, but not as a Guanine nucleotide exchange factor (GEF) for RagA/B, thus providing another avenue of control over mTORC1 translocation (Petit, Roczniak-Ferguson, & Ferguson, 2013). In addition, its intracellular positioning changes in response to amino acids: FLCN localizes in the lysosomal surface under amino acid starvation conditions, suppressing Rags activity, and moves to the cytosol in the presence of amino acids, allowing mTORC1 to be recruited to the lysosomal surface. In addition, FLCN has been shown to interact with AMPK.

AMPK is the master sensor of intracellular energy status, another of the signals that regulate mTORC1. AMPK negatively regulates mTORC1 in response to energy depletion (low ATP:ADP ratio) via TSC2 phosphorylation (Hardie, 2007). Additionally, AMPK can reduce mTORC1 activity in response to energy depletion by directly phosphorylating RAPTOR (Gwinn et al., 2008) **(Figure 4B)**.

mTORC1 activity is also affected by oxygen levels through multiple pathways. Under conditions of hypoxia, low ATP:AMP ratio activates AMPK, which promotes TSC1/2 activation and inhibits mTORC1 signaling. Hypoxia can also activate TSC1/2 through transcriptional regulation of DNA damage response 1 (REDD1). Furthermore, promyelocytic leukemia (PML) tumor suppressor and BCL2/adenovirus E1B 19 kDa protein-interacting protein 3 (BNIP3) reduce mTORC1 signaling during hypoxia by dissociating mTOR from its positive regulator RHEB (Wouters & Koritzinsky, 2008).

In addition to the four major signals described above, mTORC1 activity can be regulated by other cellular conditions and signaling pathways, such as genotoxic stress (like DNA damage), inflammation, Wnt ligand and phosphatidic acid (Laplante & Sabatini, 2012).
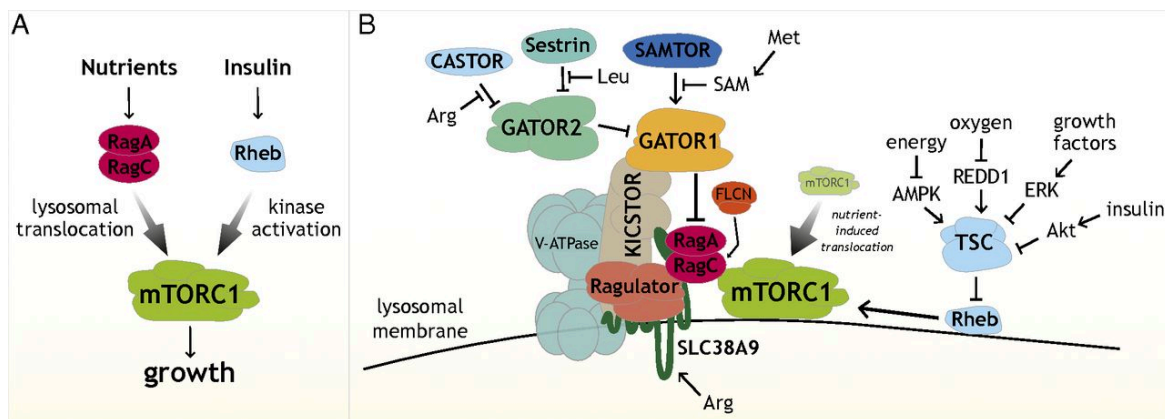

Figure 4. (*A*) Coincidence detector model for how mTORC1 integrates signals from nutrients and growth factors to regulate growth. (*B*) Schematic showing components of the nutrient-sensing pathway upstream of mTORC1 (Sabatini, 2017).

mTORC1 downstream signaling:

mTORC1 has pleiotropic functions by phosphorylating a wide range of substrates and affecting many cellular compartments, always favouring anabolic metabolism (Laplante & Sabatini, 2012, 2013).

The most known mTORC1 function is to promote protein synthesis, which is required for cell growth, through phosphorylation of its downstream targets: 4E binding protein 1 (4E-PB1) and S6K1. 4E-BP1 is a repressor of mRNA translation. When phosphorylated by mTORC1, 4E-BP1 is unable to bind to eukaryotic translation initiation factor 4E (eIF4E), which allows it to promote cap-dependent translation (Richter & Sonenberg, 2005). The main target of S6K1 is the S6 ribosomal protein. Active (phosphorylated) S6K1 increases mRNA biogenesis, cap-dependent translation and elongation, and the translation of ribosomal proteins through regulating of the activity of many proteins (Chung, Kuo, Crabtree, & Blenis, 1992).

mTORC1 is also able to promote *de novo* lipid synthesis through sterol-responsive element-binding protein (SREBP) transcription factors, which control the expression of numerous genes involved in fatty acid and cholesterol synthesis. SREBP can be activated either by S6K1 or by another mTORC1 substrate, the phosphatidate phosphatase lipin 1. By contrast, lipin 1 inhibits SREBP1 when mTORC1 signaling is inactivated (Meng, Frank, & Jewell, 2018). In addition, mTORC1 also promotes the expression and activity of PPAR-γ, the master regulator of adipogenesis (H. H. Zhang et al., 2009).

To regulate cellular metabolism and produce ATP, mTORC1 increases glycolytic flux by activating the transcription and the translation of a positive regulator of many glycolytic genes, the hypoxia inducible factor 1α (HIF1α) (Brugarolas et al., 2004; Duvel et al., 2010). Additionally, mTORC1 has been reported to increase mitochondrial DNA copy number, as well as the expression of many genes encoding proteins involved in oxidative metabolism. Even though additional evidence is needed, this happens in part by mediating the physical interaction in the nucleus between PGC1α and the transcription factor Ying-Yang 1 (YY1), which positively regulates mitochondrial biogenesis and oxidative function (Cunningham et al., 2007).

Paradoxically, mTORC1 also promotes growth by negatively regulating catabolic processes, such as autophagy, the central degradative process in cells, and lysosomal biogenesis, the creation of new degradative organelles. Both processes are

controlled by the transcription factor EB (TFEB), which is repressed by mTORC1 phosphorylation; when mTORC1 is active, phosphorylated TFEB remains inactive at the lysosomal membrane. Inactivated mTORC1 induces TFEB localization to the nucleus to activate lysosomal and autophagosomal gene transcription, thus initiating lysosomal biogenesis and autophagy. In addition, mTORC1 represses autophagy by phosphorylating and therefore repressing unc-51-like kinase 1 (ULK1) and ATG13. ULK1 can also be phosphorylated by the mTORC1 antagonist, AMPK, but in this case, to activate autophagy (Egan, Kim, Shaw, & Guan, 2011).

The complexity of mTOR signaling pathway is notable (**Figure 5**). In the recent years, much attention has been paid to this field due to its importance in many pathological conditions. As a result, more and more proteins are being identified as key players in the regulation of this signaling pathway.
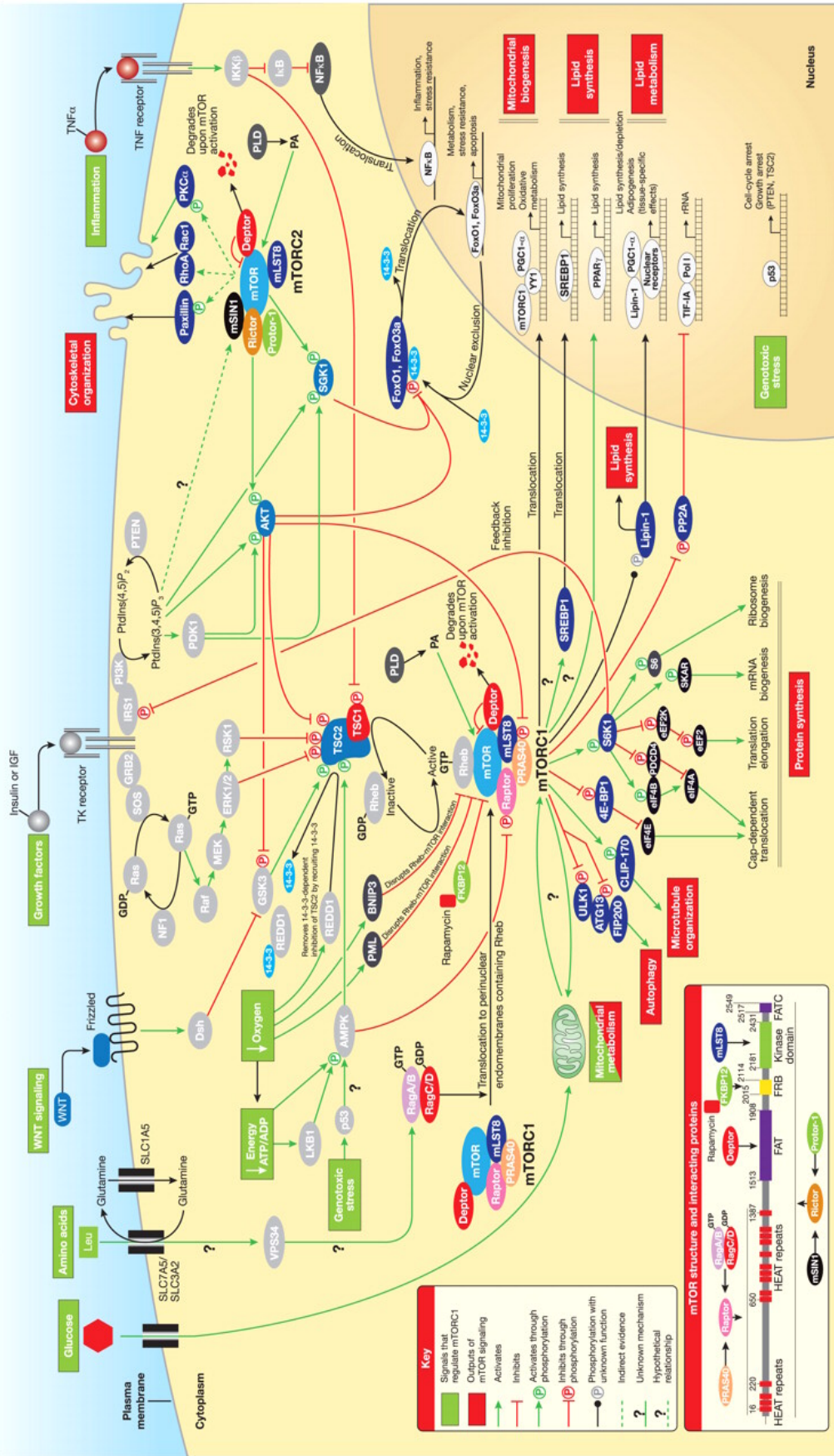
Figure 5. mTOR signaling at a glance (Laplante & Sabatini, 2009).

25

3. Lysosomes

Text adapted from the review of which I am first author, enclosed in Annex. Contribution to other articles: "Cancer: linking powerhouses to suicidal bags" (Martinez-Carreres, Nasrallah, & Fajas, 2017).

Christian de Duve first described lysosomes, also known as "suicidal bags," in 1950s as single membrane-enclosed vesicles containing hydrolases. Lysosomes function as a digestive system and are found in all eukaryotic cells, except for mature erythrocytes. The hydrolytic enzymes that they contain include proteases, nucleases, and lipases. These enzymes can break down proteins, nucleic acids, and lipids to their simplest subunits (De Duve, Pressman, Gianetto, Wattiaux, & Appelmans, 1955).

Lysosomes are formed when material from outside the cell is internalized in clathrin-coated endocytic vesicles creating early endosomes. These early endosomes undergo a process of maturation with the delivery of lysosomal acid hydrolases from the trans Golgi network, which contribute lowering of the internal pH to about 5.5. Late endosomes then mature into lysosomes as they acquire a full complement of acid hydrolases, which digest the molecules originally taken up by endocytosis, phagocytosis, and autophagy (Cooper, GM. *The Cell: A Molecular Approach.* 2000). Nevertheless, many investigations have proved that lysosomes are not only degradative organelles but also participate in metabolism of the entire cell at different levels, and their modifications can promote or repress cell proliferation.

On one hand, lysosomes repair damaged plasma membranes through a mechanism consisting in Ca^{2+} regulated exocytosis: they secreting their content into the extracellular space, and repairing their damaged plasma membranes; when the plasma membrane is injured, lysosomes quickly move to the site of damage and fuse with the plasma membrane. This allows effective resealing (Morgan, Platt, Lloyd-Evans, & Galione, 2011).

On the other hand, they can sense nutrient availability, which controls energy metabolism and mediates the starvation response (Settembre, Fraldi, Medina, & Ballabio, 2013). Zoncu et al. proposed that amino acids have to be detected in the lysosomal lumen, signaling to the Rag GTPases in a manner that is vacuolar H^+-ATPase (V-ATPase)-dependent. This is known as the "inside-out" mechanism (Zoncu

et al., 2011). Leucine, among other amino acids, must accumulate in the lumen of the lysosome to trigger the central regulator of cellular and organismal growth, mTORC1 (Bar-Peled & Sabatini, 2014). As mentioned above, mTORC1 is recruited by Rag GTPases on the lysosomal surface in response to amino acids, the site of activation by RHEB (Ras homolog enriched in brain), when growth factor-stimulated PI3K–AKT signaling is on (Dibble & Cantley, 2015; Shimobayashi & Hall, 2016). Upon amino acid and growth factors removal, Rag GTPases release mTORC1. mTORC1, then, become cytoplasmic and inactive. In those conditions, the negative regulator of RHEB, TSC2, is lysosomally localized. Thus, lysosomal proteins change depending on the nutrient status of the cells (Demetriades, Doumpas, & Teleman, 2014; Zheng et al., 2016).

In the recent years, lysosomes have also been found to be essential for many other cellular processes, such as killing of intracellular pathogens, antigen presentation, cell adhesion and migration, tumor invasion and metastasis, and gene regulation.

Additionally, the leakage of lysosomal content into the cytoplasm, known as lysosomal membrane permeabilization (LMP), can trigger apoptotic or necrotic pathways, depending on the cellular content and the extent of the leakage occurring into the cytosol. This phenomenon is called "lysosomal cell death" (Kirkegaard & Jaattela, 2009).

Overall, lysosomes are essential organelles in the cell, not only for their role in the degradation and recycling of macromolecules, but also for their roles in membrane repair, activation of metabolic pathways and cell death, among other functions. Lysosomal defects, for example the lack of a particular enzyme, perturb lysosomal homeostasis because excess products destined for breakdown and recycling remain stored in the cell. This is the main characteristic of lysosomal storage diseases (LSDs), a family of 50 rare inherited metabolic disorders. In addition to primary lysosomal dysfunction, cellular pathways associated with other membrane-bound organelles are perturbed in these disorders. The majority of LSDs are associated with neurological features, including developmental delay, behavioral/psychiatric disturbances, seizures, acroparesthesia, motor weakness, cerebrovascular ischemic events and extra-pyramidal signs (Pastores & Maegawa, 2013; Platt, Boland, & van der Spoel, 2012).

4. Autophagy

Autophagy is a catabolic process that is important for eliminating damaged components of the cell, providing a quality control of proteins and organelles, as well recycling the degraded products into biosynthetic and metabolic pathways. There are three types of autophagy in eukaryotic cells, with distinct mechanisms: macroautophagy, microautophagy and chaperone-mediated autophagy.

In this work, we focus on macroautophagy, hereafter referred to as autophagy. This process starts with an isolation membrane, known as phagophore, derived from endoplasmic reticulum and/or the trans-Golgi and endosomes (Glick, Barth, & Macleod, 2010). The phagophore is able to engulf intra-cellular cargo like protein aggregates, organelles and ribosomes, and sequesters the material in a double-membraned autophagosome. Autophagosomes filled with cargo, after some maturation steps, fuse with lysosomes. The lysosomal proteases and the acidic environment of these organelles are the optimal conditions to degrade the material from the autophagosomal cargo. Lysosomes also contain permeases and transporters on their membranes to export amino acids and other by-products of degradation to the cytoplasm for being re-used to build new macromolecules (Glick et al., 2010) **(Figure 6)**.

Autophagy has been described as a survival mechanism that is activated under physiological and stress conditions. It is also important during celular development and differentiation, and has diverse roles in innate and adaptative immunity (Z. Yang & Klionsky, 2009).

More than 30 proteins are involved in the coordination of the autophagic process. Most of them are encoded by genes belonging to the family of Autophagy-related genes (Atg). The step of autophagosome formation is mediated by two kinase complexes. The first one is composed of the class III PI3K Vps34, Atg6/Beclin1, Atg14 and Vps15/p150. The other complex is formed by ULK (in yeast Atg1), which binds to focal adhesion kinase family interacting protein 200KDa (FIP200), Atg101 and Atg13 (Zachari & Ganley, 2017).

The elongation step involves two ubiquitin-like conjugation pathways, both activated by Atg7 in an ATP-dependent manner. The first one involves Atg12 and Atg5. Both proteins are linked covalently, and their mode of conjugation is similar to

that of ubiquination. Another Atg, Atg16L (Atg16 in yeast) binds only to Atg5 and not to Atg12, and this conjugate is essential for elongation. These proteins associate with the convex surface of the isolation membrane, and dissociate from the membrane when autophagosome formation is complete; thus, this complex is not present in the mature autophagosome. The other ubiquitin-like conjugation involves one of the ortologues of the yeast Atg8, the microtubule-associated protein light chain 3 (LC3B) (other ortologues of yeast the Atg8 in mammals are GATE-16 and GABARAB). The mentioned LC3B protein has two isoforms: LC3B-I, the active and cytosolic form, and LC3B-II, after a series of ubiquitin-like reactions by Atg4. In fact, the above-mentioned Atg7 is the one that activates Atg4. LC3B-II is tightly membrane bound and is attached to phagophores and autophagosomes. This isoform is the only credible marker of the autophagosome in mammal cells, since its amounts reflect the relative abundance of autophagosomes (Mizushima, 2007; Rubinsztein, Bento, & Deretic, 2015).

In mammalian cells, autophagosome fusion with lysosomes is a complex process in which the autophagosome requires a series of maturation steps prior to its fusion with the lysosome. Some monomeric GTPases (Rab22, Rab24), mammalian orthologs of SNARE protein family members and the NSF protein are needed for the correct autophagosome maturation. Autophagosome maturation consists in their fusion with endosomes or endosome-derived vesicles. Rab7 is involved in this step. For autophagosome maturation and autophagosome-lysosome fusion, cytoskeletal elements are also crucial. After their fusion, the degradation of autophagic bodies in lysosomes requires a low pH and different proteinases and lipases to digest the material and recycle the macromolecules for use in the synthesis of essential components during nutrient stress (Y. P. Yang, Liang, Gu, & Qin, 2005).

Atg proteins as well as the whole process are regulated by nutrients, energy, and stress and their corresponding signaling pathways: mTOR, AMPK and HIF. Indeed, upon nutrient rich conditions, mTORC1 represses autophagy through phosphorylation of ULK1 (Rubinsztein et al., 2015). This phosphorylation results in suppression of ULK1 catalytic activity and inhibition of autophagy initiation. In addition, upon energy depletion, AMPK is able to modulate this complex: it does not only phosphorylate ULK1, activating its kinase activity, but also Atg13, in an inhibitory fashion, synergizing with mTORC1 phosphorylation of the complex. Therefore, the timing and context of these phosphorylation events are likely to be

critical in determining the autophagic output (Zachari & Ganley, 2017). It has been proposed that mTORC1 is also able to regulate ULK1 in a more indirect manner by phosphorylating other players of the pathway, such as autophagy and beclin 1 regulator 1 (AMBRA1). This protein is the responsible to take the E3-ligase TNF receptor associated factor 6 (TRAF6) to ULK1, thus enhancing ULK1 activity and autophagy induction (Zachari & Ganley, 2017) **(Figure 6)**.

Other than nutrient deprivation, hypoxia or reactive oxygen species can trigger autophagy by different mechanisms to prevent cell death (Fang, Tan, & Zhang, 2015). Despite being described as a survival mechanism, autophagy, however, may also induce cell death, known as autophagic cell death (ACD) (Kroemer & Levine, 2008; Yonekawa & Thorburn, 2013).
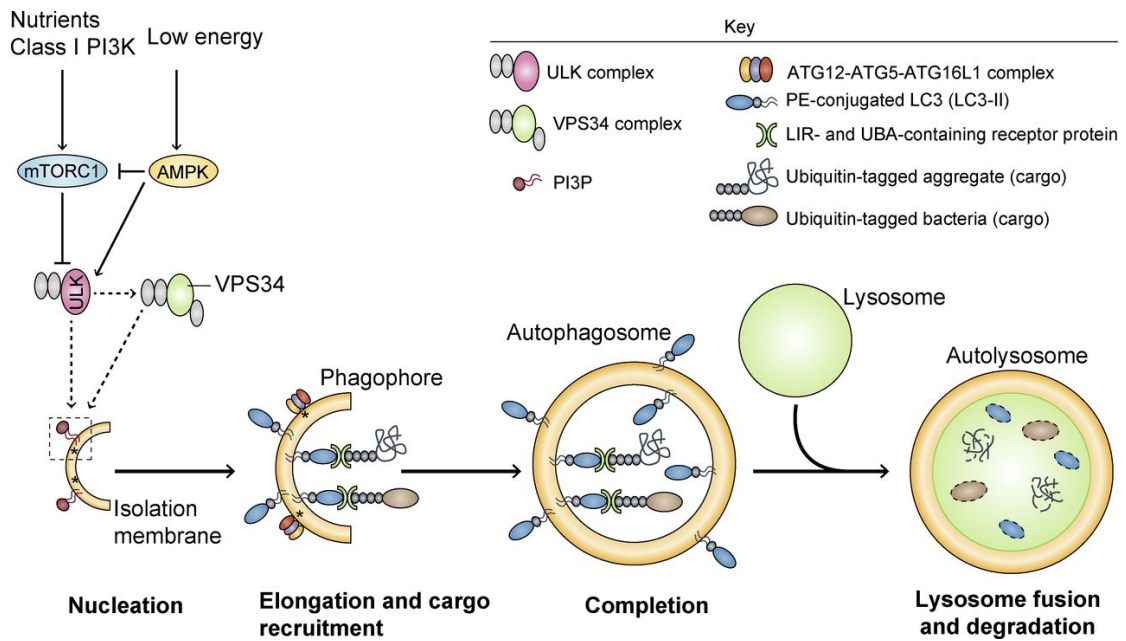

Figure 6. Autophagy scheme. Nutrient or energy deprivation trigger autophagy initiation. Autophagy consists in the processes of nucleation, elongation and cargo recruitment, completion (autophagosome maturation) and autophagosome-lysosome fusion (Rubinsztein et al., 2015).

5. Dysregulation of mTOR, lysosomes and autophagy in Cancer

Text adapted from the review of which I am first author, enclosed in Annex. Contribution to other articles: "Cancer: linking powerhouses to suicidal bags" (Martinez-Carreres et al., 2017)

mTOR promotes protein synthesis, aerobic glycolysis, *de novo* lipid synthesis, *de novo* nucleotide synthesis, and represses autophagy and lysosomal biogenesis. These anabolic processes are critical for tumorigenesis (Populo, Lopes, & Soares, 2012). Genes that encode components of the PI3K–AKT–mTOR pathway are frequently mutated in cancer, but despite few mutations have been characterized in mTOR, many tumor types present mTOR hyperactivation, thus promoting tumorigenesis (Alayev & Holz, 2013). In addition, the loss of *p53*, a very common event in cancer, promotes mTORC1 activation (Laplante & Sabatini, 2012). Importantly, inflammatory mediators, which are common in tumor angiogenesis, also signal to mTORC1 via TSC1/2 (D. F. Lee et al., 2007). Therefore, mTOR inhibition has become a great anti-cancer strategy. However, the use of mTOR inhibitors in oncology presents some limitations. The fact that the classic mTOR inhibitor, rapamycin, inhibits only some of the effects of mTOR, the existence of several feedback loops, and the crucial importance of mTOR in normal physiology are some examples of the limitations on the use of mTOR inhibitors for cancer treatment (Xie, Wang, & Proud, 2016).

On the other hand, lysosomes also undergo major changes in cancer cells. In some cases, lysosomes can become hyperactive to fulfill the needs of tumorigenic cells; they can show increased volume and protease activity, together with increased lysosomal protease secretion (Hamalisto & Jaattela, 2016). In addition, it has been recently found a correlation between lysosomal movement and tumor cell invasion, which was induced by tumor microenvironment stimuli (Steffan et al., 2014). In particular, acidic extracellular pH induced lysosomal movement toward the cell peripheries, successively leading to Cathepsin B exocytosis from the lysosomes. This eventually promoted protease-dependent tumor invasion (Friedl & Wolf, 2003, 2008). The increased secretions of lysosomal proteases render these

lysosomes pro-oncogenic, because this results in an increased neoplastic progression, *via* proteolytic pathway initiation (Mohamed & Sloane, 2006). In contrast, cathepsins are also depicted as proteases with tumor suppressor abilities for their role in inducing cell death through LMP (Jaattela, 2004; Lopez-Otin & Matrisian, 2007). Lysosome-associated membrane protein 1 (LAMP-1) has also been suggested to have a role in cell–cell adhesion and migration, since it was detected on the surface of highly metastatic cancer cells, particularly from colon cancer (Furuta et al., 2001).

Targeting lysosomes for cancer treatment is an emerging strategy (Piao & Amaravadi, 2016). The inhibition of these organelles can affect multiple activities that are needed for tumor cell survival and growth (nutrient sensing, metabolic pathways, degradation, exocytosis, immune responses, etc.) (Towers & Thorburn, 2017). The strategies currently investigated that target the lysosome in cancer are: 1) inhibiting autophagolysosome formation with drugs like hydroxychloroquine (HCQ) and Lyso 5; 2) inhibiting lysosomal acidification with inhibitors of the Vacuolar H^+-ATPase (Bafylomicin A1, Archazolid, Cleistanthin A or Manzamine A); 3) targeting the acid sphingomyelinase (ASM) with cationic amphiphilic drugs; 4) inhibiting lysosomal hydrolases with different cathepsin inhibitors; and 5) targeting HPS70, a protein which protects lysosomal membrane integrity and promotes tumor cell metastasis. Among all this agents, only HCQ has been widely tested in many clinical trials in combination with other anticancer therapies (Piao & Amaravadi, 2016). In addition, a minimally invasive anticancer modality called Photodynamic therapy (PDT) is being used for treating or relieving the symptoms of non-small cell lung cancer in patients and esophageal cancer patients. PDT combines a drug (a photosensiting agent) with a precise light wavelength, inducing ROS generation and killing tumor cells through LMP. However, this technique cannot be used for treating large tumors or metastasis (Buytaert, Dewaele, & Agostinis, 2007). Moreover, lysosomes are key players in cancer drug resistance. They can sequester cancer drugs into their acidic milieu, thus, blunting the drugs' effects (Gotink et al., 2011). This phenomenon is called "lysosomal trapping". This fact further proves that targeting lysosomes may be a promising new therapeutic strategy for cancer.

Lastly, the role of autophagy in cancer is still not clear and context specific. Some cancers are dependent on autophagy for survival and other cancers use

autophagy as a mechanism of cell death. In some models, autophagy suppresses cancer initiation by evading the toxic accumulation of damaged organelles, specifically mitochondria. On the short run, this helps in limiting oxidative stress. On the long run, it restricts chronic tissue damage and oncogenic signaling. So, in this context, autophagy stimulation might help suppress and/or prevent cancer initiation. Though, other cancers depend on autophagy for survival. In order to fit the high metabolic needs of growth and proliferation, cancers (such as the pancreatic) use autophagy-mediated recycling to their own advantage (S. Yang et al., 2011). Hence, inhibiting autophagy in this case could be an insight for selective cancer therapy, since these tumors are more dependent on autophagy than normal tissues (Guo & White, 2016).

Chapter 2. Aims of the project

In our lab, we are interested in studying the interplay between cell cycle and metabolism. The use of CDK4 inhibitors for cancer treatment has unraveled the metabolic role of CDK4 in the activation of mTOR pathway, specifically mTORC1, through a yet to know mechanism.

Our main objective is to further study the role of CDK4 in the mTOR signaling pathway. Particularly, we focused in a cancer model, since both CDK4 and mTOR are crucial for cancer progression.

Due to the kinase properties of CDK4, we would like to identify novel phosphorylation targets of CDK4 in proteins related to mTORC1 pathway. This will shed some light on the mechanism by which CDK4 regulates mTORC1.

mTORC1 activation is tightly related to lysosomes. Here, we aim to investigate whether the effects of CDK4 on mTORC1 are mediated by lysosomal changes.

Our final purpose is to evaluate the impact of our findings on cancer treatment. For this purpose, the use of an *in vivo* murine xenograft model will be fundamental.

Chapter 3. CDK4 regulates lysosomal function and mTORC1 activation to promote cancer cell survival

This chapter is based on the article "CDK4 regulates lysosomal function and mTORC1 activation to promote cancer cell survival" (Martinez-Carreres L et al 2019), which is under review in Cancer Research (submitted on February 2019).

CDK4 regulates lysosomal function and mTORC1 activation to promote cancer cell survival

Laia Martínez-Carreres[1], Meritxell Orpinell[2], Julien Puyal[3], Judit Castillo-Armengol[1], Albert Giralt[1], Catherine Moret[1], Valentin Barquissau[1], Anita Nasrallah[1], Angélique Pabois[4,5], Lianjun Zhang[4,6,7], Pedro Romero[4], Isabel C. Lopez-Mejia[1] and Lluis Fajas[1*]

[1]Center for Integrative Genomics, University of Lausanne, 1015 Lausanne, Switzerland.

[2]Department of Physiology, University of Lausanne, 1005 Lausanne, Switzerland

[3]Department of Fundamental Neurosciences, University of Lausanne, 1005 Lausanne, Switzerland.

[4]Department of Fundamental Oncology, University of Lausanne, 1066 Epalinges, Switzerland.

[5]Ludwig Institute for Cancer Research, University of Lausanne, 1066 Epalinges, Switzerland.

[6]Present address: Center for Systems Medicine, Institute of Basic Medical Sciences, Chinese Academy of Medical Sciences and Peking Union Medical College, 100005 Beijing, China.

[7]Present address: Suzhou Institute of Systems Medicine, Suzhou, Jiangsu 215123, China.

Corresponding author: Lluis Fajas, University of Lausanne, Center for Integrative Genomics, Quartier UNIL-Sorge, Bat. Genopode, CH-1015 Lausanne, Switzerland. Phone: +41.21.692.4111; E-mail: Lluis.Fajas@unil.ch.

Acknowledgements

Author contributions

L.M-C. and L.F. designed this study. L.M-C. conducted most of the experiments, with assistance from I.C.L-M., M.O., J.C-A., A.G., L.Z, V.B and A.Nasrallah. J.P performed electron microscopy experiments, acquisition and analysis. C.M. performed histological stainings. A.P. assisted in the *in vivo* work. P.R. contributed to the conception and experimental design of FACS analysis. L.M-C, I.C.L-M and L.F wrote the manuscript.

Declaration of interests

The authors declare no competing interests.

1. Abstract

CDK4 has been at the centerstage of cancer research for years. However, its role on cancer metabolism, especially in the mTOR signaling pathway, is as yet undefined. For the first time, in this study we connect CDK4 with lysosomes, the emerging metabolic organelles, crucial for mTORC1 activation. On one hand, we show that CDK4 phosphorylates the tumor suppressor FLCN, which regulates mTORC1 recruitment to the lysosomal surface in response to amino acids. On the other hand, we unravel that CDK4 has a direct role in lysosomal function and is essential for lysosomal degradation, ultimately regulating mTORC1 activity. We show here that chemical inhibition or genetic inactivation of CDK4, other than retaining FLCN at the lysosomal surface, lead to the accumulation of undigested material inside lysosomes, impairing the autophagic flux and inducing cancer cell senescence in vitro and xenograft models. Importantly, the use of CDK4 inhibitors in therapy results in cancer cell senescence but not in cell death. To overcome this resistance, and based on our findings, we increased the autophagic flux in cancer cells by using an AMPK activator in combination with a CDK4 inhibitor. We prove that the cotreatment induces autophagy (AMPK), and impairs lysosomal function (CDK4), finally resulting in cell death and tumor regression. Altogether we uncovered a previously unknown role for CDK4 in lysosomal biology and propose a novel therapeutic strategy to kill cancer cells.

2. Introduction

Cyclin-dependent kinase 4 (CDK4) has a well-established major role in cell cycle control (Malumbres and Barbacid, 2009) and CDK4-cyclin complexes are commonly deregulated in tumorigenesis (Deshpande, Sicinski, & Hinds, 2005). These complexes are of great interest as therapeutic targets, especially since the FDA has approved the specific CDK4/6 kinase inhibitors PD0332991 (palbociclib), LEE011 (ribociclib) and LY2835219 (abemaciclib) for treating advanced or metastatic hormone receptor (HR)-positive and HER2-negative breast cancer. Clinical studies

using CDK4/6 inhibitors to treat other malignancies are being conducted (O'Leary, Finn, & Turner, 2016).

Research from our group and others has shown that the role of CDK4 is not limited to the control of the cell cycle. Indeed CDK4 is also a major regulator of energy homeostasis (Aguilar & Fajas, 2010; Y. Lee et al., 2014; Salazar-Roa & Malumbres, 2017) through E2F1-RB complex (Blanchet et al., 2011), AMP-activated protein kinase (AMPK) (Lopez-Mejia et al., 2017) and insulin receptor substrate 2 (IRS2) (Lagarrigue et al., 2016). Importantly, the CDK4 pathway has been shown to cross-talk with the mechanistic target of Rapamycin (mTOR) pathway, which is a major regulator of cell growth and metabolism (Albert & Hall, 2015; Saxton & Sabatini, 2017). CDK4/6 inhibition attenuates mTOR Complex 1 (mTORC1) activity in some cancer models (Goel et al., 2016; Olmez et al., 2017), yet the effects of CDK4/6 inhibitors on mTORC1 seem to be cell-type specific, since opposite results were found in pancreatic ductal adenocarcinoma (Franco, Balaji, Freinkman, Witkiewicz, & Knudsen, 2016). Given that mTOR activity is amplified in numerous cancer types and participates in the translational regulation of several oncogenic proteins, mTOR inactivation is an attractive strategy for cancer treatment (Wang & Sun, 2009). The exact mechanism underlying the CDK4-mTOR cross-talk in mammals is unknown, although in Drosophila it occurs via the phosphorylation of TSC2 (Romero-Pozuelo, Demetriades, Schroeder, & Teleman, 2017).

Lysosomes, considered for years as only the digestive system of the cell, have since become key effectors in metabolism, due to their role as platforms in the activation of mTOR pathway (Bar-Peled & Sabatini, 2014; Dibble & Cantley, 2015; Puertollano, 2014). mTORC1 is recruited to the surface of lysosomes in a complex procedure sensitive to amino-acids (Bar-Peled & Sabatini, 2014). Among the multiple regulators of this process, we focused on FLCN, a tumor suppressor which functions as a complex with its partner FNIP. FLCN-FNIP complex interacts with the Rag GTPases in the absence of amino acids repressing their activity, and when amino acids are sensed, FLCN-FNIP complex dissociate from Rag GTPases eliciting their activation. Rag GTPases activation is crucial for mTORC1 recruitment to lysosomes (Petit, Roczniak-Ferguson, & Ferguson, 2013). Importantly, mTORC1 activation is also triggered by the accumulation of amino acids in the lysosomal lumen (Zoncu et al., 2011). Therefore, alterations in lysosomal function directly impact mTORC1 activity (Jia et al., 2018; Li et al., 2013). For this reason, and because these organelles

also play a role in cell survival and cell proliferation, lysosomes have become emerging targets for cancer therapy (Fehrenbacher & Jaattela, 2005; Martinez-Carreres, Nasrallah, & Fajas, 2017; Piao & Amaravadi, 2016).

In this study we reveal that CDK4 is capable of modulating mTORC1 activity in a direct manner, through the phosphorylation of FLCN, and in an indirect manner, by promoting lysosomal function. Indeed, CDK4 chemical inhibition or genetic inactivation prevent mTORC1 recruitment to lysosomal surface, not only due to the lack of FLCN phosphorylation, but also because of the accumulation of undigested material inside the lysosomes. This lack of lysosomal function, in turn, induces senescence in triple-negative breast cancer (TNBC) cells, as well as in a mouse xenograft model. CDK4 inhibition as single treatment reduces notably tumor size since cells enter to senescent programs. Moreover, a combination between AMPK activation and CDK4 inhibition was used in an attempt to trigger autophagy in conditions when lysosomes are dysfunctional, and results in cell death and tumor regression. This finding is of a high relevance in TNBC, a highly invasive and aggressive cancer type that does not have a clear therapeutic strategy yet (Elsamany & Abdullah, 2014).

3. Results

CDK4 activity is required for mTORC1 localization at lysosomes

It was previously demonstrated that CDK4/6 inhibition results in the deregulation of mTORC1 in certain models of human cancer, suggesting a cross-talk between the two pathways (Franco et al., 2016; Goel et al., 2016; Olmez et al., 2017). To determine the cell-type specificity of this cross-talk, eight human cancer cell lines were stimulated with IGF-1 to induce mTORC1 activation in the presence or absence of the CDK4/6 inhibitor LY2835219 (abemaciclib). The efficiency of CDK4/6 inhibition was measured by RB-Ser^{780} phosphorylation. Treatment with LY2835219 caused a decrease in p70S6K and 4E-BP1 phosphorylation (two well-known targets of mTORC1 used as a readout of its activity), both in the unstimulated and in the IGF-1 stimulated conditions (Sup. Figure 1A). mTORC1 activity showed the highest sensitivity to CDK4/6 inhibition in CCRF-CEM, MDA-MB-231 and HT29 cells, whereas IB115, MCF7 and PC3 were the least responsive. It is worth noting that,

despite showing considerable mTORC1 inhibition, some cell lines showed only a mild decrease in AKT phosphorylation in the presence of LY2835219 (HCT116, IB115, MDA-MB-231, SKOV3, PC3), suggesting that the effects observed in mTORC1 activity were at least partially independent of decreased AKT signaling.

We decided to focus our experiments on the triple negative breast cancer (TNBC) cell line MDA-MB-231 because it was one of the most responsive to CDK4/6 inhibition and due to the lack of a clearly defined treatment strategy for this cancer type. We first investigated whether CDK4 inhibition or depletion affects the translocation of mTORC1 to the lysosomal surface, a key step for mTORC1 activation. We found that MDA-MB-231 wild-type (WT) cells treated with the CDK4/6 inhibitor LY2835219 or CDK4 knock-out (KO) MDA-MB-231 cells showed impaired translocation of mTORC1 to lysosomes in response to amino acids (Figure 1A–B) and decreased mTORC1 activity, as measured by the phosphorylation of 4E-BP1 and p70S6K (Figure 1C-D). Inhibition of glutaminolysis has been shown to prevent lysosomal recruitment and subsequent activation of mTORC1 (Duran et al., 2012). To check whether mTORC1 translocation was affected due to an impairment in glutamine metabolism, we treated MDA-MB-231 cells with a cell-permeable α-ketoglutarate analog. We found that α-ketoglutarate stimulation could not rescue the defective translocation of mTORC1 to the lysosomal surface upon CDK4 inhibition or depletion (Sup. Fig 2 A-B), indicating that CDK4 inhibition or depletion does not affect mTORC1 translocation to the lysosomal surface by impairing glutamine metabolism.

Interestingly, MDA-MB-231 cells lacking E2F1 showed normal mTORC1 translocation to the lysosomal surface and increased mTORC1 activation (Sup. Fig 2 C-D-E–F) but were still sensitive to CDK4 inhibition. This suggests that the effects of CDK4 on mTORC1 activity are independent of E2F1 transcriptional activity, pointing to other cell cycle-independent targets of CDK4.

CDK4 regulates mTORC1 activity through phosphorylating FLCN

Given the kinase properties of CDK4, we hypothesize that CDK4 potentially regulates mTORC1 pathway through phosphorylation of one of its regulators. To test our hypothesis, first, we performed a bioinformatics search of the proteins of mTORC1 pathway containing the putative phosphorylation site for CDK4: [ST]Px[KRP]. Due to the tight relationship of FLCN with lysosomes and nutrient

sensing, we decided to focus on this protein. We performed *in vitro* kinase assays with CDK4/CycD3 recombinant protein and gluthatione S-transferase (GST) fusion of full length FLCN. The Mass Spectrometry analysis of post-translational modifications revealed that FLCN could be phosphorylated by recombinant CDK4/CycD3 at different sites, being S62, S73, T227 and S571 the ones with higher score (Figure 2A). Importantly, S62, S73 and S571 phosphorylation sites were found when we overexpressed and immunoprecipitated FLCN in MDA-MB-231 cells upon amino acid and IGF-1 stimulation (Figure 2B).

We, then, monitored the localization of overexpressed FLCN by immunofluorescence under amino acid depletion or stimulation in wild type MDA-MB-231 cells untreated or treated with LY2835219, and in CDK4 KO MDA-MB-231 cells. In the absence of amino acids, FLCN is localized at the surface of lysosomes, preventing mTORC1 recruitment to lysosomal surface. When amino acids are sensed, FLCN translocates to the cytoplasm, allowing the RagGTPases to recruit mTORC1. Importantly, we found that FLCN is retained at the lysosomes in the presence of amino acids upon CDK4 inhibition or depletion (Figure 2C). Therefore, our results suggests that CDK4 phosphorylations on FLCN are necessary for mTORC1 activation.

CDK4 inhibition or depletion increases lysosomal mass

Lysosomal biogenesis is a biological process coordinated by transcription factor EB (TFEB), which is repressed by mTORC1. Under nutrient-rich conditions, TFEB is phosphorylated by mTORC1, causing its retention in the cytoplasm. By contrast, when mTORC1 is inactivated, unphosphorylated TFEB translocates to the nucleus and promotes the transcription of genes encoding numerous lysosomal and autophagic proteins (Puertollano, 2014). To test whether CDK4 inhibition or depletion affected TFEB transcription and the resulting upregulation of lysosomal biogenesis genes, we treated WT and CDK4 KO MDA-MB-231 cells with complete or serum-starvation media, with or without the CDK4/6 inhibitor LY2835219, and studied the expression of TFEB target genes. As expected, under starvation conditions, WT MDA-MB-231 cells showed an increase in the expression of genes regulated by TFEB (Figure 3A; cathepsins B and D and SQSTM1). Moreover, we found that CDK4/6 inhibition synergized with starvation to further increase the expression of those genes. CDK4 KO cells also presented increased expression of

those genes under basal conditions, but no further increase was found upon CDK4/6 inhibition (Figure 3A).

We next used LysoTracker staining and flow cytometry to look at the percentage of lysosome-positive cells upon CDK4 inhibition or depletion. The percentage of LysoTracker positive cells and the size of the LysoTracker positive particles were consistently and markedly increased in the absence of CDK4 activity (Figure 3B-C-D). Similarly, when we quantified the size of lysosomal-associated membrane protein 1 (LAMP1)-positive particles, we found a significant increase in lysosomal density in CDK4 KO cells compared to WT MDA-MB-231 cells (Figure 3E-F). These results suggested a new function of CDK4 in the control of lysosomal biology.

CDK4 is required for lysosomal function

It is well known that the inhibition of mTORC1 results in the induction of autophagy, a conserved catabolic process that triggers the degradation of intracellular constituents and organelles in the lysosome (Kaur & Debnath, 2015). To investigate the effects of CDK4 inhibition on autophagy, we treated MDA-MB-231 cells for 24h with LY2835219. Also we used the mTOR inhibitor rapamycin and serum-starvation (-FBS) media as autophagy inducers. Then, we measured the amounts of the autophagosome marker LC3-II and the degradation marker SQSTM1. As expected, serum-starvation conditions, as well as mTOR inhibition by rapamycin, increased the amounts of the autophagosome marker LC3-II (Figure 4A-B, long exposure). CDK4/6 inhibition also increased LC3-II levels to the same extent (Figure 4A-B). Moreover, CDK4 KO cells showed increased levels of LC3-II in basal conditions and were more sensitive to starvation-mediated autophagic stimuli (Figure 4A-B). The observed increase of LC3-II levels suggested that there is either an increase of autophagosome biogenesis or an impairment of the autophagic flux. Indeed, these effects could be secondary to mTOR inactivation, since the decreased mTORC1 activity caused by CDK4 inhibition or depletion shown in Figure 1 could ultimately induce lysosomal biogenesis.

To further study the autophagic flux, we treated cells as described above (Figure 4A-B), including the addition of bafilomycin A1 (BafA1), a potent V-ATPase inhibitor that blocks autophagosome-lysosome fusion. In WT cells, under starvation conditions and in the presence of rapamycin treatment, BafA1 further increased LC3-

II levels, indicating that rapamycin induces autophagosome biogenesis. In contrast, in CDK4 KO cells or cells treated with CDK4 inhibitor, BafA1 failed to cause any additional increase in LC3-II levels (Figure 4A-C). These results suggested that CDK4 does not directly participate in autophagosome biogenesis. On the other hand, no abnormal SQSTM1 accumulation was observed after CDK4 inhibition or depletion, despite observing a consistent SQSTM1 increase with BafA1 (Figure 4A). SQSTM1 protein levels are often negatively correlated with autophagic degradation. However, it has been already observed that the expression of SQSTM1 does not always inversely correlate with autophagic activity, given that they can be restored during prolonged starvation (Sahani, Itakura, & Mizushima, 2014).

Given that CDK4 inhibition or depletion result in an increase in lysosomal and autophagosomal markers, we next used transmission electron microscopy (TEM) to analyze the ultrastructure of these organelles in WT and CDK4 KO MDA-MB-231 cells incubated with serum-starvation media to trigger autophagy. As expected, serum-starvation medium induced autophagosome and lysosome formation in MDA-MB-231 WT cells. Interestingly, CDK4 KO MDA-MB-231 cells displayed higher densities of autophagosomes and lysosomes than WT cells, in agreement with our previous results. Moreover, TEM analysis revealed that the lysosomes in CDK4 KO cells were full of electron-dense material, indicating that they accumulated undigested material inside the lysosomes under both complete and serum-free conditions (Figure 5A-B-C-D, Sup. Figure 3A). LY2835219 treated WT cells yielded the same results as CDK4 KO cells (Figure 5E-F-G-H, Sup. Figure 3B). To further investigate these observations, we measured intracellular lysosomal activity and cathepsin B activity and found that both were decreased in CDK4 KO cells (Figure 5I-J).

Overall, these results suggest that CDK4 is fundamental for the activity of lysosomes and that its absence impairs autophagic flux at the lysosomal degradation step.

Dysfunctional lysosomes, but not mTORC1 inhibition, induce senescence

The above results suggest that CDK4 has a direct impact on lysosomal function and that CDK4 depletion or inhibition leads to the accumulation of enlarged and non-functional lysosomes that impair autophagic flux. Lysosomal processes are associated with aging and longevity (Carmona-Gutierrez, Hughes, Madeo, & Ruckenstuhl, 2016), and the increase of lysosomal content is characteristic of

senescence progression (Cho & Hwang, 2012). This led us to investigate the fate of cells lacking CDK4 activity. We therefore measured levels of proliferation, apoptosis and senescence in cells after treatment with CDK4/6 inhibitor. Analysis of Ki-67 levels showed that CDK4/6 inhibition significantly decreased the proliferation rate of cells in complete medium (Figure 6A). Yet, when the cells were serum-starved, no differences were observed in response to CDK4/6 inhibition (Figure 6A). Apoptosis, measured by Annexin V staining, was not significantly induced when cells were treated with the CDK4/6 inhibitor in complete medium (Figure 6B). A slight increase of apoptosis was seen when CDK4/6 inhibition was combined with serum starvation, but the overall percentage of apoptotic cells was relatively low (Figure 6B). Interestingly, when WT and CDK4 KO cells were incubated for eight days with LY2835219 in complete medium, we observed increased senescence, as measured by senescence-associated beta-galactosidase (SA-βGal) staining. Moreover, CDK4 KO cells in complete medium showed abundant SA-βGal staining under basal conditions, an indication of increased senescence (Figure 6C-D). When the same experiment was conducted in serum starvation conditions, senescence was induced in WT cells but was not further increased in CDK4 KO cells. To test whether these effects were dependent on mTORC1, we also treated cells with rapamycin. Levels of SA-βGal staining in the rapamycin treated cells were similar to those of untreated cells, indicating that the induction of senescence in the absence of CDK4 was not due to mTORC1 inhibition (Figure 6C-E).

To further characterize the senescent phenotype in cells lacking CDK4 activity, we additionally measured the expression of senescence markers in MDA-MB-231 WT cells cultured in complete medium after an eight-days treatment with DMSO, LY2835219 or rapamycin (Figure 6F). Consistently with the SA-βGal data, LY2835219 treatment induced the expression of most of the senescence-related genes evaluated (Figure 6F). Some of the genes that did not respond to CDK4/6 inhibition are p53-regulated genes, reinforcing the idea of a cell cycle-independent induction of senescence. It is worth noting that MDA-MB-231 cells lack CDKN2A, a p53 target gene that is known to promote cellular senescence. Additionally, similar to SA-βGal data in Figure 6C-E, mTOR inhibition by rapamycin failed to induce the expression of genes related to senescence. Only RKHD3 and IGFBP5 were induced by rapamycin, but always to a minor extent than with LY2835219 treatment (Figure 6F).

Our results suggest that the lysosomal dysfunction induced by CDK4 inhibition or depletion is the cause of the senescent phenotype in these cells, and that mTORC1 inhibition is a secondary effect of the impairment of lysosomal function. In fact, SA-βGal derives from a lysosomal enzyme, and the increase of this parameter in senescent cells is likely due to an expansion of the lysosomal compartment (reviewed in Kuilman et al 2010).

The CDK4 inhibitor LY2835219 alters lysosomal function, attenuates mTORC1 activity, and decreases tumor growth in a breast cancer xenograft mouse model

To investigate the effects of CDK4/6 inhibition on lysosomal function *in vivo*, we used a breast cancer xenograft model created by injecting MDA-MB-231 cells into the mammary glands of NSG mice. Intratumoral inhibition of RB phosphorylation in mice treated eight days with LY2835219 compared with vehicle confirmed that CDK4/6 was effectively inhibited in the tumor (Figure 7A-B). Consistent with the previously observed anticancer activity of CDK4 inhibition (Hamilton & Infante, 2016), we observed that the tumors from LY2835219-treated group halted their growth (Figure 7C) and reduced cell proliferation (Figure 7D-E) whereas the untreated ones continued growing and highly proliferating. Of note, the observed effects of CDK4/6 inhibition in tumor size are independent of the immune system in our model because NSG mice are immunodeficient. This was confirmed by the lack of immune cell infiltration in the H-E staining of the tumors in any of the groups (Sup. Figure 4A).

Consistent with our *in vitro* data, xenograft tumors treated with LY2835219 had increased expression levels of the lysosomal marker LAMP1 (Figure 7F-G) and increased expression levels of TFEB target genes (Sup. Figure 4B). In addition, LY2835219 treatment also decreased the activity of mTORC1, assessed by the phosphorylation of p70S6K Thr^{389} (Figure 7H-I). Ultrastructural analysis by TEM confirmed that tumors from LY2835219 treated mice had higher densities of autophagosomes and lysosomes, and that those lysosomes accumulated non-digested material (Figure 7J-K-L-M, Sup. Figure 4C). Furthermore, we show that the tumors of mice treated with LY2835219, which harbored non-functional lysosomes, had increased SA-βGal staining (Figure 7N) and increased expression of senescence

markers (Sup. Figure 4D), revealing that the tumor cells had become senescent, in agreement with our *in vitro* data. Together, these results further demonstrate that CDK4 plays an essential role in the regulation of lysosomal function in vivo, and that this alteration in lysosomal function leads to tumor cell senescence in a mouse model of breast cancer.

The CDK4 inhibitor LY2835219 in combination with the AMPK activator A769662 induces cell death in breast cancer cells and tumors.

Given that lysosomes are essential for autophagy, we set to determine the consequences of the activation of autophagy in conditions when lysosomes were dysfunctional. Thus, we tested the combination of LY2835219, to impair lysosomal function, with the AMPK activator A769662, to induce autophagy. Breast cancer xenografts of NSG mice co-treated for eight days with A769662 and LY2835219 showed smaller tumor size than the ones treated only with LY2835219, whereas tumors from mice treated only with A769662 were similar in size than the untreated ones (DMSO group) (Figure 8A-B). Strikingly, the combination treatment resulted in tumor regression; almost 50% of the tumors decreased their size upon the co-treatment using both A769662 and LY2835219. In contrast, no reduction in tumor size was observed when individual drugs were used (Figure 8C-D). Cell proliferation in tumors, assessed by Ki67 staining, significantly decreased with LY2835219 treatment. However, comparing this group with de co-treated group, there was only a light tendency for the percentage of Ki67 positive cells to further decrease in the co-treated group (Figure 8E-F). Moreover, cleaved-Caspase-3 staining revealed a significant induction of intratumoral cell death when mice were co-treated with A769662 and LY2835219, which was at least six-fold higher than the apoptosis rate in mice treated with LY2835219 as a single agent (Figure 8E-G). This result suggested that increased apoptosis was underlying the decrease in tumor size in the co-treatment group.

In vitro studies with MDA-MB-231 cell line in culture were consistent with the *in vivo* data; CDK4 inhibition and AMPK activation as single treatments failed to induce cell death after one week treatment as shown by the low levels of Annexin V-positive cells (Sup. Figure 5A). Only the combination of LY2835219 with A769662 increased notably the percentage of Annexin V-positive cells (Sup. Figure 5A).

As previously reported, CDK4 inhibition resulted in the intratumoral decrease of RB phosphorylation, but no differences were observed between LY2835219 and the co-treated tumors (Figure 8H-I). As for mTORC1 activity, LY2835219 treatment as well as AMPK activation decreased p70S6K phosphorylation (Figure 8H-J). However, mTORC1 inactivation by A769662 treatment was not sufficient to decrease tumor size in our model. Importantly, and consistent with other studies (Lopez-Mejia et al., 2017), CDK4 inhibition was able to trigger AMPK activation, as observed with the increased phosphorylation of Acetyl-CoA Carboxylase (ACC), a known target of AMPK (Figure 8H-K).

TEM analysis of the tumors revealed that the percentage of the autophagosome and lysosome area per cell was increased in the single treatments, as well as in the A769662 and LY2835219 co-treated group (Sup. Figure 5B-C-D). When we quantified the percentage of autolysosomes with digested material, we found that the mice co-treated with both A769662 and LY2835219 still display a significant decrease in this parameter, despite LY2835219 as a single treatment showed a greater decrease (Sup. Figure 5B-E). The underlying mechanism of this apparent paradox could be that A769662 induced cell death only in cells in which LY2835219 treatment impaired lysosomal function. Indeed, some of the co-treated cells displayed mixed morphological features of apoptotic cell death (highly condensed chromatin, shrinkage of the cytoplasm) and autophagic cell death (numerous autophagosomes and autolysosomes, focal swelling of the perinuclear membrane (Sup. Figure 5B (indicated by *)).

Taken together, these results showed that the combination treatment using A769662 and LY2835219 provided a better outcome than LY2835219 alone, inducing cell death and tumor regression in the MDA-MB-231 breast cancer xenograft model.

4. Discussion

We show here for the first time that CDK4 regulates lysosomal function and mTORC1 activity in cancer cells. We demonstrate that CDK4, through phosphorylation of FLCN in specific residues, facilitates the migration of mTOR to the lysosomes in order to be activated. The abrogation of mTOR activation by

51

depletion or chemical inhibition of CDK4 consequently resulted in a substantial increase in the numbers of lysosomes and autophagosomes. This proves that CDK4 is necessary for the dissociation of FLCN from the lysosomes, and for the subsequent recruitment and activation of mTORC1.

However, this increase was not correlated with greater lysosomal activity, which suggested that CDK4 has an mTOR-independent role in this process. Importantly, we prove that CDK4 inhibition or depletion leads to the accumulation of intra-lysosomal undigested material, which, through recycling of amino acids, might serve as a signal to mTORC1. mTORC1 activation is initiated at the lysosome and requires the presence of amino acids, products of macromolecule degradation, in the cytosol, but also in the lysosomal lumen (Zoncu et al., 2011). We show now that an additional mechanism by which CDK4 favors mTORC1 activation by promoting the digestion of proteins in the lysosome, in turn providing metabolic intermediates that sustain cell growth and survival via downstream effectors. This pathway would be particularly crucial during prolonged starvation conditions, such as the typical environment of some tumors.

Cells initially respond to nutrient deprivation by inactivating their energy-consuming processes, such as protein or lipid biosynthesis, and by activating catabolism. At the same time, other mechanisms are activated to recycle molecules to provide the cell with enough substrates and metabolic intermediates to survive – an important function of autophagy. In the long term, autophagy reactivates the mTORC1 pathway by replenishing the lysosomes with digested proteins and amino acids (Tan, Sim, & Long, 2017). CDK4 inhibition or depletion could therefore mimic a starvation signal. This hypothesis is in agreement with previous studies showing that CDK4/6 inhibitors induce autophagy (Bourdeau & Ferbeyre, 2016; Iriyama et al., 2018). We also observed an increase in the number of autophagosomes upon CDK4 inhibition in this study. However, when analyzing the ultimate fate of the autophagosomes, we found that they accumulate due to the impairment of lysosomal degradation upon CDK4 inhibition or depletion. Indeed, others have demonstrated that the inhibition of lysosomal activity causes decreased fusion with autophagosomes and vice-versa (Renna et al., 2011; Seranova et al., 2017; Settembre & Ballabio, 2014). In this study, we showed that inhibiting or depleting CDK4, in addition to inducing autophagy, likely through mTORC1 inactivation, impairs the autophagic

flux at the lysosomal degradation step. This observation may explain the increased susceptibility of CDK4 KO cells to autophagic stimuli.

We also found that CDK4 inhibition or depletion increased the expression of many lysosomal genes. It is well known that mTORC1 negatively regulates lysosomal biogenesis (Zhou et al., 2013). This could be secondary to mTORC1 inhibition, or due to a compensatory mechanism to create new lysosomes as the existing ones are dysfunctional and ensure their function.

CDK4/6 inhibitors have been shown to accumulate into lysosomes, a phenomenon called lysosomal trapping (Llanos et al., 2019). However, the use of CDK4 KO cells in our work demonstrates that CDK4 rather stimulates lysosomal function, and that the lysosomal trapping of the drug is secondary to the lysosomal impairment induced by CDK4 inhibition. In addition, CDK4/6 inhibition has been found to result in proteasomal activation (Miettinen et al., 2018). Moreover, a negative-feedback exist between proteasomal activity and autophagic flux (J. H. Lee, Park, Kim, & Lee, 2019). Thus, the impairment of autophagic flux at the lysosomal degradation step can result in proteasomal activation and viceversa.

Despite the known requirement for lysosomes in cell cycle progression (Hubbi et al., 2014; Jin & Weisman, 2015), little is known about the relationship between lysosomes and senescence. Importantly, in eukaryotes, autophagy impairment via lysosomal dysfunction has been described to be an important characteristic of oxidative stress-induced senescence (Tai et al., 2017). Our findings suggest that the ultimate fate of cells that lack CDK4 is the activation of senescence due to lysosomal dysfunction. The absence of senescence when cells are treated with rapamycin further demonstrates that mTORC1 inactivation is a consequence of lysosomal impairment due to CDK4 inhibition or depletion. However, the CDK4 inhibitor induced lysosomal dysfunction, was not sufficient to induce cell death in the tumors of the treated mice. Instead, cancer cells were arrested, but were still alive, which explained that the tumor burden was not decreased, but only stabilized (Figure 7). We reasoned that further forcing the autophagic flux would create an additional stress that could kill these tumor cells. With this aim, we used the AMPK activator A769662, which is known to increase autophagy, in combination with the CDK4 inhibitor. Indeed, co-treatment of the cells resulted in increased cancer cell death and therefore tumor regression (Figure 8). This is a major finding that represents a paradigm switch regarding the use of CDK4 inhibitors for the treatment of cancer. Strikingly, and

consistent with our findings, CDK4 inhibitors are not efficient as a single drug in the clinical practice and are often used in combination with other drugs (Klein, Kovatcheva, Davis, Tap, & Koff, 2018b; Ku et al., 2016; Michaloglou et al., 2018).

We show here that the effects of CDK4 in MDA-MB-231 cells are independent of E2F1, the transcription factor modulated by CDK4 during the cell cycle. It has been reported, however, that E2F1 regulates lysosomal positioning and activates mTORC1 by promoting its recruitment to the lysosomal surface (Meo-Evoli et al., 2015; Real, Meo-Evoli, Espada, & Tauler, 2011). This suggests a dual and complementary role for CDK4 in the regulation of the mTORC1 pathway: first, through regulation of the lysosomal function; and second, through FLCN phosphorylation .

It was previously described that CDK4/6 inhibitors display anti-tumor activity only in RB-positive cells (Polk, Kolmos, Kumler, & Nielsen, 2016). In addition, it was unclear whether CDK4/6 inhibition had an effect on TNBCs. Our findings are consistent with other studies showing that CDK4/6 inhibitors still have some effects on RB-negative cells (Rivadeneira et al., 2010), and that CDK4/6 inhibitors do have anti-tumor effects in TNBCs. Indeed, depending on the cell type, CDK4/6 inhibition triggers either a quiescence or senescence response, not necessarily via the canonical RB-E2F pathway (reviewed in (Klein, Kovatcheva, Davis, Tap, & Koff, 2018a); (Brown et al., 2012)).

Overall, the present study demonstrates a new role for CDK4 in the regulation of lysosomal function, which ultimately leads to senescence in cancer cells and mTORC1 inactivation. , In addition, we highlight the importance of lysosomes in cancer and we propose that CDK4/6 inhibitors could be used in combination with other drugs to target lysosomal function as a novel anticancer strategy.

5. Materials and Methods

Materials

LY2835219 (abemaciclib), a specific CDK4/6 inhibitor, was purchased from MedChem Express and used at a concentration of 0.5 μM for cancer cell lines. R[3] human IGF-1 (I11146, Sigma) was used at a concentration of 30 ng/ml. Minimal Essential Media (MEM) Amino Acids Solution (50X, ThermoFisher) was used at the

indicated concentrations. Rapamycin was kindly provided by Professor Pedro Romero (Université de Lausanne, Switzerland) and was used at the indicated concentrations. Bafilomycin A1 (BafA1) was purchased from Enzo Life Sciences (ALX-380-030-M001) and used at a concentration of 0.3 µM.

Cell culture and transfection

The cancer cell lines MDA-MB-231, CCRF-CEM, HTC116, IB115, HT29, SKOV, MCF7 and PC3 were cultured in RPMI 1640 (1×) + GlutaMAX media (Life Technologies, USA) containing 10% fetal bovine serum (FBS) (PAA Laboratories), 1% HEPES (Life Technologies) and 1% sodium pyruvate (Sigma).

MDA-MB-231 CDK4 knockout (KO) and E2F1 KO stable cell lines were generated with CRISPR/cas9 technology. The lentiCRISPR v2 plasmid was a gift from Feng Zhang (Cambridge University, Cambridge, England; Addgene plasmid # 52961); a description of this plasmid can be found in Shalem et al. 2014 (Shalem et al., 2014). The pMD2.G and psPAX2 plasmids were gifts from Didier Trono (Université de Lausanne; Addgene plasmids # 12259 and # 12260, respectively). The target sequences for the guide RNA were as follows:

Table S1. Oligonucleotides used as guide RNA in CRISPR/cas9 technology for the generation of KO stable cell lines.

CDK4	5'-CACCGCTTGCCAGCCGAAACGATCA-3'
	5'-AAACTGATCGTTTCGGCTGGCAAGC-3'
E2F1	5'-CACCGTCTGACCACCAAGCGCTTCC-3'
	5'-AACGGAAGCGCTTGGTGGTCAGAC-3'

The oligonucleotides were synthesized and cloned into the digested LentiCrispR vector as described by Shalem et al., 2014. Lentiviral production was based on the standard protocol established by Salmon and Trono, 2006 (Salmon & Trono, 2006). The resulting lentivirus (2ml) was then used to infect MDA-MB-231 cells for 72 hours. Infected cells were treated with 5 µg/ml puromycin for five consecutive days. Western blotting was performed to ensure that the protein of interest was not expressed.

For pRK5-FLAG-FLCN (Addgene #72290) transfection, cells were grown in 10cm diameter dishes. 10µg of plasmid were transfected with X-treme gene HP in a ratio 1:2 (µg DNA: µl reagent) in Optimem media. The following day the media was changed to the normal growing media, and cells were grown for 48h.

Cell treatments

For insulin pathway stimulation, the different tumor cell lines were first treated with a CDK4/6 inhibitor (or the same volume of DMSO as a control) diluted in FBS-free media for 15 h. The cells were subsequently treated with IGF-1 for 20 min before lysis or fixation.

For amino acid stimulation, after a 15 h treatment with FBS-free media with or without the CDK4/6 inhibitor, the cells were incubated for two hours in KRBB media containing 111 mM NaCl, 25 mM NaHCO$_3$, 5 mM KCl, 2.5 mM CaCl$_2$, 1 mM MgCl$_2$, 25 mM HEPES, 25 mM glucose and dialyzed FBS with or without the CDK4/6 inhibitor. For the last 20 min, 2× MEM amino acids solution and 2 mM glutamine were added to the cells.

Western blotting

Cell lysates were obtained with M-PER mammalian extraction buffer (Thermo Scientific) containing 1:100 Halt phosphatase inhibitor cocktail (Thermo Scientific) and 1:100 Halt EDTA-free protease inhibitor cocktail (Thermo Scientific). Lysate proteins were separated by SDS-PAGE and transferred onto nitrocellulose membranes. The membranes were incubated overnight at 4°C with the corresponding primary antibodies and then incubated with the corresponding secondary antibodies and developed with ECL. The band intensities on the developed films, fusion FX images and ChemiDoc images were quantified using the Fiji image-processing package (Schindelin et al., 2012). The following antibodies were used for Western blot analysis: anti-CDK4 (clone H22), anti-CDK6 (clone C21) and anti-RB (C15) from Santa Cruz Biotechnology; anti-phospho Rb-S780 (clone D59B7), anti-phospho P70S6K-T389 (clone 108D2), anti-4E-BP1 (clone 53H11), anti-phospho AKT-T308 (clone 244F9), anti-phospho AKT- S472/3 (clone D9E), anti-p70S6 kinase (49D7), anti-LC3B (polyclonal), anti-SQSTM1 (polyclonal), anti AcetylCoA Carboxylase (p-ACC) (polyclonal) and anti phospho AcetylCoA Carboxylase (p-ACC) from Cell

Signaling Technology; and anti-alpha-tubulin (clone DM1A) from Sigma-Aldrich. The bands were quantified with FIJI software (Schindelin et al., 2012).

Immunofluorescence

For in vitro immunofluorescence, cells were grown on glass coverslips. After the different treatments or stimulation, the slides were rinsed with PBS once and fixed for 15 min with 4% paraformaldehyde in PBS at room temperature (RT). The slides were rinsed twice with PBS, permeabilized with 0.01% saponin for 10 min and blocked with PBS containing 2% BSA and 0.05% Tween 20 for 30-60 min, then, incubated with the primary antibodies for 2-3 h at RT. After 3 washes with PBS, they were incubated with 1:1000 anti-mouse Alexa 488 and anti-rabbit Alexa 561 secondary antibodies for 45 min. Finally, they were washed twice with PBS for 10 minutes, and the nuclei were stained with Hoechst (1:10000 in PBS). The coverslips were mounted with Fluoromont mounting media on the glass slides. Images were obtained with a Zeiss LSM710 inverted confocal microscope with a 63× objective. The following antibodies were used for immunofluorescence experiments: anti-mTOR (7C10), anti-FLCN (clone D14G9) and anti-Lamp1 (clone D401S) from Cell Signaling Technology (USA) and anti-CDK4 (clone EPR4513) from Abcam. Images were processed with Fiji software (Schindelin et al., 2012). Colocalization was analyzed with JACoP (Just Another Colocalization Plugin) for ImageJ, and the volume of LAMP1 positive particles was analyzed with Imaris 9.0.0.

For fluorescence immunohistochemistry in tissue sections, mouse xenograft tumors were dissected, fixed in 4% paraformaldehyde and embedded in paraffin. Next, 4-μm sections were deparaffined with xylene and rehydrated in a graded ethanol series. Antigen retrieval was performed by heating the sections in the microwave at 750 W for 10 minutes in citrate buffer (0.01 M, pH 6). After cooling, the sections were washed with PBS, and blocked for 1 hour with NGS 2.5%. Primary anti-LAMP1, Ki67 and Cleaved-Caspase-3 antibodies were incubated overnight at 4°C. The following day, the sections were incubated with the corresponding Alexa 488 or 568 secondary antibody and counterstained with DAPI. The sections were mounted and observed with a 20X objective and a fluorescence microscope. Images were processed and analyzed with Fiji software (Schindelin et al., 2012).

Immunoprecipitation

48 h after pRK5-FLAG-FLCN transfection, cells were lysated as described above with M-PER buffer. With 1 mg of total protein, FLAG was over night immunoprecipitated using FLAG-M2 affinity gel. After some washes with buffer, the samples were analyzed by western blotting.

GST production

pDON-FLCN and pDON-RB were cloned in pDEST pGEX-2T and expressed in BL21 bacteria. The GST-purified proteins were resuspended in 50mM Tris.HCl (pH 8), 100 mM NaCl, 5 mM DTT and 20% glycerol buffer.

In vitro kinase assay

Kinase assays were performed using GST-FLCN and recombinant RB protein (Santa Cruz) as a substrate in kinase buffer (25 mM Tris.HCl (pH 7.5), 150 mM NaCl, 10 mM MgCl$_2$, 1 mM DTT, 5 mM Na$_4$P$_2$O$_7$, 50 mM NaF, 1 mM vanadate and protease inhibitor cocktail) with 40 μM ATP (PAMGENE ATP-Perkin Elmer) for 30 min at 30°C. Recombinant CDK4/cyclin D3 kinase (ProQinase) were used. RB was used as positive control. Boiling the samples for 5 min in the presence of denaturing sample buffer stopped the reaction. As an experimental control, westernblot with RB samples was done with phospho-RB antibody. FLCN samples were analyzed by mass spectrometry.

Mass spectrometry

Protein samples were loaded on a 10% mini polyacrylamide gel, and after Coomassie staining visible band between 75 and 100 kDa corresponding to FLCN-GST or FLCN-FLAG construct was excised and digested with sequencing-grade trypsin (Promega) as described (Shevchenko, Tomas, Havlis, Olsen, & Mann, 2006). Extracted tryptic peptides were dried and resuspended in 0.05% trifluoroacetic acid, 2% (v/v) acetonitrile, for mass spectrometry analyses. Tryptic peptide mixtures were injected on an Ultimate RSLC 3000 nanoHPLC system (Dionex, Sunnyvale, CA, USA) interfaced to an Orbitrap Fusion Tribrid or to a QExactive Plus high resolution mass spectrometer (Thermo Scientific, Bremen, Germany). Peptides were loaded onto a trapping microcolumn Acclaim PepMap100 C18 (20 mm x 100 μm ID, 5 μm, 100Å, Thermo Scientific) before separation on a

reversed-phase analytical nanocolumn at a flowrate of 0.25 µl/min, using a gradient from 4 to 76% acetonitrile in 0.1% formic acid (total time: 140min). A custom packed nanocolumn was used with Fusion MS instrument (75 µm ID × 40 cm, 1.8 µm particles, Reprosil Pur, Dr. Maisch), and an Easy-Spray PepMap C18 column was used with QExactive MS (50 cm x 75 µm ID, 2 µm, 100Å, Thermo Scientific). In Fusion instrument, full survey scans were performed at a 120'000 resolution, and a top speed precursor selection strategy was applied to maximize acquisition of peptide tandem MS spectra with a maximum cycle time of 3s. HCD fragmentation mode was used at a normalized collision energy of 32%, with a precursor isolation window of 1.6 m/z, and MS/MS spectra were acquired at a 15'000 resolution. Peptides selected for MS/MS were excluded from further fragmentation during 60s. In QExactive instrument, full MS survey scans were performed at 70'000 resolution, and the 10 most intense multiple-charge precursor ions detected in the full MS survey scan were selected for higher energy collision-induced dissociation (HCD, normalized collision energy NCE=27 %) and analysis in the orbitrap at 17'500 resolution. The window for precursor isolation was of 1.5 m/z units around the precursor and selected fragments were excluded for 60s from further analysis.

MS data were analyzed using Mascot 2.6 (Matrix Science, London, UK) set up to search the SwissProt database (www.uniprot.org) restricted to *Homo sapiens* taxonomy (December 2017 version, 20'245 sequences) and including common contaminants (keratins, digestion enzymes, etc.). Trypsin (cleavage at K,R) was used as the enzyme definition, allowing 3 missed cleavages. Mascot was searched with a parent ion tolerance of 10 ppm and a fragment ion mass tolerance of 0.02 Da. Iodoacetamide derivative of cysteine was specified in Mascot as a fixed modification. N-terminal acetylation of protein, oxidation of methionine, and phosphorylation of serine, threonine or tyrosine were specified as variable modifications.

Scaffold software (version 4.8.4, Proteome Software Inc., Portland, OR) was used to validate MS/MS based peptide and protein identifications, and to perform dataset alignment. Peptide identifications were accepted if they could be established at greater than 90.0% probability by the Scaffold Local FDR algorithm. Protein identifications were accepted if they could be established at greater than 95.0% probability and contained at least 5 identified peptides. Protein probabilities were assigned by the Protein Prophet algorithm (Nesvizhskii, Keller, Kolker, & Aebersold, 2003). Proteins that contained similar peptides and could not be differentiated based

on MS/MS analysis alone were grouped to satisfy the principles of parsimony. Proteins sharing significant peptide evidence were grouped into clusters. MsViz software (Martin-Campos et al., 2017) was used for comparison of sequence coverage and phosphorylation of FLCN protein in the different treatments.

Flow cytometry

To study cell death and proliferation following treatment with CDK4 inhibitors, the amounts of Annexin V-PE and Ki67 expression were measured by flow cytometry. Cultured cells were trypsinized and stained with Annexin V-PE (BioLegend, 640907) according to the manufacturer's protocol, and the cells were analyzed on either a Gallios™ (Beckman Coulter) or LSR II flow cytometer (BD Biosciences). For intracellular Ki67 staining, cells were fixed and permeabilized (Biolegend) according to the manufacturer's protocol. Cells were then incubated with a permeabilization buffer that detects anti-Ki67-FITC (Biolegend) for 30 min on ice. After washing twice with permeabilization buffer, the cells were resuspended in PBS prior to analysis. For each sample, at least 10000 events were acquired. Flow cytometry analysis was performed with FlowJo software (Version 7.6.5, Treestar).

For the LysoTracker experiments, fluorescence was analyzed with an ImageStreem III Flow Cytometer. After treating the cells with the CDK4 inhibitor and/or IGF1, 100 nM Lysotracker Green DND-26 (Life Technologies) was added to live cells 1 h before fixation. The cells were then trypsinized and fixed in suspension with 4% PFA for 15 min at RT and washed twice with PBS. Nuclear staining was performed with DAPI, and the cells were resuspended in PBS with 2% FBS. For each sample, 10000 events were acquired at a magnification power equivalent to 60X.

Flow cytometry was also used to analyze the intracellular lysosomal activity with a lysosomal intracellular activity assay kit (Cell-Based) (Biovision) according to the manufacturer's instructions. Briefly, a self-quenched substrate was added to the cultured cells with freshly prepared media containing 0.5% FBS, incubated for one hour at 37°C with 5% CO_2 and trypsinized; 1000 events were acquired with an ACCURI C6 flow cytometer. All flow cytometry analyses were performed with FlowJo software (Version 7.6.5, Treestar).

Quantitative Real-Time PCR Analysis.

Total RNA was prepared using Trizol reagent (Sigma) and then reverse transcribed using Super Script II (Invitrogen). qPCR analysis was performed using SYBR green (Roche Diagnostics) and a 7900HT Fast Real-Time PCR System (Applied Biosystems). Relative mRNA expression levels were calculated from the comparative threshold cycle (Ct) values of the gene of interest relative to RS9 and TBP mRNA. Specific primer sequences are listed in Table S1, S2 and S3.

Table S2. Primers used for qPCR Analysis of Transcription Factor EB (TFEB) regulated genes (human).

Gene	Forward	Reverse
ATP6V0E1	CATTGTGATGAGCGTGTTCTGG	AACTCCCCGGTTAGGACCCTTA
ATP6V1H	GGAAGTGTCAGATGATCCCCA	CCGTTTGCCTCGTGGATAAT
CTSA	CAGGCTTTGGTCTTCTCTCCA	TCACGCATTCCAGGTCTTTG
CTSB	AGTGGAGAATGGCACACCCTA	AAGAAGCCATTGTCACCCCA
CTSD	GCTGATTCAGGGCGAGTACATGAT	TGCGACACCTTGAGCGTGTA
CTSF	ACAGAGGAGGAGTTCCGCACTA	GCTTGCTTCATCTTGTTGCCA
CTSL1	CACCGGCTTTGTGGACATC	ATGACCTGCATCAATAGCAACA
CTSO	TAGATGCAGTGAGCTGGCAA	AACGGAATCTGCAATACCACA
LAMP1	ACGTTACAGCGTCCAGCTCAT	TCTTTGGAGCTCGCATTGG
SQSTM1	CACCTGTCTGAGGGCTTCTC	CACACTCTCCCCAACGTTCT
TFEB	CCAGAAGCGAGAGCTCACAGAT	TGTGATTGTCTTTCTTCTGCCG

Table S3. Primers used for qPCR Analysis of Senescence genes (human).

Gene	Forward	Reverse
CDKN1A	GACACCACTGGAGGGTGACT	CAGGTCCACATGGTCTTCCT
CDKN2A	CCAACGCACCGAATAGTTACG	GCGCTGCCCATCATCATG
COL1A1	GGAGGAATTTCCGTGCCTGG	CAATCCTCGAGCACCCTGAG
CXCL14	GGACCCAAGATCCGCTACAG	CTTCGTAGACCCTGCGCTTC
MFAP2	AGCAGTGAACGGAGTCACAAA	GCCGAGGAGTCACCTCTTGA
MMP2	TGATGTCCAGCGAGTGGATG	AAGAAGTAGCTGTGACCGCC
P311	GGGGCTTTTGTCTGTTGGTC	GAAGCCTTCCCTCCATGTCC
RKHD3	GGGCGGCAAGGTTGTAAAAT	TGTTCTTATTCCGGGAGGCG
IGFBP5	GAAAGCAGTGCAAACCTTCCC	AGGTGTGGCACTGAAAGTCC

| RBL2 | CGGGATCTCTGTGCCAAACT | ACTTCTATACACCTGGCTCCG |

Table S4. Primers used for qPCR Analysis of housekeeping genes (human).

Gene	Forward	Reverse
RS9	CACACTCTCCCCAACGTTCT	ACCACCTGCTTGCGGACCCTGATA
TBP	TGCACAGGAGCCAAGAGTGAA	CACATCACAGCTCCCCACCA

Cathepsin B activity assay kit (fluorometric)

Cathepsin B activity was assessed with a fluorometric kit (ab65300, Abcam). Cell lysates that contain cathepsin B cleave the synthetic substrate RR-AFC to release free AFC, which emits fluorescence that can be measured. Cells were lysed with chilled cell lysis buffer provided in the kit; the lysates were then incubated on ice for 10-30 minutes and centrifuged for 5 minutes at 4°C. The supernatants were saved, and the protein concentrations were measured. In a 96-well plate, 200 µg of protein was loaded per well, and 50 µl of cathepsin B reaction buffer and 2 µl of 10 mM cathepsin B substrate Ac-RR-AFC (200 µM final concentration) were added. The plates were incubated at 37°C for 1 hour in the dark, and the fluorescence was measured with a Tecan plate reader (Ex/Em = 400/505 nm).

Colorimetric detection of senescence-associated β galactosidase

Senescence-associated β-galactosidase (SA-β-Gal) analysis was performed in cultured cells and mouse xenograft tumors.

Cells in culture were fixed with 2% PFA and 0.2% glutaraldehyde for five minutes at RT, washed with PBS and stained with a solution containing 40 mM citric acid/Na phosphate buffer, 5 mM $K_4[Fe(CN)_6]$ $3H_2O$, 5 mM $K_3[Fe(CN)_6]$, 150 mM sodium chloride, 2 mM magnesium chloride and 1 mg ml^{-1} X-gal in distilled water for 15h at 37°C. After staining, the cells were washed twice with PBS and once with methanol, and the plates were allowed to air dry. Bright field images were obtained with an upright light microscope (CarlZeiss) with a 20X objective. Positive cells and the total number of cells per field were counted manually.

For SA-β-Gal analysis of mouse tumors, tissues were OCT embedded and

stored at -80°C. On the day of the experiment, the tissues were cut into 8-µm-thick sections and mounted onto glass slides. After air-drying for 30 minutes, the sections were fixed with 2% PFA and 0.2% glutaraldehyde and stained as previously for cultured cells. The sections were washed and counterstained with 0.1% Fast Red (Sigma). Images were taken at different magnifications with a bright field microscope.

Electron microscopy

Cells were plated on poly-L-lysine (0.01%, Sigma, catalog n°P4832)-coated glass slides (LabTek Chamber Slides, catalog n°177399) cultured for two days and treated with CDK4/6 inhibitor or DMSO as control. The cells were then fixed for two hours in 2.5% glutaraldehyde (Electron Microscopy Sciences, catalog n°16220) dissolved in 0.1 M phosphate buffer (PB), pH 7.4. After three washes with PB, the cells were post-fixed for one hour in 1% osmium tetroxide (Electron Microscopy Sciences, catalog n°19150) in PB and then stained with 70% ethanol containing 1% uranyl acetate (Sigma, catalog n°73943) for 20 minutes. The cells were dehydrated in a graded alcohol series and embedded in Epon (Electron Microscopy Sciences, catalog n°13940). Mouse tumors were cut into small pieces (approximately 1 mm^3) and then analysed in the same way as cells, outlined below.

For EM analysis, mouse tumors and cultured cells were fixed in a 2.5% glutaraldehyde solution (EMS, Hatfield, PA, US) in PB for one hour at RT. Then, they were rinsed three times for five minutes with PB buffer and post-fixed with a fresh mixture of 1% osmium tetroxide (EMS, Hatfield, PA, US) and 1.5% potassium ferrocyanide (Sigma, St Louis, MO, US) in PB buffer for one hour at RT. The samples were then washed three times with distilled water and dehydrated in acetone solutions (Sigma, St Louis, MO, US) of graded concentrations (30%-40 min; 50%-40 min; 70%-40 min; 100%-3x1 h). This was followed by incubation with Epon (Sigma, St Louis, MO, US) at graded concentrations (Epon 1/3 acetone-2 h; Epon 3/1 acetone-2 h, Epon 1/1-4 h; Epon 1/1-12 h) and finally polymerization for 48 h at 60°C in an oven.

Ultrathin sections of 50 nm were cut on a Leica Ultracut (Leica Mikrosysteme GmbH, *Vienna*, Austria) and picked up on a 2x1 mm copper slot grid (EMS, Hatfield, PA, US) coated with a polystyrene film (Sigma, St Louis, MO, US). Sections were

post-stained with 4% uranyl acetate (Sigma, St Louis, MO, US) in H_2O for 10 minutes, rinsed several times with H_2O followed by Reynolds lead citrate in H_2O (Sigma, St Louis, MO, US) for 10 minutes and then again with H_2O several times. Micrographs were taken with a Philips CM100 transmission electron microscope (Thermo Fisher Scientific, Waltham, MA USA) at an acceleration voltage of 80 kV with a TVIPS TemCam-F416 digital camera (TVIPS GmbH, Gauting, Germany). Large montage alignment was performed using the Blendmont command-line program from IMOD software (Kremer, Mastronarde, & McIntosh, 1996) (for the in vivo analyses) or Adobe Photoshop CC 2015 (for in vitro analyses).

The areas of autolysosomes, autophagosomes and cell cytoplasm were measured using ImageJ software. The densities of the autolysosomes and autophagosomes were expressed as a percentage of the cell area using the formula: area of the autolysosomes (or autophagosomes) / area of the cell cytoplasm x 100. The mean autolysosome area per cell and the percentage of autolysosomes containing degraded material per cell were also analyzed.

Animal studies

MDA-MB-231 cells were injected into the fourth mammary gland of eight-week-old female NSG mice (NOD.*Cg-Prkdc^{scid}Il2rg^{tm1Wjl}*/Sz strain, The Jackson Laboratory). Tumor growth and body weight were measured twice per week until the tumor size of each mouse reached 50 mm^3. Optical imaging measurements using an IVIS Xenogen system were conducted on mice under anesthesia once per week for the duration of the study to follow the progression of the primary tumor.

For the first experiment, mice were divided randomly into two groups, one (n=15) for treatment with vehicle (DMSO) and the other (n=15) for treatment with a CDK4/6 inhibitor (LY2835219, 75 mg/kg, formulated in 1% HEC in distilled water). The treatments were administered orally (gavage), with approximately 300 µl of solution (depending on the body weight) gavaged every day for a total of 8 days. During this time, body weight and tumor growth were also monitored. After eight days, the animals were anesthetized with isoflurane (3%) in an induction chamber for 3 minutes and were sacrificed by cervical dislocation. Tumors from n=10 mice from each treatment group were dissected and cut into two pieces; one piece was fixed in PFA for histological staining, and the other piece was snap frozen for protein and

RNA analysis. Tumors from n=5 mice from each treatment group were processed for transmission electron microscopy analysis and SA-β-Gal staining.

The injections and monitoring for second experiment was exactly the same. However, mice were divided into four groups of n=9-10 as follows:

1. DMSO gavage + intraperitoneal injection (IP) NaCl 0.9%

2. DMSO gavage + IP A-769662 (20mg/kg)

3. LY2835219 gavage (75 mg/Kg) + IP NaCl 0.9%

4. LY2835219 gavage (75 mg/Kg) + IP A-769662 (20mg/kg)

As before, the CDK4/6 inhibitor LY2835219 was administrated orally (gavage) in approximately 350µl of volume (depending on the body weight). A-769662 was administrated by intraperitoneal injection (IP) of 100µl in saline solution (NaCl 0.9%).

Quantification and Statistical Analyses

The results are expressed as the means ± standard error of the means (S.E.M.). Comparisons between 2 groups were performed with an unpaired two-tailed Student's t test, and multiple group comparisons were performed by unpaired one-way ANOVA and two-way ANOVA, both followed by Tukey's test or otherwise indicated. All *p-value*s below 0.05 were considered significant. Statistically significant values are represented by asterisks corresponding to $^*p < 0.05$, $^{**}p < 0.01$, $^{***}p < 0.001$ and $^{****}p < 0.0001$.
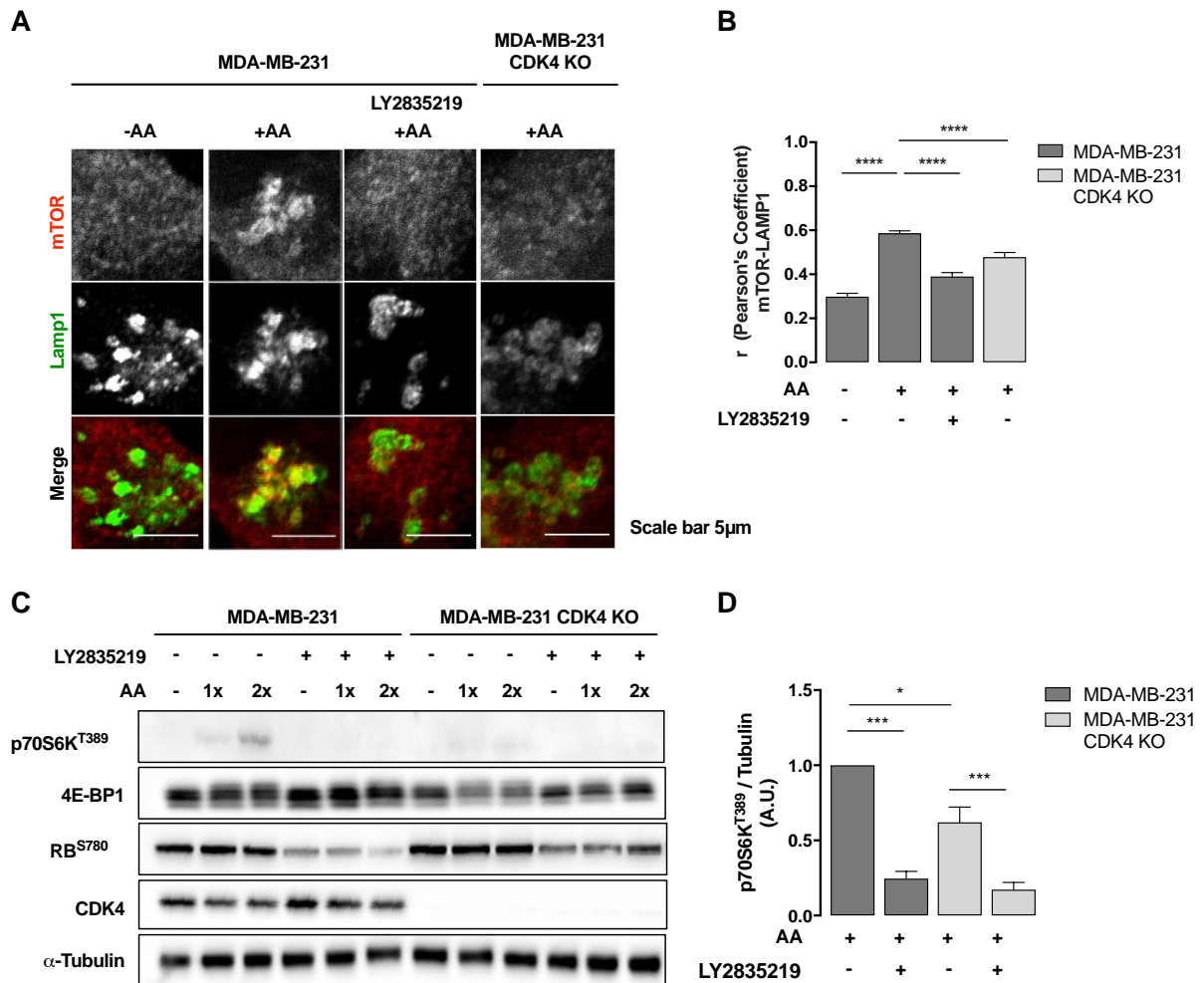
6. Figures

Figure 1.- CDK4 inhibition or depletion prevents the recruitment of mTOR to the lysosomal surface in response to amino acid stimulation. A, Confocal immunofluorescence analysis showing the colocalization of mTOR with lysosomes (visualized by LAMP1 and mTOR staining) in WT and CDK4 KO MDA-MB-231 cells, with or without amino acid stimulation and in the presence of 0.5 µM of the CDK4/6 inhibitor LY2835219 or vehicle control (DMSO). B, Quantification of mTOR-LAMP1 colocalization from A using Pearson's coefficient. At least 40 fields per treatment condition from 3 independent experiments were analyzed. C, Western blot showing levels of phospho-RB (S780), CDK4, mTORC1 target genes (phospho-p70S6K (T389) and 4E-BP1). α-tubulin was used as a loading control in WT and CDK4 KO MDA-MB-231 cells with or without amino acid stimulation and in

presence or absence of 0.5 µM LY2835219. D, Quantification of phospho-p70S6K (T389) levels from three independent experiments like C normalized to α-tubulin.
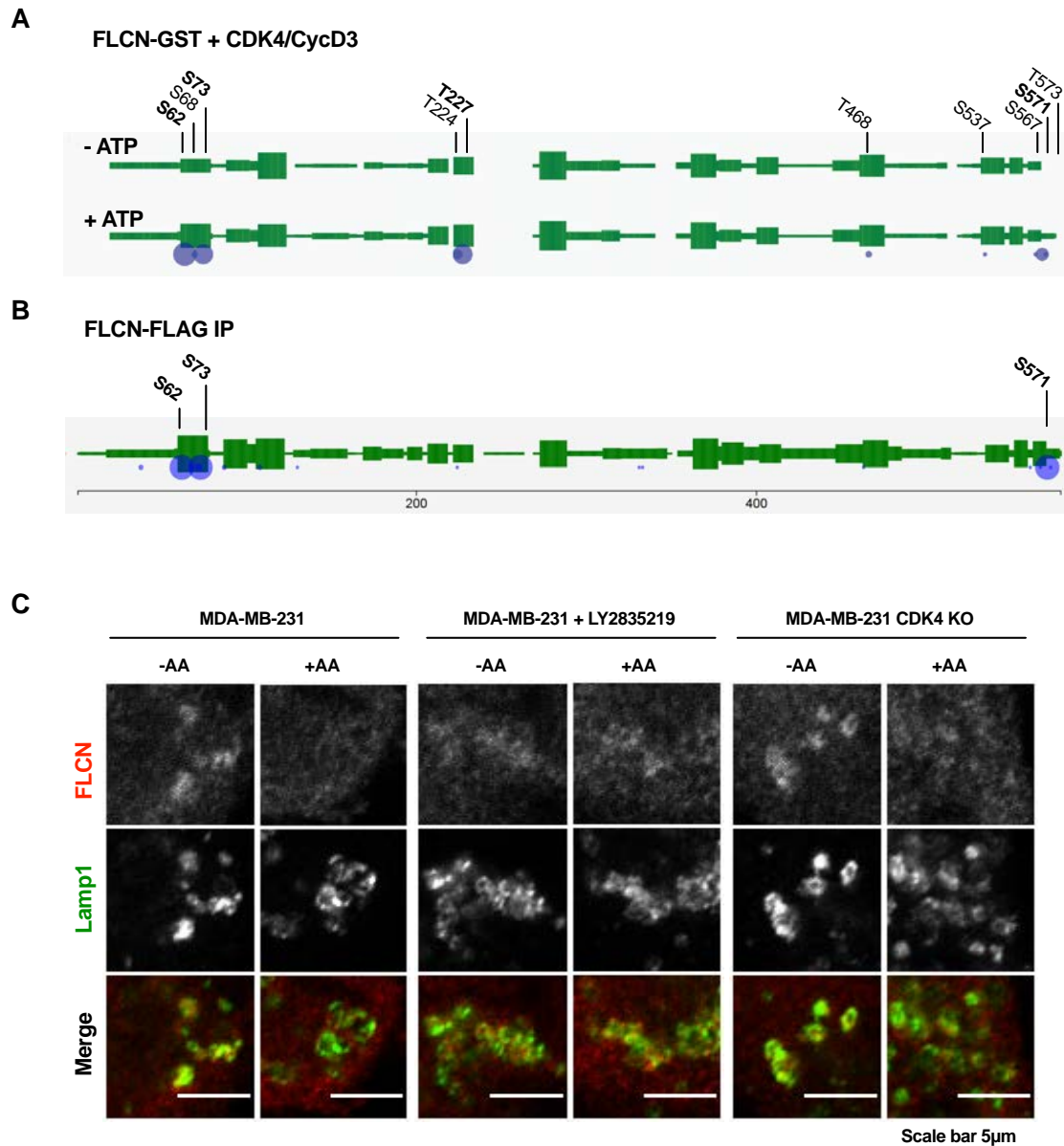
Figure 2.- CDK4 regulates mTORC1 activity through phosphorylating FLCN. A, Representation of the phosphorylation sites detected by mass spectrometry analysis in the *In vitro* kinase assay with FLCN-GST and CDK4/CyclinD3. In green is represented the protein sequence. Blue dots represent the phosphorylation sites, and their size correlates with their abundance. Conditions without ATP (-ATP) were used as negative control. B, Representation of the phosphorylation sites detected by mass spectrometry analysis in the overexpressed and immunoprecipitated FLCN-FLAG. As in A, green represents the protein sequence. Blue dots represent the phosphorylation sites, the size of which correlates with their abundance. C, Confocal

immunofluorescence analysis showing the colocalization of overexpressed FLCN with lysosomes (visualized by LAMP1 and FLCN staining) in WT and CDK4 KO MDA-MB-231 cells, with or without amino acid stimulation and in the presence of 0.5 µM of the CDK4/6 inhibitor LY2835219 or vehicle control (DMSO).
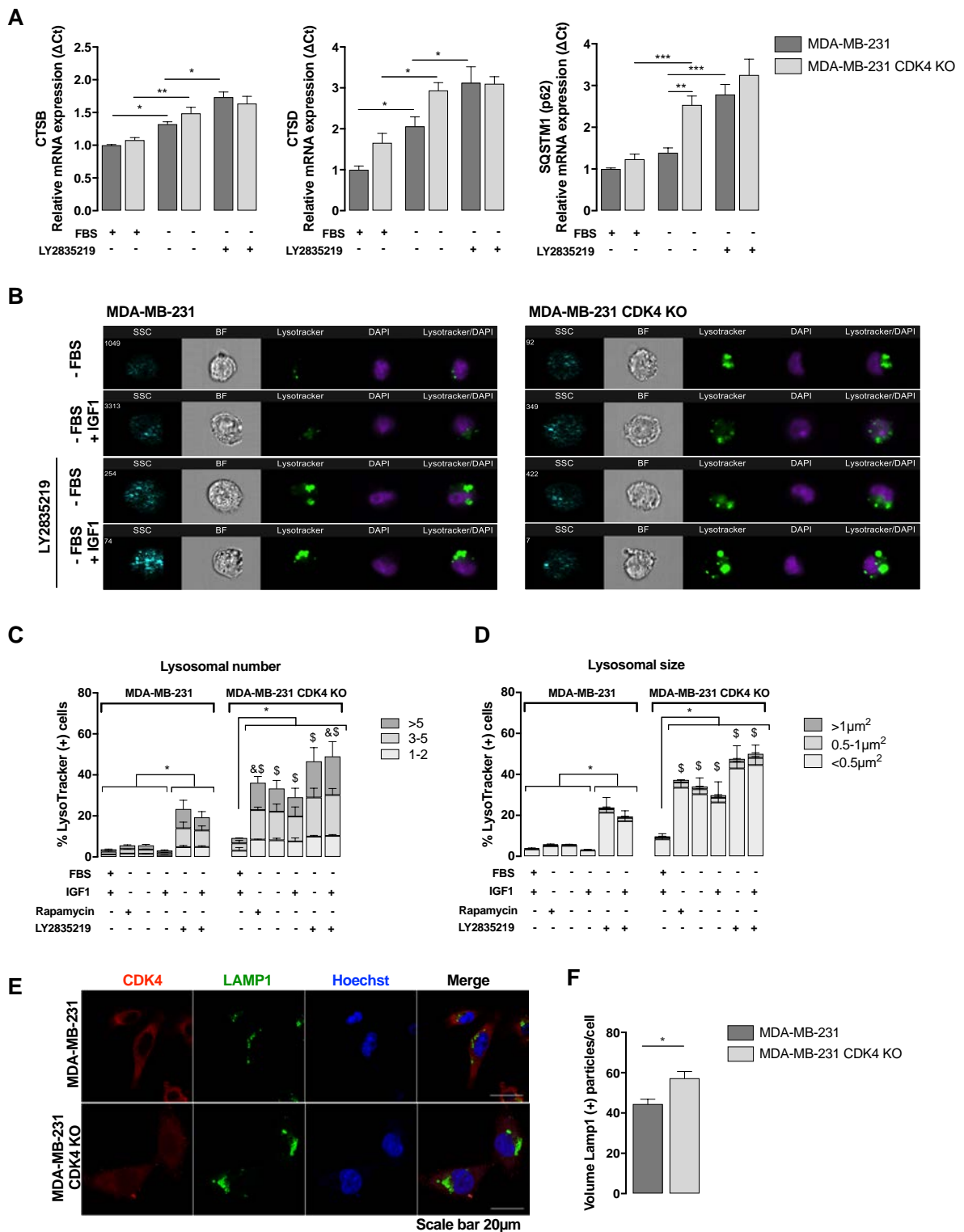
Figure 3.- CDK4 inhibition or depletion increases lysosomal mass. A, Quantitative PCR analysis showing the expression of transcription factor EB (TFEB) regulated genes that are involved in lysosomal or autophagic processes (cathepsins B and D and

SQSTM1) in WT or CDK4 KO MDA-MB-231 cells in complete (+FBS) or serum-starvation media (-FBS), treated with or without 0.5µM LY2835219. Each condition was assessed in duplicates for three independent experiments. B, Representative flow cytometry images of WT or CDK4 KO MDA-MB-231 cells treated with or without LY2835219 and stained with LysoTracker Green DND-26 under the indicated conditions. C, Proportions of cells containing lysosomes, estimated by quantification of fluorescence from LysoTracker Green DND-26 stained cells from two independent experiments. At least 10.000 events were acquired. Data are subdivided into categories of the number of lysosomes per cell. Significant differences between WT and KO MDA-MB-231 cells are indicated by: * total lysosomal particles (P<0.05); $ lysosomal particles per cell (3-5 particles) (P<0.05); & lysosomal particles per cell (>5 particles) (P<0.05); Two-way ANOVA followed by Tukey's multiple comparisons test. D, As for panel C, but subdivided into categories of the sizes of lysosomes per cell. Significant differences between WT and KO MDA-MB-231 cells are indicated by: * lysosomal particles <0.5µm^2 (P<0.05); $ lysosomal particles per cell (<0.5 µm^2) (P<0.05). E, Immunofluorescence analysis showing LAMP1 and CDK4 expression in WT and CDK4 KO MDA-MB-231 cells in complete media. F, Quantification of the total volume of LAMP1-positive particles in z-stack images. At least 30 cells in total from three independent experiments were analyzed.
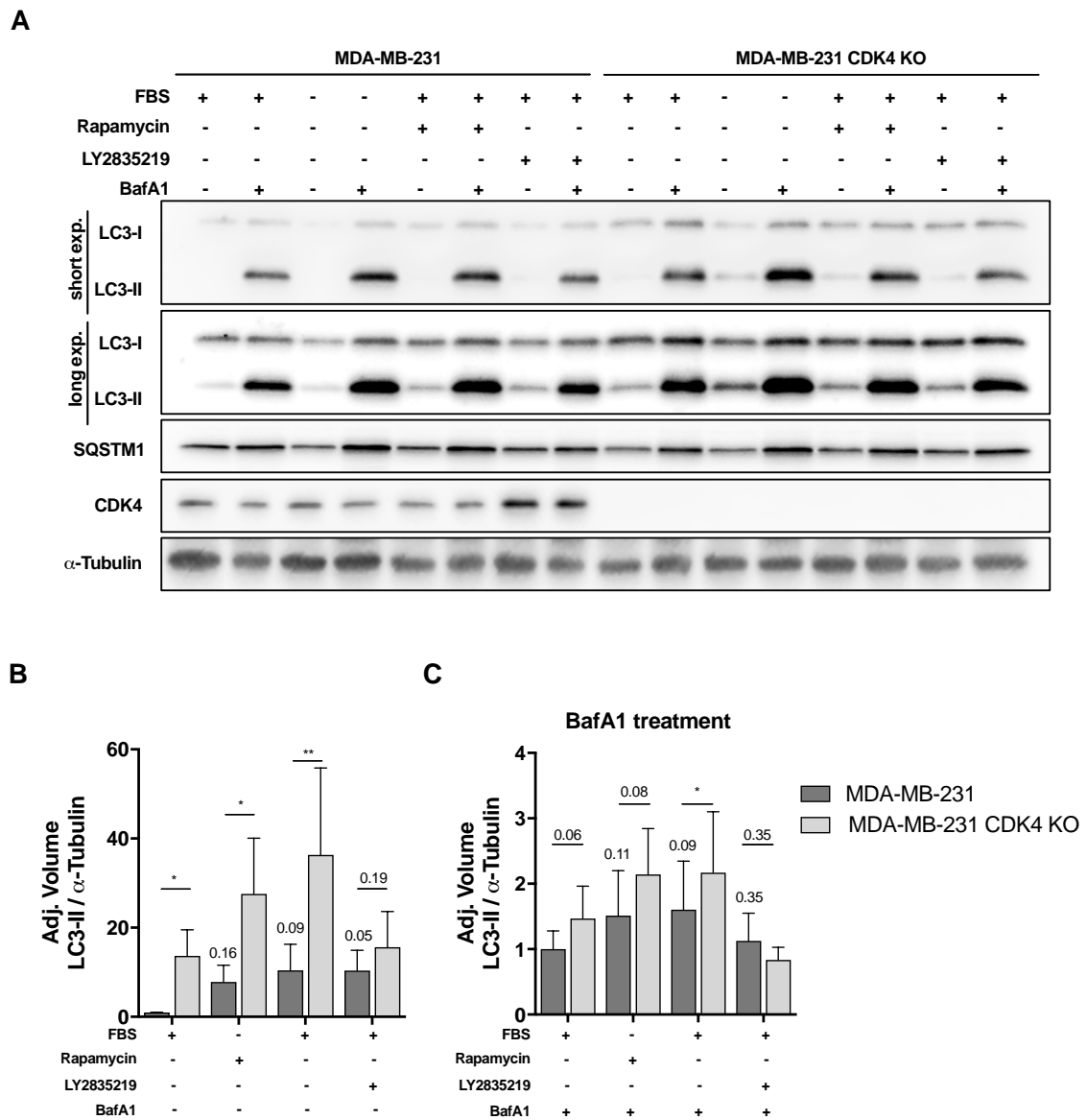
A

B

C

Figure 4.- Autophagic flux is impaired when CDK4 is inhibited or depleted. A, Western blot analysis of autophagosomal markers LC3-I, LC3-II, SQSTM1 in WT and CDK4 KO MDA-MB-231 cells treated 24h with complete media (+FBS) or serum-starvation media (-FBS), presence/absence of the mTOR inhibitor 0.5 μM rapamycin and of the CDK4 inhibitor 0.5 μM LY2835219 and presence/absence of 0.3 μM bafilomycin A1, 6 h before the treatment. B, Quantification of protein expression of LC3-II normalized to α-tubulin from three independent experiments like A, only the conditions without bafilomycin A1. C, Quantification of protein expression of LC3-II normalized to α-tubulin from three independent experiments

like A, only the conditions with bafilomycin A1. Statistical analysis was performed using a paired sample T-test.
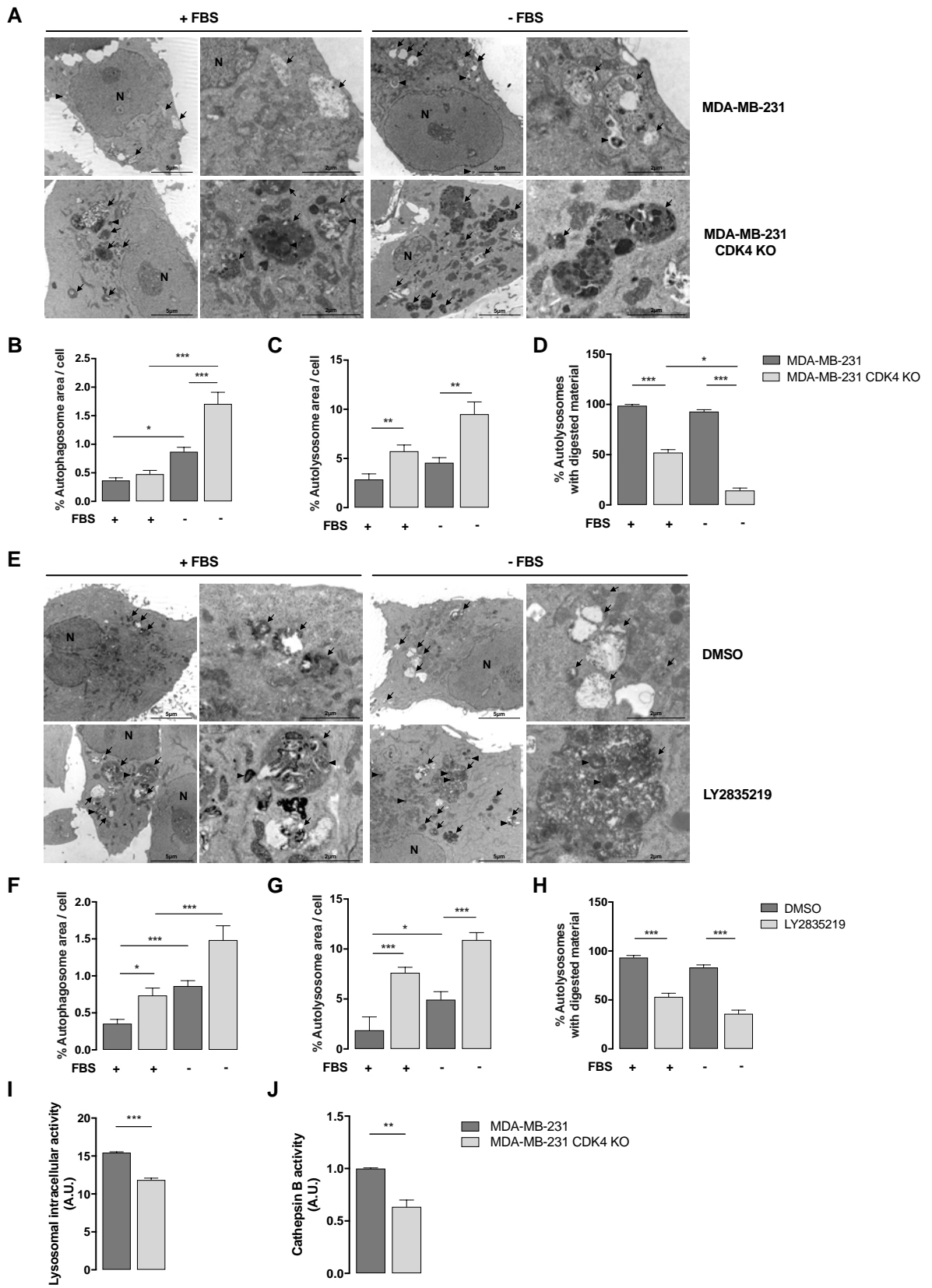
Figure 5.- Absence of CDK4 alters lysosomal function. A, Representative electron micrographs of WT and CDK4 KO MDA-MB-321 cells showing that cells lacking CDK4 have increased autolysosome (arrows) density and size. In CDK4 KO cells, autolysosomes accumulated non-degraded material, such as undegraded autophagosomes (arrowheads), in both complete (+FBS) and serum-starvation media (-FBS). In cell cultures without FBS, an increase in autophagosomes (arrowheads) was also observed in CDK4 KO cells as compared to wild-type cells. N: nucleus. B–D, Quantification of the autophagosome (B) and autolysosome (C) area per cell, and the percentage of autolysosomes containing degraded material (D), quantified for the conditions shown in Figure 4A. n = 20 cells per condition. E, Representative electron micrographs of MDA-MB-321 cells showing increased density of autolysosomes (arrows), accumulation of non-degraded materials (including undegraded autophagosomes; arrowheads) and autophagosomes (arrowheads) in DMSO or LY2835219-treated WT MDA-MB-321 cells in complete and serum-starvation media. N: nucleus. F–H, Quantification of autophagosome area per cell (F), autolysosome area per cell (G) and percentage of autolysosomes containing degraded material per cell (H) quantified for conditions shown in Figure 4E. n = 20 cells per condition. I, Quantification of intracellular lysosomal activity of WT and CDK4 KO MDA-MB-231 cells in complete media. J, Quantification of cathepsin B activity in WT and CDK4 KO MDA-MB-231 cells in complete media.
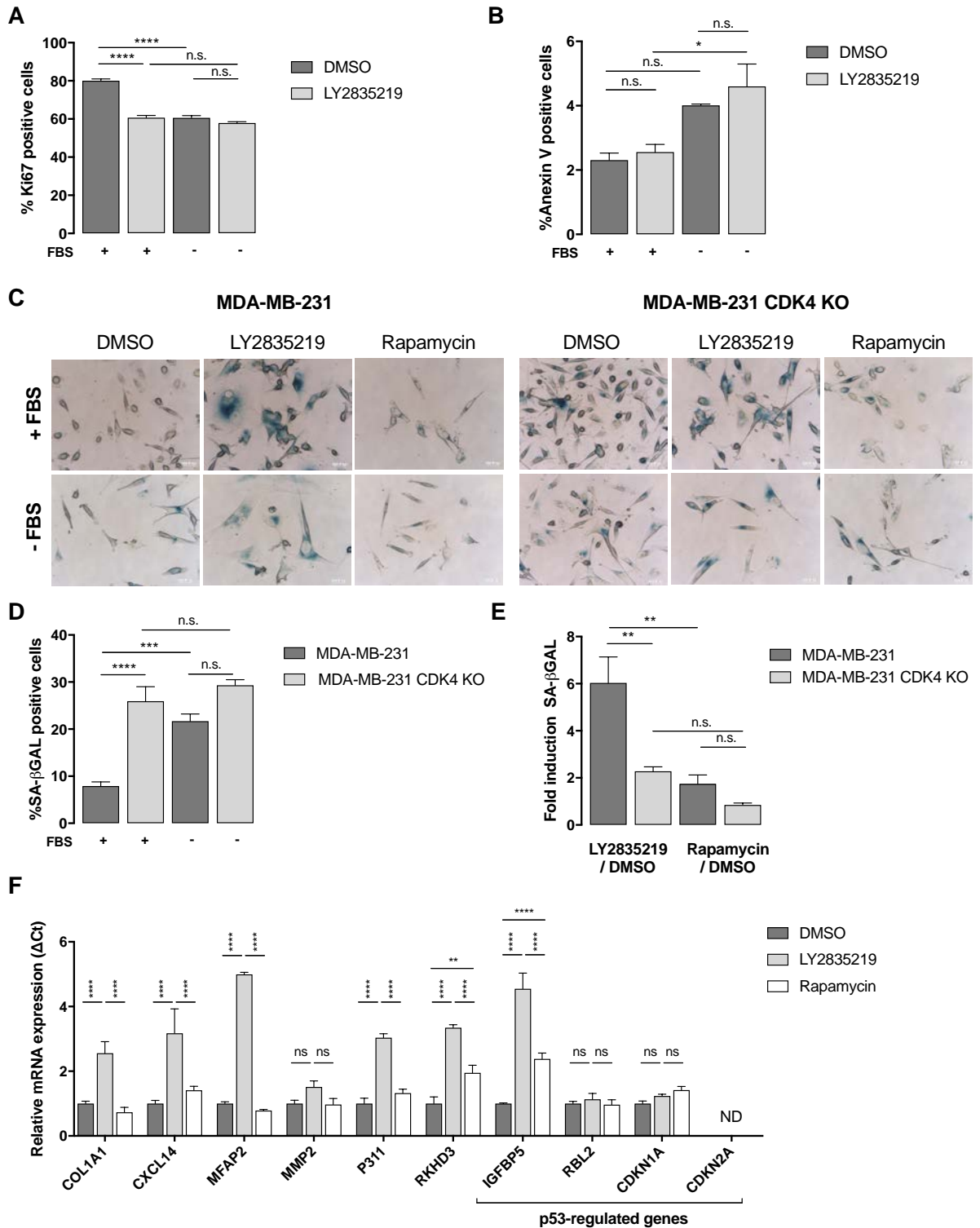
Figure 6.- Dysfunctional lysosomes, but not mTORC1 inhibition, induce senescence. A, Proliferation of WT MDA-MB-231 cells cultured in either complete (+FBS) or serum- starvation (-FBS) media, with or without LY2835219, as shown by

the percentage of Ki67-positive cells. B, Apoptosis under the same conditions, as shown by the percentage of Annexin V-positive cells. C, mTOR-independent induction of senescence by LY2835219, visualized by colorimetric senescence-associated β-Galactosidase (SA-β-Gal) staining of WT and CDK4 KO MDA-MB-231 cells cultured in -/+ FBS media for the last 16 h of 8 days' treatment with DMSO, 0.5 µM LY2835219, or 0.5µM rapamycin. D, Quantification of the percentage of SA-β-Gal-positive WT and CDK4 KO MDA-MB-231 cells from triplicates, at least five fields per replicate. E, Quantification of the fold induction of SA-β-Gal induced by LY2835219 or rapamycin treatment from triplicates, at least five fields per replicate. F, Quantitative PCR analysis showing expression of genes usually upregulated in senescence (including p53-regulated genes), in WT MDA-MB-231 cells treated for 8 days with DMSO, LY2835219, or rapamycin in complete media. Each condition was assessed in triplicates.
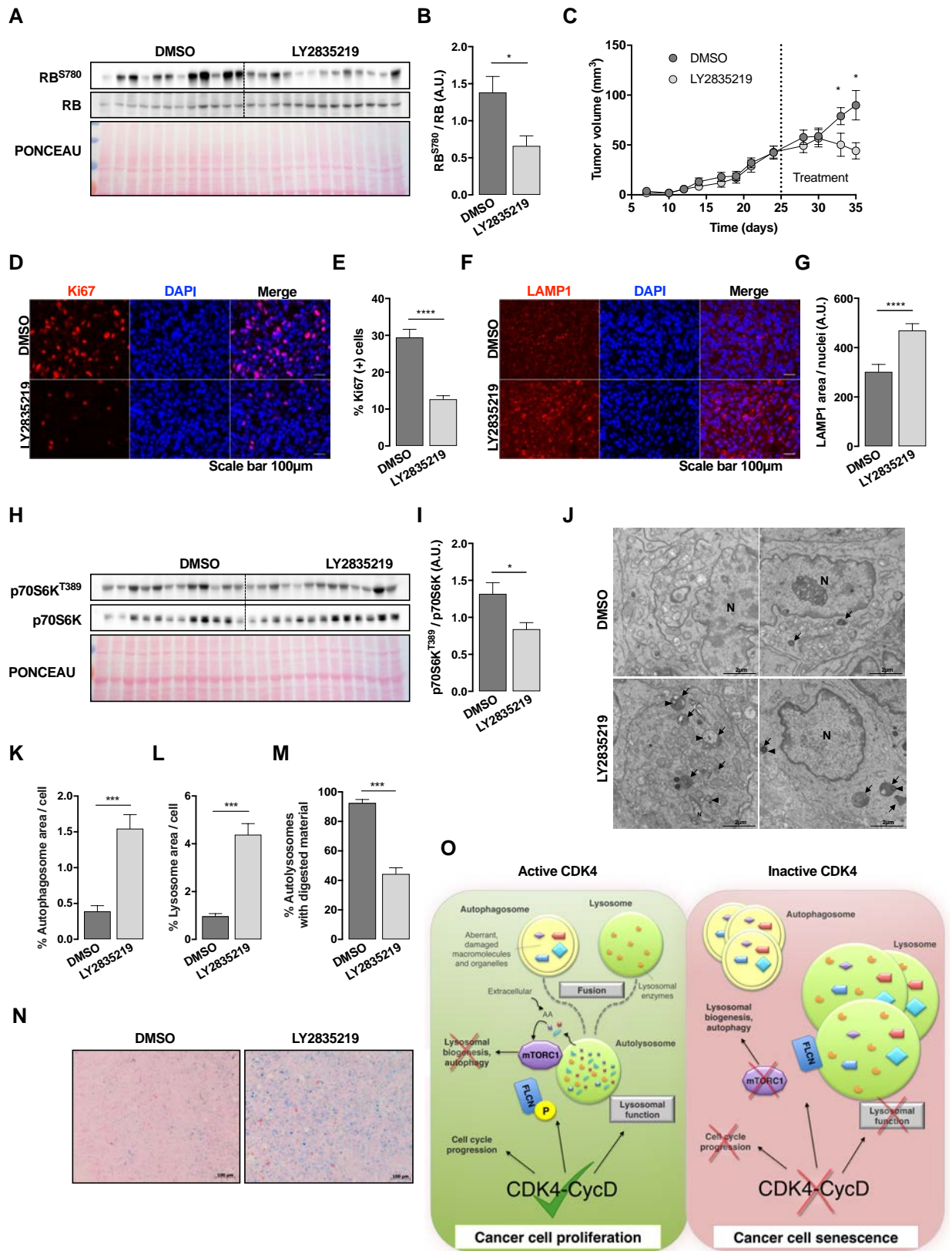
Figure 7- The CDK4/6 inhibitor LY2835219 alters lysosome morphology in a breast cancer xenograft mouse model. A, Western blot for RB and phospho-RB

(S780) in tumor protein extracts of mice from both groups as a control for CDK4/6 inhibition. B, Quantification of A, as arbitrary levels of phospho-RB (S780) normalized to total RB. C, Volume of MDA-MB-231 tumors from mice throughout the entire experiment from 8 or 9 mice per condition. When the tumors reached a volume of 50 mm^3 (day 25), gavage with either DMSO or LY2835219 started and lasted for 8 days. D, Immunohistochemistry with Ki67 antibody and DAPI for tumor sections from DMSO- or LY2835219-gavaged mice. E, Percentage of Ki67-positive cells from D. Three images per section were analyzed for 8 or 9 mice. F, Immunohistochemistry with LAMP1 antibody and DAPI of tumor sections from mouse xenograft models treated with either LY2835219 or DMSO. G, Quantification in arbitrary units of the area of LAMP1 staining normalized to the number of nuclei per field. Three images per section were analyzed for 8 or 9 mice. H, Western blot for the mTOR target protein p70S6K and its phosphorylated variant (phospho-p70S6K (T389)) from mouse tumor xenograft lysate, following gavage with either DMSO or LY2835219. I, Quantification of H, showing arbitrary levels of phospho-p70S6K (T389) normalized to total p70S6K. J, Representative electron micrographs of mouse tumor xenograft cells, showing that LY2835219 treatment increases notably the density of autolysosomes (arrows) and that these autolysosomes accumulate non-degraded materials, such as undegraded autophagosomes (arrowheads). N: nucleus. K-M, Quantification for conditions shown in J, as percentage of autophagosome area per cell (K), percentage of autolysosome area per cell (L) and the percentage of autolysosomes containing degraded material per cell (M) from EM images of mouse xenograft tumors treated with LY2835219 or control. n = 30 cells per condition. N, Colorimetric SA-β-Gal staining of tumor cell senescence in tumor xenograft sections taken from mice gavaged with LY2835219 or DMSO. O, Schematic representation of the proposed model. In cancer cells, activated CDK4 (left) promotes cancer cell proliferation through regulating cell cycle, but also through FLCN phosphorylation to ensure mTORC1 recruitment to lysosomes in the presence of amino acids (AA). In addition, CDK4 can also promote lysosomal degradation to generate amino acids, which also serve to activate mTORC1. When CDK4 is inhibited or depleted (right), cancer cell senescence is induced through impairment of cell cycle progression, and by suppressing lysosomal function, which results in mTORC1 inactivation, lysosomal biogenesis and impairment of autophagic flux. mTORC1 is dually inhibited, since

unphosphorylated FLCN is retained at the surface of lysosomes also abrogating mTORC1 recruitment.
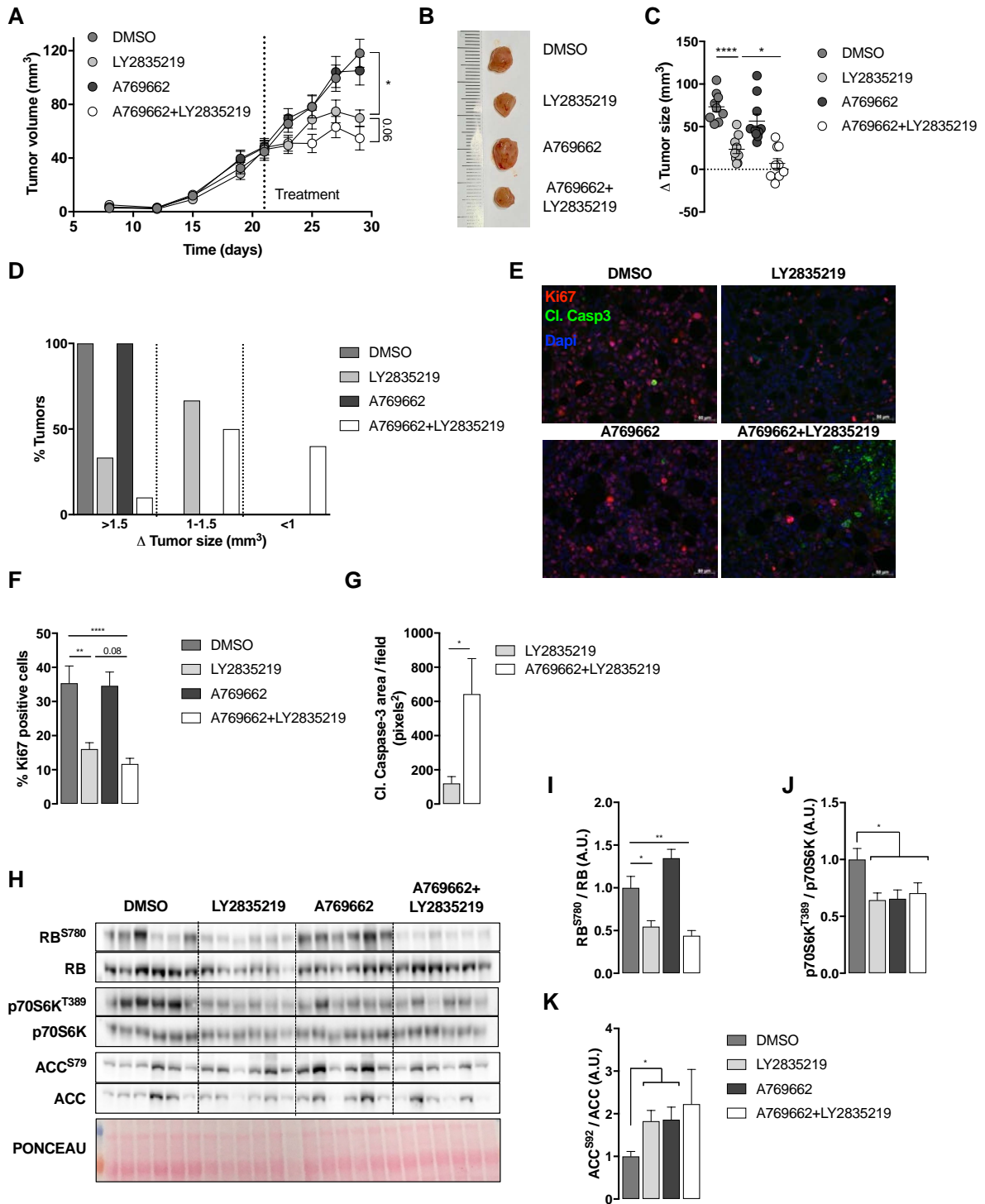
Figure 8- The CDK4 inhibitor LY2835219 in combination with the AMPK activator A769661 induces cell death in breast cancer cells and tumors. A, Tumor volume of breast cancer xenograft in NSG mice was monitored throughout the whole experiment. Treatment started on day 21 and lasted for 8 days (n=9-10). B, Representative images from tumors at the day of sacrifice, after the corresponding treatment. C, Increment of tumor volume per mouse: Vol day29/Vol day21. D,

Representation of percentage of tumors, which increases more than 1.5 fold, from 1 to 1.5 folds or less than 1 fold. E, Ki67 and Cleaved Caspase-3 immunostaining in tumor sections after the corresponding treatment. F, Quantification from E of % Ki67 positive cells. G, Quantification from E of Cleaved-Caspase-3 area per field, comparing LY2835219 and A769662+LY2935219. H, Westernblot analysis of activation of RB, p70S6K and ACC proteins in tumor samples. I, Quantification from H of phospho-RB normalized with total RB. J, Quantification from H of phospho-p70S6K normalized with total p70S6K. K, Quantification from H of phospho-ACC, normalized with total ACC.

7. Supplementary Figures

A
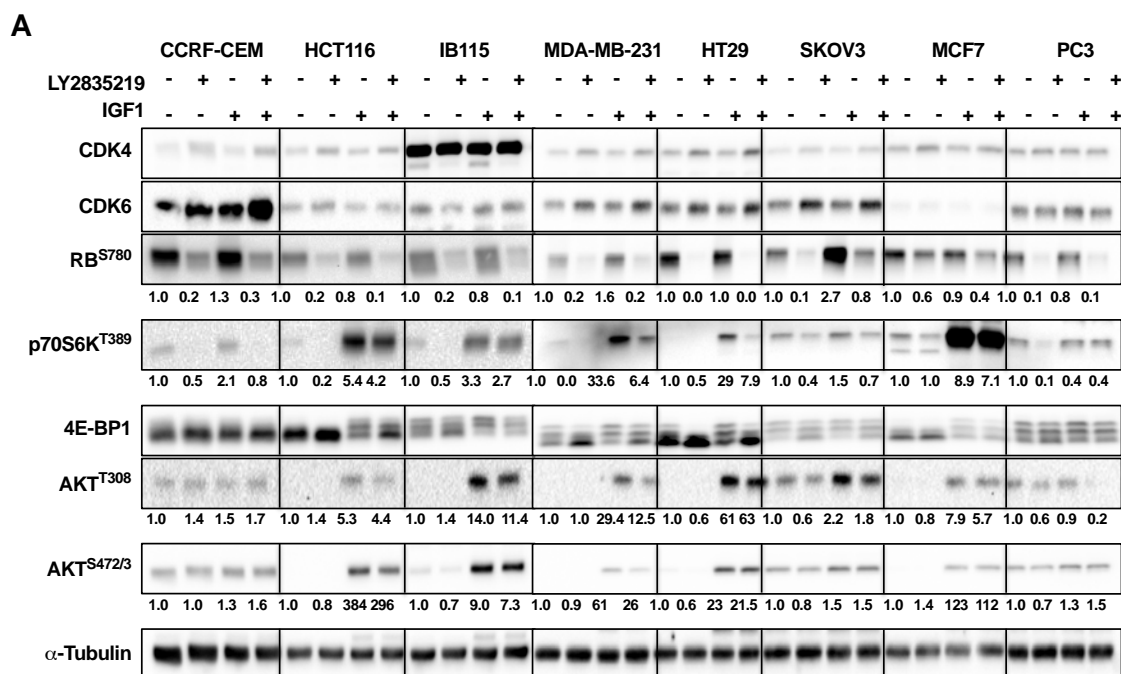
Sup. Figure 1.- CDK4 inhibition or depletion decreases mTORC1 activity in several cancer cell lines. A, Western blot showing the impact of the lack of CDK4 on downstream PI3K pathway proteins in different cancer cell lines, with or without the PI3K pathway stimulating ligand IGF-1. The relative phosphorylation level normalized to α-tubulin is indicated below the corresponding panels normalized to 1 in every cell line.
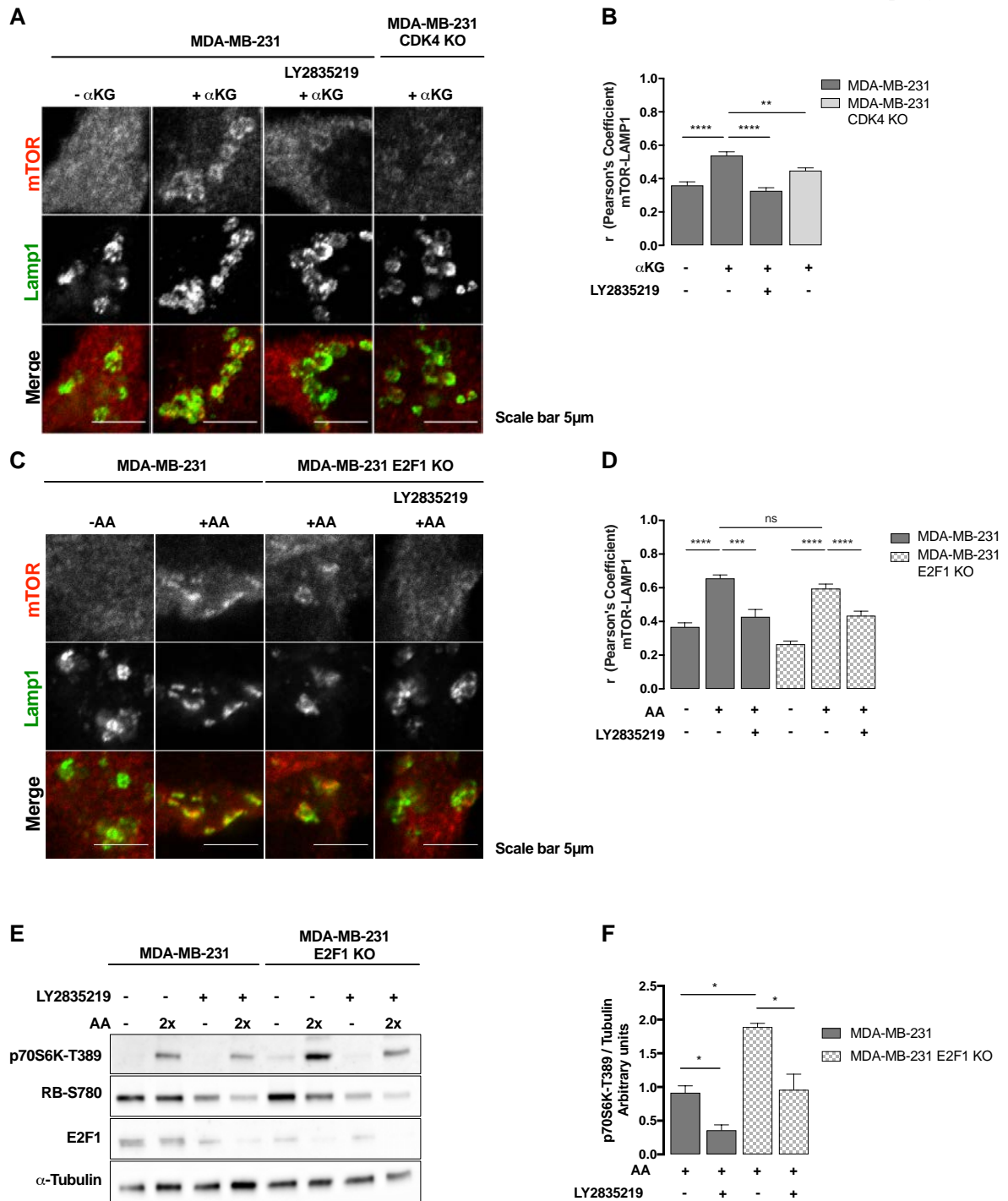
Sup. Figure 2.- CDK4 effects on mTORC1 are α-ketoglutarate and E2F1-independent. To check whether the effects of LY2835219 on MDA-MB-231 cells were due to an impairment in glutamine metabolism, we treated the cells with a cell-permeable α-ketoglutarate analog. A, Confocal immunofluorescence analysis showing mTOR colocalization with lysosomes (Lamp1) in WT and CDK4 KO MDA-MB-231, with or without 5 mM α-KG and/or 0.5 µM LY2835219. B, Quantification of

colocalization from A using Pearson's coefficient. At least 20 fields per condition were analyzed. C, Effect of CDK4 inhibition on the colocalization of mTORC1, examined using confocal immunofluorescence analysis of mTOR colocalization with lysosomes (Lamp1) in MDA-MB-231 cells lacking E2F1, and the sensitivity of these cells to LY2835219 in presence or absence of amino acid stimulation. D, Quantification of the colocalization in C using Pearson's coefficient. At least 20 fields per condition were analyzed. E, Western blot analysis of phospho-p70S6K (T389), 4E-BP1, phospho-RB (S780), E2F1 and α-tubulin in WT and E2F1 KO MDA-MB-231 cells, in the presence of glutamine and different concentrations of amino acids (AA) (0×, 1× or 2× Minimal Essential Media AA) and in the presence of DMSO or 0.5 μM LY2835219. F, Quantification of Western blot analysis in E showing phosphorylation levels of mTORC1 target molecule phospho-p70S6K (T389) normalized to α-tubulin from three independent experiments like E.

A

B
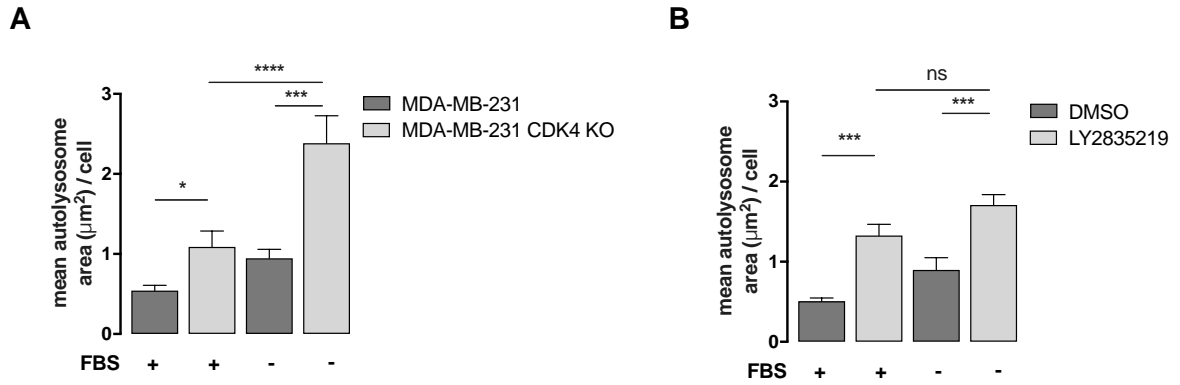
Sup. Figure 3.- CDK4 inhibition or depletion increases lysosomal mass. A, Quantifications of the mean autolysosome area per cell from electron microscope images in MDA-MB-321 WT and CDK4 KO cells, either in complete medium (+FBS) or in serum starvation conditions (-FBS). B, Quantifications of the mean autolysosome area per cell from electron microscope images in MDA-MB-321 WT cells under DMSO or LY2835219 treatment, either in complete medium or in starvation conditions (medium - FBS). n = 20 cells per condition.
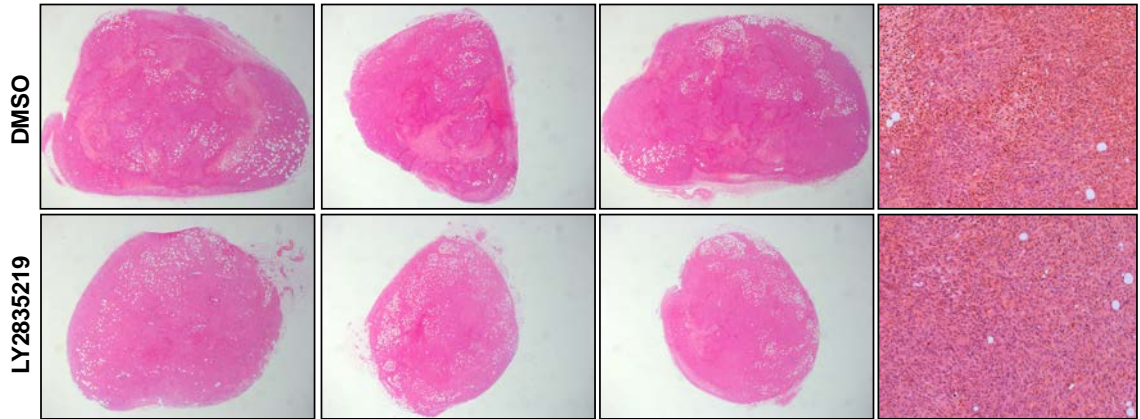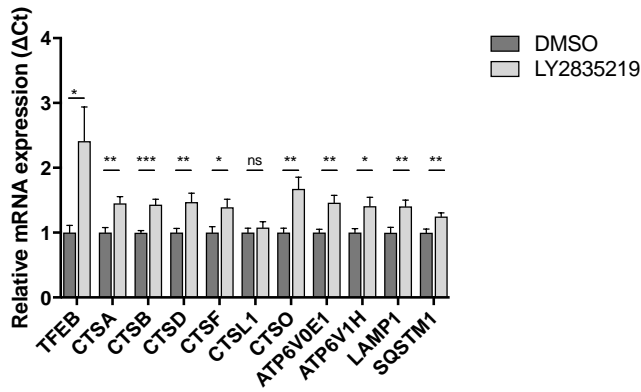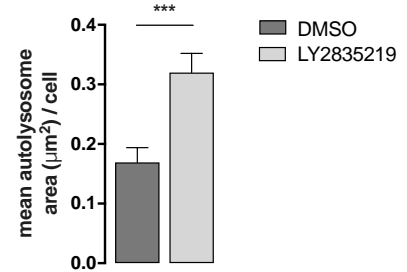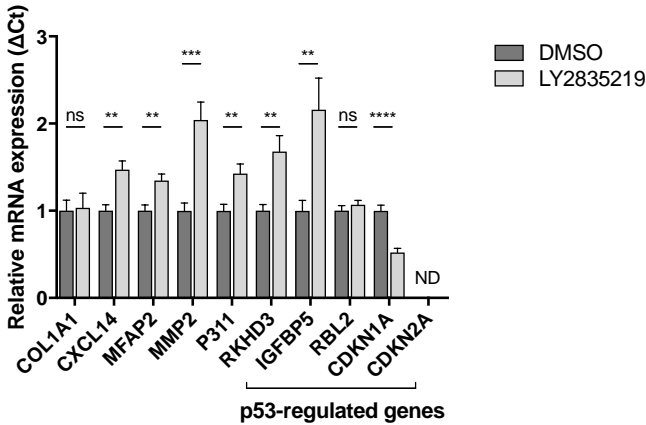
Sup. Figure 4.- Hematoxylin and eosin staining and gene expression analysis of tumors from mice treated with or without LY2835219.

A, Hematoxylin and eosin staining of tumor sections from DMSO- or LY2835219-treated mice, to confirm the lack of immune cell infiltration (whole tumor and with 20X objective). B, Gene expression of all lysosomal and autophagic genes examined by qPCR from DMSO- or LY2835219-treated mice. 8 or 9 mice per condition were analyzed C, Quantifications of the mean autolysosome area per cell from electron

microscope images of tumor sections from DMSO- or LY2835219-treated mice. n=30 cells per condition. D, Gene expression of genes usually upregulated in senescence (including p53-regulated genes) examined by qPCR from DMSO- or LY2835219-treated mice. 8 or 9 mice per condition were analyzed.

A

B

C **D** **E**
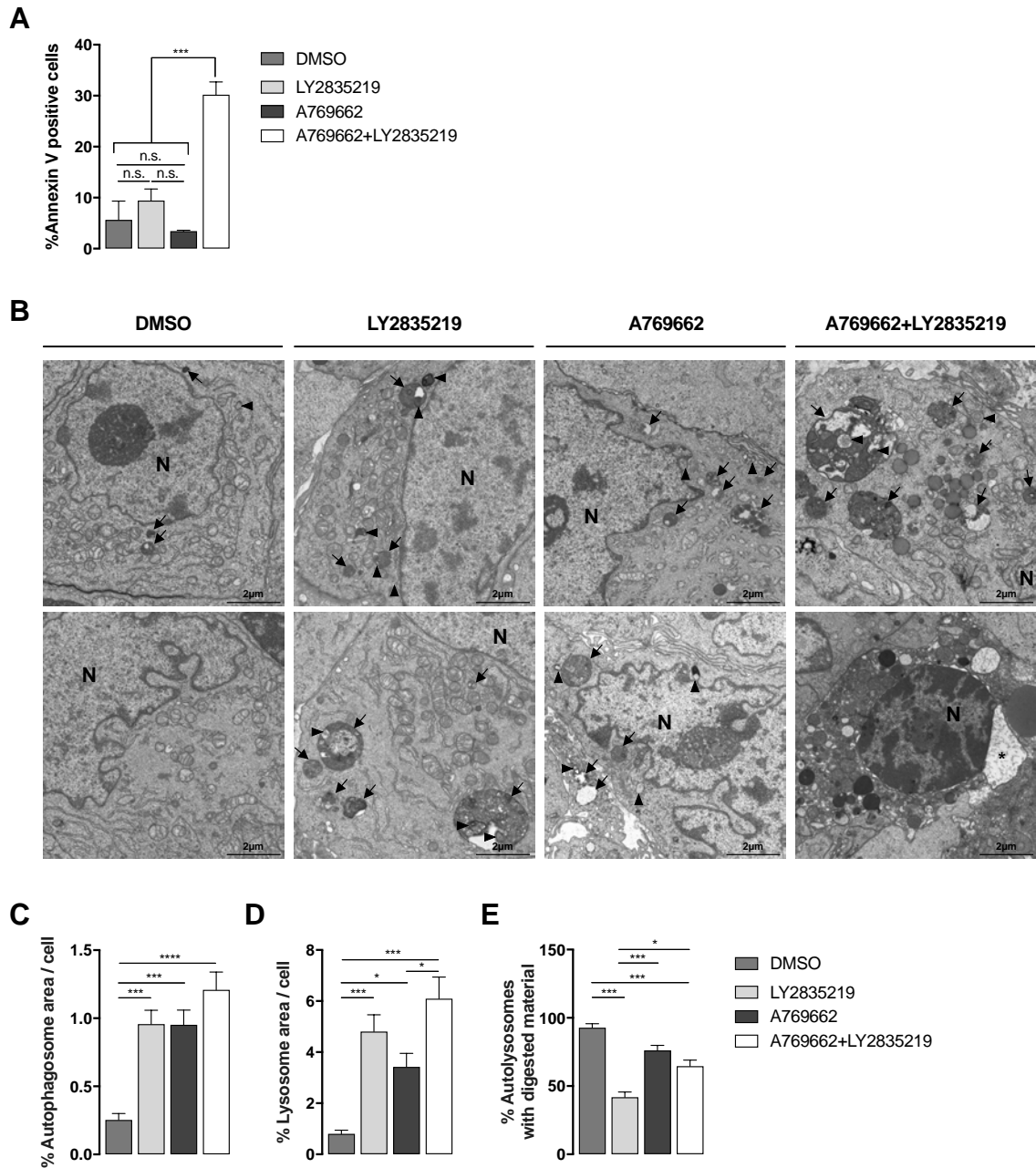
Sup. Figure 5. *In vitro* cell death analysis and *in vivo* electron microscopy analysis of tumors treated with DMSO, LY2835219, A769662 and the combination of A769662 with LY2835219. A, Percentage of Annexin V positive cells assessed by flow cytometry of MDA-MB-231 cells cultured for 8 days with the corresponding treatment. B, Representative electron micrographs of tumors from mice treated with DMSO, LY2835219, A769662 and the combination of A769662 with LY2835219. The arrowheads represent the autophagosomes and the arrows, the autolysosomes with

undigested material inside. * Indicates the focal swelling of the perinulear membrane, and N represents nucleus. C, Quantification from B, of the percentage of autophagosome area per cell. D, Quantification from B, of the percentage of lysosome area per cell. E, Quantification from B, of the percentage of autolysosomes with digested material inside. n = 30 cells per condition. Values are mean ± SEM, *$P < 0.05$;***$P < 0.001$

8. References

Aguilar, V., & Fajas, L. (2010). Cycling through metabolism. *EMBO Mol Med, 2*(9), 338-348. doi: 10.1002/emmm.201000089

Albert, V., & Hall, M. N. (2015). mTOR signaling in cellular and organismal energetics. *Curr Opin Cell Biol, 33*, 55-66. doi: 10.1016/j.ceb.2014.12.001

Bar-Peled, L., & Sabatini, D. M. (2014). Regulation of mTORC1 by amino acids. *Trends Cell Biol, 24*(7), 400-406. doi: 10.1016/j.tcb.2014.03.003

Blanchet, E., Annicotte, J. S., Lagarrigue, S., Aguilar, V., Clape, C., Chavey, C., . . . Fajas, L. (2011). E2F transcription factor-1 regulates oxidative metabolism. *Nat Cell Biol, 13*(9), 1146-1152. doi: 10.1038/ncb2309

Bourdeau, V., & Ferbeyre, G. (2016). CDK4-CDK6 inhibitors induce autophagy-mediated degradation of DNMT1 and facilitate the senescence antitumor response. *Autophagy, 12*(10), 1965-1966. doi: 10.1080/15548627.2016.1214779

Brown, N. E., Jeselsohn, R., Bihani, T., Hu, M. G., Foltopoulou, P., Kuperwasser, C., & Hinds, P. W. (2012). Cyclin D1 activity regulates autophagy and senescence in the mammary epithelium. *Cancer Res, 72*(24), 6477-6489. doi: 10.1158/0008-5472.CAN-11-4139

Carmona-Gutierrez, D., Hughes, A. L., Madeo, F., & Ruckenstuhl, C. (2016). The crucial impact of lysosomes in aging and longevity. *Ageing Res Rev, 32*, 2-12. doi: 10.1016/j.arr.2016.04.009

Cho, S., & Hwang, E. S. (2012). Status of mTOR activity may phenotypically differentiate senescence and quiescence. *Mol Cells, 33*(6), 597-604. doi: 10.1007/s10059-012-0042-1

Deshpande, A., Sicinski, P., & Hinds, P. W. (2005). Cyclins and cdks in development and cancer: a perspective. *Oncogene, 24*(17), 2909-2915. doi: 10.1038/sj.onc.1208618

Dibble, C. C., & Cantley, L. C. (2015). Regulation of mTORC1 by PI3K signaling. *Trends Cell Biol, 25*(9), 545-555. doi: 10.1016/j.tcb.2015.06.002

Duran, R. V., Oppliger, W., Robitaille, A. M., Heiserich, L., Skendaj, R., Gottlieb, E., & Hall, M. N. (2012). Glutaminolysis activates Rag-mTORC1 signaling. *Mol Cell, 47*(3), 349-358. doi: 10.1016/j.molcel.2012.05.043

Elsamany, S., & Abdullah, S. (2014). Triple-negative breast cancer: future prospects in diagnosis and management. *Med Oncol, 31*(2), 834. doi: 10.1007/s12032-013-0834-y

Fehrenbacher, N., & Jaattela, M. (2005). Lysosomes as targets for cancer therapy. *Cancer Res, 65*(8), 2993-2995. doi: 10.1158/0008-5472.CAN-05-0476

Franco, J., Balaji, U., Freinkman, E., Witkiewicz, A. K., & Knudsen, E. S. (2016). Metabolic Reprogramming of Pancreatic Cancer Mediated by CDK4/6 Inhibition Elicits Unique Vulnerabilities. *Cell Rep, 14*(5), 979-990. doi: 10.1016/j.celrep.2015.12.094

Goel, S., Wang, Q., Watt, A. C., Tolaney, S. M., Dillon, D. A., Li, W., . . . Zhao, J. J. (2016). Overcoming Therapeutic Resistance in HER2-Positive Breast Cancers with CDK4/6 Inhibitors. *Cancer Cell, 29*(3), 255-269. doi: 10.1016/j.ccell.2016.02.006

Hamilton, E., & Infante, J. R. (2016). Targeting CDK4/6 in patients with cancer. *Cancer Treat Rev, 45*, 129-138. doi: 10.1016/j.ctrv.2016.03.002

Hubbi, M. E., Gilkes, D. M., Hu, H., Kshitiz, Ahmed, I., & Semenza, G. L. (2014). Cyclin-dependent kinases regulate lysosomal degradation of hypoxia-inducible factor 1alpha to promote cell-cycle progression. *Proc Natl Acad Sci U S A, 111*(32), E3325-3334. doi: 10.1073/pnas.1412840111

Iriyama, N., Hino, H., Moriya, S., Hiramoto, M., Hatta, Y., Takei, M., & Miyazawa, K. (2018). The cyclin-dependent kinase 4/6 inhibitor, abemaciclib, exerts dose-dependent cytostatic and cytocidal effects and induces autophagy in multiple myeloma cells. *Leuk Lymphoma, 59*(6), 1439-1450. doi: 10.1080/10428194.2017.1376741

Jia, J., Abudu, Y. P., Claude-Taupin, A., Gu, Y., Kumar, S., Choi, S. W., . . . Deretic, V. (2018). Galectins Control MTOR and AMPK in Response to Lysosomal Damage to Induce Autophagy. *Autophagy*. doi: 10.1080/15548627.2018.1505155

Jin, Y., & Weisman, L. S. (2015). The vacuole/lysosome is required for cell-cycle progression. *Elife, 4*. doi: 10.7554/eLife.08160

Kaur, J., & Debnath, J. (2015). Autophagy at the crossroads of catabolism and anabolism. *Nat Rev Mol Cell Biol, 16*(8), 461-472. doi: 10.1038/nrm4024

Klein, M. E., Kovatcheva, M., Davis, L. E., Tap, W. D., & Koff, A. (2018a). CDK4/6 Inhibitors: The Mechanism of Action May Not Be as Simple as Once Thought. *Cancer Cell*. doi: 10.1016/j.ccell.2018.03.023

Klein, M. E., Kovatcheva, M., Davis, L. E., Tap, W. D., & Koff, A. (2018b). CDK4/6 Inhibitors: The Mechanism of Action May Not Be as Simple as Once Thought. *Cancer Cell, 34*(1), 9-20. doi: 10.1016/j.ccell.2018.03.023

Kremer, J. R., Mastronarde, D. N., & McIntosh, J. R. (1996). Computer visualization of three-dimensional image data using IMOD. *Journal of Structural Biology, 116*(1), 71-76. doi: Doi 10.1006/Jsbi.1996.0013

Ku, B. M., Yi, S. Y., Koh, J., Bae, Y. H., Sun, J. M., Lee, S. H., . . . Ahn, M. J. (2016). The CDK4/6 inhibitor LY2835219 has potent activity in combination with mTOR inhibitor in head and neck squamous cell carcinoma. *Oncotarget, 7*(12), 14803-14813. doi: 10.18632/oncotarget.7543

Lagarrigue, S., Lopez-Mejia, I. C., Denechaud, P. D., Escote, X., Castillo-Armengol, J., Jimenez, V., . . . Fajas, L. (2016). CDK4 is an essential insulin effector in adipocytes. *J Clin Invest, 126*(1), 335-348. doi: 10.1172/JCI81480

Lee, J. H., Park, S., Kim, E., & Lee, M. J. (2019). Negative-feedback coordination between proteasomal activity and autophagic flux. *Autophagy*, 1-3. doi: 10.1080/15548627.2019.1569917

Lee, Y., Dominy, J. E., Choi, Y. J., Jurczak, M., Tolliday, N., Camporez, J. P., . . . Puigserver, P. (2014). Cyclin D1-Cdk4 controls glucose metabolism independently of cell cycle progression. *Nature, 510*(7506), 547-551. doi: 10.1038/nature13267

Li, M., Khambu, B., Zhang, H., Kang, J. H., Chen, X., Chen, D., . . . Yin, X. M. (2013). Suppression of lysosome function induces autophagy via a feedback down-regulation of MTOR complex 1 (MTORC1) activity. *J Biol Chem, 288*(50), 35769-35780. doi: 10.1074/jbc.M113.511212

Llanos, S., Megias, D., Blanco-Aparicio, C., Hernandez-Encinas, E., Rovira, M., Pietrocola, F., & Serrano, M. (2019). Lysosomal trapping of palbociclib and its functional implications. *Oncogene*. doi: 10.1038/s41388-019-0695-8

Lopez-Mejia, I. C., Lagarrigue, S., Giralt, A., Martinez-Carreres, L., Zanou, N., Denechaud, P. D., . . . Fajas, L. (2017). CDK4 Phosphorylates AMPKalpha2

to Inhibit Its Activity and Repress Fatty Acid Oxidation. *Mol Cell, 68*(2), 336-349 e336. doi: 10.1016/j.molcel.2017.09.034

Martin-Campos, T., Mylonas, R., Masselot, A., Waridel, P., Petricevic, T., Xenarios, I., & Quadroni, M. (2017). MsViz: A Graphical Software Tool for In-Depth Manual Validation and Quantitation of Post-translational Modifications. *J Proteome Res, 16*(8), 3092-3101. doi: 10.1021/acs.jproteome.7b00194

Martinez-Carreres, L., Nasrallah, A., & Fajas, L. (2017). Cancer: Linking Powerhouses to Suicidal Bags. *Front Oncol, 7*, 204. doi: 10.3389/fonc.2017.00204

Meo-Evoli, N., Almacellas, E., Massucci, F. A., Gentilella, A., Ambrosio, S., Kozma, S. C., . . . Tauler, A. (2015). V-ATPase: a master effector of E2F1-mediated lysosomal trafficking, mTORC1 activation and autophagy. *Oncotarget, 6*(29), 28057-28070. doi: 10.18632/oncotarget.4812

Michaloglou, C., Crafter, C., Siersbaek, R., Delpuech, O., Curwen, J. O., Carnevalli, L. S., . . . Cosulich, S. C. (2018). Combined Inhibition of mTOR and CDK4/6 Is Required for Optimal Blockade of E2F Function and Long-term Growth Inhibition in Estrogen Receptor-positive Breast Cancer. *Mol Cancer Ther, 17*(5), 908-920. doi: 10.1158/1535-7163.MCT-17-0537

Miettinen, T. P., Peltier, J., Hartlova, A., Gierlinski, M., Jansen, V. M., Trost, M., & Bjorklund, M. (2018). Thermal proteome profiling of breast cancer cells reveals proteasomal activation by CDK4/6 inhibitor palbociclib. *EMBO J, 37*(10). doi: 10.15252/embj.201798359

Nesvizhskii, A. I., Keller, A., Kolker, E., & Aebersold, R. (2003). A statistical model for identifying proteins by tandem mass spectrometry. *Anal Chem, 75*(17), 4646-4658.

O'Leary, B., Finn, R. S., & Turner, N. C. (2016). Treating cancer with selective CDK4/6 inhibitors. *Nat Rev Clin Oncol, 13*(7), 417-430. doi: 10.1038/nrclinonc.2016.26

Olmez, I., Brenneman, B., Xiao, A., Serbulea, V., Benamar, M., Zhang, Y., . . . Purow, B. (2017). Combined CDK4/6 and mTOR Inhibition Is Synergistic against Glioblastoma via Multiple Mechanisms. *Clin Cancer Res, 23*(22), 6958-6968. doi: 10.1158/1078-0432.CCR-17-0803

Petit, C. S., Roczniak-Ferguson, A., & Ferguson, S. M. (2013). Recruitment of folliculin to lysosomes supports the amino acid-dependent activation of Rag GTPases. *J Cell Biol, 202*(7), 1107-1122. doi: 10.1083/jcb.201307084

Piao, S., & Amaravadi, R. K. (2016). Targeting the lysosome in cancer. *Ann N Y Acad Sci, 1371*(1), 45-54. doi: 10.1111/nyas.12953

Polk, A., Kolmos, I. L., Kumler, I., & Nielsen, D. L. (2016). Specific CDK4/6 inhibition in breast cancer: a systematic review of current clinical evidence. *ESMO Open, 1*(6), e000093. doi: 10.1136/esmoopen-2016-000093

Puertollano, R. (2014). mTOR and lysosome regulation. *F1000Prime Rep, 6*, 52. doi: 10.12703/P6-52

Real, S., Meo-Evoli, N., Espada, L., & Tauler, A. (2011). E2F1 regulates cellular growth by mTORC1 signaling. *PLoS One, 6*(1), e16163. doi: 10.1371/journal.pone.0016163

Renna, M., Schaffner, C., Winslow, A. R., Menzies, F. M., Peden, A. A., Floto, R. A., & Rubinsztein, D. C. (2011). Autophagic substrate clearance requires

activity of the syntaxin-5 SNARE complex. *J Cell Sci, 124*(Pt 3), 469-482. doi: 10.1242/jcs.076489

Rivadeneira, D. B., Mayhew, C. N., Thangavel, C., Sotillo, E., Reed, C. A., Grana, X., & Knudsen, E. S. (2010). Proliferative suppression by CDK4/6 inhibition: complex function of the retinoblastoma pathway in liver tissue and hepatoma cells. *Gastroenterology, 138*(5), 1920-1930. doi: 10.1053/j.gastro.2010.01.007

Romero-Pozuelo, J., Demetriades, C., Schroeder, P., & Teleman, A. A. (2017). CycD/Cdk4 and Discontinuities in Dpp Signaling Activate TORC1 in the Drosophila Wing Disc. *Dev Cell, 42*(4), 376-387 e375. doi: 10.1016/j.devcel.2017.07.019

Sahani, M. H., Itakura, E., & Mizushima, N. (2014). Expression of the autophagy substrate SQSTM1/p62 is restored during prolonged starvation depending on transcriptional upregulation and autophagy-derived amino acids. *Autophagy, 10*(3), 431-441. doi: 10.4161/auto.27344

Salazar-Roa, M., & Malumbres, M. (2017). Fueling the Cell Division Cycle. *Trends Cell Biol, 27*(1), 69-81. doi: 10.1016/j.tcb.2016.08.009

Salmon, P., & Trono, D. (2006). Production and titration of lentiviral vectors. *Curr Protoc Neurosci, Chapter 4*, Unit 4 21. doi: 10.1002/0471142301.ns0421s37

Saxton, R. A., & Sabatini, D. M. (2017). mTOR Signaling in Growth, Metabolism, and Disease. *Cell, 169*(2), 361-371. doi: 10.1016/j.cell.2017.03.035

Schindelin, J., Arganda-Carreras, I., Frise, E., Kaynig, V., Longair, M., Pietzsch, T., . . . Cardona, A. (2012). Fiji: an open-source platform for biological-image analysis. *Nature Methods, 9*(7), 676-682. doi: 10.1038/NMETH.2019

Seranova, E., Connolly, K. J., Zatyka, M., Rosenstock, T. R., Barrett, T., Tuxworth, R. I., & Sarkar, S. (2017). Dysregulation of autophagy as a common mechanism in lysosomal storage diseases. *Essays Biochem, 61*(6), 733-749. doi: 10.1042/EBC20170055

Settembre, C., & Ballabio, A. (2014). Lysosomal adaptation: how the lysosome responds to external cues. *Cold Spring Harb Perspect Biol, 6*(6). doi: 10.1101/cshperspect.a016907

Shalem, O., Sanjana, N. E., Hartenian, E., Shi, X., Scott, D. A., Mikkelson, T., . . . Zhang, F. (2014). Genome-scale CRISPR-Cas9 knockout screening in human cells. *Science, 343*(6166), 84-87. doi: 10.1126/science.1247005

Shevchenko, A., Tomas, H., Havlis, J., Olsen, J. V., & Mann, M. (2006). In-gel digestion for mass spectrometric characterization of proteins and proteomes. *Nat Protoc, 1*(6), 2856-2860. doi: 10.1038/nprot.2006.468

Tai, H., Wang, Z., Gong, H., Han, X., Zhou, J., Wang, X., . . . Xiao, H. (2017). Autophagy impairment with lysosomal and mitochondrial dysfunction is an important characteristic of oxidative stress-induced senescence. *Autophagy, 13*(1), 99-113. doi: 10.1080/15548627.2016.1247143

Tan, H. W. S., Sim, A. Y. L., & Long, Y. C. (2017). Glutamine metabolism regulates autophagy-dependent mTORC1 reactivation during amino acid starvation. *Nat Commun, 8*(1), 338. doi: 10.1038/s41467-017-00369-y

Wang, X., & Sun, S. Y. (2009). Enhancing mTOR-targeted cancer therapy. *Expert Opin Ther Targets, 13*(10), 1193-1203. doi: 10.1517/14728220903225008

Zhou, J., Tan, S. H., Nicolas, V., Bauvy, C., Yang, N. D., Zhang, J., . . . Shen, H. M. (2013). Activation of lysosomal function in the course of autophagy via mTORC1 suppression and autophagosome-lysosome fusion. *Cell Res, 23*(4), 508-523. doi: 10.1038/cr.2013.11

Zoncu, R., Bar-Peled, L., Efeyan, A., Wang, S., Sancak, Y., & Sabatini, D. M. (2011). mTORC1 senses lysosomal amino acids through an inside-out mechanism that requires the vacuolar H(+)-ATPase. *Science, 334*(6056), 678-683. doi: 10.1126/science.1207056

Chapter 4. General discussion

1. General discussion

The role of CDKs in the control of cell cycle has been extensively studied. Cell cycle progression requires great metabolic adaptation, given the high demand of energy for anabolic processes (Lopez-Mejia & Fajas, 2015). Growing evidence about cell cycle regulators being the sensors and effectors of this metabolic adaptation is found. Cell cycle regulators respond to mitogenic extracellular stimuli (Duronio & Xiong, 2013). In addition, many metabolic targets of CDKs have been identified, including metabolic enzymes, metabolic regulators and molecules involved in organismal energy homeostasis. These findings highlight, not only the tight link between cell cycle and metabolism, but also the role of CDKs in the regulation of metabolism (Solaki & Ewald, 2018).

The laboratory of Prof. Fajas has focused for years on elucidating the metabolic roles of cell cycle regulators, including CDK4. It is well known that CDK4 promotes the transition from the G_1 to S phase of the cell cycle. This occurs in the nucleus of the cell. However, CDK4 is also found in the cytoplasm playing additional roles in metabolism (Aguilar & Fajas, 2010). It is known that CDK4 is translocated to the cytoplasm once it accomplishes its cell cycle task. However, it was thought that this translocation occurs for CDK4 to be degraded. It is yet to be elucidated whether two pools of CDK4 co-exist in a cell, or whether the same CDK4, once it accomplishes its task in the nucleus, is translocated to the cytoplasm to perform metabolic functions.

During my PhD, I contributed in unraveling new roles of CDK4 in metabolism. In 2016 we published that CDK4, through phosphorylation of IRS2, maintains the insulin signaling pathway activated in adipocytes (Lagarrigue et al., 2016) (enclosed in ANNEX. Contribution to other articles). These findings place CDK4 at the initiation of the insulin signaling pathway, a pathway usually deregulated in metabolic disorders such as obesity and insulin resistance. The following year, we found that CDK4 represses catabolism by directly targeting the α2 subunit of AMPK in mouse embryonic fibroblasts and also *in vivo*, in muscle tissues

from mice. This finding uncovered the role of CDK4 in the control of the whole-body energy homeostasis and exercise performance (Lopez-Mejia et al., 2017) (enclosed in ANNEX. Contribution to other articles). Interestingly, in both cases, CDK4 acts independently of E2F1 to regulate metabolism. In addition, it also has been shown that one of the main proteins of insulin signaling pathway, AKT, can negatively regulate AMPK through phosphorylating its α1 subunit (Hawley et al., 2014). This places CDK4 at two different levels of the same signaling pathway with the same purpose: to promote anabolism and repress catabolism.

The results shown in this thesis (Chapter 3) depicted a new role of CDK4 in metabolism. We show here that this kinase, also independently of E2F1, regulates lysosomal function and mTORC1 activation in a TNBC model. Once again, we are describing that CDK4 promotes an anabolic process, but this time, through a novel mechanism. We show for the first time that CDK4 can phosphorylate FLCN, a regulator of mTORC1, and that CDK4 phosphorylations on FLCN are necessary for mTORC1 activation at the surface of lysosomes. In addition, we show that CDK4 inhibition or depletion impairs lysosomal function, thus, also resulting in mTORC1 inhibition. The lack of evidences of FLCN playing a role in lysosomal function suggested these dual effects with the same result. Lysosomal function is important mainly for autophagy, to degrade damaged organelles or proteins to be recycled to create new ones, or to be exported outside the cell. mTORC1, since is the main promoter protein synthesis, can sense amino acids resulting from lysosomal degradation to become activated and start its functions. mTORC1 is also activated by insulin signaling pathway. In addition, it is a negative regulator of AMPK and vice versa. The results shown in Chapter 3 further places CDK4 as an important regulator of the insulin signaling pathway, this time regulating mTORC1 activity. However, these three studies are conducted in different models. Further investigations are needed to elucidate whether all these roles of CDK4 in metabolism can occur in the same cell type, or they are context specific.

The role of CDK4 in the regulation of lysosomal function is specially important for cancer treatment. Firstly, CDK4 appears to be hyperactive in many cancer types, and the use of CDK4 inhibitors have already provided successful results in clinical trials. In addition, lysosomes play multiple roles in the cell, they can be deregulated in tumorigenesis, and targeting these organelles is an emerging strategy to treat cancer. Our investigations were conducted in a TNBC model, a highly

aggressive breast cancer type, and provide a new therapeutic strategy to treat this form of disease.

It was already known that CDK4 inhibition does not induce cell death but senescence in cancer cells (Yoshida & Diehl, 2015). We have found that senescent cells with impaired lysosomal function (treated with CDK4 inhibitors) eventually die, if they are additionally treated with an activator of AMPK, which induces autophagy. The combination of both drugs reduced tumor size and offered a better outcome than single treatments. These findings highlight the importance of targeting lysosomes for cancer treatment, and offer another application for CDK4 inhibitors.

In summary, our research uncovers the interesting roles of CDK4 in metabolism, that are not only essential for basic cell cycle biology, but may open new avenues for the treatment of different pathologies, such as metabolic disorders or cancer.

2. Conclusions

- CDK4 is not only a cell cycle regulator. It is also an important metabolic effector that promotes anabolism while repressing catabolism.
- In MDA-MB-231 *in vitro* and in xenografts models of TNBC, CDK4 inhibition or depletion impairs lysosomal function. As a result, mTORC1 pathway is downregulated. Cells with impaired lysosomal degradation become senescent.
- As cancer treatment, the combination of the CDK4 inhibitor LY2835219 together with A769662 induces cell death and provides a better outcome for TNBC.
- Targeting lysosomes is a promising approach to treat cancer.

3. Future perspectives

The results described in this thesis leave unresolved questions and open new perspectives in the study of the relationship between CDK4, mTOR and lysosomes.

Despite demonstrating that CDK4 promotes lysosomal function in a TNBC model, the underlying mechanism of this finding is still unknown. In order to find the pathways differentially activated in the presence or absence of CDK4, the use of PamStation, a new technology developed by PamGene and available in the lab, it would be very informative. This automated instrument contains different chips with more than 100 known peptides immobilized in array format. These peptides can be phosphorylated by the proteins from a cell or tissue lysate. A fluorescently labeled antibody detects the levels of phosphorylation of each peptide, which correlates with the intensity of the fluorescence. Later on, upstream analysis of the phosphorylated peptides can reveal which kinases are affected by CDK4 inhibition or depletion, and eventually the involved pathways. This will lead to the discovery of new potential CDK4 targets.

In order to find its direct phosphorylation targets, we could use an analog-sensitive CDK4. We would need to mutate the ATP binding site of the kinase and perform a kinase assay with labeled ATP. Only the direct CDK4 targets will acquire the labeled phosphate and they can be identified by immunoprecipitation. This technique has already been tested in the lab. However, further optimization is needed, given that the non-mutated CDK4 was able to use labeled ATP to phosphorylate our positive control, RB protein.

In addition, preliminary data indicated that CDK4 KO MDA-MB-231 cells have increased basal respiration and increased mitochondria in number and size as compared to WT cells. With these observations, and also taking into account that lysosomal function is impaired in CDK4 KO cells, the next question to address would be if mitophagy is also altered in these conditions. Analysis of some mitophagy markers or analysis of electron microscopy images would be useful to elucidate this question.

Furthermore, it would be interesting to study if the results obtained in a cancer model are also obtained in physiological conditions. For this purpose, since we have CDK4$^{-/-}$ mice available in our lab, it would be interesting to study whether they have defects in lysosomal function, and if so, what the metabolic impact of this phenotype is. For example, preliminary data indicates that the livers from CDK4$^{-/-}$ mice present enlargement of lysosomes as compared to CDK4$^{+/+}$ mice, as measured by immunohistochemistry of LAMP1 in liver sections. Lysosomes have been shown to be essential for liver regeneration (Dwivedi, Kaur, Srivastava, & Krishna Murti,

1985), and their enlargement in CDK4$^{-/-}$ mice could be an indication of defects of this process. In addition, autophagy-lysosome system is a pathway of critical importance in the brain, where it contributes to neuronal plasticity and must protect nonreplaceable neurons from the potentially harmful accumulation of cellular waste (Sharma, di Ronza, Lotfi, & Sardiello, 2018). Some neurodegenerative diseases such as Alzheimer's or Parkinson's disease, present deregulations in lysosomes (Dehay et al., 2013; McBrayer & Nixon, 2013). In addition, the majority of LSDs are associated with neurological problems (Onyenwoke & Brenman, 2015). Therefore, it would be interesting to study whether CDK4$^{-/-}$ mice present abnormalities in lysosomes in the brain, and to explore whether they present the neurological characteristics of the mentioned diseases.

Overall, this work has led to the creation of a new line of investigation in Prof. Fajas lab to further study the role of CDK4 in lysosomal biology in various physiological and pathological models.

ANNEX. Contribution to other articles

1. **"Cancer: Linking lysosomes to suicidal bags"**
   Martinez-Carreres, L., Nasrallah, A., and Fajas, L. (2017). Cancer: Linking Powerhouses to Suicidal Bags. Frontiers in oncology *7*, 204.

During my PhD I had the opportunity to write a literature review about the interplay between two essential organelles of the cell: mitochondria and lysosomes. Both organelles are crucial for cell proliferation and cell fate; their interaction in some cases can result in cell death, and in others, in tumorigenesis. This literature review explains the main mechanisms or processes by which this two organelles are connected and their deregulations in cancer. In addition, it explains the current treatments that target the interplay of both organelles and their implications for cancer therapy.

Cancer: Linking Powerhouses to Suicidal Bags

Laia Martinez-Carreres†, Anita Nasrallah† and Lluis Fajas*

Cancer and Metabolism Laboratory, Center for Integrative Genomics, University of Lausanne, Lausanne, Switzerland

Membrane-bound organelles are integrated into cellular networks and work together for a common goal: regulating cell metabolism, cell signaling pathways, cell fate, cellular maintenance, and pathogen defense. Many of these interactions are well established, but little is known about the interplay between mitochondria and lysosomes, and their deregulation in cancer. The present review focuses on the common signaling pathways of both organelles, as well as the processes in which they both physically interact, their changes under pathological conditions, and the impact on targeting those organelles for treating cancer.

Keywords: cancer, mitochondria, lysosomes, mammalian target of rapamycin, Rab7, AMP-activated protein kinase, mitophagy, lysosomal membrane permeabilization

INTRODUCTION

Cancer is characterized by the unrestricted cellular growth and proliferation of abnormal cells. It exhibits properties of motility, invasion, angiogenesis, and metastasis. Recent studies identified diverse mechanisms of metabolic plasticity in cancer cells. These include increased glucose uptake in most tumors, elevated glycolytic intermediates, increased pentose phosphate pathway activities, increased glutamine catabolism, and increased use of lactate as a fuel in selective tumors [1].

According to the American Cancer Society, it is estimated that, in the US, almost 1.7 million new cases of cancer will be diagnosed in 2017. Mostly, general cancer treatments are limited to radiation, chemotherapy, and surgery. However, these treatments encounter non-specific distribution of chemotherapeutic agents, insufficient drug concentrations to reach the tumor, and restricted ability to survey therapeutic responses [2]. More efforts are targeted to find new therapies to help overpass these obstacles. Subcellular targeting is beneficial for therapy in several scenarios [3]: (1) basic organelle malfunctions could be targeted, making the process more selective; (2) the quantity of drug required could be significantly reduced because of its specificity, which eventually helps in decreasing side effects; and (3) most importantly, intracellular drug targeting may surpass dangerous drawbacks of drug actions in cancer therapy, i.e., multidrug resistance [4, 5].

In most of the mechanisms of cancer initiation and progression, different organelles are involved, especially mitochondria and lysosomes, for their relevance in energy homeostasis and cell death [6]. The purpose of this review is to shed light on the roles of mitochondria and lysosomes in cancer, as well as them being prominent targets for cancer therapy.

THE ROLE OF MITOCHONDRIA IN CANCER

Mitochondria, also called "powerhouses" of cells, are double membrane organelles, with their own genome, thought to have been originated from an ancient symbiosis that resulted when a nucleated cell engulfed an aerobic prokaryote. Through evolution, mitochondria conserved only a small part of prokaryotic bacterial genes, including the ones encoding 13 proteins of the respiratory chain [7].

In this manner, mitochondria gained a central role in the regulation of metabolism, cell proliferation, and apoptosis, while many tasks were transmitted to the host cells (8).

Other than being cell's powerhouses, mitochondria function as signaling organelles. They coordinate distinct metabolic pathways, producing metabolites required for cell survival and proliferation (9). In fact, mitochondria are key players in the calcium-signaling pathway (10). When toxic stimuli damage the cell, mitochondria release pro-apoptotic molecules, such as cytochrome c, thus regulating cell death (11). Moreover, mitochondria are established as the major site of production of free radicals, which are major signaling molecules in the cell (12). Recently, it has been shown that mitochondrial metabolites do not only have intermediary roles in energy generation but can also promote regulatory effects on post-translational modifications of proteins (13), as well as affecting chromatin structure and function (14).

Multiple human diseases have been strongly associated with impaired mitochondrial homeostasis. These include liver and cardiovascular diseases, neurological and muscular disorders, seizures, susceptibility to infections, and cancer (15–18). In cancer, mitochondrial roles vary as a function of genetic and environmental differences, as well as the tissue-of-origin of the diverse types of cancer. The main mitochondrial processes contributing to tumorigenesis include mitochondrial biogenesis and mitophagy, fission and fusion dynamics, metabolism, oxidative stress, and cell death (19).

Compared to normal cells, cancer cells show many alterations in energy metabolism. In the 1920s, cancer metabolism studies commenced with Otto Warburg's observation: to produce energy, cancer cells rely less on mitochondrial respiration and more on glycolysis. Warburg hypothesized that mitochondria must be dysfunctional, taking into consideration that glycolysis gives a lot less energy as compared to mitochondrial respiration (20). However, other scientists believed that the reduced mitochondrial activity is due to higher glycolysis. In some cases, Warburg's proposal holds true. Nevertheless, there are reports showing that the mitochondrial function in cancer cells in some cases is intact, or mitochondrial biogenesis is increased (21).

Mitochondrial biogenesis could be described as the division and growth of pre-existing mitochondria. It is regulated at the transcriptional and post-transcriptional levels of gene expression (22). Regulating mitochondrial biogenesis is an attractive target of key oncogenic signaling pathways, since cancer cells induce it to increase ATP production for cellular proliferation. PGC-1α, through its interactions with numerous transcription factors, is a central regulator of mitochondrial biogenesis (23). It portrays a dual effect on cancer viability. On the one hand, PGC-1α acts as a tumor suppressor in some cancers, resulting in induced apoptosis upon overexpression. In human epithelial ovarian cancer, apoptosis was induced *via* the organized regulation of Bcl-2 and Bcl-2-associated X protein (BAX) expression by PGC-1α (24). PGC-1α is considered a tumor suppressor not only because it induces apoptosis but also because it has been found to suppress the metastatic abilities of tumor cells *via* the direct regulation of transcriptional machinery (25, 26). For example, PGC-1α directly increases ID2 transcription that binds

to the transcription factor TCF4, rendering it inactive. This in turn leads to a downregulation in metastasis-related genes, such as integrins, that are able to influence metastasis and invasion (25). On the other hand, the ability of PGC-1α in sustaining metabolic homeostasis can also promote cancer cell survival and tumor metastasis (27). In cancer cells, silencing PGC-1α resulted in deferred invasive potential and weakened metastatic ability without affecting proliferation and tumor growth. Consistently, the transition from primary lung tumor cells to metastatic cancer cells was coupled with more dependence on mitochondrial respiration, *via* PGC-1α, leading to an upregulation of PGC-1β, ERRα, and NRF1, which are mitochondrial-related biogenesis genes (28).

Another key activator of mitochondrial biogenesis in cancer is c-Myc, a transcription factor regulating cell cycle, proliferation, metabolism and cell death. Studies have demonstrated that the loss or gain of Myc decreases or increases mitochondrial mass, respectively. This is due to the fact that over 400 mitochondrial genes are identified as targets of c-Myc (29). A third effector of mitochondrial biogenesis is mammalian target of rapamycin (mTOR). It controls mitochondrial gene expression through the activation of PGC-1α/YY1 and represses the inhibitory 4E-BPs (eukaryotic translation initiation factor 4E-binding protein 1) that downregulates the translation of mitochondrial proteins (30).

During tumorigenesis, mitochondrial dynamics is very important. It determines the equilibrium between cell death programs and mitochondrial energy production. Several studies demonstrated, in cancer, an imbalance in mitochondrial fission and fusion activities, depicted in decreased fusion, and/or elevated fission that resulted in fragmented mitochondrial networks *via* the K-Ras-DRK1/2-Drp1 pathway (31, 32). Also, c-Myc affects mitochondrial dynamics by altering the expression of proteins implicated in the fission and fusion processes (33).

Furthermore, mitochondria have a tight relationship with the intrinsic (also called mitochondrial) apoptotic cell death program, since B-cell lymphoma-2 (BCL-2) family of proteins regulates the integrity of the outer mitochondrial membrane (OMM). Mainly two members of this family, BAX and Bcl-2-associated killer (BAK) can break the OMM in response to apoptotic stimuli. This releases apoptogenic factors from inside mitochondria, such as cytocrome c, inducing activation of caspases and subsequent cell death. In some cases, mitochondria can also participate in the extrinsic apoptotic pathway, which is initiated by cell membrane death receptors. For example, FAS receptor can truncate Bid protein, another member of the BCL-2 family, *via* caspase 8. Truncated Bid (tBid) can then translocate to mitochondria to induce apoptosis (34).

Mitochondrial morphology is a hallmark for apoptotic susceptibility. Even though fission and fusion do not regulate apoptosis *per se*, the generated mitochondrial morphology supports the interaction with pro-apoptotic Bcl-2 proteins. Thus, mitochondrial hyper-fragmentation causes resistance to apoptosis due to the inability of mitochondrial membranes to interact with pro-apoptotic proteins (35).

Mitochondria play major roles in metabolic reprograming, including the synthesis of macromolecules and cellular survival (1). One mechanism by which cancer drives these alterations in

metabolism is limiting pyruvate utilization by the mitochondria. This is achieved by regulating pyruvate kinases such as PKM isoforms (36), as well as downregulating mitochondrial pyruvate carriers: MPC1 and MPC2 (37). Moreover, in some tumor types, mutations in the enzymes of the tricarboxylic acid (TCA) cycle render the mitochondria dysfunctional. Cells from such tumors use glutamine-dependent reductive carboxylation rather than oxidative metabolism as the major pathway of citrate formation. This, in turn, leads to the major reprograming of amino acid metabolism and lipid synthesis (38).

There are multiple levels at which both mitochondrial biology and tumorigenic signaling vastly intersect. First, cellular physiology and tumorigenesis are affected by direct signals from mitochondria. Metabolites generated by the mitochondrial pathways affect gene transcription through chromatin modification, and cytosolic signaling pathways (19). For example, the TCA cycle intermediate α-ketoglutarate (α-KG) is a co-substrate for many enzymes in the cytoplasm and nucleus, including families of chromatin-modifying ones. In the case of chromatin regulation, glutamine-derived α-KG contributes to TET-dependent demethylation reactions (38). Second, many mutations were identified as directly associated with cancer risk (39). Cancer can be caused by mutations in nuclear-encoding genes, such as electron transporter chain (ETC) genes. For example, patients suffering from paraganglioma often presents dysfunctions in succinate dehydrogenase (SDH). Mutations of the same complex have also been found in other cancers, such as gastrointestinal stromal cancer, breast cancer, or renal carcinomas. Other enzymes such as fumarate hydratase (FH) have also found to be mutated in other cancers. When the function of these enzymes is lost, the metabolic intermediates fumarate and succinate accumulate, which in turn function as oncometabolites when found in excess (40, 41). In addition, mitochondrial DNA mutations (amplifications, deletions, point mutations, etc.) have been associated with various cancers (42). For example, point mutations in MT-ND1 gene modify complex I activity, having an influence on the tumorigenic characteristics of cells. Finally, and in order to support tumorigenesis, classical oncogenic signaling pathways alter mitochondrial functions. These include the c-Myc, p53, mTOR, and k-Ras signaling pathways (19). In addition, a main function of mitochondria is synthesizing aspartate for nucleotide synthesis, inducing cellular proliferation (43).

Mitochondria are complex organelles affecting cancer at many levels: initiation, proliferation, survival, or metastasis. One type of the various organelles that communicate with mitochondria is lysosomes. Mainly, this crosstalk depends on mitochondrial stress and/or destabilization of lysosomal membranes (44).

THE ROLE OF LYSOSOMES IN CANCER

Also known as "suicidal bags," lysosomes were first described in 1950s by Christian de Duve as membrane-enclosed vesicles containing hydrolases. Functioning as a digestive system, they are found in all eukaryotic cells, except for mature erythrocytes. The hydrolytic enzymes that they contain include proteases, nucleases, and lipases that can break down proteins, nucleic acids, and lipids, respectively, to their simplest subunits (45).

Lysosomes are formed when material from outside the cell is internalized in clathrin-coated endocytic vesicles forming early endosomes. Endosomal maturation occurs with the delivery of lysosomal acid hydrolases from the trans Golgi network, which contribute lowering of the internal pH to about 5.5. Late endosomes then mature into lysosomes as they acquire a full complement of acid hydrolases, which digest the molecules originally taken up by endocytosis, phagocytosis, and autophagy (46). Nevertheless, many investigations have proved that lysosomes are not only degradative organelles but also participate in metabolism of the entire cell at different levels, and their modifications can promote or repress cell proliferation.

On one hand, lysosomes undergo Ca^{2+} regulated exocytosis, which is secreting their content into the extracellular space, and repairing their damaged plasma membranes; when the plasma membrane is injured, lysosomes quickly move to the site of damage and fuse with the plasma membrane. This allows effective resealing (47). On the other hand, they can sense nutrient availability, which controls energy metabolism and mediates the starvation response (48). Zoncu et al. proposed that amino acids have to be detected in the lysosomal lumen, signaling to the Rag GTPases in a manner that is vacuolar H^+-ATPase (V-ATPase)-dependent. This is known as the "inside-out" mechanism (49). Leucine, among other amino acids, must accumulate in the lumen of the lysosome to trigger the central regulator of cellular and organismal growth, mammalian target of rapamycin complex I (mTORC1) (50). mTORC1 is recruited by Rag GTPases on the lysosomal surface in response to amino acids, the site of activation by Rheb (Ras homolog enriched in brain), when growth factor-stimulated PI3K–Akt signaling is on (51, 52). Upon amino acid and growth factors removal, Rag GTPases releases mTORC1, causing it to become cytoplasmic and inactive. In those conditions, the negative regulator of Rheb, tuberous sclerosis complex 2 (TSC2), is lysosomally localized. Thus, lysosomal proteins change depending on the nutrient status of the cells (53, 54).

Lysosomal biogenesis as well as autophagy is controlled by the main regulator of lysosomal genes, known as TFEB or transcription factor EB; when mTORC1 is active, TFEB remains inactive at the lysosomal membrane. Inactivated mTORC1 induces TFEB localization to the nucleus to activate lysosomal gene transcription (52, 55).

Since lysosomes also serve as platforms of activation of mTORC1, it is important to mention the dysregulation of this pathway in cancer. Indeed, mTORC1 regulates several anabolic processes that are critical for tumorigenesis: it promotes protein synthesis, aerobic glycolysis, *de novo* lipid synthesis, *de novo* nucleotide synthesis, and represses autophagy and lysosomal biogenesis (56–59). Genes that encode components of the PI3K–Akt–mTOR pathway are frequently mutated in cancer, but despite few mutations have been characterized in mTOR, many tumor types present mTOR hyperactivation, thus promoting tumorigenesis (60, 61).

In addition, lysosomal intracellular positioning is important for adhesion and motility (62), and important for mTOR signaling, autophagosome formation, and autophagosome-lysosome fusion, and changes depending on the nutrient availability. During starvation, mTORC1 activity is repressed, which

induces autophagosome formation. Starvation increases pH, causing lysosomes to cluster near the microtubule-organizing center (MTOC), facilitating autophagosome–lysosome fusion. Conversely, nutrient replenishment restores basal pH inducing lysosomal scattering, which brings lysosomal mTORC1 to the cell periphery and stimulates its activity by increasing its coupling to the gradient of signaling molecules emanating from the plasma membrane (63). Given that peripheral lysosomes inside the cell are responsible for cell adhesion and motility, targeting those lysosomes in cancer cells is also a good strategy for cancer treatment (62).

As de Duve already stated in the 1950s, lysosomal membrane permeabilization (LMP), consequently leading to the leakage of lysosomal content into the cytoplasm, induced what is known as "lysosomal cell death" (45, 64). Major players of this mechanism are lysosomal cathepsin proteases. They have apoptotic and/or necrotic features, depending on the cellular context and the extent of leakage occurring into the cytosol (65).

Lysosomes in cancer cells undergo major changes. In some cases, they have an increased volume and protease activity, along with an improved lysosomal protease secretion, as compared to lysosomes in normal cells. Thus, they become hyperactivated as a reaction to fulfill the needs of the challenging microenvironment of the tumorigenic cells (62). For example, they require the ingestion of huge amounts of adhesion molecules and extracellular matrix molecules, leading to an upregulation in exocytosis. Also, they have to move inside the cell to repair damaged membranes (66, 67). Recently, a correlation between lysosomal movement and tumor cell invasion was also established, which was induced by tumor microenvironment stimuli (68). In particular, acidic extracellular pH induced lysosomal movement toward the cell peripheries, successively leading to Cathepsin B exocytosis from the lysosomes. This eventually promoted protease-dependent tumor invasion (69, 70). *In vitro* studies with glioma cells have shown that inhibition of lysosomal exocytosis with vacuolin-1 is a good strategy for fighting against invasion in cancer (71).

As explained above, changes in the lysosomal compartment, in the presence of increased secretions of cysteine cathepsins, render these lysosomes pro-oncogenic. This results in an increased neoplastic progression, *via* proteolytic pathway initiation (72). Other than matrix remodeling, lysosomal role in degradation is crucial in tumorigenesis. This has been observed in reports revealing that specific intracellular cathepsin inhibitors are able to block collagen degradation, promoting tumor viability (73). However, cathepsins are also depicted as proteases with tumor suppressor abilities for their role in inducing cell death through LMP (74, 75).

Due to their role in cell death, autophagy, and deregulating metabolism, targeting lysosomes have a great therapeutic potential in cancer. Lysosomal proteins are indeed good targets for cancer treatment (76), such as lysosome-associated membrane protein 1 (LAMP-1). LAMP-1 is suggested to have a role in cell–cell adhesion and migration, since it was detected on the surface of highly metastatic cancer cells, particularly from colon cancer (77). V-ATPase is another significant lysosomal membrane protein participating in cancer. It functions as a pump of protons to create an acidic pH of lysosomes. Also, it regulates endocytic

trafficking and affects the tumor microenvironment, by extruding protons into the extracellular matrix (78). Moreover, in tumor malignancy, V-ATPase participates not only in the dysregulation of lysosomal trafficking but also in mTORC1 activation and autophagy (79).

In addition, lysosomes are key players in cancer drug resistance. They can sequester cancer drugs into their acidic milieu, thus, blunting the drugs' effects (80). This further proves that targeting lysosomes may be a promising new therapeutic strategy for cancer.

Since both organelles, mitochondria and lysosomes, share the power of majorly impacting the process of tumorigenesis, we will next further describe the main crosstalk between these two important organelles, shedding light on their interplay in cancer and their impact on cancer therapy.

THE MITOCHONDRIAL–LYSOSOMAL INTERPLAY IN CANCER

In cancer, several important changes occur in all the organelles. However, the interplay between mitochondria and lysosomes is of high importance, because both organelles can interact to promote, in some cases cell death and in others tumorigenesis. There are two processes in which mitochondria and lysosomes work together: the first is LMP, a process in which enzymes from lysosomes can induce mitochondrial death pathway, and the second is mitophagy, a process in which lysosomes can degrade mitochondria, resulting in cell survival or cell death. Other than these two processes, there are several common effectors that play important roles in both organelles, which are also affected in cancer.

Mitochondrial–Lysosomal Mechanisms
Lysosomal Membrane Permeabilization
As mentioned above, LMP is a mechanism that induces two types of cell death: apoptosis induced by partial and selective LMP, and necrosis provoked by the complete disruption of lysosomes. One of the causes of apoptosis during LMP is the activation of caspases in the mitochondrial death pathway by mitochondrial outer membrane permeabilization (MOMP) (65).

Reactive oxygen species (ROS) and cathepsins are well-known mediators of LMP-triggered cell death (81). It has been reported that only cathepsin D in the cytoplasm is enough to induce MOMP and apoptosis in human fibroblasts. However, cathepsin D alone is not in all cases of LMP sufficient to induce cell death (65).

As shown in **Figure 1**, MOMP can be triggered by LMP in two manners: either Bid dependent or Bid independent. Bid is known as BH3-interacting-domain death agonist and belongs to the pro-apoptotic BH3-only Bcl-2 family. The Bid-dependent process occurs when Bid is cleaved by the active cathepsins at cytosolic pH (specially cathepsins B and D), after which Bid is capable to form pores at the OMM inducing MOMP and releasing cytochrome *c* from the mitochondria (81). Despite tBid is also known to activate BAX and BAK, in some cases, LMP can induce MOMP in a Bid-independent manner; cathepsins or
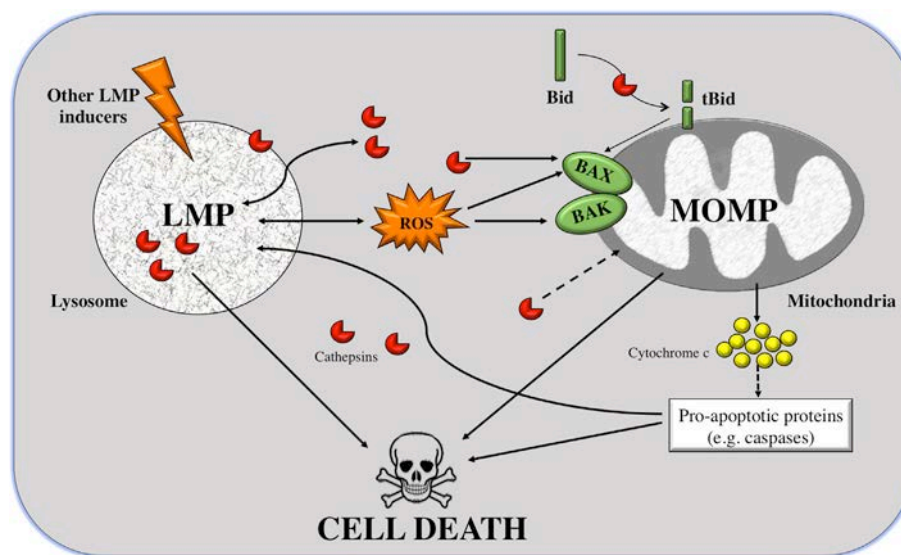
FIGURE 1 | From lysosomal membrane permeabilization (LMP) to cell death through mitochondrial outer membrane permeabilization (MOMP). LMP is a process in which intralysosomal content (mostly cathepsins but also ROS) is leaked to the cytoplasm. Massive disruption of lysosomes induces cell death by necrosis, but selective LMP can induce apoptosis by MOMP. Cathepsins can promote, on the one hand, the cleavage of the pro-apoptotic protein Bid; and on the other hand, the translocation of Bcl-2-associated killer (BAK) and BAX to the outer mitochondrial membrane (OMM) where they form pores. Truncated Bid (tBid) can itself form pores to the OMM but can also activate BAK/BAX. These two processes can induce apoptosis, *via* release of cytocrome *c* and in a caspase-dependent way or independently of caspases. A positive feedback loop exists given that caspases and cathepsins are also inducers of LMP.

stress stimuli can directly activate the proteins BAX and/or BAK (82, 83). After their activation and translocation to the mitochondria, BAX and BAK make pores at the OMM. This permits the translocation of numerous molecules bigger than 100 kDa, without inducing membrane rupture leading to apoptosis (84–86). Furthermore, cathepsin B has a major role in linking LMP to MOMP *via* the generation of lipid mediators, such as arachidonic acid that induces MOMP (87). Alternatively, other than ROS and cathepsins, there is a large list of agents capable of inducing this mitochondrial membrane permeabilization, such as sphingolipids, phospholipase A2, etc. (64). Some of these stimuli, like the pro-apoptotic proteins or caspases, are derived from mitochondria, suggesting that there is a positive feedback loop: mitochondrial damage also induces LMP (**Figure 1**).

In addition, the mechanism by which cathepsins are released from the lysosomes is not yet clear. There are three possible hypotheses: (i) through the rupture of the lysosomal membrane, (ii) through specific pores, or (iii) by special transporters. In an attempt to find which of the three hypotheses is valid, fluorescently labeled dextran molecules of different sizes were used. When inducing LMP, it was shown that only small molecules (size of 10 kDa) were released to the cytoplasm in most of the cells. In almost half of the cells, 40-kDa molecules were redistributed to the cytoplasm, and molecules larger that 70 kDa remained inside lysosomes. Based on the fact that cathepsins are relatively small proteins, around 40 kDa in size, it is inferred that cathepsins are among these released molecules. Furthermore, the low intralysosomal pH was maintained, suggesting that lysosomes were still active (88). However, it is still not enough to rule out any of the possible mechanisms.

Until now, several explanations may account for the higher vulnerability to LMP of cancer cell lysosomes. Since lysosomes are relatively large in cancer cells (89), one possibility would be that they are more prone to inducing cell death than lysosomes with normal sizes (90). Another possibility lies in the observation that cancer cells have higher metabolic rates. This is accompanied by an elevated turnover of proteins that contains iron, leading to iron accumulation in the lysosomes. Subsequently, these lysosomes will undergo an iron-mediated predisposition to a ROS-induced LMP (91). In other words, a characteristic of cancer cells is the increased levels of ROS, which is associated with an amplified release of cathepsins from the lysosomes. Since cancer cells appear to be more susceptible to LMP, its induction will eventually facilitate cancer cell death (92).

Autophagy and Mitophagy

Macroautophagy is a process in which intracellular proteins or organelles are degraded in the lysosomes. Degraded products are then released from lysosomes and recycled into biosynthetic and metabolic pathways. Through the elimination of those damaged components, autophagy basically provides quality control over proteins and organelles, as well as sustains mitochondrial metabolic function and energy homeostasis (93). More than 30 proteins coordinate the autophagic processes, generating autophagosomes from essentially all membrane sources from the cell. Autophagy-related genes (Atg) control the processes of autophagy. The products of Atg genes are regulated by nutrients (mTOR), energy [AMP-activated protein kinase (AMPK)], and stress [hypoxia-inducible factor (HIF)], which can turn the pathway on and off (94). Nevertheless, autophagy may also induce cell

death, known as autophagic cell death (ACD). This specifically occurs when chromatin condensation is absent (95).

Autophagy's role in cancer is still not clear. Some cancers are dependent on autophagy for survival and other cancers use autophagy as a mechanism of cell death. In some models, autophagy suppresses cancer initiation by evading the toxic accumulation of damaged organelles, specifically mitochondria. On the short run, this helps in limiting oxidative stress. On the long run, it restricts chronic tissue damage and oncogenic signaling. So, in this context, autophagy stimulation might help suppress and/or prevent cancer initiation. Though, other cancers depend on autophagy for survival. In order to fit the high metabolic needs of growth and proliferation, cancers (such as the pancreatic) use autophagy-mediated recycling to their own advantage (96). Hence, inhibiting autophagy in this case could be an insight for selective cancer therapy, since these tumors are more dependent on autophagy than normal tissues (93).

Degradation of entire organelles can also occur: mitophagy (mitochondria), reticulophagy (endoplasmic reticulum), lipophagy (lipid droplets), peroxophagy (peroxisomes), and xenophagy (microbes). Mitophagy or autophagy of mitochondria is required to eliminate dysfunctional mitochondria to maintain appropriate metabolic and cell survival signals (97). Here, we will focus only on mitophagy, a key process for the control of mitochondrial quality. It is of substantial importance for the normal development of cells and tissues. The most studied mechanism of mitophagy initiation involves the E3 ubiquitin ligase Parkin and the serine–threonine kinase PINK1 (PTEN-induced putative kinase 1). PINK1 is a mitophagy receptor found at the OMM that accumulates when mitochondria are damaged or undergo any stress leading to mitochondrial membrane potential loss. This PINK1 accumulation at the OMM recruits Parkin from the cytosol. Parkin ubiquitinates proteins at the OMM. These ubiquitinated proteins are recognized by p62, also known as Sequestrome 1 (SQSTM 1). P-62 binds to LC3/Atg8 and takes p62-containing aggregates to the autophagosome to be degraded (98).

In the recent years, the role of mitophagy in cancer has been extensively reviewed. Parkin is frequently genetically inactivated in cancer. Although certain cancers, such as sarcomas and uterine cancer, have amplifications in PARK2 gene, the majority of tumors with lesions in PARK2, including ovarian, breast, and lung cancers, harbor deletions or loss of function mutations. This is mainly because the PARK2 gene is found on a fragile location on chromosome 6 (99). Parkin has been evidenced to control cell cycle regulators, such as cyclin-dependent kinases (CDKs) and cyclins, promoting acceleration of cell cycle progression. It can also lead to the accumulation of damaged mitochondria and elevated ROS production, triggering DNA damage and tumorigenesis (100). In addition, PINK1 and Parkin can promote apoptosis through targeting and ubiquitinating anti-apoptotic Mcl-1 leading to degradation; they operate as molecular switches by dictating cell fate as a response to diverse cellular stresses (101, 102). However, mitophagy can happen in cancer cells without active Parkin, known as mitophagy-independent Parkin function. OMM proteins, such as FUNDC1, BNIP3, and NIX, are autophagy receptors, independently of ubiquitinization. Furthermore, other factors such as the phospholipid cardiolipin

can induce mitophagy, as well as ubiquitin ligases, such as SMURF1 and MAPL (103–105).

During hypoxia, HIFs can induce mitophagy through the transcription of NIX and BNIP3. In addition to its transcriptional activation by HIF-1, FoxO3A, PPARα, RB/E2Fs, NF-κB, oncogenic Ras, and p53 also transcriptionally regulate BNIP3 (103), while NIX is transcriptionally regulated by HIF-1 and p53 (106, 107). Upon hypoxia or high oxidative phosphorylation, the small GTPase Rheb translocates to the OMM, where it can interact with BNIP3 and NIX to induce mitophagy, resulting in mTOR inactivation (108, 109). The role of BNIP3-dependent mitophagy in cancer presents some controversies. BNIP3-dependent mitophagy is required to limit mitochondrial mass and ROS levels in growing tumors; its loss leads to HIF-1α-dependent increases in tumor growth and increased progression to metastasis (110). However, other studies show that BNIP3 has a pro-tumorigenic role; its inactivation reduced cell migration and its upregulation suppressed the mTOR/S6K1 pathway. It is hypothesized that the dual role of BNIP3 can be explained by alternative splicing or variable transcriptional regulation *via* transcription factor Sp3 (111, 112).

Contrary to BNIP3, the role of NIX and FUNDC1 in tumor progression remains relatively unknown, requiring further investigation. They can induce mitophagy under hypoxic conditions (113). However, their role in cancer mitophagy is still to be raveled (107).

Signaling Pathways Involved in the Mitochondria–Lysosomal Crosstalk

As shown in **Figure 2**, the master regulator of cell growth and metabolism mTORC1 and proteins of the same pathway are the main linkers of mitochondria and lysosomes. As described

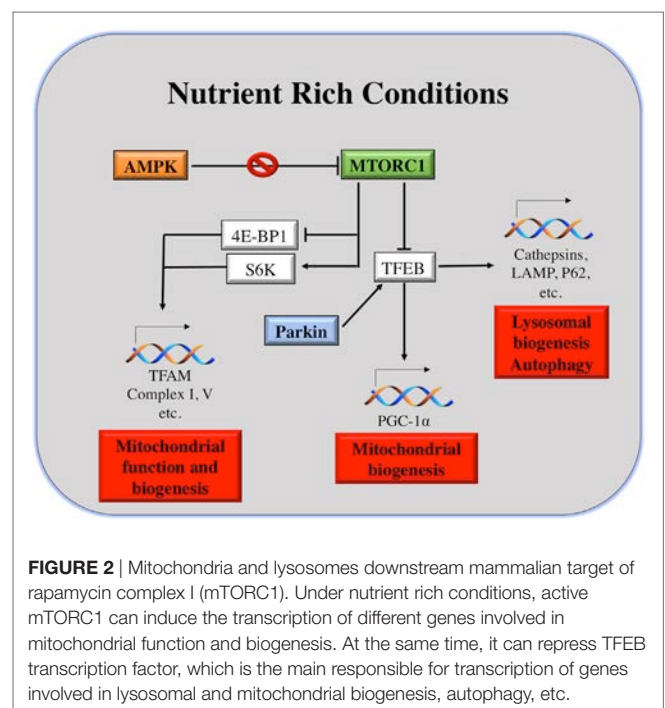**FIGURE 2 |** Mitochondria and lysosomes downstream mammalian target of rapamycin complex I (mTORC1). Under nutrient rich conditions, active mTORC1 can induce the transcription of different genes involved in mitochondrial function and biogenesis. At the same time, it can repress TFEB transcription factor, which is the main responsible for transcription of genes involved in lysosomal and mitochondrial biogenesis, autophagy, etc.

earlier, under nutrient-rich conditions, mTORC1 is activated at the lysosomal surface. mRNA translation of many genes occurs, *via* the activation and repression of S6K and 4E-BP1, respectively. Among the genes repressed by 4E-BP are TFAM, Complex I and Complex V of the mitochondria, regulating mitochondrial activity and biogenesis (114).

On the other hand, under starvation conditions, mTORC1 is inhibited and TFEB positively regulates the expression of lysosomal and autophagy genes, as well as the expression of PGC-1α. PGC-1α coactivates numerous biological programs in diverse tissues; it is a key regulator of lipid metabolism (115), but also it promotes mitochondrial biogenesis (30). Notably, TFEB activation can be induced by mitophagy as well, in an attempt to induce mitochondrial biogenesis after eliminating malfunctioning or damaged ones. The mechanism of TFEB activation by mitophagy is different than that under starvation conditions. Parkin promotes TFEB nuclear translocation, inducing lysosomal and mitochondrial biogenesis (98). In addition to that, upon energy depletion, AMPK is activated. AMPK serves as a fuel gage as it becomes active when ATP/AMP ratio is low, thus maintaining energy homeostasis (116). AMPK inhibits mTORC1 by the direct phosphorylation of Raptor, a molecule of the mTORC1 complex. This explains why AMPK has been considered as a tumor suppressor. AMPK activation is essential for increased mitochondrial biogenesis under glucose-limited conditions, since AMPK activation increases the expression of PGC-1α and TFAM (117) (**Figure 2**).

When mTORC1 is active, there is an increase of mitochondrial biogenesis. This increase in mitochondrial biogenesis will result in a gain of ATP production capacity, a mandatory energy source for translation (114). By contrast, mitochondrial biogenesis induced by AMPK is an attempt to accelerate ATP generation, for restoring its level in favor of cell survival. This takes place under limiting nutrient availability or metabolic stress (118).

To further emphasize the link between mitochondria and lysosomes, it has been shown that mTOR not only binds to lysosomes (when mTORC1 is activated when amino acids are present) but it can also be associated with MOM. This is needed to integrate different stress signals that affect the function of mitochondria and regulate a checkpoint implicating p70S6K, one of the well-known targets of mTORC1 (119). Recent studies link mitochondrial dynamics to the equilibrium between nutrient supply and energy demand, suggesting variations in mitochondrial architecture as an adaptive mechanism to metabolic demands (120).
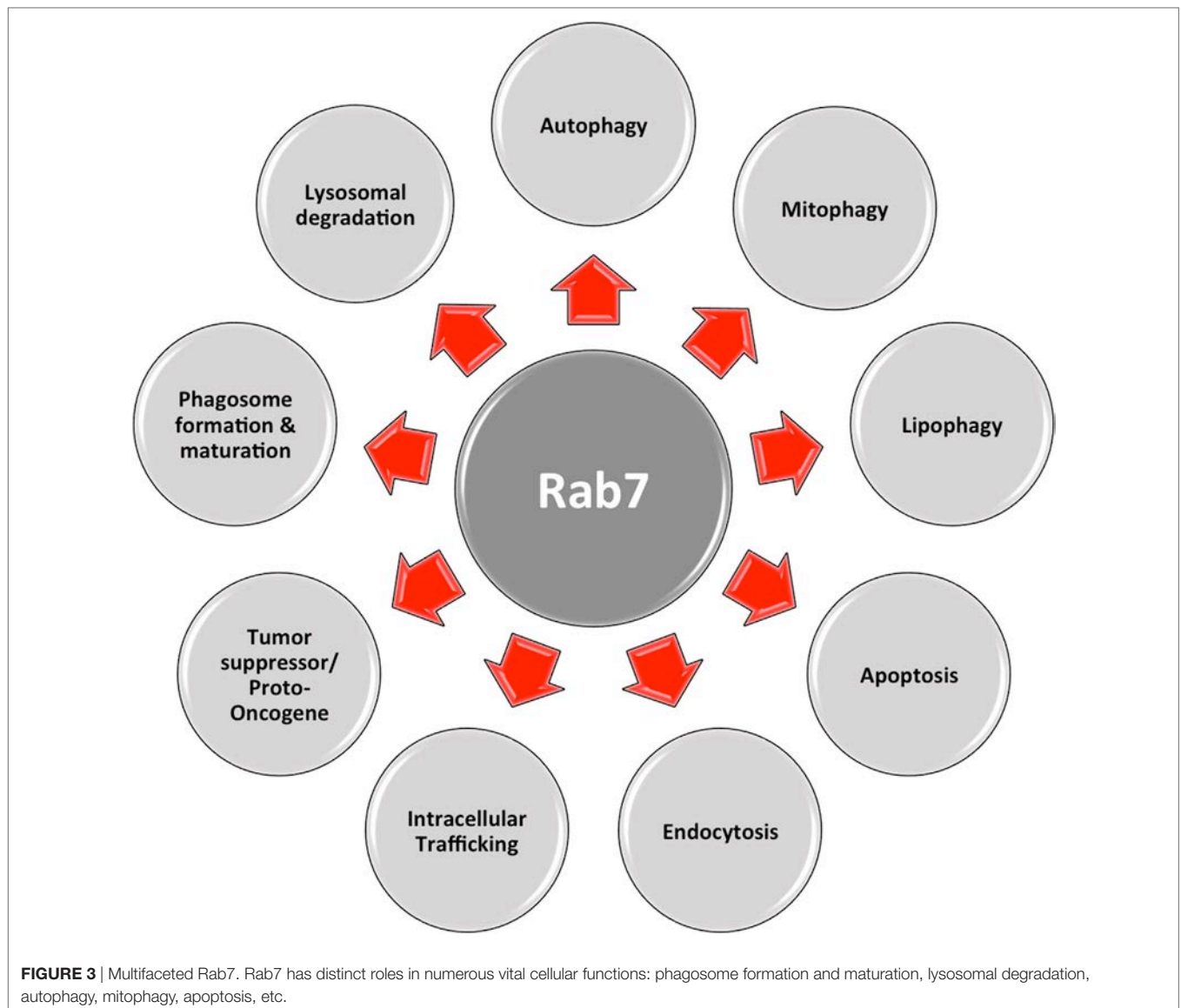
Another important regulator is Rab7, which belongs to the RAB family, a RAS-related group of GTP-binding proteins. This family of proteins includes important regulators of vesicle transportation and is localized in certain intracellular compartments (121). Numerous studies indicate that Rab7 plays major roles in controlling maturation of endosomes and transportation to lysosomes, as well as in phagocytosis, retromere regulation, cytoskeleton regulation, autophagy, and mitophagy (122, 123).

Normally, Rab7 is found on late endosomes and this acquisition is complemented by Rab5 loss, an early endosome marker. The switch from Rab5 to Rab7 is a process in which both proteins cooperate sequentially and dynamically. This determines Rab5 recruitment to early endosomes and Rab7 recruitment

and Rab5 loss at late endosomes (124–126). Late endosomes can fuse with lysosomes and other late endosomes, only if the Rab5 to Rab7 switch is accompanied by variations in fusion and tethering machinery. This allows direct contact in between organelles (127).

Other than being a marker of late endosomes, Rab7 is vital for mitophagy (**Figure 3**), as it is a downstream effector of Parkin (128). This occurs with the help of TBC1D15/17 and Fis1. The first protein belongs to the TBC family (Tre2/Bub2/Cdc16), having RabGAP functions (129, 130), while the latter is a fission protein with cytosolic N-terminal, bound to the OMM at its C-terminal (131, 132). In the absence or inactivity of TBC1D15, membranes that are labeled with LC3 excessively accumulate and lose their cargo orientation. In turn, membrane tubules are sent along microtubule tracks away from the mitochondria. Therefore, it is inferred that, during mitophagy, TBC1D15 binds to Fis1 and LC3 inducing Rab7 activity, which leads to the shaping of the autophagosome isolation membrane. In fact, besides promoting microtubule-associated trafficking and autophagosomal membrane growth, the activity of Rab7 is affected by TBC1D15/17 activity, inducing autophagosomal membrane expansion to correctly surround the mitochondria (128). This indicates that, in case of Parkin-regulated mitophagy, Rab7 is essential for expanding LC3-labeled isolation membranes. Otherwise, inactive Rab7 might help in mediating the release of LC3-positive membranes from microtubules (133). The above-described model substantially differs from the well-known role of Rab7 in controlling autophagosome maturation and fusion with lysosomes (134, 135). In addition, it was shown an increase in the interaction between Rab7 and Mitofusin2 (MFN2), a mitochondrial fusion-related protein, as a response to starvation. This suggests the contribution of Rab7 during autophagosomal membrane maturation, as an adaptor protein used by MFN2 (136). Hence, Rab7 has a dual role in mitophagy, i.e., autophagosome formation and maturation.

As shown in **Figure 3**, this multifaceted small GTPase also participates in other important processes in the cell, such as in apoptosis and the activation of stress response pathways (137). One of these pathways is the mTORC1 pathway, through which mTORC1 moves toward a Rab7-containing compartment in the presence of amino acids (138). The direct interaction between Rab7 and mTOR has been proved by co-immunoprecipitation experiments (139). During bioenergetic stress, several groups showed a Rab7-dependent lysosomal crosstalk with apoptosis and its regulatory machinery, i.e., intramitochondrial recruitment of endolysosomes mediates apoptosis. As explained before, in the presence of growth factors, mTOR and AKT are activated initiating downstream signaling cascades. Under these conditions, nutrient transporter proteins facilitate the import of extracellular nutrients, supporting cellular bioenergetics by supplying the mitochondria with metabolic substrates. In this case, one important apoptotic mediator, cytochrome *c* is retained at the mitochondrial intermembrane. When there is nutrient starvation, these same signaling cascades are silenced, and genes are no longer transcribed. Existing transporters are trafficked to the lysosomes by Rab7, where they are degraded and removed from the cell. This decrease in cellular bioenergetics results in substrate limitation at the mitochondrial site, loss of homeostasis,

FIGURE 3 | Multifaceted Rab7. Rab7 has distinct roles in numerous vital cellular functions: phagosome formation and maturation, lysosomal degradation, autophagy, mitophagy, apoptosis, etc.

and cytochrome *c* release, eventually leading to apoptosis. This process can be rescued by inhibiting Rab7. For example, transporter proteins destined to enter the endocytic pathway and be trafficked to lysosomes for degradation, instead, are recycled and re-expressed on the cellular surface. As a result, extracellular nutrients are continually imported, and cellular bioenergetics is maintained, as well as mitochondrial homeostasis, in the absence of growth factors (140). In this case, Rab7 has a proapoptotic function, by limiting cell autonomous uptake of extracellular nutrients (141).

In cancer, the specific role of Rab7 is not fully understood. In the literature, Rab7 has been depicted as either a tumor suppressor (68, 141, 142) or a proto-oncogene (143–146), depending on tumor type, morphology, and metastatic and invasive abilities (122) (**Figure 3**). Particularly, synergy between HSP90 inhibition and Rab7 depletion decreases EGFR and Her2 levels, through proteasomal degradation, and promotes apoptosis, depicting

a proto-oncogenic role of Rab7 (147, 148). During melanoma development, Myc is activated, inducing Rab7 overexpression. Subsequently, Rab7 expression is downregulated to support the invasive and metastatic characteristics of melanoma (145). Moreover, the knockdown of Rab7 in prostate cancer cells led to the overexpression of c-Met, a protein involved in the promotion of cell invasion and metastasis (149).

In fact, since Rab7 is mainly accountable for intracellular trafficking, which is linked to the metastatic/invasive ability of tumors, and the degradation of many organelles and molecules, such as adhesion molecules and signaling receptors, it is a key regulator in governing cellular homeostasis. Certainly, Rab7 is a central molecule of cell survival, differentiation, and apoptosis. Current data suggest that the regulation of Rab7 expression and activity can reduce several pathologies, such as cancer (122). Of course, further work will be needed to investigate this possibility.

THERAPEUTIC APPROACHES IN CANCER TREATMENT

Cancer cells exhibit a significant number of metabolic alterations associated with mitochondria, lysosomes, and other sub-cellular organelles. These organelles exhibit a number of deregulations, which have been identified as potential drug targets for successful rational drug design and therapy. For their involvement in bio-energetics, redox balancing, and survival, targeting mitochondria for therapeutic benefits is already in practice to induce apoptotic cell death (150, 151). In addition, the advances in lysosome research have highlighted their importance for degradation, signaling pathways, and cell death in pathophysiological conditions; thus, targeting lysosomes has also been considered a new therapeutic strategy for cancer treatment (76).

In this review, we highlighted the interplay between lysosomes and mitochondria and its importance in cell fate. We propose that targeting this crosstalk between both organelles might be crucial for fighting cancer.

Inducing LMP

Indeed, many compounds are described to induce LMP and subsequent cell death in various human cancer cells and animal models but are not in clinical use (152, 153). Besides, little is known about the endogenous inhibitors preventing LMP and which mechanisms suppress lysosomal hydrolases in the cytoplasm of both, normal and cancer cells. Inducing LMP-dependent death could activate self-destructive processes in tumor cells, particularly if those cells were dependent on such inhibitors. Future investigations are needed to clarify if antagonists of LMP inducers may be useful synergistically with the current clinical treatments (64).

Interestingly, a minimally invasive anticancer modality called Photodynamic therapy (PDT) is able to induce LMP. PDT combines a drug (a photosensitizing agent) with a precise light wavelength, inducing ROS generation and killing tumor cells (154). The location where the photosensitizing agent is directed is very important, as it determines where the primary damage occurs. Usually photosensitizing agents accumulate either in mitochondria, inducing rapid apoptosis, or in lysosomes, inducing LMP and subsequent cell death (64). To date, PDT is used for treating or relieving the symptoms of non-small cell lung cancer patients and esophageal cancer patients. PDT still presents some limitations, since only tumors on the skin or just underneath it, or in internal organ linings and/or cavities can be treated with this technique. But it cannot be used for treating large tumors or metastasis (155–158).

Targeting Mitophagy

Targeting mitophagy as an approach to adjuvant chemotherapy has been already questioned by Chourasia et al. (107). They claim that the deletion or inhibition of Parkin and BNIP3 induces the Warburg effect, thus favoring tumorigenesis. Nevertheless, acute chemical inhibition of mitophagy is still an effective approach for advanced tumors that have switched to glycolytic metabolism but still depend on mitochondria for further metabolic purposes (107). Of course, this approach has still to be therapeutically tested.

Targeting Common Effectors between Mitochondria and Lysosomes

Other than targeting processes in which mitochondria and lysosomes are linked, inhibitors of their main common effectors, i.e., AMPK or mTOR have been already tested for cancer therapy. The role of AMPK in cancer cells is paradoxical. It can be a tumor suppressor, but can also promote tumorigenesis, stimulating cell survival in glucose-deficient situations and preserving metabolic homeostasis (117). Despite that, the use of the anti-diabetic drug Metformin, non-steroidal anti-inflammatory drugs, such as Aspirin, AICAR, and some natural products known to be AMPK activators, has shown to decrease tumorigenesis in animal models and cancer cell lines (159, 160). In addition, preclinical evidence suggests that Metformin appears to prevent the proliferation and growth of certain tumor types. There are currently more than 100 ongoing or clinical studies assessing the role of metformin in the therapy cancer (161, 162). It is well understood that metformin targets the mitochondrial complex I. However, it has been suggested that metformin could directly influence the V-ATPase activity of lysosomes (163), so this fact further supports the importance of lysosomal–mitochondrial link for cancer treatment.

Targeting mTOR may be crucial for cancer treatment not only for cell growth and proliferation but also for reversing the Warburg effect characteristic of tumor cells (164). At the molecular level, mTORC1 inhibition may induce mitochondrial biogenesis *via* PGC-1α, as well as repression of transcription of mitochondrial genes *via* 4E-BP1 (114) depending on the model. mTORC1 inhibition induces lysosomal biogenesis and also initiates several feedback loops to upstream pathways, activation of which might be beneficial for the survival of tumor cells and metastasis. The best-known mTOR inhibitor is Rapamycin, which does not inhibit directly mTOR's kinase (catalytic) activity. Together with FKBP12, it binds specifically to mTORC1 (at high concentrations also to mTORC2). The binding occurs next to the kinase active site. Consequently, it can only inhibit a number of mTORC1 functions. Given this, and the importance of mTOR for cancer, several groups have developed other inhibitors to target mTOR's catalytic subunit (PP242, Torin 1 and 2, etc.). As reviewed by Xie and al., some mTOR inhibitors are already in clinical trials for treating cancer (165). Despite that, the utility of such inhibitors in oncology still appears to be limited, given that autophagy can be induced by mTOR inhibition, thus promoting cancer cell survival.

As reviewed above, RAB7 is a prominent target for cancer treatment (143). In addition, there are already drugs that target RAB7. It has been shown that liensinine, a major isoquinoline alkaloid that inhibits RAB7A recruitment to lysosomes, not autophagosomes. In this way, autophagy/mitophagy is impaired, enhancing the efficacy of chemotherapy in breast cancer cell lines (166).

Using Nanomedicine for Inducing Cell Death

Nanotechnology is the science of controlling matter, at the molecular level, to generate devices with new biological, physical, and/or chemical characteristics. It is in the spotlight of therapeutic

innovation. The use of nanomaterial is a particularly promising tool not only to improve the diagnosis but also to generate new cancer treatments and overcome the drawbacks of traditional therapies (167). In particular, the discovery of gold nanorods (GNRs) has provided a new method to induce apoptosis specifically in cancer cells, while posing a negligible impact on normal cells. They are able to induce apoptosis in cancer cells through lysosomal permeability, as indicated by cathepsin D release, and a decrease in mitochondrial membrane potential (168). These findings are promising for the further implementation of nanotechnology at the clinical practice.

CONCLUSION AND FUTURE PERSPECTIVES

Intracellular organelles, as thoroughly discussed, are the major players of cellular networks. Even though physical contact among these organelles was exhaustively described through out the years, research is now shifting toward revealing the crosstalk of these entities on the signaling levels, as well as their physiological relevance. Mainly, organelle interactions are needed for metabolite exchange, and more interestingly, in membrane dynamics, intracellular organelle distribution, and the assembly of dynamic signaling platforms depending on cellular requirements.

In tumors, cells significantly display metabolic aberrations, associated directly or indirectly with mitochondria and lysosomes. These anomalies promote cancer cell growth and survival, while exhibiting distinctive properties that render cancer cells vulnerable to specific anticancer agents. In other words, the deregulation of these organelles in cancer cells as compared to their counterparts in healthy cells is a main reason for promising targeted drug therapy. Though substantial advancement has been made regarding elucidating the role of these anomalies in oncogenesis and chemotherapy-resistance, a better interpretation of the main pathophysiological differences between organelles of

normal and tumor cells can undoubtedly compliment the efforts to improve selective targeted anti-cancer agents.

Lysosomes and mitochondria have common regulators and can physically interact to maintain cell homeostasis or induce cell death. However, in cancer everything becomes a paradox; all of the processes in which lysosomes and mitochondria interact, except for LMP, and the common regulators (mTOR, AMPK, Rab7, etc.) present a dual role: on the one hand, they can promote tumorigenesis and, on the other hand, they can induce cell death. The relative contribution of these pathways would depend on tumor type, state, metastatic ability, microenvironment, metabolic reprograming, etc. This reflects the importance of these two organelles for cancer treatment. New potential targets have been proposed, i.e., PGC-1α, TFEB, Rab7, etc. However, will these targets overpass the problem of having a paradoxical role in cancer treatment? As we have seen already, every case needs to be studied independently, in order to predict whether the treatment would be beneficial or not. This is known as personalized medicine.

AUTHOR CONTRIBUTIONS

LC, AN, and LC discussed the ideas and wrote the paper.

ACKNOWLEDGMENT

FUNDING

REFERENCES

1. Pavlova NN, Thompson CB. The emerging hallmarks of cancer metabolism. *Cell Metab* (2016) 23:27–47. doi:10.1016/j.cmet.2015.12.006

2. Drabu S, Khatri S, Babu S, Verma D. Nanotechnology: an introduction to future drug delivery system. *J Chem Pharm Res* (2010) 2(1):444–57.

3. Sakhrani NM, Padh H. Organelle targeting: third level of drug targeting. *Drug Des Devel Ther* (2013) 7:585–99. doi:10.2147/DDDT.S45614

4. Cheng SM, Boddapati SV, D'Souza G, Weissig V. DQAsomes as mitochondria-targeted nanocarries for anti-cancer drugs. *Nanotechnol Cancer Ther* (2006) 38:787–802. doi:10.1201/9781420006636.ch38

5. Rajendran L, Knolker HJ, Simons K. Subcellular targeting strategies for drug design and delivery. *Nat Revi Drug Discov* (2010) 9(1):29–42. doi:10.1038/nrd2897

6. Flierl A, Jackson C, Cottrell B, Murdock D, Seibel P, Wallace DC. Targeted delivery of DNA to the mitochondrial compartment via import sequence-conjugated peptide nucleic acid. *Mol Ther* (2003) 7(4):550–7. doi:10.1016/S1525-0016(03)00037-6

7. Antico Arciuch VG, Elguero ME, Poderoso JJ, Carreras MC. Mitochondrial regulation of cell cycle and proliferation. *Antioxid Redox Signal* (2012) 16(10):1150–80. doi:10.1089/ars.2011.4085

8. Detmer SA, Chan DC. Functions and dysfunctions of mitochondrial dynamics. *Nat Rev Mol Cell Biol* (2007) 8:870–9. doi:10.1038/nrm2275

9. Frezza C. Mitochondrial metabolites: undercover signalling molecules. *Interface Focus* (2017) 7:1–6. doi:10.1098/rsfs.2016.0100

10. Rizzuto R, De Stefani D, Raffaello A, Mammucari C. Mitochondria as sensors and regulators of calcium signalling. *Nat Rev Mol Cell Biol* (2012) 13:566–78. doi:10.1038/nrm3412

11. Tait SWG, Green DR. Mitochondria and cell death: outer membrane permeabilization and beyond. *Nat Rev Mol Cell Biol* (2010) 11:621–32. doi:10.1038/nrm2952

12. Schieber M, Chandel NS. ROS function in redox signaling and oxidative stress. *Curr Biol* (2014) 24:453–62. doi:10.1016/j.cub.2014.03.034

13. Menzies KJ, Zhang H, Katsyuba E, Auwerx J. Protein acetylation in metabolism – metabolites and cofactors. *Nat Rev Endocrinol* (2016) 12:43–60. doi:10.1038/nrendo.2015.181

14. Sullivan LB, Gui DY, Heiden MGV. Altered metabolite levels in cancer: implications for tumour biology and cancer therapy. *Nat Rev Cancer* (2016) 16:680–93. doi:10.1038/nrc.2016.85

15. Arnoult D, Carneiro L, Tattoli I, Girardin SE. The role of mitochondria in cellular defense against microbial infection. *Semin Immunol* (2009) 21:223–32. doi:10.1016/j.smim.2009.05.009

16. Fillano JJ, Goldenthal MJ, Rhodes CH, Marin-Garcia J. Mitochondrial dysfunction in patients with hypotonia, epilepsy, autism, and developmental delay: HEADD syndrome. *J Child Neurol* (2002) 17:435–9. doi:10.1177/088307380201700607

17. Oka T, Hikoso S, Yamaguchi O, Taneike M, Takeda T, Tamai T, et al. Mitochondrial DNA that escapes from autophagy causes inflammation and heart failure. *Nature* (2012) 485:251–5. doi:10.1038/nature10992

18. Zsurka G, Kunz WS. Mitochondrial dysfunction and seizures: the neuronal energy crisis. *Lancet Neurol* (2015) 14:956–66. doi:10.1016/S1474-4422(15)00148-9

19. Vyas S, Zaganjor E, Haigis MC. Mitochondria and cancer. *Cell* (2016) 166:555–66. doi:10.1016/j.cell.2016.07.002

20. Warburg O. The metabolism of carcinoma cells. *J Cancer Res* (1925) 9:148–63. doi:10.1158/jcr.1925.148

21. Senyilmaz D, Teleman AA. Chicken or the egg: Warburg effect and mitochondrial dysfunction. *F1000Prime Rep* (2015) 7(41):1–13. doi:10.12703/P7-41

22. Jornayvaz FR, Shulman GI. Regulation of mitochondrial biogenesis. *Essays Biochem* (2010) 47:69–84. doi:10.1042/bse0470069

23. Puigserver P, Wu Z, Park CW, Graves R, Wright M, Spiegelman BM. A cold-inducible coactivator of nuclear receptors linked to adaptive thermogenesis. *Cell* (1998) 92(6):829–39. doi:10.1016/S0092-8674(00)81410-5

24. Zhang Y, Ba Y, Liu C, Sun G, Ding L, Gao S, et al. PGC-1alpha induces apoptosis in human epithelial ovarian cancer cells through a PPARgamma-dependent pathway. *Cell Res* (2007) 17(4):363–73. doi:10.1038/cr.2007.11

25. Luo C, Lim JH, Lee Y, Granter SR, Thomas A, Vazquez F, et al. A PGC1α-mediated transcriptional axis suppresses melanoma metastasis. *Nature* (2016) 537(7620):422–6. doi:10.1038/nature19347

26. Torrano V, Valcarcel-Jimenez L, Cortazar AR, Liu X, Urosevic J, Castillo-Martin M, et al. The metabolic co-regulator PGC1α suppresses prostate cancer metastasis. *Nat Cell Biol* (2016) 18(6):645–56. doi:10.1038/ncb3357

27. Tan Z, Luo X, Xiao L, Tang M, Bode AM, Dong Z, et al. The role of PGC1α in cancer metabolism and its therapeutic implications. *Mol Cancer Ther* (2016) 15:774–82. doi:10.1158/1535-7163.MCT-15-0621

28. LeBleu VS, O'Connell JT, Gonzalez Herrera KN, Wikman H, Pantel K, Haigis MC, et al. PGC1α mediates mitochondrial biogenesis and oxidative phosphorylation in cancer cells to promote metastasis. *Nat Cell Biol* (2014) 16:992–1015. doi:10.1038/ncb3039

29. Li F, Wang Y, Zeller KI, Potter JJ, Wonsey DR, O'Donnell KA, et al. Myc stimulates nuclearly encoded mitochondrial genes and mitochondrial biogenesis. *Mol Cell Biol* (2005) 25:6225–34. doi:10.1128/MCB.25.14.6225-6234.2005

30. Morita M, Gravel SP, Hulea L, Larsson O, Pollak M, St-Pierre J, et al. mTOR coordinates protein synthesis, mitochondrial activity and proliferation. *Cell Cycle* (2015) 14:473–80. doi:10.4161/15384101.2014.991572

31. Senft D, Ronai ZA. Regulators of mitochondrial dynamics in cancer. *Curr Opin Cell Biol* (2016) 39:43–52. doi:10.1016/j.ceb.2016.02.001

32. Serasinghe MN, Wieder SY, Renault TT, Elkholi R, Asciolla JJ, Yao JL, et al. Mitochondrial division is requisite to RAS-induced transformation and targeted by oncogenic MAPK pathway inhibitors. *Mol Cell* (2015) 51:521–36. doi:10.1016/j.molcel.2015.01.003

33. Graves JA, Wang Y, Sims-Lucas S, Cherok E, Rothermund K, Branca MF, et al. Mitochondrial structure, function and dynamics are temporally controlled by c-Myc. *PLoS One* (2012) 7(5):e37699. doi:10.1371/journal.pone.0037699

34. Wang C, Youle RJ. The role of mitochondria in apoptosis. *Annu Rev Genet* (2009) 43:95–119. doi:10.1146/annurev-genet-102108-134850

35. Renault TT, Floros KV, Elkholi R, Corrigan KA, Kushnareva Y, Wieder SY, et al. Mitochondrial shape governs BAX-induced membrane permeabilization and apoptosis. *Mol Cell* (2015) 57:69–82. doi:10.1016/j.molcel.2014.10.028

36. Christofk HR, Vander Heiden MG, Harris MH, Ramanathan A, Gerszten RE, Wei R, et al. The M2 splice isoform of pyruvate kinase is important for cancer metabolism and tumour growth. *Nature* (2008) 452:230–3. doi:10.1038/nature06734

37. Schell JC, Olson KA, Jiang L, Hawkins AJ, Van Vranken JG, Xie J, et al. A role for the mitochondrial pyruvate carrier as a repressor of Warburg effect and colon cancer cell growth. *Mol Cell* (2014) 56:400–13. doi:10.1016/j.molcel.2014.09.026

38. Mullen AR, Wheaton WW, Jin ES, Chen PH, Sullivan LB, Cheng T, et al. Reductive carboxylation supports growth in tumour cells with detective mitochondria. *Nature* (2011) 481:385–8. doi:10.1038/nature10642

39. van Gisbergen MW, Voets AM, Starmans MH, de Coo IF, Yadak R, Hoffmann RF, et al. How do changes in the mtDNA and mitochondrial dysfunction influence cancer and cancer therapy? Challenges, opportunities and models. *Mutat Res Rev Mutat Res* (2015) 764:16–30. doi:10.1016/j.mrrev.2015.01.001

40. Dang L, White DW, Gross S, Bennett BD, Bittinger MA, Driggers EM, et al. Cancer-associated IDH1 mutations produce 2-hydroxyglutarate. *Nature* (2009) 462:739–44. doi:10.1038/nature08617

41. Ward PS, Patel J, Wise DR, Abdel-Wahab O, Bennett BD, Coller HA, et al. The common feature of leukemia-associated IDH1 and IDH2 mutations is a neomorphic enzyme activity converting alpha-ketoglutarate to 2-hydroxyglutarate. *Cancer Cell* (2010) 17:225–34. doi:10.1016/j.ccr.2010.01.020

42. Reznik E, Miller ML, Şenbabaoğlu Y, Riaz N, Sarungbam J, Tickoo SK, et al. Mitochondrial DNA copy number variation across human cancers. *Elife* (2016) 5:1–20. doi:10.7554/eLife.10769

43. Birsoy K, Wang T, Chen WW, Freinkman E, Abu-Remaileh M, Sabatini DM. An essential role of the mitochondrial electron transport chain in cell proliferation is to enable aspartate synthesis. *Cell* (2015) 162(3):540–51. doi:10.1016/j.cell.2015.07.016

44. Aits S, Jaattela M. Lysosomal cell death at a glance. *J Cell Sci* (2013) 126:1905–12. doi:10.1242/jcs.091181

45. de Duve C, Pressman BC, Gianetto R, Wattiaux R, Appelmans F. Tissue fractionation studies: intracellular distribution patterns of enzymes in rat-liver tissue. *Biochem J* (1955) 60(4):604–17. doi:10.1042/bj0600604

46. Cooper GM. *The Cell: A Molecular Approach.* Sunderland, MA: Sinauer Associates (2000).

47. Morgan AJ, Platt FM, Lloyd-Evans E, Galione A. Molecular mechanisms of endolysosomal Ca2+ signalling in health and disease. *Biochem J* (2011) 439(3):349–74. doi:10.1042/BJ20110949

48. Settembre C, Fraldi A, Medina DL, Ballabio A. Signals from the lysosome: a control centre for cellular clearance and energy metabolism. *Nat Rev Mol Cell Biol* (2013) 14:283–96. doi:10.1038/nrm3565

49. Zoncu R, Bar-Peled L, Efeyan A, Wang S, Sancak Y, Sabatini DM. mTORC1 senses lysosomal amino acids through an inside-out mechanism that requires the vacuolar H(+)-ATPase. *Science* (2011) 334(6056):678–83. doi:10.1126/science.1207056

50. Bar-Peled L, Sabatini DM. Regulation of mTORC1 by amino acids. *Trends Cell Biol* (2014) 24(7):400–6. doi:10.1016/j.tcb.2014.03.003

51. Dibble CC, Cantley LC. Regulation of mTORC1 by PI3K signaling. *Trends Cell Biol* (2015) 25(9):545–55. doi:10.1016/j.tcb.2015.06.002

52. Shimobayashi M, Hall MN. Multiple amino acid sensing inputs to mTORC1. *Cell Res* (2016) 26:7–20. doi:10.1038/cr.2015.146

53. Demetriades C, Doumpas N, Teleman AA. Regulation of TORC1 in response to amino acid starvation via lysosomal recruitment of TSC2. *Cell* (2014) 156(4):786–99. doi:10.1016/j.cell.2014.01.024

54. Zheng L, Zhang W, Zhou Y, Li F, Wei H, Peng J. Recent advances in understanding amino acid sensing mechanisms that regulate mTORC1. *Int J Mol Sci* (2016) 17(10):1635–50. doi:10.3390/ijms17101636

55. Sardiello M, Palmieri M, di Ronza A, Medina DL, Valenza M, Gennarino VA, et al. A gene network regulating lysosomal biogenesis and function. *Science* (2009) 325(5939):473–7. doi:10.1126/science.1174447

56. Pópulo H, Lopes JM, Soares P. The mTOR signalling pathway in human cancer. *Int J Mol Sci* (2012) 13(2):1886–918. doi:10.3390/ijms13021886

57. Dibble CC, Manning BD. Signal integration by mTORC1 coordinates nutrient input with biosynthetic output. *Nat Cell Biol* (2013) 15:555–64. doi:10.1038/ncb2763

58. Francipane MG, Lagasse E. mTOR pathway in colorectal cancer: an update. *Oncotarget* (2014) 5(1):49–66. doi:10.18632/oncotarget.1548

59. Hare SH, Harvey AJ. mTOR function and therapeutic targeting in breast cancer. *Am J Cancer Res* (2017) 7(3):383–404.

60. Tardy C, Codogno P, Autefage H, Levade H, Andrieu-Abadie N. Lysosomes and lysosomal proteins in cancer cell death (new players of an old struggle). *Biochim Biophys Acta* (2006) 1765(2):101–25. doi:10.1016/j.bbcan.2005.11.003

61. Alayev A, Holz MK. mTOR signaling for biological control and cancer. *J Cell Physiol* (2013) 228(8):1658–64. doi:10.1002/jcp.24351

62. Hämälistö S, Jäättelä M. Lysosomes in cancer—living on the edge (of the cell). *Curr Opin Cell Biol* (2016) 39:69–76. doi:10.1016/j.ceb.2016.02.009

63. Korolchuk VI, Saiki S, Lichtenberg M, Siddiqi FH, Roberts EA, Imarisio S, et al. Lysosomal positioning coordinates cellular nutrient responses. *Nat Cell Biol* (2011) 13(4):453–60. doi:10.1038/ncb2204

64. Boya P, Kroemer G. Lysosomal membrane permeabilization in cell death. *Oncogene* (2008) 27:6434–51. doi:10.1038/onc.2008.310

65. Kirkegaard T, Jäättelä M. Lysosomal involvement in cell death and cancer. *BBA Mol Cell Res* (2009) 1793(4):746–54. doi:10.1016/j.bbamcr.2008.09.008

66. Kallunki T, Olsen OD, Jaattela M. Cancer-associated lysosomal changes: friends or foes? *Oncogene* (2013) 32:1995–2004. doi:10.1038/onc.2012.292

67. Xu H, Ren D. Lysosomal physiology. *Ann Rev Physiol* (2015) 77:57–80. doi:10.1146/annurev-physiol-021014-071649

68. Steffan JJ, Dykes SS, Coleman DT, Adams LK, Rogers D, Carroll JL, et al. Supporting a role for the GTPase Rab7 in prostate cancer progression. *PLoS One* (2014) 9(2):e87882. doi:10.1371/journal.pone.0087882

69. Friedl P, Wolf K. Tumor-cell invasion and migration: diversity and escape mechanisms. *Nat Rev Cancer* (2003) 3(5):362–74. doi:10.1038/nrc1075

70. Friedl P, Wolf K. Tube travel: the role of proteases in individual and collective cancer cell invasion. *Cancer Res* (2008) 68(18):7247–9. doi:10.1158/0008-5472.CAN-08-0784

71. Liu Y, Zhou Y, Zhu K. Inhibition of glioma cell lysosome exocytosis inhibits glioma invasion. *PLoS One* (2012) 7:e45910. doi:10.1371/journal.pone.0045910

72. Mohamed MM, Sloane BF. Cysteine cathepsins: multifunctional enzymes in cancer. *Nat Rev Cancer* (2006) 6(10):764–75. doi:10.1038/nrc1949

73. Sameni M, Moin K, Sloane BF. Imaging proteolysis by living human breast cancer cells. *Neoplasia* (2000) 2:496–504. doi:10.1038/sj.neo.7900116

74. Lopez-Otin C, Matrisian LM. Emerging roles of proteases in tumour suppression. *Nat Rev Cancer* (2007) 7:800–8. doi:10.1038/nrc2228

75. Jäättelä M. Multiple cell death pathways as regulators of tumour initiation and progression. *Oncogene* (2004) 23:2746–56. doi:10.1038/sj.onc.1207513

76. Piao S, Amaravadi RK. Targeting the lysosome in cancer. *Ann N Y Acad Sci* (2016) 1371(1):45–54. doi:10.1111/nyas.12953

77. Furuta K, Ikeda M, Nakayama Y, Nakamura K, Tanaka M, Hamasaki N, et al. Expression of lysosome-associated membrane proteins in human colorectal neoplasms and inflammatory diseases. *Am J Pathol* (2001) 159(2):449–55. doi:10.1016/S0002-9440(10)61716-6

78. Dettmer J, Hong-Hermesdorf A, Stierhof YD, Schumacher K. Vacuolar H+-ATPase activity is required for endocytic and secretory trafficking in arabidopsis. *Plant Cell* (2006) 18(3):715–30. doi:10.1105/tpc.105.037978

79. Meo-Evoli N, Almacellas E, Massucci FA, Gentilella A, Ambrosio S, Kozma SC, et al. V-ATPase: a master effector of E2F1-mediated lysosomal trafficking, mTORC1 activation and autophagy. *Oncotarget* (2015) 6(29):28057–70. doi:10.18632/oncotarget.4812

80. Gotink KJ, Broxterman HJ, Labots M, de Haas RR, Dekker H, Honeywell RJ, et al. Lysosomal sequestration of sunitinib: a novel mechanism of drug resistance. *Clin Cancer Res* (2011) 17(23):7337–46. doi:10.1158/1078-0432.CCR-11-1667

81. Cirman T, Oresič K, Mazovec GD, Turk V, Reed JC, Myers RM, et al. Selective disruption of lysosomes in HeLa cells triggers apoptosis mediated by cleavage of Bid by multiple papain-like lysosomal cathepsins. *J Biol Chem* (2004) 279(5):3578–87. doi:10.1074/jbc.M308347200

82. Kroemer G, Jäättelä M. Lysosomes and autophagy in cell death control. *Nat Rev Cancer* (2005) 5:886–97. doi:10.1038/nrc1738

83. Boya P, Andreau K, Poncet D, Zamzami N, Perfettini JL, Metivier D, et al. Lysosomal membrane permeabilization induces cell death in a mitochondrion-dependent fashion. *J Exp Med* (2003) 197(10):1323–34. doi:10.1084/jem.20021952

84. Kuwana T, Bouchier-Hayes L, Chipuk JE, Bonzon C, Sullivan BA, Green DR, et al. BH3 domains of BH3-only proteins differentially regulate Bax-mediated mitochondrial membrane permeabilization both directly and indirectly. *Mol Cell* (2005) 17(4):525–35. doi:10.1016/j.molcel.2005.02.003

85. Kågedal K, Johansson AC, Johansson U, Heimlich G, Roberg K, Wang NS, et al. Lysosomal membrane permeabilization during apoptosis—involvement of Bax? *Int J Exp Pathol* (2005) 86(5):309–21. doi:10.1111/j.0959-9673.2005.00442.x

86. Feldstein AE, Werneburg NW, Li Z, Bronk SF, Bronk SF, Gores GJ. Bax inhibition protects against free fatty acid-induced lysosomal permeabilization. *Am J Physiol Gastrointest Liver Physiol* (2006) 290(6):G1339–46. doi:10.1152/ajpgi.00509.2005

87. Jäättelä M, Tschopp J. Caspase-independent cell death in T lymphocytes. *Nat Immunol* (2003) 4(5):416–23. doi:10.1038/ni0503-416

88. Bidère N, Lorenzo HK, Carmona S, Laforge M, Harper F, Dumont C, et al. Cathepsin D triggers bax activation, resulting in selective apoptosis-inducing factor (AIF) relocation in T lymphocytes entering the early commitment phase to apoptosis. *J Biol Chem* (2003) 278(33):31401–11. doi:10.1074/jbc.M301911200

89. Glunde K, Guggino SE, Solaiyappan M, Pathak AP, Ichikawa Y, Bhujwalla ZM. Extracellular acidification alters lysosomal trafficking in human breast cancer cells. *Neoplasia* (2003) 5(6):533–45. doi:10.1016/S1476-5586(03)80037-4

90. Ono K, Kim SO, Han J. Susceptibility of lysosomes to rupture is a determinant for plasma membrane disruption in tumor necrosis factor alpha-induced cell death. *Mol Cell Biol* (2003) 23(2):665–76. doi:10.1128/MCB.23.2.665-676.2003

91. Eaton JW, Qian M. Molecular bases of cellular iron toxicity. *Free Radic Biol Med* (2002) 32(9):833–40. doi:10.1016/S0891-5849(02)00772-4

92. Gyrd-Hansen M, Nylandsted J, Jäättelä M. Heat shock protein 70 promotes cancer cell viability by safeguarding lysosomal integrity. *Cell Cycle* (2004) 3(12):1484–5. doi:10.4161/cc.3.12.1287

93. White E, Mehnert JM, Chan CS. Autophagy, metabolism, and cancer. *Clin Cancer Res* (2015) 21(22):5037–46. doi:10.1158/1078-0432.CCR-15-0490

94. Lorin S, Hamaï A, Mehrpour M, Codogno P. Autophagy regulation and its role in cancer. *Semin Cancer Biol* (2013) 23:361–79. doi:10.1016/j.semcancer.2013.06.007

95. Kroemer G, Levine B. Autophagic cell death: the story of a misnomer. *Nat Rev Mol Cell Biol* (2008) 9(12):1004–10. doi:10.1038/nrm2529

96. Yang S, Wang X, Contino G, Liesa M, Sahin E, Ying H, et al. Pancreatic cancers require autophagy for tumor growth. *Genes Dev* (2011) 25(7):717–29. doi:10.1101/gad.2016111

97. Klionsky DJ, Cuervo AM, Seglen PO. Methods for monitoring autophagy from yeast to human. *Autophagy* (2007) 3(3):181–206. doi:10.4161/auto.3678

98. Pankiv S, Clausen TH, Lamark T, Brech A, Bruun JA, Outzen H, et al. p62/SQSTM1 binds directly to Atg8/LC3 to facilitate degradation of ubiquitinated protein aggregates by autophagy. *J Biol Chem* (2007) 282(33):24131–45. doi:10.1074/jbc.M702824200

99. Gong Y, Zack TI, Morris LG, Lin K, Hukkelhoven E, Raheja R, et al. Pan-cancer genetic analysis identifies PARK2 as a master regulator of G1/S cyclins. *Nat Genet* (2014) 46:588–94. doi:10.1038/ng.2981

100. Palikaras K, Tavernarakis N. Measuring oxygen consumption rate in caenorhabditis elegans. *Bio Protoc* (2016) 6:23. doi:10.21769/BioProtoc.2049

101. Zhang C, Lee S, Peng Y, Bunker E, Giaime E, Shen J, et al. PINK1 triggers autocatalytic activation of parkin to specify cell fate decisions. *Curr Biol* (2014) 18(24):1854–65. doi:10.1016/j.cub.2014.07.014

102. Esteban-Martínez L, Doménech E, Boya P, Salazar-Roa M, Malumbres M. Mitophagy in mitosis: more than a myth. *Autophagy* (2015) 11(12):2379–80. doi:10.1080/15548627.2015.1108509

103. Chourasia AH, Macleod KF. Tumor suppressor functions of BNIP3 and mitophagy. *Autophagy* (2015) 11(10):1937–8. doi:10.1080/15548627.2015.1085136

104. Bernardini JP, Lazarou M, Dewson G. Parkin and mitophagy in cancer. *Oncogene* (2017) 36(10):1315–27. doi:10.1038/onc.2016.302

105. Drake LE, Springer MZ, Poole LP, Kim CJ, Macleod KF. Expanding perspectives on the significance of mitophagy in cancer. *Semin Cancer Biol* (2017) S1044-579X(17):30102–5. doi:10.1016/j.semcancer.2017.04.008

106. Palikaras K, Lionaki E, Tavernarakis N. Mitophagy: in sickness and in health. *Mol Cell Oncol* (2016) 3(1):1–2. doi:10.1080/23723556.2015.1056332

107. Chourasia AH, Boland ML, Macleod KF. Mitophagy and cancer. *Cancer Metab* (2015) 3(4):1–11. doi:10.1186/s40170-015-0130-8

108. Melser S, Chatelain EH, Lavie J, Mahfouf W, Jose C, Obre E, et al. Rheb regulates mitophagy induced by mitochondrial energetic status. *Cell Metab* (2013) 17(5):719–30. doi:10.1016/j.cmet.2013.03.014

109. Li Y, Wang Y, Kim E, Beemiller P, Wang CY, Swanson J, et al. Bnip3 mediates the hypoxia-induced inhibition on mTOR by interacting with Rheb. *J Biol Chem* (2007) 282(49):35803–13. doi:10.1074/jbc.M705231200

110. Palikarasa K, Daskalakia I, Markaki M, Tavernarakisa N. Mitophagy and age-related pathologies: development of new therapeutics by targeting mitochondrial turnover. *Pharmacol Ther* (2017). doi:10.1016/j.pharmthera.2017.04.005

111. Chang JY, Yi HS, Kim HW, Shong M. Dysregulation of mitophagy in carcinogenesis and tumor progression. *Biochim Biophys Acta* (2017) 1858(8):633–40. doi:10.1016/j.bbabio.2016.12.008

112. Huang Y, Shen P, Chen X, Chen Z, Zhao T, Chen N, et al. Transcriptional regulation of BNIP3 by Sp3 in prostate cancer. *Prostate* (2015) 75(14):1556–67. doi:10.1002/pros.23029

113. Kulikov AV, Luchkina EA, Gogvadze V, Zhivotovsky B. Mitophagy: link to cancer development and therapy. *Biochem Biophys Res Commun* (2017) 482(3):432–9. doi:10.1016/j.bbrc.2016.10.088

114. Morita M, Gravel SP, Chénard V, Sikström K, Zheng L, Alain T, et al. Mtorc1 controls mitochondrial activity and biogenesis through 4E-BP-dependent translational regulation. *Cell Metab* (2013) 18(5):698–711. doi:10.1016/j.cmet.2013.10.001

115. Settembre C, De Cegli R, Mansueto G, Saha PK, Vetrini F, Visvikis O, et al. TFEB controls cellular lipid metabolism through a starvation-induced autoregulatory loop. *Nat Cell Biol* (2013) 15(6):647–58. doi:10.1038/ncb2718

116. Hardie DG, Carling D. The AMP-activated protein kinase – fuel gauge of the mammalian cell? *Eur J Biochem* (1997) 246(2):259–73. doi:10.1111/j.1432-1033.1997.00259.x

117. Chaube B, Malvi P, Singh SV, Mohammad N, Violle B, Bhat MK. AMPK maintains energy homeostasis and survival in cancer cells via regulating p38/PGC-1ALPHA-mediated mitochondrial biogenesis. *Cell Death Discov* (2015) 1(15063):1–11. doi:10.1038/cddiscovery.2015.63

118. Kahn BB, Alquier T, Carling D, Hardie DG. AMP-activated protein kinase: ancient energy gauge provides clues to modern understanding of metabolism. *Cell Metab* (2005) 1(1):15–25. doi:10.1016/j.cmet.2004.12.003

119. Desai BN, Myers BR, Schreiber SL. FKBP12-rapamycin-associated protein associates with mitochondria and senses osmotic stress via mitochondrial dysfunction. *Proc Natl Acad Sci U S A* (2002) 99(7):4319–24. doi:10.1073/pnas.261702698

120. Liesa M, Shirihai OS. Mitochondrial dynamics in the regulation of nutrient utilization and energy expenditure. *Cell Metab* (2013) 17(4):491–506. doi:10.1016/j.cmet.2013.03.002

121. Agola JO, Jim PA, Ward HH, Basuray S, Wandinger-Ness A. Rab GTPases as regulators of endocytosis, targets of disease and therapeutic opportunities. *Clin Genet* (2011) 80(4):305–18. doi:10.1111/j.1399-0004.2011.01724.x

122. Guerra F, Bucci C. Multiple roles of the small GTPase Rab7. *Cells* (2016) 5(3):34–62. doi:10.3390/cells5030034

123. Zhang M, Chen L, Wang S, Wang T. Rab7: roles in membrane trafficking and disease. *Biosci Rep* (2009) 29(3):193–209. doi:10.1042/BSR20090032

124. Rink J, Ghigo E, Kalaidzidis Y, Zerial M. Rab conversion as a mechanism of progression from early to late endosomes. *Cell* (2005) 122(5):735–49. doi:10.1016/j.cell.2005.06.043

125. Vonderheit A, Helenius A. Rab7 associates with early endosomes to mediate sorting and transport of Semliki orest virus to late endosomes. *PLoS Biol* (2005) 3(7):e233. doi:10.1371/journal.pbio.0030233

126. Poteryaev D, Datta S, Ackema K, Zerial M, Spang A. Identification of the switch in early-to-late endosome transition. *Cell* (2010) 141(3):497–508. doi:10.1016/j.cell.2010.03.011

127. Luzio JP, Pryor PR, Bright NA. Lysosomes: fusion and function. *Nat Rev Mol Cell Biol* (2007) 8:622–32. doi:10.1038/nrm2217

128. Yamano K, Fogel AI, Wang C, van der Bliek AM, Youle RJ. Mitochondrial Rab GAPs govern autophagosome biogenesis during mitophagy. *Elife* (2014) 3:1–24. doi:10.7554/eLife.01612

129. Frasa MA, Koessmeier KT, Ahmadian MR, Braga VM. Illuminating the functional and structural repertoire of human tbc/rabgaps. *Nat Rev Mol Cell Biol* (2013) 13(476):67–73. doi:10.1038/nrm3267

130. Fukuda M. Tbc proteins: GAPs for mammalian small GTPase Rab? *Biosci Rep* (2011) 31(3):159–68. doi:10.1042/BSR20100112

131. Mozdy AD, McCaffery JM, Shaw JM. Dnm1p GTPase-mediated mitochondrial fission is a multi-step process requiring the novel integral membrane component Fis1p. *J Cell Biol* (2000) 151(2):367–80. doi:10.1083/jcb.151.2.367

132. Suzuki M, Jeong SY, Karbowski M, Youle RJ, Tjandra N. The solution structure of human mitochondria fission protein Fis1 reveals a novel TPR-like helix bundle. *J Mol Biol* (2003) 334(3):445–58. doi:10.1016/j.jmb.2003.09.064

133. Pankiv S, Alemu EA, Brech A, Bruun JA, Lamark T, Overvatn A, et al. FYCO1 is a Rab7 effector that binds to LC3 and PI3P to mediate microtubule plus end–directed vesicle transport. *J Cell Biol* (2010) 188(2):253–69. doi:10.1083/jcb.200907015

134. Jager S, Bucci C, Tanida I, Ueno T, Kominami EL. Role for Rab7 in maturation of late autophagic vacuoles. *J Cell Sci* (2004) 117(20):4837–48. doi:10.1242/jcs.01370

135. Zhou J, Tan SH, Nicolas V, Bauvy C, Yang ND, Zhang J, et al. Activation of lysosomal function in the course of autophagy via mTORC1 suppression and autophagosome-lysosome fusion. *Cell Res* (2013) 23(4):508–23. doi:10.1038/cr.2013.11

136. Zhao T, Huang X, Han L, Wang X, Cheng H, Zhao Y, et al. Central role of mitofusin 2 in autophagosome-lysosome fusion in cardiomyocytes. *J Biol Chem* (2012) 287(28):23615–25. doi:10.1074/jbc.M112.379164

137. Snider MD. A role for Rab7 GTPase in growth factor-regulated cell nutrition and apoptosis. *Mol Cell* (2003) 12(4):796–7. doi:10.1016/S1097-2765(03)00401-5

138. Sancak Y, Bar-Peled L, Zoncu R, Markhard AL, Nada S, Sabatini DM. Ragulator-Rag complex targets mTORC1 to the lysosomal surface and is necessary for its activation by amino acids. *Cell* (2010) 141(2):290–303. doi:10.1016/j.cell.2010.02.024

139. Ding X, Zhang W, Zhao T, Yan C, Du H. Rab7 GTPase controls lipid metabolic signaling in myeloid-derived suppressor cells. *Oncotarget* (2017) 8(18):30123–37. doi:10.18632/oncotarget.16280

140. Edinger AL. Growth factors regulate cell survival by controlling nutrient transporter expression. *Biochem Soc Trans* (2005) 33(1):225–7. doi:10.1042/BST0330225

141. Edinger AL, Cinalli RM, Thompson CB. Rab7 prevents growth factor-independent survival by inhibiting cell-autonomous nutrient transporter expression. *Dev Cell* (2003) 5(4):571–82. doi:10.1016/S1534-5807(03)00291-0

142. Steffan JJ, Cardelli JA. Thiazolidinediones induce Rab7-RILP-MAPK-dependent juxtanuclear lysosome aggregation and reduce tumor cell invasion. *Traffic* (2010) 11(2):274–86. doi:10.1111/j.1600-0854.2009.01012.x

143. Wang T, Zhang M, Ma Z, Guo K, Tergaonkar V, Zeng Q, et al. A role of Rab7 in stabilizing EGFR-HER2 and in sustaining Akt survival signal. *J Cell Physiol* (2012) 227(6):2788–97. doi:10.1002/jcp.23023

144. Williams KC, Coppolino MG. Phosphorylation of membrane type 1-matrix metalloproteinase (mt1-mmp) and its vesicle-associated membrane protein 7 (Vamp7)-dependent trafficking facilitate cell invasion and migration. *J Biol Chem* (2011) 286(50):43405–16. doi:10.1074/jbc.M111.297069

145. Alonso-Curbelo D, Riveiro-Falkenbach E, Pérez-Guijarro E, Cifdaloz M, Karras P, Osterloh L, et al. Rab7 controls melanoma progression by exploiting a lineage-specific wiring of the endolysosomal pathway. *Cancer Cell* (2014) 26(1):61–76. doi:10.1016/j.ccr.2014.04.030

146. Lackner MR, Kindt RM, Carroll PM, Brown K, Cancilla MR, Chen C, et al. Chemical genetics identifies Rab geranylgeranyl transferase as an apoptotic target of farnesyl transferase inhibitors. *Cancer Cell* (2005) 7(4):325–36. doi:10.1016/j.ccr.2005.03.024

147. Ceresa BP, Bahr SJ. Rab7 activity affects epidermal growth factor: epidermal growth factor receptor degradation by regulating endocytic trafficking from the late endosome. *J Biol Chem* (2006) 281(2):1099–106. doi:10.1074/jbc.M504175200

148. Sakane A, Hatakeyama S, Sasaki T. Involvement of Rabring7 in EGF receptor degradation as an E3 ligase. *Biochem Biophys Res Commun* (2007) 357(4):1058–64. doi:10.1016/j.bbrc.2007.04.052

149. Benvenuti S, Comoglio PM. The MET receptor tyrosine kinase in invasion and metastasis. *J Cell Physiol* (2007) 213(2):316–25. doi:10.1002/jcp.21183

150. Ubah OC, Wallace HM. Cancer therapy: targeting mitochondria and other sub-cellular organelles. *Curr Pharm Des* (2014) 20:201–22. doi:10.2174/13816128113199990031

151. Wen S, Zhu D, Huang P. Targeting cancer cell mitochondria as a therapeutic approach. *Future Med Chem* (2013) 5(1):53–67. doi:10.4155/fmc.12.190

152. Rigo A, Vinante F. The antineoplastic agent α-bisabolol promotes cell death by inducing pores in mitochondria and lysosomes. *Apoptosis* (2016) 21(8):917–27. doi:10.1007/s10495-016-1257-y

153. Erdal H, Berndtsson M, Castro J, Brunk U, Shoshan MC, Linder S. Induction of lysosomal membrane permeabilization by compounds that activate p53-independent apoptosis. *Proc Natl Acad Sci U S A* (2005) 102(1):192–7. doi:10.1073/pnas.0408592102

154. Buytaert E, Dewaele M, Agostinis P. Molecular effectors of multiple cell death pathways initiated by photodynamic therapy. *Biochim Biophys Acta* (2007) 1776(1):86–107. doi:10.1016/j.bbcan.2007.07.001

155. Capella MA, Capella LS. A light in multidrug resistance: photodynamic treatment of multidrug-resistant tumors. *J Biomed Sci* (2003) 10(4):361–6. doi:10.1159/000071155

156. Vrouenraets MB, Visser GW, Snow GB, van Dongen GA. Basic principles, applications in oncology and improved selectivity of photodynamic therapy. *Anticancer Res* (2003) 23(1B):505–22.

157. Gudgin Dickson EF, Goyan RL, Pottier RH. New directions in photodynamic therapy. *Cell Mol Biol* (2002) 48(8):939–54.

158. Dougherty TJ, Gomer CJ, Henderson BW, Jori G, Kessel D, Korbelik M, et al. Photodynamic therapy. *J Natl Cancer Instit* (1998) 90(12):889–905. doi:10.1093/jnci/90.12.889

159. Li W, Saud SM, Young MR, Chen G, Hua B. Targeting AMPK for cancer prevention and treatment. *Oncotarget* (2015) 6(10):7365–78. doi:10.18632/oncotarget.3629

160. Luo Z, Zang M, Guo W. AMPK as a metabolic tumor suppressor: control of metabolism and cell growth. *Future Oncol* (2010) 6(3):457–70. doi:10.2217/fon.09.174

161. Griss T, Vincent EE, Egnatchik R, Chen J, Ma EH, Faubert B, et al. Metformin antagonizes cancer cell proliferation by suppressing mitochondrial-dependent biosynthesis. *PLoS Biol* (2015) 13(12):e1002309. doi:10.1371/journal.pbio.1002309

162. Kasznicki J, Sliwinska A, Drzewos J. Metformin in cancer prevention and therapy. *Ann Transl Med* (2014) 2(6):57–68. doi:10.3978/j.issn.2305-5839.2014.06.01

163. Kim J, You YJ. Regulation of organelle function by metformin. *IUBMB Life* (2017) 69(7):459–69. doi:10.1002/iub.1633

164. Lu CL, Qin L, Liu HC, Candas D, Fan M, Li JJ. Tumor cells switch to mitochondrial oxidative phosphorylation under radiation via mTOR-mediated hexokinase II inhibition – a Warbourg-Reversing effect. *PLoS One* (2015) 10(3):e0121046. doi:10.1371/journal.pone.0121046

165. Xie J, Wang X, Proud CG. mTOR inhibitors in cancer therapy. *F1000 Fac Rev* (2016) 5(2078):1–11. doi:10.12688/f1000research.9207.1

166. Zhou J, Li G, Zheng Y, Shen HM, Hu X, Ming QL, et al. A novel autophagy/mitophagy inhibitor liensinine sensitizes breast cancer cells to chemotherapy through DNM1L-mediated mitochondrial fission. *Autophagy* (2015) 11(8):1259–79. doi:10.1080/15548627.2015.1056970

167. Kodiha M, Wang YM, Hutter E, Maysinger D, Stochaj U. Off to the organelles – killing cancer cells with targeted gold nanoparticles. *Theranostics* (2015) 5(4):357–70. doi:10.7150/thno.10657

168. Zhang F, Zhu X, Gong J, Sun Y, Chen D, Wang J, et al. Lysosome-mitochondria-mediated apoptosis specifically evoked in cancer cells induced by gold nanorods. *Nanomedicine* (2016) 11(15):1993–2006. doi:10.2217/nnm-2016-0139

2. CDK4 phosphorylates AMPKα2 to inhibit its activity and repress fatty acid oxidation

Lopez-Mejia, I. C., Lagarrigue, S., Giralt, A., Martinez-Carreres, L., Zanou, N., Denechaud, P. D., Castillo-Armengol, J., Chavey, C., Orpinell, M., Delacuisine, B.*, et al.* (2017). CDK4 Phosphorylates AMPKalpha2 to Inhibit Its Activity and Repress Fatty Acid Oxidation. Molecular cell *68*, 336-349 e336.

This paper describes a new metabolic function of CDK4 in the regulation of AMPK, and its implications, specially in muscle tissue. Here, it is shown that CDK4 can repress AMPK by phosphorylating its α2 subunit in mouse embryonic fibroblasts and in mouse muscles. This results in an increase of anaerobic glycolysis and in a repression of fatty acid oxidation. Thus, CDK4 -/- mice showed increased oxidative metablism and exercice capacity, in an AMPK-dependent manner. This represents a novel mechanism by which CDK4 is promoting anabolism by blocking a catalytic process (fatty acid oxydation) through AMPK phosphorylation.

I contributed to demonstrate this finding by testing the exercise capacity of different mice strains, as well as by analyzing the activation of AMPK in muscle tissues from the same mice.

Molecular Cell

CDK4 Phosphorylates AMPKα2 to Inhibit Its Activity and Repress Fatty Acid Oxidation

Graphical Abstract
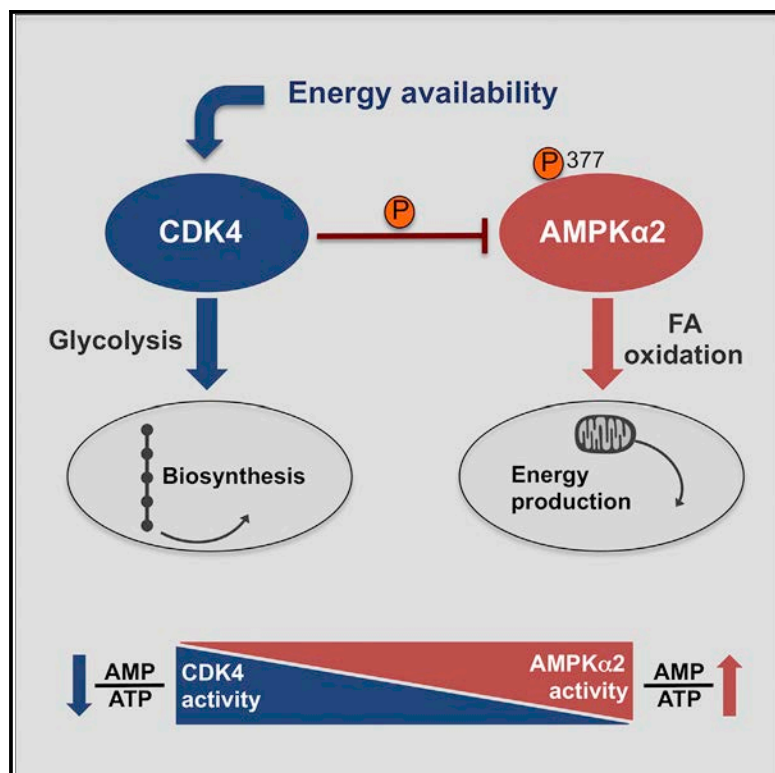
Authors

Isabel C. Lopez-Mejia,
Sylviane Lagarrigue, Albert Giralt, ...,
Benoît Viollet, D. Grahame Hardie,
Lluis Fajas

Correspondence

lluis.fajas@unil.ch

In Brief

Lopez-Mejia et al. show in this study that CDK4, a protein that is usually involved in the control of cell division, is an important regulator of the energy balance of the cell through the direct inhibition of the activity of AMPK, which is a major regulator of energy consuming processes.

Highlights

- CDK4 promotes glycolysis and inhibits fatty acid oxidation

- CDK4 inhibits AMPK activity through direct phosphorylation of the AMPK-α2 subunit

- Mice treated with CDK4 inhibitor have AMPK-dependent increased oxidative metabolism

CellPress

CellPress

CDK4 Phosphorylates AMPKα2 to Inhibit Its Activity and Repress Fatty Acid Oxidation

Isabel C. Lopez-Mejia,[1,2] Sylviane Lagarrigue,[2] Albert Giralt,[1] Laia Martinez-Carreres,[1] Nadège Zanou,[2,3]
Pierre-Damien Denechaud,[1,2] Judit Castillo-Armengol,[1] Carine Chavey,[4] Meritxell Orpinell,[2] Brigitte Delacuisine,[1,2]
Anita Nasrallah,[1] Caterina Collodet,[5,6] Lianjun Zhang,[7] Benoît Viollet,[8,9,10] D. Grahame Hardie,[11] and Lluis Fajas[1,2,12,*]
[1]Center for Integrative Genomics, University of Lausanne, 1015 Lausanne, Switzerland
[2]Department of Physiology, University of Lausanne, 1005 Lausanne, Switzerland
[3]Institute of Sport Sciences, University of Lausanne, 1015 Lausanne, Switzerland
[4]IGMM, Université de Montpellier, UMR 5535 CNRS, 34293 Montpellier, France
[5]Nestlé Institute of Health Sciences SA, EPFL Innovation Park, 1015 Lausanne, Switzerland
[6]École Polytechnique Fédérale de Lausanne, School of Life Sciences, 1015 Lausanne, Switzerland
[7]Ludwig Center for Cancer Research, University of Lausanne, 1066 Epalinges, Switzerland
[8]Institut Cochin, INSERM U1016, Paris, France
[9]CNRS, UMR 8104, Paris, France
[10]Université Paris Descartes, Sorbonne Paris Cité, Paris, France
[11]School of Life Sciences, University of Dundee, Dundee, Scotland, UK
[12]Lead Contact
*Correspondence: lluis.fajas@unil.ch
https://doi.org/10.1016/j.molcel.2017.09.034

SUMMARY

The roles of CDK4 in the cell cycle have been extensively studied, but less is known about the mechanisms underlying the metabolic regulation by CDK4. Here, we report that CDK4 promotes anaerobic glycolysis and represses fatty acid oxidation in mouse embryonic fibroblasts (MEFs) by targeting the AMP-activated protein kinase (AMPK). We also show that fatty acid oxidation (FAO) is specifically induced by AMPK complexes containing the α2 subunit. Moreover, we report that CDK4 represses FAO through direct phosphorylation and inhibition of AMPKα2. The expression of non-phosphorylatable AMPKα2 mutants, or the use of a CDK4 inhibitor, increased FAO rates in MEFs and myotubes. In addition, $Cdk4^{-/-}$ mice have increased oxidative metabolism and exercise capacity. Inhibition of CDK4 mimicked these alterations in normal mice, but not when skeletal muscle was AMPK deficient. This novel mechanism explains how CDK4 promotes anabolism by blocking catabolic processes (FAO) that are activated by AMPK.

INTRODUCTION

Promitotic signals such as growth factors increase the levels of D-type cyclins (cyclins D1, D2, and D3), which bind and activate CDK4/6 to trigger the phosphorylation of the retinoblastoma-associated protein pRB and other pocket proteins (i.e., p107 and p130) (Malumbres and Barbacid, 2005). Rb phosphorylation enables release of the E2F transcription factors that promote the

transcription of genes necessary for the replication of the genome (Malumbres and Barbacid, 2005). The role of CDK4 in the regulation of cell-cycle progression has been extensively studied in eumetazoan organisms, and alterations in CDK4 activity have been associated with cancer development and progression (Malumbres and Barbacid, 2001, 2009; O'Leary et al., 2016). For example, the R24C mutation, which is used in this study, renders CDK4 resistant to inhibition by INK4 inhibitors and has been reported to confer a genetic predisposition to melanoma (Rane et al., 1999, 2002; Wölfel et al., 1995).

Cell division requires substantial amounts of ATP, and numerous metabolic intermediates to support biosynthesis of essential molecules, such as lipids and nucleic acids. Proliferating cells preferentially use anaerobic glycolysis to generate large amounts of ATP and provide metabolic intermediates to support cell growth (Jones and Thompson, 2009). Growing evidence demonstrates that regulatory crosstalk exists between metabolic pathways and regulators of cell-cycle progression. Mitochondrial respiration and metabolism are coordinated with cell-cycle progression by cell-cycle regulators (Lopez-Mejia and Fajas, 2015; Salazar-Roa and Malumbres, 2016). Our laboratory and others have demonstrated that CDK4 is one such "metabolic" cell-cycle regulator (Blanchet et al., 2011; Icreverzi et al., 2012; Lagarrigue et al., 2016; Lee et al., 2014). Indeed, we have previously shown that CDK4 regulates oxidative metabolism via the E2F1 transcription factor in muscle and brown adipose tissue (Blanchet et al., 2011) and promotes the insulin-signaling pathway in mature adipocytes (Lagarrigue et al., 2016). Overall, the participation of cell-cycle regulators in the control of energy homeostasis occurs mainly through the activation of anabolic processes (Aguilar and Fajas, 2010). The AMP-activated protein kinase (AMPK) is a central inhibitor of such anabolic processes and might therefore be repressed by cell-cycle regulators. Under conditions of low cellular energy, AMP and ADP are increased relative to ATP, and this is sensed by AMPK.

CrossMark

AMPK exists as heterotrimeric complexes composed of a cata-lytic subunit (α) and two regulatory subunits (β and γ); the α and β subunits exist as two isoforms ($\alpha1/\alpha2$ and $\beta1/\beta2$, encoded by the *PRKAA1/2* and *PRKAB1/2* genes), and the γ subunit exists as three isoforms ($\gamma1/\gamma2/\gamma3$, encoded by *PRKAG1/2/3*), thus gener-ating up to 12 combinations of heterotrimeric complex (Carling, 2004; Grahame Hardie, 2016; Hardie et al., 2012; Ross et al., 2016b). AMPK is regulated both by phosphorylation/dephos-phorylation and by the relative cellular concentrations of adenine nucleotides, with the two mechanisms being intimately linked. First, the upstream kinases LKB1 (liver kinase B1) (Hawley et al., 2003; Shaw et al., 2004; Woods et al., 2003) or CaMKK2 (calmodulin-dependent kinase kinase-2/-β) (Hawley et al., 2005; Hurley et al., 2005; Woods et al., 2005) activate AMPK through the phosphorylation of Thr^{172} of the α subunit (Hawley et al., 1996). Second, AMPK is regulated through the competitive binding of ATP or AMP and ADP at up to three sites on the γ sub-unit. When cellular energy levels are low, binding of AMP or ADP enhances Thr^{172} phosphorylation by LKB1 and inhibits Thr^{172} dephosphorylation by protein phosphatases, while binding of AMP (but not ADP) causes further allosteric activation (Ross et al., 2016a). Metabolic stresses that reduce intracellular ATP concentrations are therefore the best-characterized activators of AMPK, although it has recently been shown that glucose deprivation can activate AMPK by an adenine nucleotide-inde-pendent mechanism (Zhang et al., 2017). Once activated, AMPK promotes catabolic pathways that generate ATP (e.g., fatty acid oxidation [FAO]) while switching off anabolic pathways and other ATP-requiring processes to restore cellular ATP levels (Carling, 2004; Grahame Hardie, 2016; Hardie et al., 2012; Ross et al., 2016b).

Other kinase activities that are induced by growth stimuli are known to inhibit AMPK. This includes AKT a key effector of the insulin/insulin growth factor 1 (IGF1)-signaling pathway that antagonizes the AMPK pathway through phosphorylation of AMPK$\alpha1$ on Ser^{487} (Horman et al., 2006), or extracellular signal-regulated kinase (ERK), which was shown to phosphor-ylate the same residue (López-Cotarelo et al., 2015). The cyclic-AMP-dependent protein kinase (PKA) also phosphory-lates and negatively regulates AMPK (Djouder et al., 2010; Hurley et al., 2006), and Thr^{481} and Ser^{477} on AMPK$\alpha1$ are phosphorylated by glycogen synthase kinase 3 (GSK3) (Suzuki et al., 2013), following a "priming" phosphorylation of Ser^{487} by AKT.

Muscle function requires a finely tuned balance between anabolism and catabolism in order to respond to physiological challenges within the available energy supply. AMPK is a major coordinator of energy intake and utilization in exercising muscle (Hoffman et al., 2015), functioning to enhance energy availability. Among other effects, AMPK promotes FAO to maintain ATP cellular stores, although the exact role of AMPK in regulation of muscle FAO has been controversial (Mounier et al., 2015).

In this study, we sought to determine whether CDK4 partici-pates in energy homeostasis by inhibiting catabolic processes. The mechanisms by which the activity of AMPK is inhibited under anabolic conditions, such as during cell-cycle progression or in resting muscle, have not been thoroughly studied. We report

here that CDK4 enhances anaerobic glycolysis and represses fatty acid oxidation. Surprisingly, the AMPK$\alpha1$ and $\alpha2$ subunits play distinct roles. We provide here a molecular mechanism whereby CDK4-CycD3 complexes directly repress $\alpha2$-contain-ing complexes to inhibit FAO. We show that chemical and ge-netic inhibition of CDK4 also promotes oxidative metabolism *in vivo*, as evidenced by decreased respiratory exchange ratio (RER) and increased exercise performance in mice lacking CDK4 activity.

RESULTS

CDK4 Modulates FAO in an E2F1-Independent Manner

We previously demonstrated that CDK4 is a major mediator of in-sulin signaling and therefore contributes to the positive regula-tion of biosynthetic processes, such as fatty acid synthesis, and the inhibition of catabolic pathways, such as lipolysis (Lagar-rigue et al., 2016). To further investigate the contribution of CDK4 to metabolic regulation, Seahorse analyses were performed. *Cdk4$^{R24C/R24C}$* mouse embryonic fibroblasts (MEFs), which ex-press a hyperactive CDK4 mutant, exhibited a significant in-crease in anaerobic glycolysis, as measured by the extracellular acidification rate (ECAR), whereas *Cdk4$^{-/-}$* MEFs had impaired anaerobic glycolysis (Figures 1A and 1B). In contrast, CDK4 activity was inversely correlated with FAO. *Cdk4$^{R24C/R24C}$* MEFs metabolized palmitate at a low rate, whereas *Cdk4$^{-/-}$* MEFs showed increased palmitate oxidation (Figures 1C and 1D). Interestingly, the effects of CDK4 on substrate use were independent of E2F1 activity, since deletion of E2F1 in *Cdk4$^{R24C/R24C}$* MEFs failed to reverse the effects of *Cdk4^{R24C}* on anaerobic glycolysis or palmitate oxidation (Figures 1E–1H). These results suggest that CDK4 controls substrate utilization in MEFs independently of E2F1.

CDK4 Regulation of FAO Is AMPK Dependent

The decrease in FAO observed in response to constitutive acti-vation of CDK4 is the opposite of the effect seen with AMPK acti-vation (Fullerton et al., 2013; Hardie, 2015; Hardie and Pan, 2002; O'Neill et al., 2014). Therefore, we analyzed the involvement of AMPK in the CDK4-mediated regulation of FAO in MEFs. Basal levels of phosphorylated ACC (pACC), which is a known target and marker of AMPK activity, were decreased in *Cdk4$^{R24C/R24C}$* MEFs but increased 3-fold in the *Cdk4$^{-/-}$* cells (Figures 2A, 2B, S1A, and S1B), suggesting that CDK4 antagonizes AMPK function. Moreover, the activation of AMPK by the specific acti-vator A769662 (Göransson et al., 2007; Moreno et al., 2008) was reduced in *Cdk4$^{R24C/R24C}$* MEFs (Figures 2A and 2B), suggesting that CDK4 can prevent AMPK activation. In addition, increased AMP/ATP and ADP/ATP ratios were observed in MEFs express-ing the hyperactive CDK4 mutant, which suggested a lower cata-bolic rate (Figures 2C and 2D). Interestingly, in *Cdk4$^{-/-}$* MEFs, comparable pACC levels were measured both in the basal state and upon AMPK stimulation (Figures 2A and 2B). This finding im-plies that in the absence of CDK4, AMPK reaches its activated state without need for any further stimulation. Likewise in *Cdk4$^{-/-}$* cells and wild-type (WT) MEFs treated with A769662, we observed a significant decrease of AMP/ATP and ADP/ATP ratios (Figures 2C–2F).
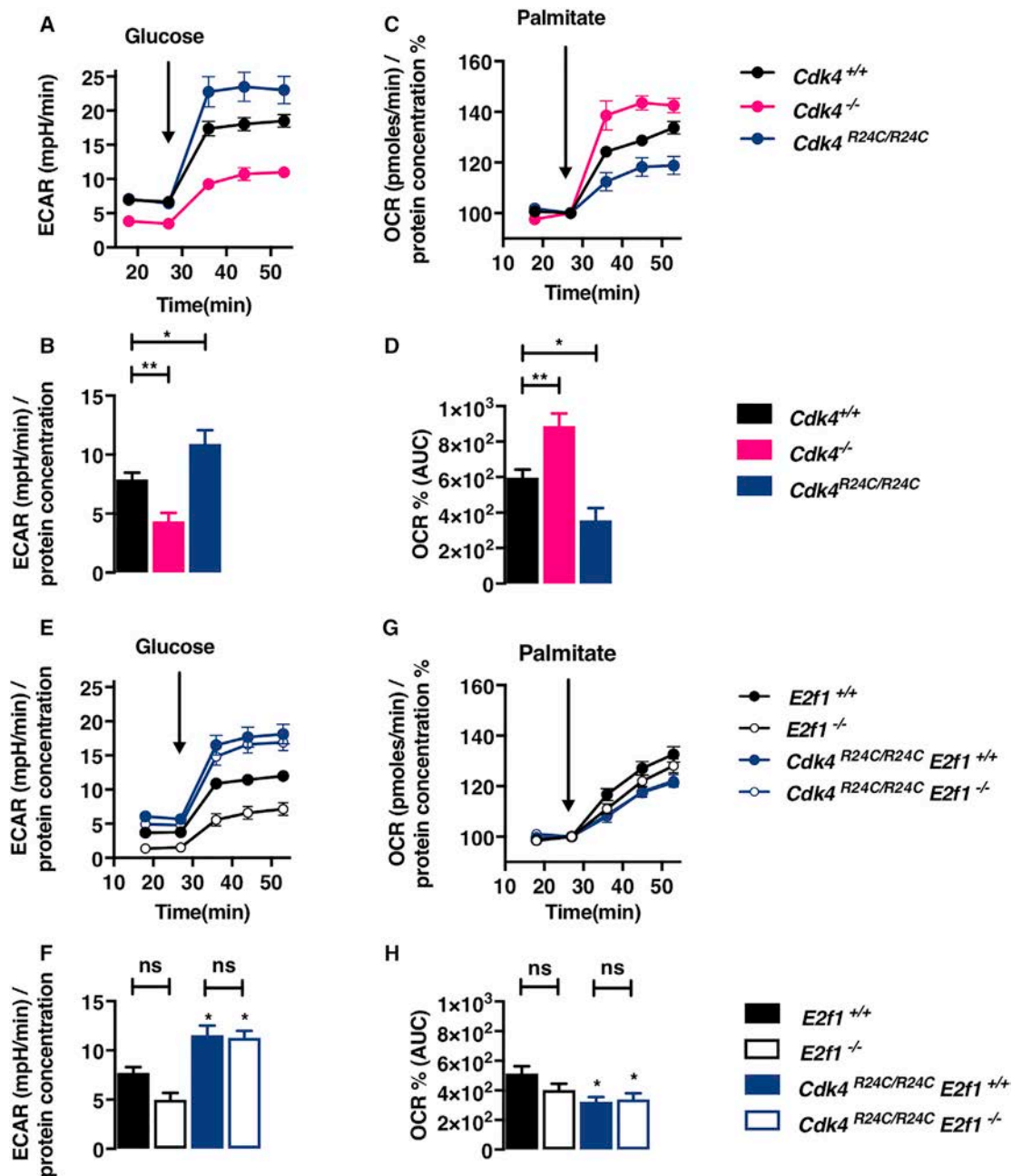
Figure 1. CDK4 Modulates FAO in an E2F1-Independent Manner

(A–D) $Cdk4^{+/+}$, $Cdk4^{-/-}$, and $Cdk4^{R24C/R24C}$ MEFs were submitted to a glycolysis assay, during which ECAR was measured at the basal level and upon glucose injection (A), or to a FAO assay, in which the palmitate induced OCR was measured (in % OCR compared to the basal OCR) (C). The glycolytic rate was calculated (B). The area under curve of the palmitate induced OCR was quantified (D).

(E–H) $E2f1^{+/+}$, $E2f1^{-/-}$, $Cdk4^{R24C/R24C}$ $E2f1^{+/+}$, and $Cdk4^{R24C/R24C}$ $E2f1^{-/-}$ MEFs were submitted to a glycolysis assay, during which ECAR was measured at the basal level and upon glucose injection (E), or to a FAO assay, in which the palmitate induced OCR was measured (in % OCR compared to the basal OCR) (G). The glycolytic rate was calculated in (F). The area under curve of the palmitate induced OCR was quantified in (H).

Data are expressed as mean ± SEM.

Next, we studied the physiological relevance of the increase in AMPK activity in $Cdk4^{-/-}$ cells using FAO assays in MEFs treated with A769662 and with the non-selective AMPK inhibitor compound C. As expected, the levels of palmitate oxidation in WT MEFs were at least 25% higher in A769662-treated cells (Figures 2G, S1C, and S1D). However, $Cdk4^{-/-}$ cells did not respond in the same assay to A769662 treatment. By contrast, AMPK activation by A769662 in $Cdk4^{R24C/R24C}$ MEFs was only able to
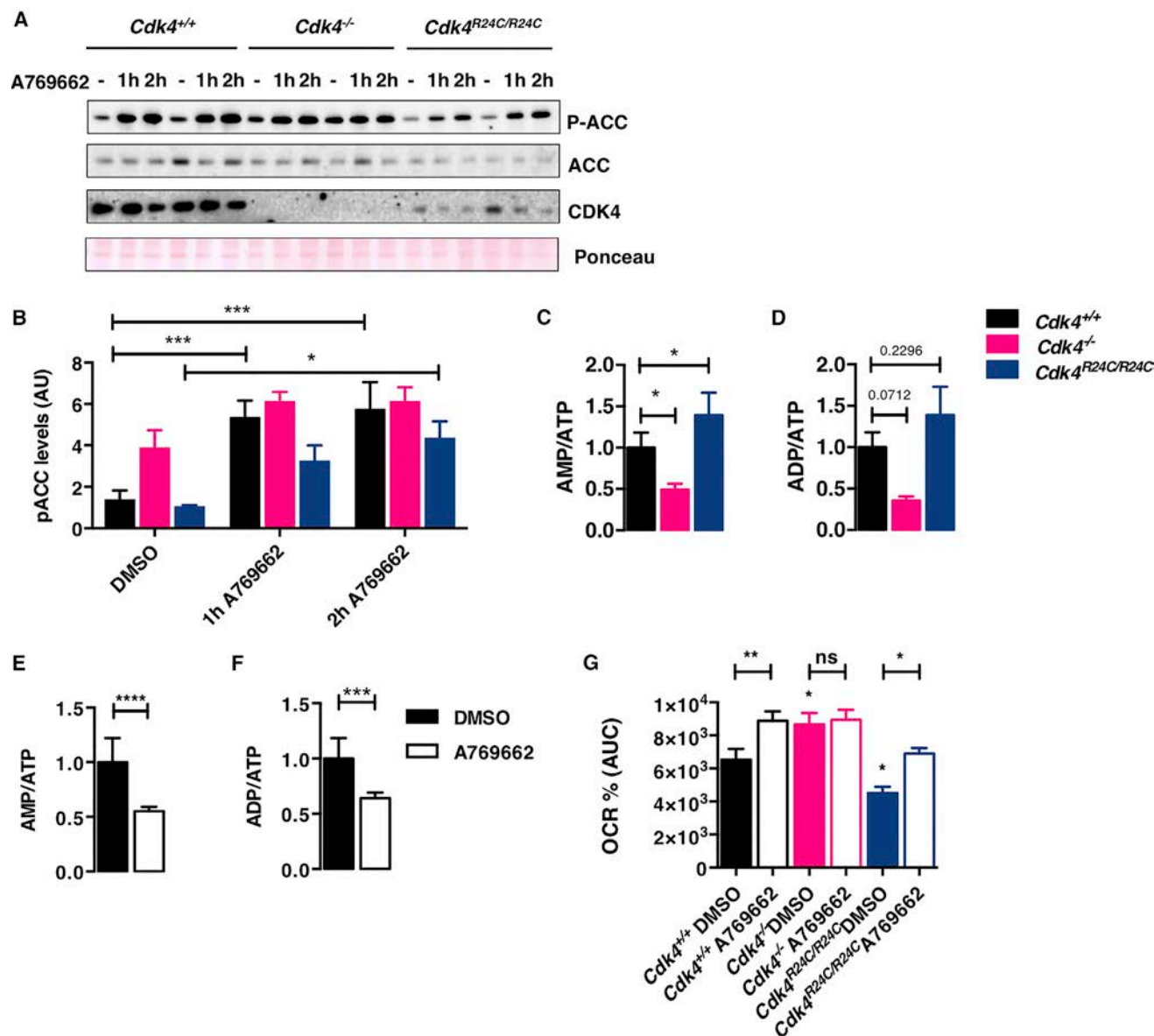
Figure 2. CDK4 Regulation of FAO Is AMPK Dependent

(A) $Cdk4^{+/+}$, $Cdk4^{-/-}$, and $Cdk4^{R24C/R24C}$ MEFs were starved for 3 hr and then stimulated with 50 μM A769662; western blot analysis shows the A769662-induced ACC phosphorylation in $Cdk4^{+/+}$, $Cdk4^{-/-}$, and $Cdk4^{R24C/R24C}$ cells.

(B) Quantification of pACC levels.

(C and D) SV40 immortalized cells were placed in KHB medium containing 1.5 mM carnitine and 300 μM oleate for AMP, ADP, and ATP quantification by HPLC, and AMP/ATP (C) and ADP/ATP (D) ratios are shown.

(E and F) AMP/ATP (E) and ADP/ATP (F) ratios of WT SV40 immortalized cells treated with 50 μM A769662 for 8 hr.

(G) $Cdk4^{+/+}$, $Cdk4^{-/-}$, and $Cdk4^{R24C/R24C}$ MEFs were treated with DMSO or 50 μM A769662 for 2 hr in KHB medium and submitted to a FAO assay in which the palmitate induced OCR was measured (in % OCR compared to the basal OCR). The area under curve of the palmitate-induced OCR was quantified.

Data are expressed as mean ± SEM. See also Figure S1.

restore WT levels of FAO (Figures 2G, S1C, and S1D). AMPK inhibition in $Cdk4^{-/-}$ cells (albeit by the non-selective inhibitor compound C) produced consistent results. The levels of pACC in CDK4-null MEFs, as well as the increased FAO levels, were restored back to basal levels (Figures S1E–S1G). Taken together, these results suggest that CDK4 inhibits the AMPK pathway.

The AMPKα2 Subunit Is Required for Efficient FAO in MEFs

Our results suggested that CDK4 has a negative effect on FAO via the regulation of AMPK activity, raising the question of which AMPK subunits contribute to this effect. Interestingly, the deletion of either AMPKα subunit in MEFs resulted in increased

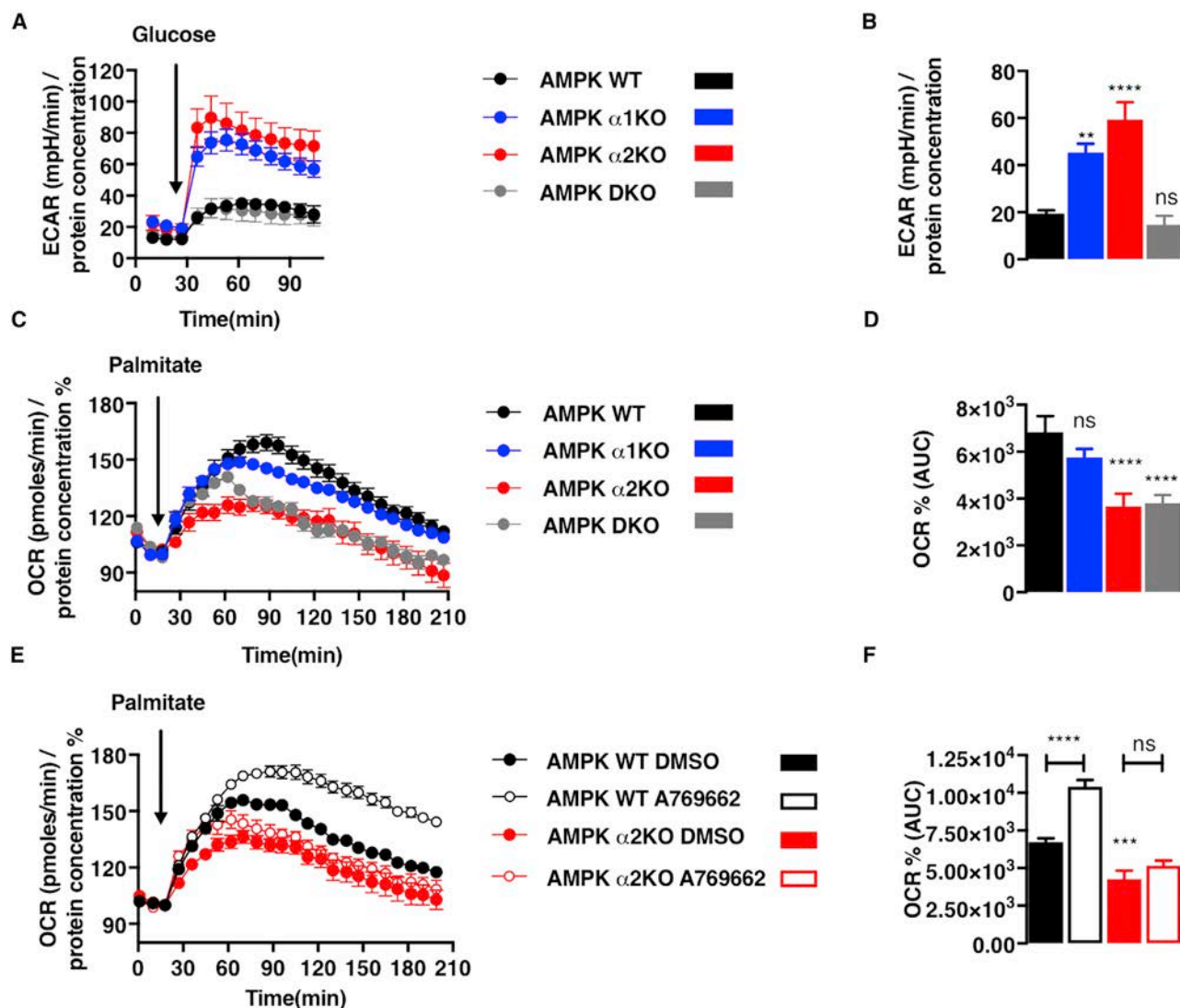**Figure 3. The AMPKα2 Subunit Is Required for Efficient Fatty Acid Oxidation in MEFs**

(A–D) AMPK WT, AMPK α1 KO, AMPK α2 KO, and AMPK DKO SV40-immortalized MEFs were submitted to a glycolysis assay, during which ECAR was measured at the basal level and upon glucose injection (A), or to a FAO assay, in which the palmitate induced OCR was measured (in % OCR compared to the basal OCR) (C). The glycolytic rate was calculated (B). The area under curve of the palmitate induced OCR was quantified (D).

(E and F) AMPK WT and AMPK α2 KO SV40-immortalized MEFs were treated for 2 hr with DMSO or 50 μM A769662 for 2 hr in KHB medium and submitted to a FAO assay in which the palmitate induced OCR was measured (in % OCR compared to the basal OCR) (E). The area under curve of the palmitate induced OCR was quantified (F).

Data are expressed as mean ± SEM. See also Figure S2.

ECAR, indicating increased glycolysis, whereas the complete abrogation of AMPK activity had no effect, perhaps due to disruption of glucose transport into the cells (Figures 3A and 3B). However, although AMPKα1 knockout (KO) MEFs metabolized palmitate as efficiently as control cells, both AMPKα2KO and AMPK α1/α2 double-knockout (DKO) cells exhibited significantly reduced levels of FAO (Figures 3C and 3D). Consistently, A769662 failed to trigger FAO in cells lacking the α2 subunit (both α2KO and DKO). Thus, despite being more abundant in MEFs (Morizane et al., 2011), the AMPKα1 subunit cannot substitute for the α2 subunit in the control of FAO, even when allosterically

activated by A769662 (Figures 3E, 3F, S1H, and S1I). In addition, ACC phosphorylation could be detected upon stimulation with A769662 in both AMPK α1KO and AMPK α2KO MEFs (Figure S1J), suggesting that both AMPK subunits can phosphorylate ACC1 and therefore inhibit lipid synthesis, but only AMPKα2 can promote FAO. Taken together, these results suggest that AMPK complexes containing α2 specifically control FAO.

CDK4 Phosphorylates the AMPK α2 Subunit

The inhibition of AMPKα2-dependent FAO could be the result of a direct phosphorylation by CDK4. *In vitro* kinase assays showed
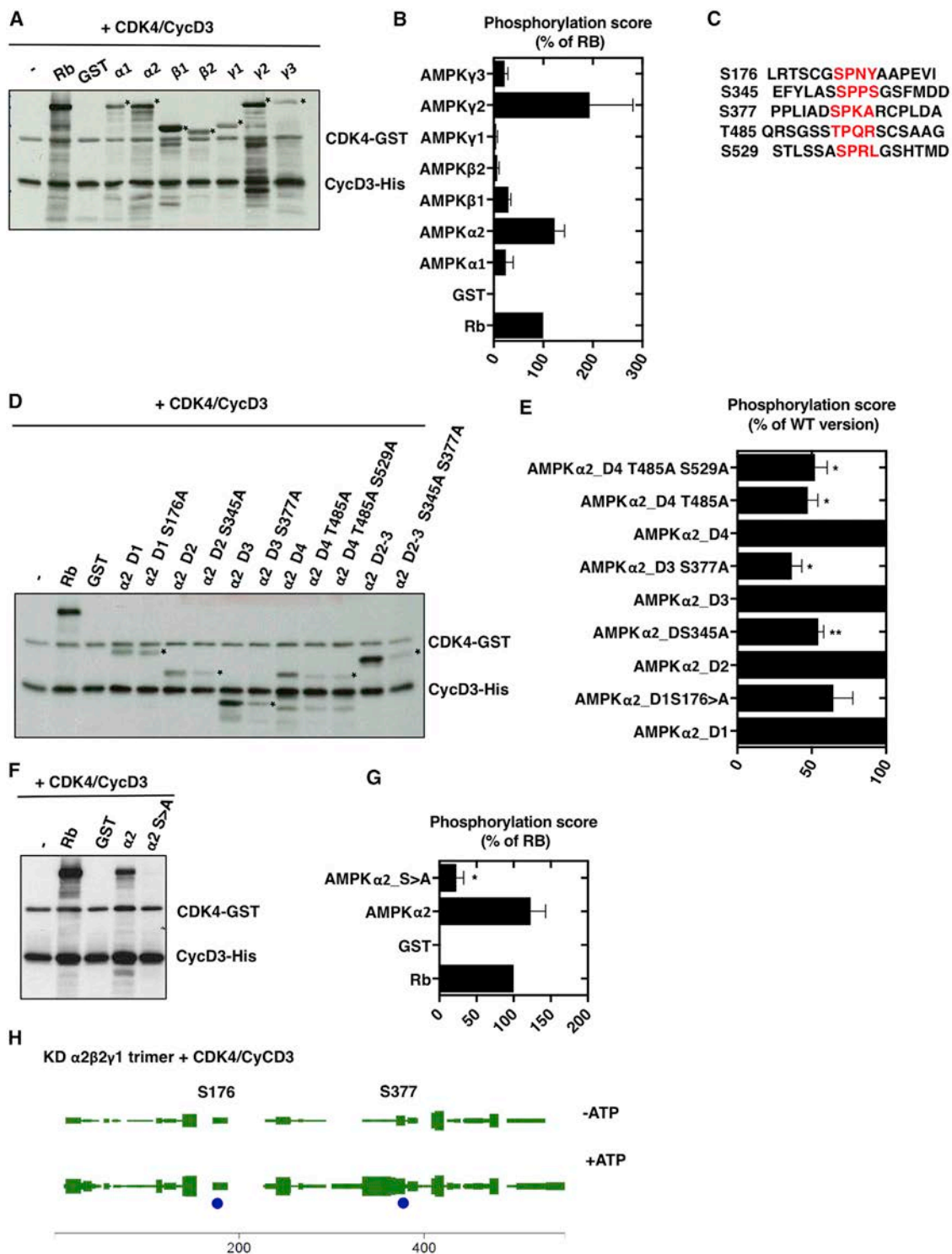
Figure 4. CDK4 Phosphorylates the AMPKα2 Subunit

(A) Cyclin D3-CDK4 directly phosphorylates full-length GST-AMPK subunits *in vitro* (n = 3). Asterisks mark the proteins of interest.

(B) Phosphorylation score (in percentage of RB phosphorylation).

(C) CDK consensus sites in human AMPKα2 (*PRKAA2*).

(D) *In vitro* phosphorylation of WT and mutated (Ser or Thr to Ala) GST-AMPK α2 fragments (D1, 1–245 aa; D2, 246–356 aa; D3, 357–422 aa; D4, 432–522; and D2–D3, 246–422 aa) by cyclin D3/CDK4 (n = 3).

that recombinant CDK4/CycD3 phosphorylated all glutathione S-transferase (GST) fusions of AMPK subunits tested at different levels (Figure 4A; loading control in Figure S2A). Interestingly, AMPKα2 and AMPKγ2 were phosphorylated by CDK4 to a greater extent than pRB, which is the canonical CDK4 substrate (Figure 4B). Since the specificity of CDKs is partially determined by substrate docking on the cyclin subunit, kinase assays were also performed using recombinant CDK4/CycD1 instead of CDK4/CycD3. The phosphorylation of the AMPK subunits was very low under these conditions (Figure S2B), suggesting that AMPK phosphorylation by CDK4 requires recognition by cyclin D3.

AMPKα2 was predicted to contain 6 CDK4 phosphorylation sites (Thr^{85}, Ser^{176}, Ser^{345}, Ser^{377}, Thr^{485}, and Ser^{529}). Out of these six potential sites, five were listed in the phosphoNET database (Figure 4C). Site-directed mutagenesis (S > A or T > A) combined with protein truncation studies (Figure S3C) identified Ser^{345}, Ser^{377}, Thr^{485}, and Ser^{529} as CDK4 phosphorylation sites (Figures 4D and 4E; loading control in Figure S3D). Phosphorylation by CDK4 was completely abrogated in a full-length recombinant protein carrying Ser to Ala or Thr to Ala mutations at the four CDK4 phosphosites (α2 S > A mutant), suggesting that the four newly identified residues account for all sites phosphorylated on GST-AMPKα2 by CDK4 in cell-free assays (Figure 4F and 4G; loading control in Figure S2E). The phosphorylation of Ser^{377} and Thr^{485} has been previously described in proteomic studies (Figure S2F) (Dinkel et al., 2011; Gnad et al., 2011; Hornbeck et al., 2015), including cell-cycle-related phosphoproteomes (Daub et al., 2008; Kettenbach et al., 2011), and in liver upon insulin stimulation (Humphrey et al., 2015), suggesting that the regulation of AMPK by CDK4 is important for cell-cycle progression and for the insulin signaling pathway. Moreover, we found the four newly identified CDK4 phosphosites to be conserved among the AMPKα2 subunits of several mammalian species (Figure S3A), but not between the AMPKα1 and AMPKα2 isoforms (Figure S3B).

In intact cells, AMPK is found as a heterotrimeric complex; therefore recombinant kinase-inactive α2β2γ1 complexes were also used as substrate for recombinant CDK4-CycD3 complexes. After mass spectrometry analysis, we obtained 83% coverage of the AMPKα2 subunit and observed the phosphorylation in Ser^{176} and Ser^{377} (Figure 4H). A targeted analysis to increase coverage showed phosphorylation of Thr^{485} and Ser^{529} with low detectability. The phosphorylation of Ser^{345} and Ser^{377} was also detected in myotubes and muscle tissue, which express high levels of the α2 subunit (Figures S4A and S4B; Table S1). Interestingly, our results suggest that these phosphorylations are present when AMPK is inactive, since the activating Thr^{172} phosphorylation was not found in 5 out of 6 experiments

(Figures S4A and S4B). Taken together, these data indicate that the α2 subunit of AMPK is a substrate for CDK4-CycD3 complexes in cell-free assays and that some of these phosphorylations occur *in vivo*, in conditions in which CDK4 is active (Blanchet et al., 2011; Lagarrigue et al., 2016) but AMPK is inactive.

AMPKα2 Phosphorylation Is Necessary and Sufficient for FAO Repression by CDK4

To elucidate the functional relevance of the phosphorylation of AMPKα2 by CDK4, we compared the regulatory activities of AMPKα2 S > A, AMPKα2, and AMPKα1 in the context of FAO. Transfection of AMPK DKO MEFs with the AMPKα2 S > A mutant conferred ACC phosphorylation levels that where higher than those observed in AMPKα1- or α2-transfected cells in the basal state and upon stimulation by A769662 (Figure 5A). Similarly, ectopic expression of the AMPKα2 S > A mutant in the FAO-defective AMPK DKO MEFs rescued palmitate oxidation to a greater extent than that observed upon transfection with WT AMPKα2 (Figures 5B and S5A). Taken together, these results indicate that defective targeting of AMPKα2 by CDK4 at Ser^{345}, Ser^{377}, Thr^{485}, and Ser^{529} results in increased AMPKα2 FAO-promoting activity.

In order to demonstrate that CDK4 represses FAO by inhibiting AMPK activity, WT and AMPK mutant cells were treated with CDK4 inhibitors. Inhibition of CDK4 activity by LY2835219 significantly increased FAO after 24 hr (Figures 5C and S5B) or 2 hr (Figure S5C) of treatment. Strikingly, the CDK4 inhibitor failed to increase FAO in both AMPK α2KO and AMPK DKO cells, but not in AMPK α1KO cells, demonstrating that CDK4 targets AMPKα2 to alter cellular metabolism (Figures 5C, S5B, and S5E–S5G). The overall positive effect of CDK4 inhibition on AMPK activity was confirmed by analyzing ACC phosphorylation. Indeed, LY2835219 treatment induced a dose-dependent increase in the phosphorylation of ACC (Figures S5H and S5I). This effect correlated with decreased CDK4 activity given that phosphorylation of RB Ser^{780} was also reduced (Figure S5I). Of note, increased ACC phosphorylation and increased FAO could be detected after 2 hr of CDK4 inhibition, whereas inhibition of RB phosphorylation required longer treatments. Moreover, LY2835219 had an effect comparable to that of A769662, significantly decreasing AMP/ATP and ADP/ATP ratios in WT MEFs (Figures 2E, 2F, 5D, and 5E). The use of LY2835219 suggests that CDK4 inhibition promotes catabolic processes in an AMPKα2-subunit-dependent manner.

We next decided to validate our findings in a more physiological cellular model. LY2835219 treatment induced an increase in FAO in C2C12 myotubes, which are known to express high levels of AMPKα2 (Figures S6A and S6B). In this model, CDK4 inhibition correlated with a dose-dependent increase of the

(E) Phosphorylation score (in percentage of the WT fragment).
(F) *In vitro* phosphorylation of full-length WT GST-AMPKα2 and full-length S > A GST-AMPKα2 by cyclin D3/CDK4 (n = 3).
(G) Phosphorylation score (in percentage of RB phosphorylation).
(H) Kinase-dead AMPK α2β2γ1 trimers were used as a substrate for cyclin D3-CDK4 complex and analyzed by mass spectrometry. A graphical overview of the sequence coverage of AMPKα2 human protein in samples displayed by MsViz is depicted. The thickness of the green bars is a function of the number of spectra matching the sequence region, while modification sites are labeled and shown as circles with size proportional to the number of spectra matching a given position. A truncated form of RB (hRB; 379–928 aa) was used as a positive control. A representative autoradiography for each kinase assay is shown.
See also Figure S3.
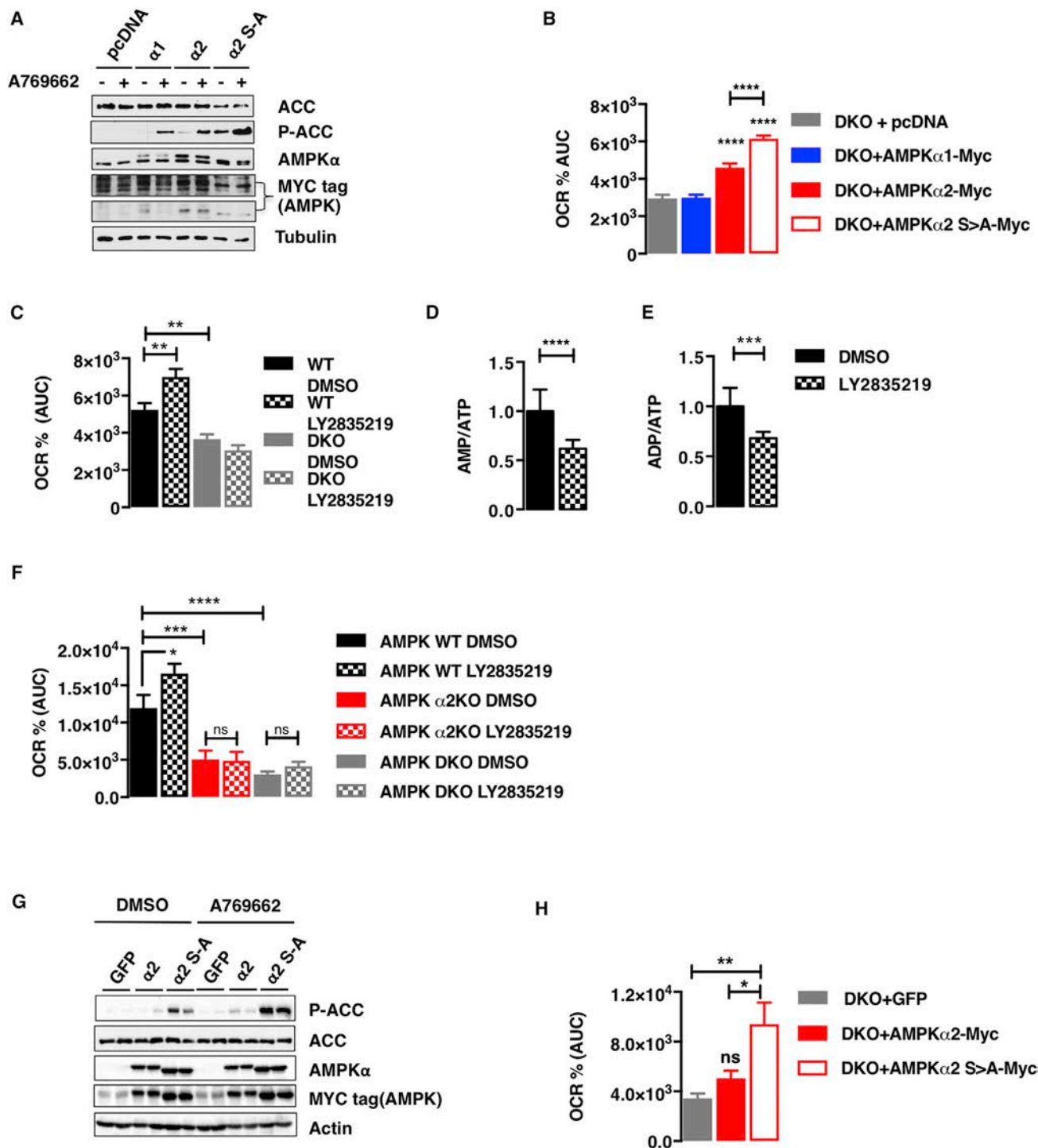
Figure 5. AMPKα2 Phosphorylation Is Necessary and Sufficient for FAO Repression by CDK4

(A) AMPK DKO SV40-immortalized MEFs were electroporated with plasmids encoding Myc-tagged AMPK α1, Myc-tagged AMPK α2 and Myc-tagged AMPK α2 S > A. 48 hr later, MEFs were starved for 3 hr and treated for 2 hr with DMSO or 50 μM A769662 before protein extraction. Western blot analysis shows the A769662-induced ACC phosphorylation in transfected cells.

(B) Electroporated MEFs were submitted to a FAO assay 48 hr after transfection, in which the palmitate induced OCR was measured (in % OCR compared to the basal OCR). The area under curve of the palmitate induced OCR was quantified.

(C) AMPK WT and AMPK DKO SV40-immortalized MEFs were treated with DMSO or LY2835219 (1.5 μM) for 24 hr and submitted to a FAO assay, in which the palmitate-induced OCR was measured (in % OCR compared to the basal OCR). The area under curve of the palmitate induced OCR was quantified.

(legend continued on next page)

phosphorylation of ACC, without significant increase of AMPK Thr^{172} phosphorylation (Figures S6C–S6E). The direct involvement of AMPKα2 was confirmed by analyzing myotubes lacking AMPKα2 or both the α1 and α2 subunits (Lantier et al., 2010). Like in MEFs, FAO was impaired in the α2KO and DKO myotubes. Similarly, the CDK4 inhibitor failed to increase FAO in α2KO and DKO myotubes (Figures 5F and S6F). Rescue of AMPK DKO myotubes with the AMPKα2 S > A mutant triggered ACC phosphorylation levels that where higher than those observed in AMPK α2-transfected cells both in the basal state or upon stimulation with A769662 (Figure 5G). Similarly, ectopic expression of the AMPKα2 S > A mutant in the FAO-defective AMPK DKO myotubes rescued palmitate oxidation to levels similar to those of WT myotubes (Figures 5H and S6G). Taken together, these results in muscle cells confirm that CDK4 modulates FAO through the specific inhibition of AMPKα2 activity and that a non-phosphorylatable AMPKα2 mutant has a FAO-promoting activity.

CDK4 Modulates Oxidative Metabolism and Exercise Capacity *In Vivo*

We next investigated the contribution of CDK4 to oxidative metabolism and muscle function *in vivo*. Isolated mitochondria from *Cdk4*$^{-/-}$ muscles showed increased oxygen consumption, suggesting increased fatty acid oxidation capacity (Figures 6A and 6B). Increased FAO was further demonstrated by using intact muscle fibers from flexor digitorum brevis (FDB) muscle (Figure 6C). Fibers from *Cdk4*$^{-/-}$ FDB muscle metabolized palmitate at a higher rate (Figures 6C and 6D) and were capable to reach a higher maximal respiration (Figures 6C and 6E). The increased capacity of the muscles of *Cdk4*$^{-/-}$ mice to oxidize fatty acids suggested an overall metabolic phenotype in these mice.

Cdk4$^{-/-}$ mice have decreased body weight (Figure 6F). Consistent with increased AMPK activity, *Cdk4*$^{-/-}$ mice exhibit increased exercise capacity and decreased RER, indicating a preference toward fat oxidation (Figures 6G–6I). An 8-day treatment with LY2835219 did not trigger significant alterations in body weight and food intake (Figures 6J and S7D), although it induced a consistent albeit non-significant decrease in fat mass (Figure S7C) and a modest but significant increase in exercise performance (Figure 6K). A decrease in RER was observed after 4–5 days of treatment (Figures 6L and 6M). *In vivo*, the inhibition of CDK4 triggered an increase in the phosphorylation of ACC in quadriceps muscle (Figures S7E and S7G), suggesting increased AMPK activity. This was accompanied by an increase of the slow-twitch fiber marker MyHC I (Figure S7I). MyHC I mRNA levels were also increased in gastrocnemius and tibialis muscles from LY2835219-treated animals (Figures S7H–S7J).

Overall, these data suggest that CDK4 is a negative regulator of exercise capacity and whole-body oxidative metabolism in mice.

CDK4 Regulation of Oxidative Metabolism and Exercise Capacity *In Vivo* Requires Muscle AMPK

To determine if the effects of CDK4 inhibition in exercise performance and whole-body oxidative metabolism require muscle AMPK, we treated muscle-specific AMPK α1/α2 KO mice (MDKO) (Lantier et al., 2014) with the CDK4 inhibitor. Consistently, treatment with LY2835219 did not trigger significant alterations in body weight or food intake (Figures 7A and S7M) in control or in AMPK MDKO animals. In control animals, LY2835219 was sufficient to trigger a decrease (albeit not significant [p = 0.1243]) in fat mass, a modest increase in exercise performance, and a decrease in RER (Figures 7B–7D and S7L). In agreement with previous reports (Lantier et al., 2014; O'Neill et al., 2011), AMPK MDKO animals showed decreased RER and decreased exercise capacity (Figures 7B–7D). However, they were not affected by the treatment with LY2835219 under our experimental conditions (Figures 7A–7D and S7K–S7M). Taken together, these results show that the negative effects of CDK4 in oxidative metabolism and exercise performance *in vivo* involve muscle AMPK activity.

DISCUSSION

The contribution of CDK4 to the control of cell-cycle progression, via pocket proteins and E2F transcription factors, has been extensively studied (Malumbres, 2014) for more than two decades. However, the CDK4/6-pRB/E2F1 pathway was only recently implicated in metabolic regulation (Aguilar and Fajas, 2010; Blanchet et al., 2011; Denechaud et al., 2016; Lagarrigue et al., 2016; Lee et al., 2014; Lopez-Mejia and Fajas, 2015; Petrov et al., 2016; Salazar-Roa and Malumbres, 2016). Our study provides evidence that the cell-cycle kinase CDK4 is a key player in the control of cellular energy homeostasis and can also act independently of E2F1 to regulate metabolic pathways.

Three major findings are described here. First, we found that CDK4 negatively regulates the AMPK pathway and thus inhibits FAO through phosphorylation of the AMPKα2 subunit. Indeed, *Cdk4*$^{-/-}$ MEFs behaved like cells treated with an AMPK activator and exhibited high FAO levels and low levels of anaerobic glycolysis. Consistently, *Cdk4*$^{R24C/R24C}$ cells exhibited increased anaerobic glycolysis and very low FAO levels. A similar phenotype was observed in AMPK α2KO MEFs. Therefore, CDK4 activity is inversely correlated with AMPKα2-dependent activity. These findings indicate that CDK4 plays a central role in

---

(D and E) AMPK WT SV40 immortalized cells were treated for 8 hr with DMSO or LY2835219 (1.5 μM). AMP, ADP, and ATP were quantified by HPLC. The AMP/ATP (D) and ADP/ATP (E) ratios are shown.

(F–H) AMPK WT, AMPK α2 KO and AMPK DKO myotubes were treated with DMSO or 1.5μM LY2835219 for 24, and submitted to a FAO assay, in which the palmitate induced OCR was measured (in % OCR compared to the basal OCR). The area under curve of the palmitate induced OCR was quantified in (F). AMPK DKO myotubes were transfected with plasmids encoding Myc-tagged AMPK α2 and Myc-tagged AMPK α2 S > A. B. 48 hr later, myotubes were treated for 2 hr with DMSO or 50 μM A769662 before protein extraction; western blot analysis shows the A769662-induced ACC phosphorylation in transfected cells (G). Transfected myotubes were submitted to a FAO assay in which the palmitate-induced OCR was measured (in % OCR compared to the basal OCR). The area under curve of the palmitate-induced OCR was quantified in (H).

Data are expressed as mean ± SEM. See also Figure S4 and S5.
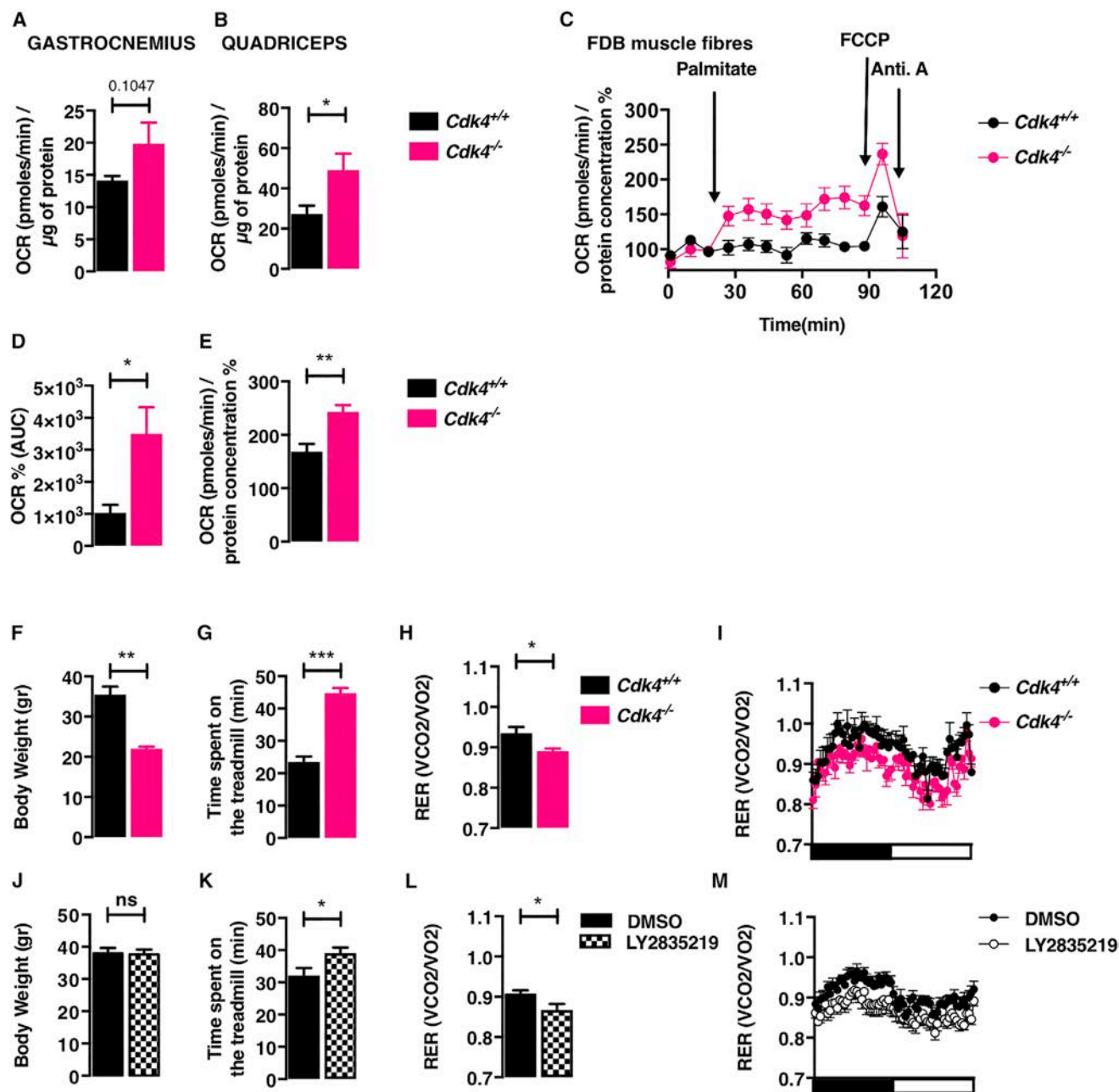
Figure 6. CDK4 Modulates Oxidative Metabolism and Exercise Capacity *In Vivo*

(A–E) Mitochondria isolated from gastrocnemius (A) and quadriceps (B) muscle from $Cdk4^{+/+}$ and $Cdk4^{-/-}$ mice were submitted to a respiration assay using fatty acids as a substrate. Isolated FDB muscle fibers from $Cdk4^{+/+}$ and $Cdk4^{-/-}$ mice were submitted to a FAO assay in which the palmitate-induced OCR was measured (in % OCR compared to the basal OCR) (C). The area under curve of the palmitate-induced OCR is shown (D). The maximal respiration was induced by FCCP (E).

(F) Body weight of 25- to 30-week-old male $Cdk4^{+/+}$ and $Cdk4^{-/-}$ mice was measured.

(G) $Cdk4^{+/+}$ and $Cdk4^{-/-}$ were submitted to an exercise capacity testing on treadmill, and the time before exhaustion was recorded.

(H and I) RER of the aforementioned mice is depicted.

(J and K) 30-week-old WT mice were gavaged with 37 mg/kg LY2835219 or vehicle for 8 days. Body weight (K) and exercise capacity (K) were measured the day after the last treatment.

(L and M) RER of the aforementioned mice after 5 days of treatment is depicted.

Data are expressed as mean ± SEM. See also Figure S6.
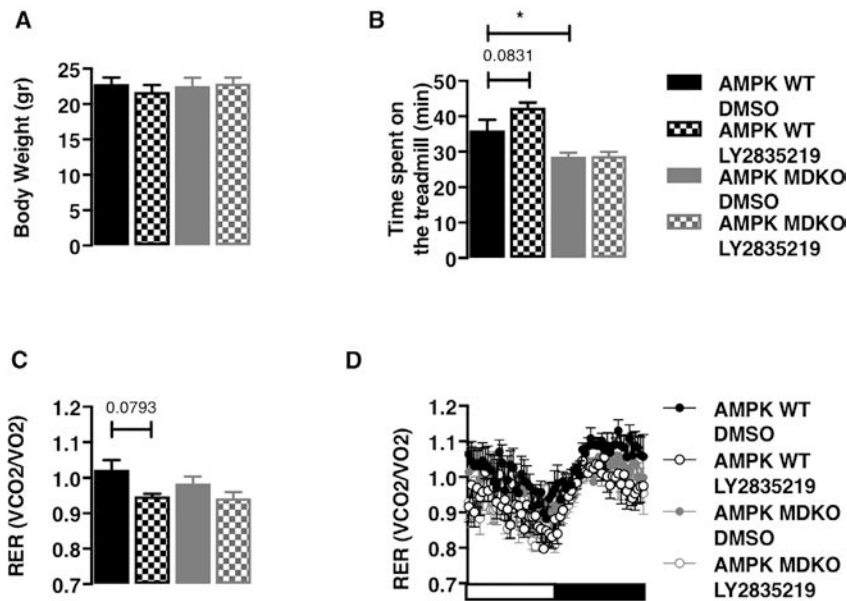
Figure 7. CDK4 Regulation of Oxidative Metabolism and Exercise Capacity *In Vivo* Requires Muscle AMPK

(A) Body weight of 12- to 16-week-old AMPK WT and AMPK MDKO females gavaged with 37 mg/kg LY2835219 or vehicle for 8 days was measured.

(B–D) Body weight of 12–16 weeks old AMPK WT and AMPK MDKO females gavaged with 37mg/kg of LY2835219 or vehicle for 8 days was measured in (A). To measure exercise capacity on treadmill, the time before exhaustion was recorded in (B). RER of the aforementioned mice is depicted in (C) and (D).

Data are expressed as mean ± SEM. See also Figure S7.

mitochondrial FAO that involves AMPKα2 inhibition and is independent of other downstream effectors, such as E2F1.

Cell division requires high cellular energy levels. Despite the recent evidence that underscores the existence of a crosstalk between cell-cycle regulators and energy metabolism (Lopez-Mejia and Fajas, 2015; Salazar-Roa and Malumbres, 2016), the molecular mechanisms coupling energy production and cell-cycle progression remain to be elucidated. Based on our results, we propose that to exert its role in both cell-cycle progression and the insulin-signaling pathway, CDK4 represses catabolism by directly targeting at least one of the catalytic subunits of AMPK, namely the α2 subunit. Interestingly, AKT, another key player of the insulin-signaling pathway, phosphorylates the α1 subunit of AMPK, thus reducing α1 Thr172 phosphorylation and the subsequent activation of the AMPK heterotrimer (Hawley et al., 2014; Horman et al., 2006). Remarkably, previous evidence from our laboratory demonstrates that CDK4 is a key effector of the AKT pathway (Lagarrigue et al., 2016). Surprisingly, GSK3 has been reported to inhibit AMPK activity after phosphorylation of the α subunit by AKT (Suzuki et al., 2013). This finding is somehow unexpected, since GSK3 activity is negatively regulated via phosphorylation by AKT upon insulin stimulation. Moreover, GSK3 is known to inhibit rather than promote anabolic pathways, like the synthesis of glycogen (Cohen and Frame, 2001).

The second major finding in our study is the observation that the function of AMPK heterotrimers can differ depending on their α subunit isoform. Few studies have focused on the specific function of each AMPK subunit (but see a recent review by Ross et al., 2016b), and models completely lacking AMPK activity are often used to study the function of AMPK. Liver-specific deletion or overexpression of the AMPKα2 subunit suggested that this isoform is involved in regulating the balance between lipid synthesis and FAO (Andreelli et al., 2006; Foretz et al., 2005), but these studies did not assess the differences in spec-

ificity between α1 and α2. Interestingly, leptin was shown to directly trigger FAO in muscle (Minokoshi et al., 2002) and trigger an anorexigenic response in hypothalamus (Minokoshi et al., 2004) in an AMPKα2-dependent manner. The effect on food intake may be triggered through AKT signaling via phosphorylation of AMPKα2 by p70S6K (Dagon et al., 2012). Other positive energy balance signals can also reduce food intake via AMPKα2 activity in the brain (Claret et al., 2007; Kim et al., 2004). The isoform-specific roles of the different AMPK subunits in whole-body energy homeostasis were further highlighted by the fact that the AMPKα2 subunit is essential for nicotine-triggered lipolysis in adipocytes (Wu et al., 2015). However, the specific regulation of energy homeostasis by AMPKα2, and the molecular mechanisms regulating α2-isoform specific AMPK activity have remained largely unknown.

The third major finding in our study is that the modulation of CDK4 activity *in vivo* can result in modifications in whole-body energy homeostasis and exercise performance. These modifications require the expression of AMPK in skeletal muscle. Our results are in agreement with previous studies demonstrating that the use of 5-aminoimidazole-4-carboxamide ribonucleotide (AICAR) can increase exercise performance in sedentary mice while increasing the proportion of slow-twitch fibers (Narkar et al., 2008). However, the exact mechanisms that mediate this phenotype remain to be studied. Global approaches to determine muscle reprograming at the proteomics and gene expression level will allow further study of the involvement of CDK4 in muscle biology, particularly during exercise. Given that muscle expresses the AMPKα2 subunit highly and responds to exercise by downregulating CDK activity (Hoffman et al., 2015), we believe that the study of the CDK4-AMPKα2 interaction in skeletal muscle will be very relevant to the discovery of pharmacological interventions to promote or enhance the beneficial effects of exercise on general health.

By identifying 4 new specific CDK4 phosphosites in the α2 subunit of AMPK, we have discovered a specific role for this subunit in the control of fatty acid metabolism that we could not demonstrate for the α1 subunit. Interestingly, we detected the phosphorylation of two of these residues, Ser[377] and Ser[345], in

muscle samples from resting mice and myotubes stimulated with insulin or IGF1.

FAO repression by CDK4 emerges as an additional level of metabolic regulation by this kinase, which also mediates other effects of the insulin-signaling pathway (Lagarrigue et al., 2016), including lipid synthesis, glycolysis (Denechaud et al., 2016), and proliferation (Malumbres and Barbacid, 2005).

In conclusion, our results demonstrate that CDK4 is a major regulator of cellular energy homeostasis. By combining experimental data from cellular metabolism analyses, biochemistry and molecular biology studies, and *in vivo* experiments, our work provides insights into the complex regulation of anabolic and catabolic pathways. These novel findings can have broad implications not only in the regulation of cell metabolism during proliferation but also in the control of energy utilization at the level of the whole organism. Moreover, they highlight the need to delve deeper into the specific functions of the different AMPK heterotrimers, as well as in the regulation of AMPK inactivation.

STAR★METHODS

Detailed methods are provided in the online version of this paper and include the following:

- KEY RESOURCES TABLE
- CONTACT FOR REAGENT AND RESOURCE SHARING
- EXPERIMENTAL MODEL AND SUBJECT DETAILS
  - Cell culture
  - Animal studies
- METHOD DETAILS
  - Materials
  - Immunoblot
  - Plasmid constructs and mutagenesis
  - GST production
  - CDK4 Kinase assay
  - Mitochondrial isolation
  - Isolation of adult skeletal muscle fibers
  - Seahorse analyses
  - Immunoprecipitation
  - Mass spectrometry
  - HPLC
  - mRNA analysis
- QUANTIFICATION AND STATISTICAL ANALYSES

SUPPLEMENTAL INFORMATION

Supplemental Information includes seven figures and three tables and can be found with this article online at https://doi.org/10.1016/j.molcel.2017.09.034.

AUTHOR CONTRIBUTIONS

I.C.L.-M. and L.F. designed this study. I.C.L.-M. guided and performed most experiments, with assistance from S.L., A.G., L.M.-C., P.-D.D., N.Z., C. Chavey, B.D., J.C.-A., A.N., L.Z., and C. Collodet. M.O. performed HPLC analysis for AMP-ADP-ATP quantification. B.V. generated the *Prkaa1*$^{-/-}$, *Prkaa2*$^{-/-}$ individual KOs and *Prkaa1*$^{-/-}$; *Prkaa2*$^{-/-}$ double-KO MEF cells and myoblasts, as well as the muscle-specific *Prkaa1*$^{-/-}$; *Prkaa2*$^{-/-}$ double-KO mice. D.G.H. helped to design the experiments and provided AMPK constructs. I.C.L.-M. and L.F. wrote the manuscript.

REFERENCES

Aguilar, V., and Fajas, L. (2010). Cycling through metabolism. EMBO Mol. Med. *2*, 338–348.

Andreelli, F., Foretz, M., Knauf, C., Cani, P.D., Perrin, C., Iglesias, M.A., Pillot, B., Bado, A., Tronche, F., Mithieux, G., et al. (2006). Liver adenosine monophosphate-activated kinase-alpha2 catalytic subunit is a key target for the control of hepatic glucose production by adiponectin and leptin but not insulin. Endocrinology *147*, 2432–2441.

Blanchet, E., Annicotte, J.S., Lagarrigue, S., Aguilar, V., Clapé, C., Chavey, C., Fritz, V., Casas, F., Apparailly, F., Auwerx, J., and Fajas, L. (2011). E2F transcription factor-1 regulates oxidative metabolism. Nat. Cell Biol. *13*, 1146–1152.

Carling, D. (2004). Ampk. Curr. Biol. *14*, R220.

Claret, M., Smith, M.A., Batterham, R.L., Selman, C., Choudhury, A.I., Fryer, L.G., Clements, M., Al-Qassab, H., Heffron, H., Xu, A.W., et al. (2007). AMPK is essential for energy homeostasis regulation and glucose sensing by POMC and AgRP neurons. J. Clin. Invest. *117*, 2325–2336.

Cohen, P., and Frame, S. (2001). The renaissance of GSK3. Nat. Rev. Mol. Cell Biol. *2*, 769–776.

Dagon, Y., Hur, E., Zheng, B., Wellenstein, K., Cantley, L.C., and Kahn, B.B. (2012). p70S6 kinase phosphorylates AMPK on serine 491 to mediate leptin's effect on food intake. Cell Metab. *16*, 104–112.

Daub, H., Olsen, J.V., Bairlein, M., Gnad, F., Oppermann, F.S., Körner, R., Greff, Z., Kéri, G., Stemmann, O., and Mann, M. (2008). Kinase-selective enrichment enables quantitative phosphoproteomics of the kinome across the cell cycle. Mol. Cell *31*, 438–448.

Denechaud, P.D., Lopez-Mejia, I.C., Giralt, A., Lai, Q., Blanchet, E., Delacuisine, B., Nicolay, B.N., Dyson, N.J., Bonner, C., Pattou, F., et al. (2016). E2F1 mediates sustained lipogenesis and contributes to hepatic steatosis. J. Clin. Invest. *126*, 137–150.

Dinkel, H., Chica, C., Via, A., Gould, C.M., Jensen, L.J., Gibson, T.J., and Diella, F. (2011). Phospho.ELM: a database of phosphorylation sites–update 2011. Nucleic Acids Res. *39*, D261–D267.

Djouder, N., Tuerk, R.D., Suter, M., Salvioni, P., Thali, R.F., Scholz, R., Vaahtomeri, K., Auchli, Y., Rechsteiner, H., Brunisholz, R.A., et al. (2010). PKA phosphorylates and inactivates AMPKalpha to promote efficient lipolysis. EMBO J. *29*, 469–481.

Foretz, M., Ancellin, N., Andreelli, F., Saintillan, Y., Grondin, P., Kahn, A., Thorens, B., Vaulont, S., and Viollet, B. (2005). Short-term overexpression of a constitutively active form of AMP-activated protein kinase in the liver leads to mild hypoglycemia and fatty liver. Diabetes *54*, 1331–1339.

Fullerton, M.D., Galic, S., Marcinko, K., Sikkema, S., Pulinilkunnil, T., Chen, Z.P., O'Neill, H.M., Ford, R.J., Palanivel, R., O'Brien, M., et al. (2013). Single phosphorylation sites in Acc1 and Acc2 regulate lipid homeostasis and the insulin-sensitizing effects of metformin. Nat. Med. *19*, 1649–1654.

Gnad, F., Gunawardena, J., and Mann, M. (2011). PHOSIDA 2011: the posttranslational modification database. Nucleic Acids Res. *39*, D253–D260.

Göransson, O., McBride, A., Hawley, S.A., Ross, F.A., Shpiro, N., Foretz, M., Viollet, B., Hardie, D.G., and Sakamoto, K. (2007). Mechanism of action of A-769662, a valuable tool for activation of AMP-activated protein kinase. J. Biol. Chem. *282*, 32549–32560.

Grahame Hardie, D. (2016). Regulation of AMP-activated protein kinase by natural and synthetic activators. Acta Pharm. Sin. B *6*, 1–19.

Hardie, D.G. (2015). AMPK: positive and negative regulation, and its role in whole-body energy homeostasis. Curr. Opin. Cell Biol. *33*, 1–7.

Hardie, D.G., and Pan, D.A. (2002). Regulation of fatty acid synthesis and oxidation by the AMP-activated protein kinase. Biochem. Soc. Trans. *30*, 1064–1070.

Hardie, D.G., Ross, F.A., and Hawley, S.A. (2012). AMPK: a nutrient and energy sensor that maintains energy homeostasis. Nat. Rev. Mol. Cell Biol. *13*, 251–262.

Hawley, S.A., Davison, M., Woods, A., Davies, S.P., Beri, R.K., Carling, D., and Hardie, D.G. (1996). Characterization of the AMP-activated protein kinase kinase from rat liver and identification of threonine 172 as the major site at which it phosphorylates AMP-activated protein kinase. J. Biol. Chem. *271*, 27879–27887.

Hawley, S.A., Boudeau, J., Reid, J.L., Mustard, K.J., Udd, L., Mäkelä, T.P., Alessi, D.R., and Hardie, D.G. (2003). Complexes between the LKB1 tumor suppressor, STRAD alpha/beta and MO25 alpha/beta are upstream kinases in the AMP-activated protein kinase cascade. J. Biol. *2*, 28.

Hawley, S.A., Pan, D.A., Mustard, K.J., Ross, L., Bain, J., Edelman, A.M., Frenguelli, B.G., and Hardie, D.G. (2005). Calmodulin-dependent protein kinase kinase-beta is an alternative upstream kinase for AMP-activated protein kinase. Cell Metab. *2*, 9–19.

Hawley, S.A., Ross, F.A., Gowans, G.J., Tibarewal, P., Leslie, N.R., and Hardie, D.G. (2014). Phosphorylation by Akt within the ST loop of AMPK-α1 down-regulates its activation in tumour cells. Biochem. J. *459*, 275–287.

Hoffman, N.J., Parker, B.L., Chaudhuri, R., Fisher-Wellman, K.H., Kleinert, M., Humphrey, S.J., Yang, P., Holliday, M., Trefely, S., Fazakerley, D.J., et al. (2015). Global phosphoproteomic analysis of human skeletal muscle reveals a network of exercise-regulated kinases and AMPK substrates. Cell Metab. *22*, 922–935.

Horman, S., Vertommen, D., Heath, R., Neumann, D., Mouton, V., Woods, A., Schlattner, U., Wallimann, T., Carling, D., Hue, L., and Rider, M.H. (2006). Insulin antagonizes ischemia-induced Thr172 phosphorylation of AMP-activated protein kinase alpha-subunits in heart via hierarchical phosphorylation of Ser485/491. J. Biol. Chem. *281*, 5335–5340.

Hornbeck, P.V., Zhang, B., Murray, B., Kornhauser, J.M., Latham, V., and Skrzypek, E. (2015). PhosphoSitePlus, 2014: mutations, PTMs and recalibrations. Nucleic Acids Res. *43*, D512–D520.

Humphrey, S.J., Azimifar, S.B., and Mann, M. (2015). High-throughput phosphoproteomics reveals in vivo insulin signaling dynamics. Nat. Biotechnol. *33*, 990–995.

Hurley, R.L., Anderson, K.A., Franzone, J.M., Kemp, B.E., Means, A.R., and Witters, L.A. (2005). The Ca2+/calmodulin-dependent protein kinase kinases are AMP-activated protein kinase kinases. J. Biol. Chem. *280*, 29060–29066.

Hurley, R.L., Barré, L.K., Wood, S.D., Anderson, K.A., Kemp, B.E., Means, A.R., and Witters, L.A. (2006). Regulation of AMP-activated protein kinase by multisite phosphorylation in response to agents that elevate cellular cAMP. J. Biol. Chem. *281*, 36662–36672.

Icreverzi, A., de la Cruz, A.F., Van Voorhies, W.A., and Edgar, B.A. (2012). Drosophila cyclin D/Cdk4 regulates mitochondrial biogenesis and aging and sensitizes animals to hypoxic stress. Cell Cycle *11*, 554–568.

Jones, R.G., and Thompson, C.B. (2009). Tumor suppressors and cell metabolism: a recipe for cancer growth. Genes Dev. *23*, 537–548.

Kettenbach, A.N., Schweppe, D.K., Faherty, B.K., Pechenick, D., Pletnev, A.A., and Gerber, S.A. (2011). Quantitative phosphoproteomics identifies substrates and functional modules of Aurora and Polo-like kinase activities in mitotic cells. Sci. Signal. *4*, rs5.

Kim, M.S., Park, J.Y., Namkoong, C., Jang, P.G., Ryu, J.W., Song, H.S., Yun, J.Y., Namgoong, I.S., Ha, J., Park, I.S., et al. (2004). Anti-obesity effects of alpha-lipoic acid mediated by suppression of hypothalamic AMP-activated protein kinase. Nat. Med. *10*, 727–733.

Laderoute, K.R., Amin, K., Calaoagan, J.M., Knapp, M., Le, T., Orduna, J., Foretz, M., and Viollet, B. (2006). 5'-AMP-activated protein kinase (AMPK) is induced by low-oxygen and glucose deprivation conditions found in solid-tumor microenvironments. Mol. Cell. Biol. *26*, 5336–5347.

Lagarrigue, S., Lopez-Mejia, I.C., Denechaud, P.D., Escoté, X., Castillo-Armengol, J., Jimenez, V., Chavey, C., Giralt, A., Lai, Q., Zhang, L., et al. (2016). CDK4 is an essential insulin effector in adipocytes. J. Clin. Invest. *126*, 335–348.

Lantier, L., Mounier, R., Leclerc, J., Pende, M., Foretz, M., and Viollet, B. (2010). Coordinated maintenance of muscle cell size control by AMP-activated protein kinase. FASEB J. *24*, 3555–3561.

Lantier, L., Fentz, J., Mounier, R., Leclerc, J., Treebak, J.T., Pehmøller, C., Sanz, N., Sakakibara, I., Saint-Amand, E., Rimbaud, S., et al. (2014). AMPK controls exercise endurance, mitochondrial oxidative capacity, and skeletal muscle integrity. FASEB J. *28*, 3211–3224.

Lee, Y., Dominy, J.E., Choi, Y.J., Jurczak, M., Tolliday, N., Camporez, J.P., Chim, H., Lim, J.H., Ruan, H.B., Yang, X., et al. (2014). Cyclin D1-Cdk4 controls glucose metabolism independently of cell cycle progression. Nature *510*, 547–551.

López-Cotarelo, P., Escribano-Díaz, C., González-Bethencourt, I.L., Gómez-Moreira, C., Deguiz, M.L., Torres-Bacete, J., Gómez-Cabañas, L., Fernández-Barrera, J., Delgado-Martín, C., Mellado, M., et al. (2015). A novel MEK-ERK-AMPK signaling axis controls chemokine receptor CCR7-dependent survival in human mature dendritic cells. J. Biol. Chem. *290*, 827–840.

Lopez-Mejia, I.C., and Fajas, L. (2015). Cell cycle regulation of mitochondrial function. Curr. Opin. Cell Biol. *33*, 19–25.

Malumbres, M. (2014). Cyclin-dependent kinases. Genome Biol. *15*, 122.

Malumbres, M., and Barbacid, M. (2001). To cycle or not to cycle: a critical decision in cancer. Nat. Rev. Cancer *1*, 222–231.

Malumbres, M., and Barbacid, M. (2005). Mammalian cyclin-dependent kinases. Trends Biochem. Sci. *30*, 630–641.

Malumbres, M., and Barbacid, M. (2009). Cell cycle, CDKs and cancer: a changing paradigm. Nat. Rev. Cancer *9*, 153–166.

Manfredi, G., Yang, L., Gajewski, C.D., and Mattiazzi, M. (2002). Measurements of ATP in mammalian cells. Methods *26*, 317–326.

Martín-Campos, T., Mylonas, R., Masselot, A., Waridel, P., Petricevic, T., Xenarios, I., and Quadroni, M. (2017). MsViz, a graphical software tool for in-depth manual validation and quantitation of post-translational modifications. J. Proteome Res. *16*, 3092–3101.

Minokoshi, Y., Kim, Y.B., Peroni, O.D., Fryer, L.G., Müller, C., Carling, D., and Kahn, B.B. (2002). Leptin stimulates fatty-acid oxidation by activating AMP-activated protein kinase. Nature *415*, 339–343.

Minokoshi, Y., Alquier, T., Furukawa, N., Kim, Y.B., Lee, A., Xue, B., Mu, J., Foufelle, F., Ferré, P., Birnbaum, M.J., et al. (2004). AMP-kinase regulates food intake by responding to hormonal and nutrient signals in the hypothalamus. Nature *428*, 569–574.

Moreno, D., Knecht, E., Viollet, B., and Sanz, P. (2008). A769662, a novel activator of AMP-activated protein kinase, inhibits non-proteolytic components of the 26S proteasome by an AMPK-independent mechanism. FEBS Lett. *582*, 2650–2654.

Morizane, Y., Thanos, A., Takeuchi, K., Murakami, Y., Kayama, M., Trichonas, G., Miller, J., Foretz, M., Viollet, B., and Vavvas, D.G. (2011). AMP-activated protein kinase suppresses matrix metalloproteinase-9 expression in mouse embryonic fibroblasts. J. Biol. Chem. *286*, 16030–16038.

Mounier, R., Théret, M., Lantier, L., Foretz, M., and Viollet, B. (2015). Expanding roles for AMPK in skeletal muscle plasticity. Trends Endocrinol. Metab. *26*, 275–286.

Narkar, V.A., Downes, M., Yu, R.T., Embler, E., Wang, Y.X., Banayo, E., Mihaylova, M.M., Nelson, M.C., Zou, Y., Juguilon, H., et al. (2008). AMPK and PPARdelta agonists are exercise mimetics. Cell *134*, 405–415.

Nesvizhskii, A.I., Keller, A., Kolker, E., and Aebersold, R. (2003). A statistical model for identifying proteins by tandem mass spectrometry. Analytical Chemistry *75*, 4646–4658.

O'Leary, B., Finn, R.S., and Turner, N.C. (2016). Treating cancer with selective CDK4/6 inhibitors. Nat. Rev. Clin. Oncol. *13*, 417–430.

O'Neill, H.M., Maarbjerg, S.J., Crane, J.D., Jeppesen, J., Jørgensen, S.B., Schertzer, J.D., Shyroka, O., Kiens, B., van Denderen, B.J., Tarnopolsky, M.A., et al. (2011). AMP-activated protein kinase (AMPK) beta1beta2 muscle null mice reveal an essential role for AMPK in maintaining mitochondrial content and glucose uptake during exercise. Proc. Natl. Acad. Sci. USA *108*, 16092–16097.

O'Neill, H.M., Lally, J.S., Galic, S., Thomas, M., Azizi, P.D., Fullerton, M.D., Smith, B.K., Pulinilkunnil, T., Chen, Z., Samaan, M.C., et al. (2014). AMPK phosphorylation of ACC2 is required for skeletal muscle fatty acid oxidation and insulin sensitivity in mice. Diabetologia *57*, 1693–1702.

Petrov, P.D., Ribot, J., López-Mejía, I.C., Fajas, L., Palou, A., and Bonet, M.L. (2016). Retinoblastoma protein knockdown favors oxidative metabolism and glucose and fatty acid disposal in muscle cells. J. Cell. Physiol. *231*, 708–718.

Rane, S.G., Dubus, P., Mettus, R.V., Galbreath, E.J., Boden, G., Reddy, E.P., and Barbacid, M. (1999). Loss of Cdk4 expression causes insulin-deficient diabetes and Cdk4 activation results in beta-islet cell hyperplasia. Nat. Genet. *22*, 44–52.

Rane, S.G., Cosenza, S.C., Mettus, R.V., and Reddy, E.P. (2002). Germ line transmission of the Cdk4(R24C) mutation facilitates tumorigenesis and escape from cellular senescence. Mol. Cell. Biol. *22*, 644–656.

Ross, F.A., Jensen, T.E., and Hardie, D.G. (2016a). Differential regulation by AMP and ADP of AMPK complexes containing different γ subunit isoforms. Biochem. J. *473*, 189–199.

Ross, F.A., MacKintosh, C., and Hardie, D.G. (2016b). AMP-activated protein kinase: a cellular energy sensor that comes in 12 flavours. FEBS J. *283*, 2987–3001.

Salazar-Roa, M., and Malumbres, M. (2016). Fueling the cell division cycle. Trends Cell Biol. *27*, 69–81.

Schindelin, J., Arganda-Carreras, I., Frise, E., Kaynig, V., Longair, M., Pietzsch, T., Preibisch, S., Rueden, C., Saalfeld, S., Schmid, B., et al. (2012). Fiji: an open-source platform for biological-image analysis. Nat. Methods *9*, 676–682.

Shaw, R.J., Kosmatka, M., Bardeesy, N., Hurley, R.L., Witters, L.A., DePinho, R.A., and Cantley, L.C. (2004). The tumor suppressor LKB1 kinase directly activates AMP-activated kinase and regulates apoptosis in response to energy stress. Proc. Natl. Acad. Sci. USA *101*, 3329–3335.

Suzuki, T., Bridges, D., Nakada, D., Skiniotis, G., Morrison, S.J., Lin, J.D., Saltiel, A.R., and Inoki, K. (2013). Inhibition of AMPK catabolic action by GSK3. Mol. Cell *50*, 407–419.

Wölfel, T., Hauer, M., Schneider, J., Serrano, M., Wölfel, C., Klehmann-Hieb, E., De Plaen, E., Hankeln, T., Meyer zum Büschenfelde, K.H., and Beach, D. (1995). A p16INK4a-insensitive CDK4 mutant targeted by cytolytic T lymphocytes in a human melanoma. Science *269*, 1281–1284.

Woods, A., Johnstone, S.R., Dickerson, K., Leiper, F.C., Fryer, L.G., Neumann, D., Schlattner, U., Wallimann, T., Carlson, M., and Carling, D. (2003). LKB1 is the upstream kinase in the AMP-activated protein kinase cascade. Curr. Biol. *13*, 2004–2008.

Woods, A., Dickerson, K., Heath, R., Hong, S.P., Momcilovic, M., Johnstone, S.R., Carlson, M., and Carling, D. (2005). Ca2+/calmodulin-dependent protein kinase kinase-beta acts upstream of AMP-activated protein kinase in mammalian cells. Cell Metab. *2*, 21–33.

Wu, Y., Song, P., Zhang, W., Liu, J., Dai, X., Liu, Z., Lu, Q., Ouyang, C., Xie, Z., Zhao, Z., et al. (2015). Activation of AMPKα2 in adipocytes is essential for nicotine-induced insulin resistance in vivo. Nat. Med. *21*, 373–382.

Zhang, C.S., Hawley, S.A., Zong, Y., Li, M.Q., Wang, Z.C., Gray, A., Ma, T., Cui, J.W., Feng, J.W., Zhu, M.J., et al. (2017). Fructose-1,6-bisphosphate and aldolase mediate glucose sensing by AMPK. Nature *548*, 112–116.

STAR★METHODS

KEY RESOURCES TABLE

REAGENT or RESOURCE	SOURCE	IDENTIFIER
Antibodies		
Rabbit polyclonal anti-ACC	Cell Signaling Technology	Cat#3662
Rabbit polyclonal anti-Phospho-ACC	Cell Signaling Technology	Cat#3661
Rabbit polyclonal anti-AMPKa	Cell Signaling Technology	Cat#2532
Rabbit monoclonal anti-Phospho-AMPKa(Thr172)(40H9)	Cell Signaling Technology	Cat#2535
Mouse monoclonal anti-Myc-Tag (9B11)	Cell Signaling Technology	Cat#2276
Rabbit monoclonal anti-Phospho Rb (ser780)(D59B7)	Cell Signaling Technology	Cat#8180
Rabbit polyclonal anti-Cdk4 (C-22)	Santa Cruz biotechnology	Sc-260
Mouse monoclonal anti-Rb (C-2)	Santa Cruz biotechnology	Sc-74562
Goat polyclonal anti-AMPK a2 (C-20)	Santa Cruz biotechnology	Sc-19131
Goat polyclonal anti-Actin (C11)	Santa Cruz biotechnology	Sc-1615
Rabbit polyclonal anti-Myc-Tag	Abcam	Ab9106
Mouse monoclonal anti-a-Tubulin	Sigma-Aldrich	T6199
Chemicals, Peptides, and Recombinant Proteins		
LY2835219	MedChemExpress	HY-16297
PD0332991	MedChemExpress	HY-50767
LEE011	MedChemExpress	HY-15777
A769662	MedChemExpress	HY-50662
Compound C	MedChemExpress	HY-13418
FCCP	Sigma Aldrich	C2920
Antimycine A	Sigma Aldrich	A8674
CDK4/CycD3	ProQinase	0142-0373-1
CDK4/CycD1	ProQinase	0142-0143-1
Recombinant kinase dead AMPK trimers ($\alpha2\beta2\gamma1$)	DG. Hardie lab.	
Experimental Models: Cell Lines		
C2C12	ATCC	CRL-1772
Primary and SV40 immortalized $Cdk4^{-/-}$ MEFs	This paper	N/A
Primary and SV40 immortalized $Cdk4^{+/+}$ MEFs,	This paper	N/A
Primary and SV40 immortalized $Cdk4^{R24C/R24C}$ MEFs	This paper	N/A
Primary $E2f1^{+/+}$ MEFs	This paper	N/A
Primary $E2f1^{-/-}$ MEFs	This paper	N/A
Primary $Cdk4^{R24C/R24C}$ $E2f1^{+/+}$ MEFs	This paper	N/A
Primary $Cdk4^{R24C/R24C}$ $E2f1^{-/-}$ MEFs	This paper	N/A
$Prkaa1^{-/-}$ SV40 immortalized MEFs	(Laderoute et al., 2006)	N/A
$Prkaa2^{-/-}$ SV40 immortalized MEFs	(Laderoute et al., 2006)	N/A
$Prkaa1^{-/-}$; $Prkaa2^{-/-}$ double KO SV40 immortalized MEFs	(Laderoute et al., 2006)	N/A
AMPK alpha2 KO Myoblasts	(Lantier et al., 2010)	N/A
AMPK alpha1, alpha2 double KO Myoblasts	(Lantier et al., 2010)	N/A
AMPK WT Myoblasts	(Lantier et al., 2010)	N/A
Experimental Models: Organisms/Strains		
Skeletal muscle AMPK-deficient mice [AMPK_1fl/fl _2fl/fl human skeletal actin (HSA)-Cre_ mice on a C57Bl6- 129Sv mixed background]	(Lantier et al., 2014)	N/A
The generation of $Cdk4^{-/-}$, that lack CDK4 in all tissues except pancreatic beta cells and were referred as $Cdk4^{nc/nc}$ in our previous study.	(Lagarrigue et al., 2016)	N/A
C57BL/6JRj mice.		Janvier Labs

(Continued on next page)

Continued

REAGENT or RESOURCE	SOURCE	IDENTIFIER
Oligonucleotides		
See Table S2		N/A
See Table S3		N/A
Recombinant DNA		
pDONR223-hPRKAA1	Addgene	(ref:23871)
pDONR223-hPRKAA2	Addgene	(ref:23671)
pDONR223-hPRKAB1	Addgene	(ref:23360)
pDONR223-hPRKAB2	Addgene	(ref:23647)
pDONR223-hPRKAG1,	Addgene	(ref:23718)
pDONR223-hPRKAG2	Addgene	(ref:23689)
pDONR223-hPRKAG3	Addgene	(ref:23549)
pDEST pGEX-2T-hPRKAA1	This paper	N/A
pDEST pGEX-2T -hPRKAA2	This paper	N/A
pDEST pGEX-2T -hPRKAB1	This paper	N/A
pDEST pGEX-2T -hPRKAB2	This paper	N/A
pDEST pGEX-2T -hPRKAG1,	This paper	N/A
pDEST pGEX-2T -hPRKAG2	This paper	N/A
pDEST pGEX-2T -hPRKAG3	This paper	N/A
pDEST pGEX-2T -hPRKAA2 D1	This paper	N/A
pDEST pGEX-2T -hPRKAA2 D1 S176A	This paper	N/A
pDEST pGEX-2T -hPRKAA2 D2	This paper	N/A
pDEST pGEX-2T -hPRKAA2 D2 S345A	This paper	N/A
pDEST pGEX-2T -hPRKAA2 D3	This paper	N/A
pDEST pGEX-2T -hPRKAA2 D3 S377A	This paper	N/A
pDEST pGEX-2T -hPRKAA2 D4	This paper	N/A
pDEST pGEX-2T -hPRKAA2 D4 T485A	This paper	N/A
pGEX-2T -hPRKAA2 D4 T485A S529A	This paper	N/A
pDEST pGEX-2T -hPRKAA2 D2-D3	This paper	N/A
pDEST pGEX-2T -hPRKAA2 D2-D3 S345A S377A	This paper	N/A
pDEST pGEX-2T -hPRKAA2 S377A S345A T485A S529A	This paper	N/A
pCDNA3 MYC hPRKAA1	This paper	N/A
pCDNA3 MYC hPRKAA2	This paper	N/A
pCDNA3 MYC hPRKAA2 S377A S345A T485A S529A	This paper	N/A
Software and Algorithms		
Protein Prophet algorithm	(Nesvizhskii et al., 2003)	N/A
MsViz software	(Martín-Campos et al., 2017)	N/A
Fiji image processing package	(Schindelin et al., 2012).	N/A

CONTACT FOR REAGENT AND RESOURCE SHARING

Further information and requests for resources and reagents should be directed to and will fulfilled by Lluis Fajas (lluis.fajas@unil.ch).

EXPERIMENTAL MODEL AND SUBJECT DETAILS

Cell culture

MEFs were derived from embryos that were dissected 13.5 days after vaginal plugs. The $Cdk4^{-/-}$ ($Cdk4^{nc}$), $Cdk4^{R24C/R24C}$ and $E2f1^{-/-}$ mice have been previously described (Denechaud et al., 2016; Lagarrigue et al., 2016).

Prkaa1$^{-/-}$, *Prkaa2$^{-/-}$* individual KOs; and *Prkaa1$^{-/-}$*; *Prkaa2$^{-/-}$* double KO SV40 immortalized MEF cells were prepared as described (Laderoute et al., 2006). They are referred in the manuscript as AMPK α1KO, AMPK α2KO and AMPK DKO.

MEFs were cultured in DMEM/F12 supplemented with 10% fetal bovine serum (FBS, PAA Laboratories), glutamax (1mM), sodium pyruvate (1mM), non-essential amino-acids, 2-Mercapto-ethanol (50μM) and antibiotics in 5% CO_2 37°C incubator.

C2C12 myoblasts were obtained from ATCC and were cultured in low-glucose DMEM with 10% FBS in 5% CO_2 37°C incubator. For myotube differentiation, when the cells reached 80%–90% confluency, the culture medium was switched to DMEM containing 2% horse serum. The medium was changed every 2 days until day 5 to 7 of differentiation.

Primary myoblasts were grown in collagen coated plates cultured DMEM/F12 supplemented with 20% fetal bovine serum, 2mM Glutamine and FGF (5ng/ml) in 5% CO_2 37°C incubator. For myotube differentiation, cells were plated on matrigel-coated plates when the cells reached 80%–90% confluency, the culture medium was switched to DMEM/F12 supplemented with 2% horse serum and 2mM Glutamine. The medium was changed every 2 days until day 4-5 of differentiation. For rescue experiments, myotubes were transfected using lipofectamine 3000 (Thermo Fisher Scientific), at day 1 and day 3 of differentiation. The cells were assayed 48 hr after the 2nd round of transfection.

Primary *Cdk4$^{+/+}$, Cdk4$^{-/-}$* and *Cdk4$^{R24C/R24C}$* MEFs, as well as primary *E2f1$^{+/+}$, E2f1$^{-/-}$, Cdk4$^{R24C/R24C}$ E2f1$^{+/+}$* and *Cdk4$^{R24C/R24C}$ E2f1$^{-/-}$* MEFs, between P2 and P5, were used for Figures 1 and 2. SV40 immortalized MEFs were used for all other figures.

Animal studies

The generation of *Cdk4$^{-/-}$*, that lack CDK4 in all tissues except pancreatic beta cells and were referred as *Cdk4$^{nc/nc}$* in our previous study, was described in (Lagarrigue et al., 2016). Male mice were used.

For gavage experiments, C57BL/6J male mice were obtained from Janvier Labs. Animals were gavaged daily with 37mg/kg of LY2835219 or vehicle for 8 days. Mice were acclimated and submitted to indirect calorimetry between day 4 and day 6. Exercise capacity testing was performed the day after the last gavage. Body weight was controlled daily. Food intake was measured in the metabolic cages.

To obtain skeletal muscle AMPK-deficient mice [AMPK_1fl/fl _2fl/fl human skeletal actin (HSA)-Cre_ mice on a C57Bl6- 129Sv mixed background], AMPK_1$^{fl/fl}$-2$^{fl/fl}$ mice were interbred with transgenic mice expressing Cre recombinase under the control of the HSA promoter. Female mice were used.

The mice were housed in a facility on a 12-h light-dark cycle with free access to standard rodent chow and water.

Mice were familiarized to the motorized rodent treadmill (Columbus Instruments, Columbus OH) on the J-2 and J-1 before the evaluation of exercise capacity. Familiarization consisted of an initial 10 min period where the treadmill speed and incline were set to zero with a slight electric shock grid at the back of the carpet set to 20 V, 0.34 mA, and 2 Hz. The treadmill speed was then increased steadily to 10 m/min (J-2) and 12 m/min (J-1) for an additional 10 min.

The day immediately following familiarization to the treadmill, mice were subjected to an exercise capacity test. For this, the mice were acclimated to the treadmill for 10 min, with the speed and incline set initially to zero. The treadmill speed was then increase to 8.5 m/min with an angle of inclination set to 0° for 9 min. Next, the treadmill speed and incline was increased to 10 m/min and 5°, respectively, for 3 min. The speed was then increased by 2.5 m/min every 3 min to a maximum speed of 40 m/min, while inclination was increased by 5° every 9 min until a maximum incline of 15°.

Strict a priori criteria for exercise-induced exhaustion consisted in: (1) 10 consecutive seconds on the electric grid; (2) spending more than 50% of time on the grid; and/or (3) lack of motivation to manual prodding. Mice were immediately removed from their respective lane once one or more of these criteria were reached.

Following the protocol, mice were killed by cervical dislocation and skeletal muscles were isolated for analysis.

All animal care and treatment procedures were performed in accordance with Swiss guidelines and were approved by the Canton of Vaud, Service de la Consommation et des Affaires Vétérinaires (SCAV) (authorization VD 3121.a).

METHOD DETAILS

Materials

All cell culture reagents were purchased from GIBCO (Thermo Fisher Scientific). All chemicals, except if stated otherwise, were purchased from Sigma-Aldrich. The CDK4 *inhibitor (LY2835219) and* Compound C. were purchased from MedChem Express. Experiments were done using 1μM of LY2835219, unless stated otherwise. The AMPK allosteric activator was purchased from Abcam or MedChem Express. Unless stated otherwise, A769662 was used at a concentration of 50μM. γ-^{33}P-ATP was purchased from Perkin Elmer.

Immunoblot

For western blot analysis, the cells were seeded in 6-well plates 48 hr before the experiment, serum starved for 3 hr, and treated with either LY2835219 or A769662 for 2 hr.

Total proteins extracts were subjected to SDS-PAGE analysis and transferred to nitrocellulose membranes for immunoblotting. The following antibodies were obtained from Cell Signaling Technology: ACC (no. 3662), phosphorylated ACC (ser79) (no. 3661), AMPK (no.2532), phosphorylated AMPK (Thr172) (no 2535), Myc-tag (no. 2276), phosphorylated RB (Ser780) (no. 8180). The

following antibodies were obtained from Santa Cruz Technology: Cdk4 (C-22; sc-260), Rb (C-2; sc-74562), AMPK α2 (sc-19131). A second Myc-tag antibody was used to analyze myotube samples (Abcam ab9106)

The α Tubulin (no. T6199) antibody was obtained from Sigma Aldrich, the actin (sc-1615) was obtained from Santa Cruz Technology.

The levels of total proteins and the levels of phosphorylation of proteins were analyzed on separate gels. The band intensities on developed films, fusion FX images or chemidoc images or were quantified using Fiji image processing package (Schindelin et al., 2012).

Plasmid constructs and mutagenesis

pDONR223-hPRKAA1 (ref:23871), pDONR223-hPRKAA2 (ref:23671), pDONR223-hPRKAB1 (ref:23360), pDONR223-hPRKAB2 (ref:23647), pDONR223-hPRKAG1 (ref:23718), pDONR223-hPRKAG2 (ref:23689), pDONR223-hPRKAG3 (ref:23549) were provided from Addgene. The different GST subunits of human AMPK were obtained using the pDEST pGEX-2T vector of Gateway Cloning Technology (Invitrogen) starting from previously described pDONR223AMPK constructs. The different serine-to-alanine mutants of GST-hPRKAA2 were generated using a Quick-Change Site-Directed Mutagenesis kit (Stratagene) with the following primers (Table S2). A similar strategy was used to obtain the truncated versions of GST-hPRKAA2 and the different serine-to-alanine mutants using the following primers (Table S2).

The Myc-hPRKAA1, the Myc-hPRKAA2 and the Myc-hPRKAA2-S345A-S377A-T485A-S529A were obtained using the pDEST pCDNA3 MYC vector previously and the above described pDONR223-human AMPK constructs. pDONR-hRB 379-928aa was subcloned from pCMV human RB and generated using the pDONR221 vector of Gateway Cloning Technology. The pGEX-2T hRB 379-928aa was obtained using the pDEST pGEX-2T from Gateway Cloning Technology.

GST production

Independent AMPK subunits were cloned in the pDEST pGEX-2T and expressed in BL21 bacteria. GST-purified proteins were re-suspended in 50mM Tris.HCl [pH 8], 100 mM NaCl, 5 mM DTT and 20% glycerol buffer.

CDK4 Kinase assay

Kinase assays were performed using independent AMPK subunits proteins and 500ng of recombinant RB protein (Santa Cruz) as a substrate in kinase buffer (25 mM Tris.HCl [pH 7.5], 150 mM NaCl, 10 mM MgCl$_2$, 1 mM DTT, 5 mM Na$_4$P$_2$O$_7$, 50 mM NaF, 1 mM vanadate and protease inhibitor cocktail) with 40 μM ATP and 8 μCi γ-^{33P}ATP (Perkin Elmer) for 30 min at 30°C. Recombinant CDK4/cyclin D3 kinase and CDK4/Cyclin D1 (ProQinase) were used. RB was used as a positive control.

Boiling the samples for 5 min in the presence of denaturing sample buffer stopped the reaction. Samples were subsequently subjected to SDS–PAGE, and transferred to a nitrocellulose membrane before being exposed to an X-ray film at −80°C during 4 hr or over night. Recombinant protein loading was confirmed by SYPRO Ruby protein Blot Staining (Life Technologies).

For mass spectrometry, recombinant kinase dead AMPK trimers (α2β2γ1) were used as a substrate for CDK4/CyCD3. Recombinant kinase dead AMPK trimers (α2β2γ1) were produced by the DG. Hardie lab.

Mitochondrial isolation

Quadriceps muscle from $Cdk4^{+/+}$ or $Cdk4^{-/-}$ mice were homogenized in 2ml cold buffer I. Tissue homogenization was obtained at 1500rpm after 30 strokes. The homogenized extract was then centrifuged at 600 g for 10 min at 4°C in order to remove cellular debris. This step was performed three times. The mitochondrial fraction was pelleted at 10000 g for 10 min at 4°C and subsequently washed using buffer II. The mitochondrial pellet was suspended in 80ul cold buffer II. Mitochondria were immediately used for seahorse analysis. Buffers I composition is as follows: 210 mM mannitol, 70 mM sucrose, 5 mM HEPES, 1 mM EGTA, 0.5% BSA pH to 7.4. Buffer II composition is as follows: 210 mM mannitol, 70 mM sucrose, 10 mM MgCl2, 5 mMK2HPO4, 10 mM MOPS, 1 mM EGTA pH to 7.4.

Isolation of adult skeletal muscle fibers

Flexor digitorum brevis (FDB) muscles were incubated for 45 min at 37°C in an oxygenated 'Krebs-HEPES' solution containing 0.2% collagenase type IV (GIBCO). Muscles were then washed twice in DMEM/F12 supplemented with 2% fetal bovine serum and mechanically dissociated by repeated passages through fire-polished Pasteur pipettes of progressively decreasing diameter. Dissociated fibers were plated directed onto Seahorse XF24 tissue culture dishes coated with Matrigel and allowed to adhere to the bottom of the dish for 2h. After checking the adhesion of the fibers, a seahorse Fatty acid oxidation was performed as described

The Krebs-HEPES solution contains NaCl 135.5mM, MgCl$_2$ 1.2mM, KCl 5.9mM, glucose 11.5mM, HEPES 11.5mM and CaCl$_2$ mM.

Seahorse analyses

For seahorse analysis, the cells were seeded 16 hr before the experiment.

Mitochondrial function was determined with an XF-24 extracellular flux analyzer (Seahorse Bioscience). Oxygen consumption Rate (OCR) and Extracellular acidification rate (ECAR) was measured in adherent MEFs. Control and mutant fibroblast cells were seeded in an XF 24-well cell culture microplate at a density of 7×10^5 cells per cell in 200 μL DMEM/F12 media. Cells were incubated for 16 hr at 37°C in 5% CO$_2$ before the assay. OCR was expressed as pmol of O$_2$ per minute and was normalized by protein content a Pierce BCA

Protein Assay protocol (Thermo Fisher Scientific). ECAR was expressed as mpH per minute and was normalized by protein content a Pierce BCA Protein Assay protocol (Thermo Fisher Scientific).

For glycolysis experiments, just before the experiment the cells were washed, and the growth medium was replaced with DMEM medium containing only 2mM Glutamine. Cells were then pre-incubated for 1 hr at 37°C without CO_2 to allow cells to pre-equilibrate with the assay media before starting the glycolysis test procedure. After measuring baseline ECAR, ECAR was measured after an acute injection of 25mM Glucose. The glycolytic rate was calculated as glucose dependent ECAR. It was calculated as follows: Glucose induced ECAR-basal ECAR.

For fatty acid oxidation experiments, just before the experiment the cells are washed, and the growth medium was replaced with KHB containing 2.5mM Glucose and 1.5mM of carnitine. Cells were then pre-incubated for 1 hr at 37°C without CO_2 to allow cells to pre-equilibrate with the assay media before starting the fatty acid oxidation procedure. After measuring baseline OCR as an indication of basal respiration, OCR was measured after an acute injection of 400µM or 150µM of palmitate coupled to BSA (for MEFs and myotubes respectively).

For FDB muscle fibers 125µM of palmitate coupled to BSA, 400nM of FCCP and 1µM of Antimycine A were injected directly onto the fibers using the seahorse analyzer. Fatty acid oxidation was induced by the palmitate injection. The uncoupling agent FCCP induced the maximal respiration.

OCR was expressed as pmol of O_2 per minute and was normalized by total DNA content.

For mitochondrial respiration, 50 µL of mitochondrial suspension (containing 10µg of freshly isolated mitochondria) were used per well. The XF24 cell culture microplate was centrifuged at 2000 g for 20 min at 4°C. The assay medium contained 250 mM sucrose, 15 mM KCl, 1 mM EGTA, 5 mMMgCl2, 30 mM K2HPO4, 2mM HEPES and 0.2% FFA-Free BSA. 0.5mM Malate, 80µM PalmitoylCoA, 240µM Carnitine and 4mM ADP diluted in assay medium were added after the centrifugation of the mitochondria to obtain a final volume of 525µl per well. After 10 min of incubation at 37°C without CO2 the mitochondrial respiration was measured using the seahorse analyzer.

Immunoprecipitation

Myotubes or liquid N2 grinded muscle samples were lysed in M-PER buffer (Thermo Fisher Scientific) and incubated in agitation for one hour at 4°C. 2-5 mg of protein was immunoprecipitated overnight with an AMPKα2 antibody (Santa Cruz, sc-19131) and Protein G coupled with magnetic beads (Sigma, 1004D) in the following buffer (IP buffer): 25 mM TRIS pH 7.9, 5 mM $MgCl_2$, 10% Glycerol, 100 mM KCl, 0.1% NP40, 0.3 mM DTT. Next day, beads were washed for times with the IP buffer and frozen. Samples were used for mass spectrometry.

Mass spectrometry

In the *in vitro* assays, protein samples were loaded on a 12% mini polyacrylamide gel and migrated about 3 cm, while in the immunoprecipitation experiments proteins were loaded on an 8% gel and fully migrated. After Coomassie staining, visible band between 50 and 75 kDa corresponding to AAPK2 was excised and digested with sequencing-grade trypsin (Promega). Extracted tryptic peptides were dried and resuspended in 0.05% trifluoroacetic acid, 2% (v/v) acetonitrile for mass spectrometry analyses.

Tryptic peptide mixtures were injected on an Ultimate RSLC 3000 nanoHPLC system (Dionex, Sunnyvale, CA, USA) interfaced via a nanospray source to a high resolution mass spectrometer based on Orbitrap technology: Fusion Tribrid or QExactive Plus (Thermo Fisher, Bremen, Germany), depending on the experiments considered. Peptides were loaded onto a trapping microcolumn Acclaim PepMap100 C18 (20 mm x 100 µm ID, 5 µm, Dionex) before separation on a C18 reversed-phase analytical nanocolumn at a flowrate of 0.25 µl/min, using a gradient from 4 to 76% acetonitrile in 0.1% formic acid (total time: 65min).

The *in vitro* experiments were analyzed with a Fusion mass spectrometer interfaced to a custom packed 40-cm C18 column (75 µm ID, 100Å, Reprosil Pur 1.9 um particles). Full MS survey scans were performed at 120'000 resolution. Data-dependent acquisition was controlled by Xcalibur 3.0 software (Thermo Fisher) and applied a top speed precursor selection strategy to maximize acquisition of peptide tandem MS spectra with a maximum cycle time of 3 s. Multiple-charge precursor ions were isolated in the quadrupole with a window of 1.6 m/z width and then dynamically excluded from further selection during 60 s. HCD fragmentation was performed in the ion routing multipole with 32% normalized collision energy and fragment ions were measured in the ion trap.

The immunoprecipitation experiments were analyzed with a Q-Exactive Plus instrument interfaced to an Easy Spray C18 PepMap column (50cm x 75µm ID, 2µm, 100Å, Dionex). Full MS survey scans were performed at 70'000 resolution. In data-dependent acquisition controlled by Xcalibur 3.1 software (Thermo Fisher), the 10 most intense multiple-charge precursor ions detected in the full MS survey scan were selected for higher energy collision-induced dissociation (HCD, normalized collision energy NCE = 27%) and analysis in the orbitrap at 17'500 resolution. The window for precursor isolation was of 1.5 m/z units around the precursor and selected fragments were excluded for 60 s from further analysis.

MS data were analyzed using Mascot 2.6 (Matrix Science, London, UK) set up to search the UniProt database (www.uniprot.org) restricted to *Homo sapiens* (*in vitro* experiments) or *Mus musculus* (immunoprecipitation experiments) taxonomy (SwissProt, November 2016 version: 20'130 and 16'846 sequences, respectively). Trypsin (cleavage at K,R) was used as the enzyme definition, allowing 3 missed cleavages. Mascot was searched with a parent ion tolerance of 10 ppm and a fragment ion mass tolerance of 0.5

(Fusion MS data) or 0.02 Da (QExactive MS data). Iodoacetamide derivative of cysteine was specified in Mascot as a fixed modification. N-terminal acetylation of protein, oxidation of methionine, and phosphorylation of serine, threonine or tyrosine were specified as variable modifications.

Scaffold software (version 4.7.5, Proteome Software Inc., Portland, OR) was used to validate MS/MS based peptide and protein identifications, and to perform dataset alignment. Peptide identifications were accepted if they could be established at greater than 90.0% probability by the Scaffold Local FDR algorithm. Protein identifications were accepted if they could be established at greater than 95.0% probability and contained at least 2 identified peptides. Protein probabilities were assigned by the Protein Prophet algorithm. Proteins that contained similar peptides and could not be differentiated based on MS/MS analysis alone were grouped to satisfy the principles of parsimony. Proteins sharing significant peptide evidence were grouped into clusters.

MsViz software (Martín-Campos et al., 2017) was used to compare sequence coverage and phosphorylation of the AMPK alpha 2 protein in the *in vitro* experiments.

HPLC

Cells were grown in 10 cm dishes and treated as indicated in the figure legends. Culture medium was removed by aspiration, rinsed with ultra pure water, flash frozen with liquid nitrogen, thawed on ice, and followed by immediate addition of ice-cold 0.4M perchloric acid (500 μl). Cells were scrapped off thoroughly, and transferred to 1.5 mL microfuge eppendorf tubes. Samples were incubated at 4°C for 45 min, and centrifuged at 14,000 rpm at 4C for 10 min. The supernatant (500 μl) was collected, mixed with 500μl K_2CO_3 4M, and incubated at least 1h at −80°C. The samples were again centrifugated at 4C for 10 min, the supernatant collected and tested on HPLC.

External standards stocks were prepared in ultra pure water, at 10 mg/ml, and treated in exactly the same way as the samples.

For normalization, protein measurements were performed using a Pierce BCA Protein Assay protocol (Thermo Fisher Scientific). In parallel DNA was extracted from the pellets and quantified.

The gradient elution was performed as described (Manfredi et al., 2002) on a 4.6-mmi.d, 150-mm, Kinetex 5u EVO C18 100A HPLC column (Phenomenex) with two buffers at a rate of 0.5 ml/min. Buffer A contained 25mM NaH2PO4, 100 mg/liter tetrabutylammonium hydrogen sulfate, pH 5. Organic buffer B was composed of 10% (v/v) acetonitrile in 200mM NaH2PO4, 100 mg/liter tetrabutylammonium hydrogen sulfate, pH 4.0. Buffers were filtered and degassed. The gradient was 100% buffer A from 0–5 min, 100% buffer A to 100% buffer B from 5–20 min, and 100% buffer A from 20 to 31 min for column reequilibration, which was sufficient to achieve stable baseline conditions. 25 μl of prepared sample was autoinjected and UV monitored at 260nm from 0 to 31 min for phosphorylated nucleotides. Peaks were identified by their retention times and by using co-chromatography with standards.

Each standard of interest was first subjected to chromatography individually to obtain its retention time (Manfredi et al., 2002) and to be able to later identify each compound in a standard mixture. A standard curve for each compound was constructed by plotting peakheight s (IV) versus concentration. Linear curves were obtained with R^2 values > 0.95. The quantification of nucleotides in the sample was performed using the external standard calibration, integrating sample peak heights against corresponding standard curves.

mRNA analysis

Muscle tissues were grinded to powder in liquid nitrogen. mRNAs from muscle was isolated using TRIREAGENT according to the manufacturer's protocol. One microgram of the RNA was subsequently reverse-transcribed (Superscript II, Life Technologies) and quantified via real-time quantitative PCR using an ABI 7900HT instrument. qPCR analysis was performed using a 7900HT Fast Real-Time PCR System (Applied Biosystems) and SYBR Green detection of the amplified products. The relative quantification for a given gene was corrected to RS9 mRNA values (oligonucleotide sequences are provided in Table S3).

QUANTIFICATION AND STATISTICAL ANALYSES

The results were expressed as means ± standard error of the means (s.e.m). Comparisons between 2 groups were performed with an unpaired 2-tailed Student's t test and multiple group comparisons were performed by unpaired 1-way ANOVA followed by Tukey's test and 2-way ANOVA, followed by Tukey's test. All *p-value*s below 0.05 were considered significant. Statistical significance values were represented by asterisks corresponding to *p < 0.05, **p < 0.01, ***p < 0.001 and ****p < 0.0001.

3. CDK4 is an essential insulin effector in adipocytes

Lagarrigue, S., Lopez-Mejia, I. C., Denechaud, P. D., Escote, X., Castillo-Armengol, J., Jimenez, V., Chavey, C., Giralt, A., Lai, Q., Zhang, L.*, et al.* (2016). CDK4 is an essential insulin effector in adipocytes. The Journal of clinical investigation *126*, 335-348.

This paper shows that CDK4 is a major regulator of insulin signaling in white adipose tissue. Three major findings are described in this paper. Firstly, that CDK4 represses lipolysis and promotes lipogenesis. Secondly, that CDK4 is activated by insulin, and third, that CDK4 is able to phosphorylate IRS2 protein in adipocytes, thus maintaining the insulin signaling pathway activated in the presence of growth factors.

Given my previous experience in mice surgery, I tested to transplant white adipose tissue from CDK4 knock-out mice to wild-type mice to reveal that CDK4 was the responsable of IRS2 phosphorylation in adipocytes. However, we could not include this data in the paper, because, due to the re-vascularization the transplanted pieces had CDK4 expression, we could not validate wether the transplanted tissue was from CDK4 knock-out mice. Despite this, I contributed to the histological procedure and analysis of the adipose tissue from different mice genotypes.

CDK4 is an essential insulin effector in adipocytes

Sylviane Lagarrigue,[1,2] Isabel C. Lopez-Mejia,[1] Pierre-Damien Denechaud,[1] Xavier Escoté,[1] Judit Castillo-Armengol,[1]
Veronica Jimenez,[3] Carine Chavey,[2] Albert Giralt,[1] Qiuwen Lai,[1] Lianjun Zhang,[4] Laia Martinez-Carreres,[1]
Brigitte Delacuisine,[1] Jean-Sébastien Annicotte,[2,5] Emilie Blanchet,[2] Sébastien Huré,[1,2] Anna Abella,[6]
Francisco J. Tinahones,[7,8] Joan Vendrell,[9] Pierre Dubus,[10] Fatima Bosch,[3] C. Ronald Kahn,[11] and Lluis Fajas[1,2]

[1]Department of Physiology, Université de Lausanne, Lausanne, Switzerland. [2]Institut de Génétique Moléculaire de Montpellier (IGMM), Université de Montpellier, Montpellier, France.
[3]Center of Animal Biotechnology and Gene Therapy and Department of Biochemistry and Molecular Biology, School of Veterinary Medicine, Universitat Autònoma de Barcelona, Bellaterra,
and Centro de Investigación Biomédica en Red de Diabetes y Enfermedades Metabólicas Asociadas, Barcelona, Spain. [4]Translational Tumor Immunology, Ludwig Center for Cancer Research,
Université de Lausanne, Epalinges, Switzerland. [5]European Genomic Institute for Diabetes, Université Lille Nord de France, UMR 8199 CNRS, Lille, France. [6]INSERM U834, Montpellier, France.
[7]Unidad de Gestión Clínica de Endocrinología y Nutrición, Hospital Universitario Virgen de la Victoria, Málaga, Spain. [8]Centro de Investigación Biomédica en Red-Fisiopatología de la Obesidad y la Nutrición
(CIBERobn CB06/003), Instituto de Salud Carlos III, Madrid, Spain. [9]CIBERDEM, Institut d'Investigació Pere Virgili, Universitat Rovira i Virgili, Hospital Universitari Joan XXIII, Tarragona, Spain.
[10]EA2406, Histologie et pathologie moléculaire des tumeurs, Université de Bordeaux, Bordeaux, France. [11]Section on Integrative Physiology and Metabolism, Joslin Diabetes Center,
Harvard Medical School, Boston, Massachusetts, USA.

Insulin resistance is a fundamental pathogenic factor that characterizes various metabolic disorders, including obesity and type 2 diabetes. Adipose tissue contributes to the development of obesity-related insulin resistance through increased release of fatty acids, altered adipokine secretion, and/or macrophage infiltration and cytokine release. Here, we aimed to analyze the participation of the cyclin-dependent kinase 4 (CDK4) in adipose tissue biology. We determined that white adipose tissue (WAT) from CDK4-deficient mice exhibits impaired lipogenesis and increased lipolysis. Conversely, lipolysis was decreased and lipogenesis was increased in mice expressing a mutant hyperactive form of CDK4 (CDK4^{R24C}). A global kinome analysis of CDK4-deficient mice following insulin stimulation revealed that insulin signaling is impaired in these animals. We determined that insulin activates the CCND3-CDK4 complex, which in turn phosphorylates insulin receptor substrate 2 (IRS2) at serine 388, thereby creating a positive feedback loop that maintains adipocyte insulin signaling. Furthermore, we found that CCND3 expression and IRS2 serine 388 phosphorylation are increased in human obese subjects. Together, our results demonstrate that CDK4 is a major regulator of insulin signaling in WAT.

Introduction

Insulin signaling is a versatile system that coordinates growth, proliferation, and development of multiple tissues and organs by controlling metabolic processes that accommodate the energy needs of cellular function (1). Defects in insulin signaling contribute to insulin resistance, a common complication of obesity that occurs early in the pathogenesis of type 2 diabetes and cardiovascular disease (2, 3). Insulin response depends on tissue and cellular functions. In white adipose tissue (WAT), insulin signaling regulates lipid synthesis (1) and glucose transport (4–6) and represses lipolysis (7). However, the exact mechanism by which insulin signaling coordinates regulated cellular functions is not fully understood. Cyclin-dependent kinase 4 (CDK4) plays an important role in the G$_1$/S transition of the cell cycle. Its kinase activity is regulated through interaction with the D-type cyclins (CCND1, CCND2, and CCND3) (8). The resulting cyclin D–CDK4 complexes catalyze the phosphorylation of the members of the retinoblastoma (RB) protein family (RB1, RBL1, and RBL2). Phosphorylation of RB1 by cyclin D–CDK4 releases the E2F

transcription factors, thereby ensuring the expression of genes required for cell-cycle progression (9). Conversely, members of the family of CDK inhibitors (INK and CIP/KIP) block CDK activity in response to quiescence stimuli. Many studies have assessed the roles of CDK4 in cell growth, proliferation, and cancer (10), but the role of CDK4 in adipose tissue function has never been explored. The most marked phenotypes of mice lacking CDK4 (*Cdk4$^{neo/neo}$*) are reduced body size and insulin-deficient diabetes due to a severe decrease in pancreatic β cell growth (11). β Cell–specific reexpression of the *Cdk4^{R24C}* allele renders CDK4 resistant to the inhibitory effects of INK4 proteins (12) and restores β cell proliferation and normoglycemic conditions (13). Interestingly, CDK4 reexpression in pancreatic β cells does not rescue body size reduction, suggesting that this phenotype is not due to endocrine defects secondary to decreased insulin levels. We previously demonstrated that CDK4 regulates adipogenesis, suggesting a role of CDK4 in WAT function (14).

Results

CDK4 activity is positively correlated with WAT mass. The first suggestion of a role of CDK4 in adipose tissue biology came from the finding that CDK4 and 2 D-type cyclins (CCND2 and CCND3) are highly expressed in epididymal WAT (eWAT) compared with the other tissues analyzed (Figure 1A). The high levels of expres-
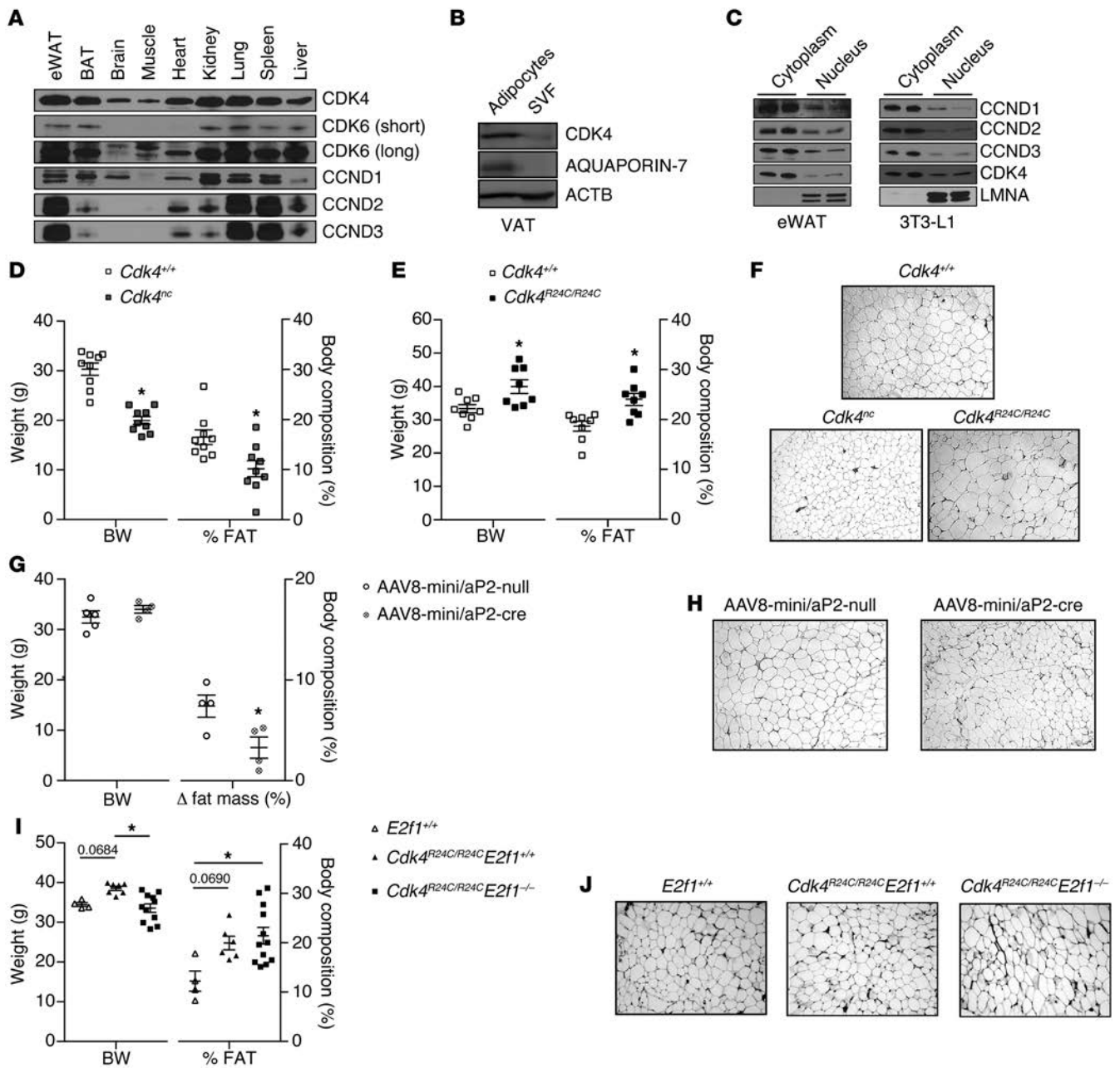
Figure 1. Positive correlation between CDK4 activity and WAT mass. (**A**) Expression levels of CCND1, CCND2, CCND3, CDK4, and CDK6 proteins in mouse eWAT, BAT, brain, muscle, heart, kidney, lung, spleen, and liver. Representative blot of several animals analyzed is shown. (**B**) CDK4 protein level in the SVF and mature adipocytes isolated from VAT. (**C**) Subcellular localization of CCND1, CCND2, CCND3, and CDK4 proteins in cytoplasm and nuclear fractions of eWAT and mature 3T3-L1 adipocytes. LMNA was used as a control for the nuclear fraction. (**B** and **C**) Representative blots out of 3 independent experiments are shown. (**D** and **E**) Body weight and percentage of fat mass of 20-week-old $Cdk4^{+/+}$ and $Cdk4^{nc}$ mice ($n = 9$) (**D**) and 30-week-old $Cdk4^{+/+}$ and $Cdk4^{R24C/R24C}$ mice ($n = 8$) (**E**) as obtained using EchoMRI technology. (**F**) H&E staining of eWAT sections from $Cdk4^{+/+}$, $Cdk4^{nc}$, and $Cdk4^{R24C/R24C}$ mice. (**G**) Body weight, Δ fat mass of 20-week-old $Cdk4^{flox/flox}$ mice infected with AAV8-mini/aP2-null ($n = 5$) or AAV8-mini/aP2-cre ($n = 4$) analyzed by EchoMRI technology (we show the difference between the percentage of fat before and the percentage of fat 3 weeks after infection). (**H**) H&E staining of eWAT sections from $Cdk4^{flox/flox}$ mice infected with AAV8-mini/aP2-null or AAV8-mini/aP2-cre. (**I**) Body weight and percentage of fat mass of 30-week-old $E2f1^{+/+}$ ($n = 4$), $Cdk4^{R24C/R24C} E2f1^{+/+}$ ($n = 6$), and $Cdk4^{R24C/R24C} E2f1^{-/-}$ mice ($n = 12$). (**J**) H&E staining of eWAT sections from $E2f1^{+/+}$, $Cdk4^{R24C/R24C} E2f1^{+/+}$, and $Cdk4^{R24C/R24C} E2f1^{-/-}$ mice. Statistically significant differences were determined with unpaired 2-tailed Student's t tests (**D**, **E**, and **G**) or 1-way ANOVA followed by Tukey's multiple comparisons test (**I**). *$P < 0.05$. Original magnification, ×100.

sion of CCND3 in eWAT (Figure 1A and Supplemental Figure 1, A and B; supplemental material available online with this article; doi:10.1172/JCI81480DS1) are consistent with previous findings showing increased CCND3 expression during adipogenesis (15).

Protein expression analysis in visceral adipose tissue (VAT) cellular fractions showed that CDK4 was better expressed in mature adipocytes compared with the stromal vascular fraction (SVF) (Figure 1B and Supplemental Figure 1C). Furthermore, CDK4 expression
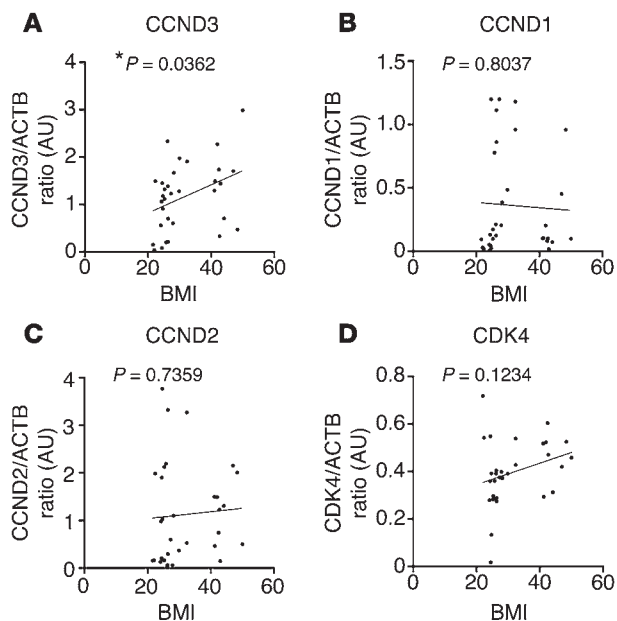
Figure 2. Positive correlation between CCND3 expression and human VAT mass. (**A**–**D**) Correlation between the CCND3/ACTB ratio ($n = 32$, Pearson's $r = 0.3717$, $P < 0.05$) (**A**), the CCND1/ACTB ratio ($n = 32$, Pearson's $r = -0.04574$, $P < 0.05$) (**B**), the CCND2/ACTB ratio ($n = 32$, Pearson's $r = 0.06203$, $P < 0.05$) (**C**), and the CDK4/ACTB ratio ($n = 30$, Pearson's $r = 0.2875$, $P < 0.05$) (**D**) and BMI in VAT of human subjects. Data are normalized to ACTB. *$P < 0.05$.

engineering of white and brown adipocytes in adult mice and has very poor tropism for macrophages (17). We infected *Cdk4^flox/flox^* mice (Supplemental Figure 1I) with AAV8 vectors expressing the Cre recombinase under the control of the mini/aP2 adipose tissue–specific promoter (AAV8-mini/aP2-cre) or with the control vector (AAV8-mini/aP2-null). First of all, we determined the tissues that were infected by assessing the presence of viral genome (vg) using Cre PCR. The vg was only present in brown adipose tissue (BAT), eWAT, s.c. WAT, and liver, whereas we could not detect it in pancreas and muscle (Supplemental Figure 1J). Quantitative reverse-transcription–PCR (RT-qPCR) analysis showed a significant decrease of *Cdk4* mRNA in eWAT and s.c. WAT, whereas no changes were observed in liver and BAT (Supplemental Figure 1K). After 3 weeks, the systemic administration of AAV8-mini/aP2-cre triggered a decrease in fat mass gain; indeed, AAV8-mini/aP2-cre–infected mice gained significantly less fat mass (Figure 1G) and experienced a reduction in adipocyte size (Figure 1H). However, no differences were found in body weight and lean mass in *Cdk4^flox/flox^* mice infected with AAV8-mini/aP2-cre vector (Figure 1G and Supplemental Figure 1L). The use of this adipose tissue–specific *Cdk4* depletion model supports a cell-autonomous contribution for CDK4 in adipose tissue. Overall, these 3 models (*Cdk4^nc^*, *Cdk4^R24C/R24C^*, and *Cdk4^flox/flox^* mice infected with AAV8 mini/aP2-cre) clearly demonstrate a positive correlation between CDK4 activity and WAT mass/size.

E2F1, a known proproliferative downstream effector of CDK4, was previously shown to promote adipogenesis (16). Therefore, in order to determine whether adipocyte proliferation was not affected with the modulation of CDK4 activity, we generated *Cdk4^R24C/R24C^ E2f1^-/-^* mice. No significant changes were observed in adiposity, adipocyte size, lean mass, or adipocyte proliferation as measured by Ki67 expression in *Cdk4^R24C/R24C^ E2f1^-/-^* compared with *Cdk4^R24C/R24C^ E2f1^+/+^* mice (Figure 1, I and J, and Supplemental Figure 1, M and N). These results demonstrate that when CDK4 is hyperactive, the deletion of E2f1 does not affect fat mass, mature adipocyte size, and proliferation. Because *Cdk4^R24C/R24C^* mice develop a wide spectrum of tumors (18, 19), we investigated to determine whether the WAT phenotype observed in these mice could be secondary to tumor development. We could not find any correlation between fat mass and tumor development. Indeed, all mice used in this study were tumor free (Supplemental Figure 1O). Moreover, tumor development was negatively correlated with fat mass in 60-week-old *Cdk4^R24C/R24C^* mice, proving that the increased WAT mass in these mice was not secondary to tumor formation (Supplemental Figure 1P).

CCND3 is positively correlated with WAT mass in human subjects. Our data suggesting the involvement of CCND3-CDK4 in adipose tissue was further supported by the positive correlation between CCND3 protein expression in visceral WAT samples from human subjects and their BMI (Figure 2A and Supplemental Figure 1, Q

was also higher in differentiated 3T3-L1 adipocytes compared with nondifferentiated 3T3-L1 preadipocytes (Supplemental Figure 1C). Interestingly, the subcellular localization of CDK4 and CCND3 as well as of the other D-type cyclins revealed that these proteins are not only found in the nucleus; rather, they are mainly localized in the cytoplasm of adipocytes (Figure 1C and Supplemental Figure 1D), suggesting a role for CDK4 that is independent of the RB/E2F pathway in these cells. Moreover, since the duplication rate in mature adipocytes is low (16), these results suggested a novel cell-cycle independent role for CDK4. In order to analyze the participation of CDK4 in adipose tissue biology, we set to determine the phenotype of CDK4 mutant mice. The previously generated *Cdk4^neo/neo^* mice are diabetic and have impaired pancreatic β cell development and decreased insulin levels (11). Analysis of adipose tissue function in these mice would be confusing, since any observed effect could be secondary to insulin deficiency. We therefore used *Cdk4^neo/neo^ Rip-Cre* (*Cdk4^neo/neo;cre/cre^*; herein referred to as *Cdk4^nc^*) mice that reexpress *Cdk4* in β cells and thus have normal insulin levels (13). We also used a mouse model of CDK4 hyperactivation, the R24C model. *Cdk4^R24C/R24C^* mice express a mutant CDK4 protein that is not sensitive to INK4a inhibitors (11) and is consequently more active. A first analysis showed that *Cdk4^nc^* mice had decreased body weight, whereas *Cdk4^R24C/R24C^* mice exhibited increased body weight compared with *Cdk4^+/+^* mice (Figure 1, D and E). Significant changes in WAT mass accounted for body weight variation. *Cdk4^nc^* and *Cdk4^R24C/R24C^* mice had decreased and increased WAT mass, respectively, as measured by EchoMRI (Figure 1, D and E, and Supplemental Figure 1, E and F). Changes in fat mass were consistent with variation in adipocyte size (Figure 1F and Supplemental Figure 1G). Overall, severe atrophy could be observed in fat pads from *Cdk4^nc^* mice, whereas *Cdk4^R24C/R24C^* mice developed adipose tissue hypertrophy (Supplemental Figure 1H).

To demonstrate that the effects of Cdk4 deletion in adipose tissue were cell autonomous, we used an approach involving systemic administration of adeno-associated viral vectors of serotype 8 (AAV8), which has been previously reported as leading to genetic
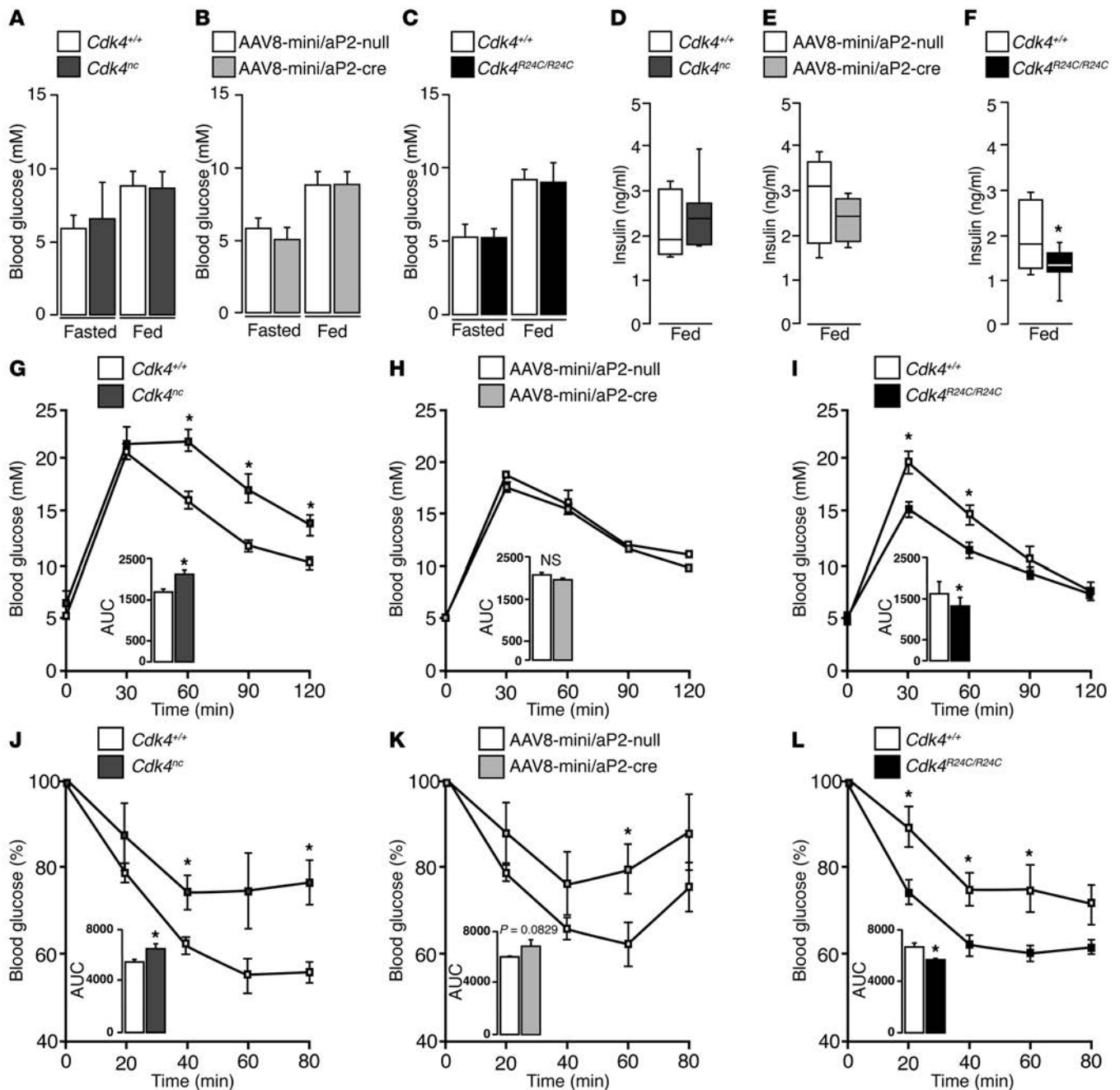
Figure 3. CDK4 promotes insulin sensitivity in vivo. (A–C) Fasting glycemia in *Cdk4*^{+/+} and *Cdk4*[nc] (*n* = 8) mice (**A**), *Cdk4*[flox/flox] infected with AAV8-mini/aP2-null or AAV8-mini/aP2-cre vectors (*n* = 5–4) (**B**), and *Cdk4*^{+/+} and *Cdk4*[R24C/R24C] (*n* = 12) mice (**C**). (**D–F**) Fed serum insulin in *Cdk4*^{+/+} and *Cdk4*[nc] (*n* = 7) (**D**), *Cdk4*[flox/flox] infected with AAV8-mini/aP2-null or AAV8-mini/aP2-cre vectors (*n* = 5–4) (**E**), and *Cdk4*^{+/+} and *Cdk4*[R24C/R24C] mice (*n* = 8) (**F**). (**G–I**) GTT in *Cdk4*^{+/+} and *Cdk4*[nc] (*n* = 7) (**G**), *Cdk4*[flox/flox] infected with AAV8-mini/aP2-null or AAV8-mini/aP2-cre (*n* = 5–4) (**H**), and *Cdk4*^{+/+} and *Cdk4*[R24C/R24C] (*n* = 6) mice (**I**). (**J–L**) ITT in *Cdk4*^{+/+} and *Cdk4*[nc] (*n* = 5) (**J**), *Cdk4*[flox/flox] infected with AAV8-mini/aP2-null or AAV8-mini/aP2-cre vectors (*n* = 5–4) (**K**), and *Cdk4*^{+/+} and *Cdk4*[R24C/R24C] (*n* = 12) mice (**L**). AUC for GTT and ITT was analyzed and is shown below the curves. Data were expressed as mean ± SEM. Statistically significant differences were determined with unpaired 2-tailed Student's *t* tests. *$P < 0.05$.

and R). No association was found for CCND1, CCND2, or CDK4 (Figure 2, B–D). These results confirmed a positive correlation between WAT mass and CCND3-CDK4 expression and activity and suggested that these proteins participate in WAT function.

CDK4 promotes insulin sensitivity in vivo. No differences in fasting and feeding glycemia were observed in *Cdk4*[nc] or *Cdk4*[flox/flox] infected with AAV8-mini/aP2-cre vector and *Cdk4*[R24C/R24C] mice

compared with their respective control mice (Figure 3, A–C). Insulin quantification in plasma showed, however, a significant decrease in *Cdk4*[R24C/R24C] mice, whereas no differences were observed in *Cdk4*[nc] or *Cdk4*[flox/flox] mice infected with AAV8-mini/aP2-cre vector in fed conditions (Figure 3, D–F). Decreased insulin levels are indicative of either better insulin sensitivity or of a defect in insulin secretion by pancreatic β cells. *Cdk4*[nc] mice were glucose intolerant (Figure 3G)
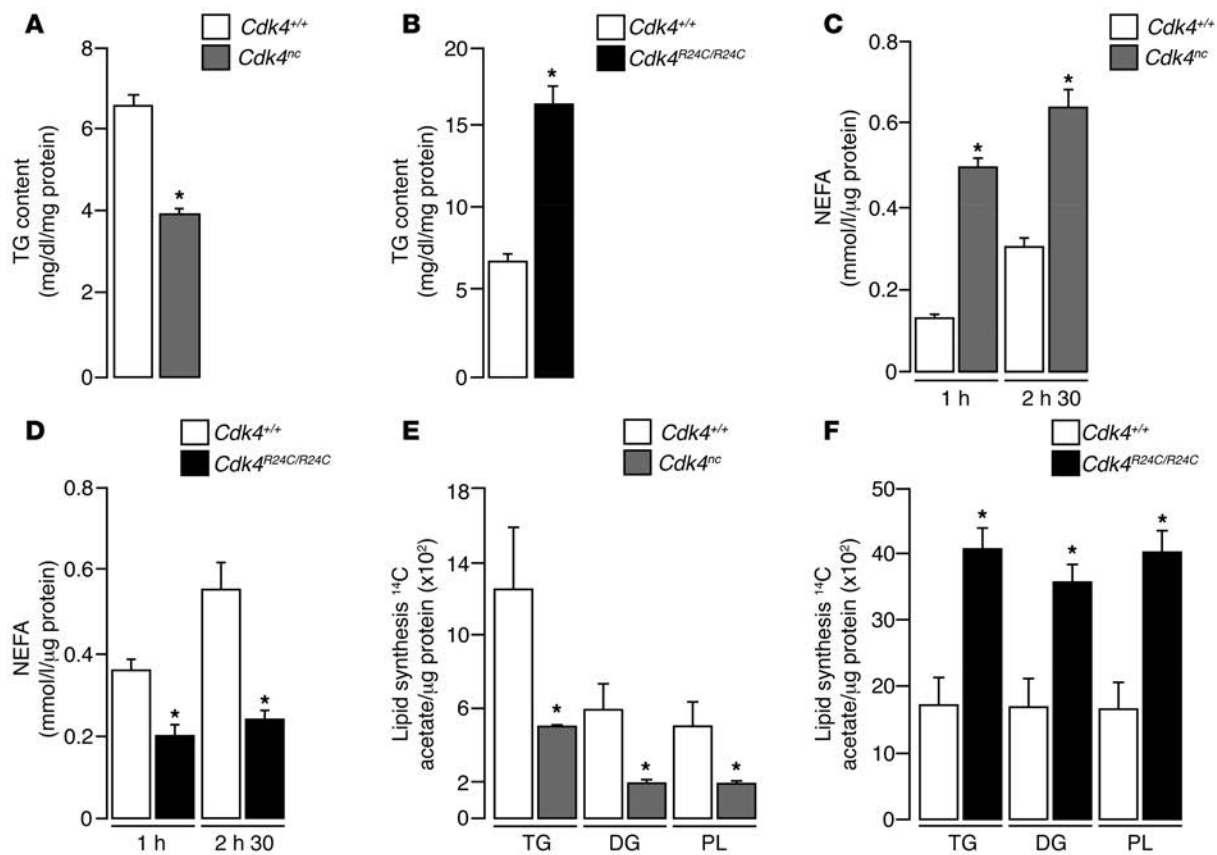
Figure 4. CDK4 represses lipolysis and is a positive modulator of lipogenesis. (**A**) Quantification of TG content of eWAT from *Cdk4⁺/⁺* and *Cdk4ⁿᶜ* mice (*n* = 3). (**B**) Quantification of TG content of eWAT of *Cdk4⁺/⁺* and *Cdk4^R24C/R24C* mice (*n* = 3). (**C**) Rate of NEFA release in eWAT explants from fasting *Cdk4⁺/⁺* and *Cdk4ⁿᶜ* mice (*n* = 3). (**D**) Rate of NEFA release in eWAT explants from fasting *Cdk4⁺/⁺* and *Cdk4^R24C/R24C* mice (*n* = 6). (**E**) Ex vivo lipogenesis experiments in eWAT explants using labeled ¹⁴C-acetate incorporation to detect TG, DG, and PL synthesis in *Cdk4⁺/⁺* and *Cdk4ⁿᶜ* mice (*n* = 3). (**F**) Ex vivo lipogenesis experiments in eWAT explants from *Cdk4⁺/⁺* and *Cdk4^R24C/R24C* mice. ¹⁴C-acetate incorporation was used to detect TG, DG, and PL synthesis by TLC (*n* = 3). Data are expressed as mean ± SEM. Statistically significant differences were determined with unpaired 2-tailed Student's *t* tests. *$P < 0.05$.

and cleared glucose at a slower rate than *Cdk4⁺/⁺* mice, a characteristic of insulin resistance (Figure 3J). We did not observe any significant differences in glucose tolerance tests (GTTs) in *Cdk4^flox/flox* mice infected with AAV8-mini/aP2-cre vector; however, these mice had a trend toward insulin resistance compared with *Cdk4^flox/flox* mice infected with AAV8-mini/aP2-null vector ($P = 0.0829$) (Figure 3, H and K). In contrast, *Cdk4^R24C/R24C* mice were more glucose tolerant and insulin sensitive than *Cdk4⁺/⁺* mice (Figure 3, I and L). Together, these results show that CDK4 activity is positively correlated with insulin sensitivity.

CDK4 represses lipolysis and stimulates lipogenesis. We previously showed the participation of CDK4 and CCND3 in adipogenesis. We proved that these proteins control the activity of the master regulator of adipocyte differentiation, PPARγ (14). In this study, we analyze the participation of CDK4 in the function of mature adipocytes. Lipids are mobilized from WAT through lipolysis, a breakdown of triglycerides (TG) into glycerol and free fatty acids (FFA) (20). As expected, changes in WAT mass were positively correlated with alterations in TG content in our mouse models: *Cdk4ⁿᶜ* and *Cdk4^R24C/R24C* mice had less and more TG in eWAT, respectively (Figure 4, A and B). Decreased TG content in *Cdk4ⁿᶜ* eWAT was likely the result of an imbalanced lipogenesis/lipolysis ratio. Indeed, treatment of fully differentiated 3T3-L1

adipocytes with a chemical CDK4 inhibitor (PD0332991) (21) resulted in the delipidation of these adipocytes and in a 40% decrease in their TG content (Supplemental Figure 2, A and B). Lipolysis experiments in eWAT explants from mice revealed a 4-fold increase of nonesterified fatty acid (NEFA) release in *Cdk4ⁿᶜ* eWAT compared with *Cdk4⁺/⁺* eWAT (Figure 4C). Similarly, glycerol release was also increased in these mice (Supplemental Figure 2C). Conversely, *Cdk4^R24C/R24C* eWAT showed significantly decreased NEFA (Figure 4D) and glycerol release (Supplemental Figure 2D), which suggested impaired lipolysis. Interestingly, eWAT explants from *Cdk4ⁿᶜ* mice, in addition to increased lipolysis, had reduced lipogenesis, as measured by acetate incorporation into the distinct TG, diacyclycerols (DG), and phospholipid (PL) lipid fractions (Figure 4E). On the other hand, eWAT explants from mice expressing the hyperactive *Cdk4^R24C* allele showed increased lipogenesis (Figure 4F). However, we could not detect any differences in liver TG content in *Cdk4⁺/⁺*, *Cdk4ⁿᶜ*, and *Cdk4^R24C/R24C* mice (Supplemental Figure 2, E and F). This validated a positive correlation between CDK4 activity and lipogenesis and a negative correlation between CDK4 activity and lipolysis. Strikingly, these are exactly the effects of insulin in adipocytes, suggesting that CDK4 could mediate the effects of insulin in adipose tissue.
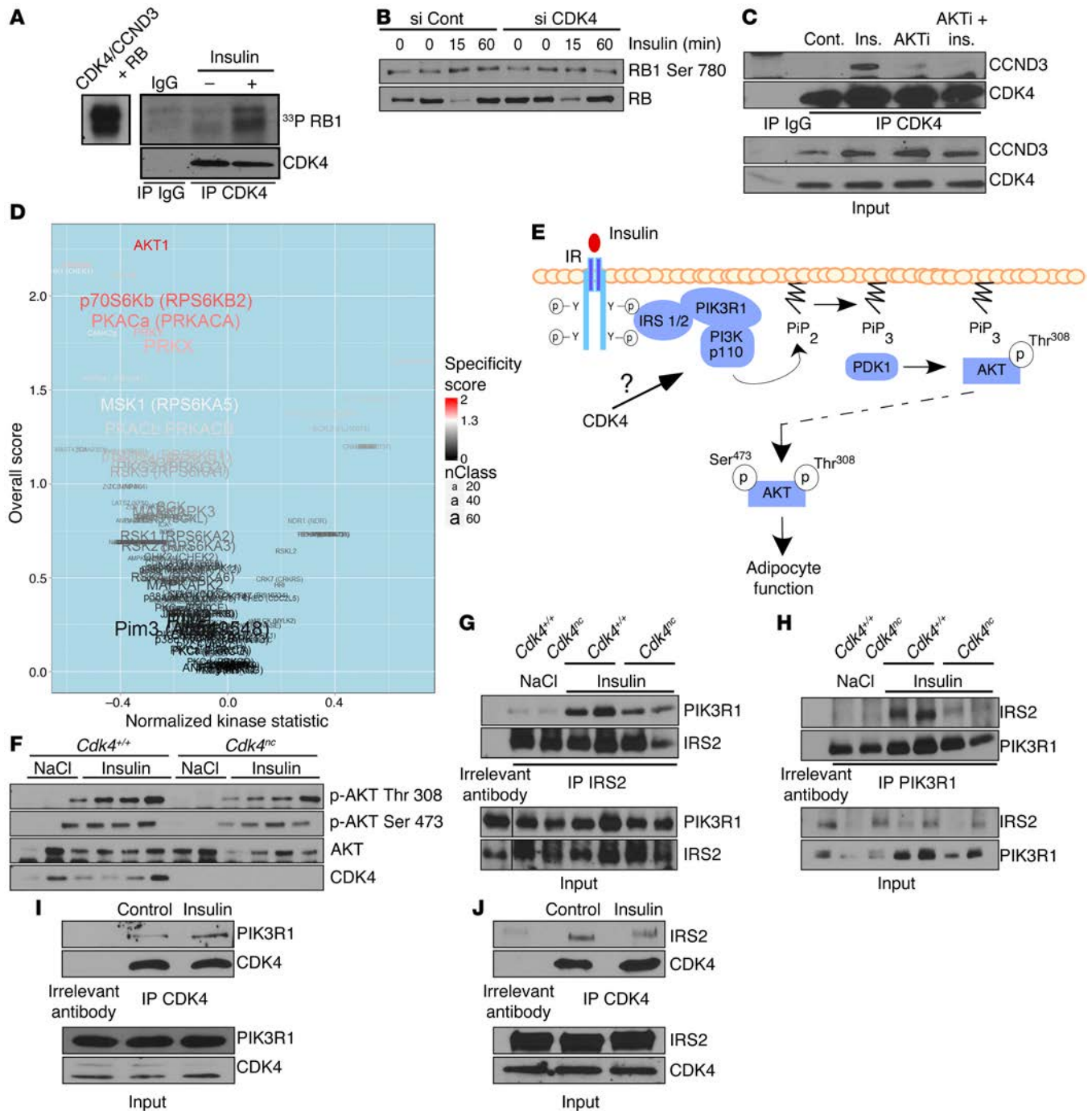
Figure 5. CDK4 is activated by insulin and translates insulin signaling in adipocytes. (**A**) CDK4 activity in vivo. SDS-PAGE autoradiography showing RB1 phosphorylation by CDK4 immunoprecipitated from 3T3-L1 mature adipocytes after insulin stimulation. The left panel shows RB1 phosphorylation by recombinant CDK4 used as a positive control. (**B**) Western blot analysis showing the inhibition of insulin-induced RB1 phosphorylation on Ser780 by CDK4 knockdown in mature 3T3-L1 adipocytes. (**C**) CCND3 and CDK4 association is increased upon insulin stimulation, but decreased upon cotreatment with insulin and AKT inhibitor in mature 3T3-L1 adipocytes. (**D**) Volcano plot showing differences in putative kinase activities between control and *Cdk4^nc^* mice injected (portal vein) with insulin for 3 minutes (*n* = 4). Kinases with a positive kinase statistic show higher activity in *Cdk4^nc^* samples compared with control samples, whereas kinases with negative kinase statistic show lower activity in *Cdk4^nc^* samples compared with control samples. (**E**) Based on the upstream kinase activity (**D**) results and on the GeneGO analysis of the PamGene experiment, the putative role of CDK4 upstream of AKT in the insulin signaling pathway is represented. (**F**) Immunoblot showing AKT phosphorylation on Thr308 and Ser473 in response to insulin injection (3 minutes) in fasted control and *Cdk4^nc^* mice (*n* = 2 for NaCl and *n* = 4 for insulin treatment). (**G** and **H**) Coimmunoprecipitation experiments showing the interaction between endogenous IRS2 and PIK3R1. IRS2 (**G**) and PIK3R1 (**H**) were immunoprecipitated and the presence of PIK3R1 (**G**) and IRS2 (**H**) was detected by Western blot analysis in *Cdk4^+/+^* and *Cdk4^nc^* mice treated with insulin for 3 minutes (*n* = 2 for NaCl and *n* = 3 for insulin treatment). (**I** and **J**) Coimmunoprecipitation experiments showing the interaction between endogenous PIK3R1 or IRS2 and CDK4. CDK4 was immunoprecipitated and the presence of PIK3R1 (*n* = 3) (**I**) and IRS2 (*n* = 1) (**J**) was detected by Western blot analysis in 3T3-L1 mature adipocytes treated with insulin. A representative Western blot is shown. Unless specified otherwise, all experiments are representative of 3 independent experiments.

Table 1. CDK consensus sites in mouse IRS1, IRS2, PDKP1, and PIK3R1

Protein	Site position	Sequence	CDK4 Interaction
PIK3R1	Thr86	TPKP	+
PDPK1	Thr357	TPPP	–
	Thr521	TPNP	
IRS1	Ser1209	SPRR	+
IRS2	Ser388	SPGP	+
	Thr576	TPAR	
	Ser980	SPKP	
	Ser1004	SPYP	
	Ser1226	SPMR	

CDK4 is activated by insulin and mediates insulin signaling in adipocytes. We wanted next to uncover the mechanisms of CDK4 activation following insulin stimulation in adipocytes. CDK4 activity was stimulated by insulin in differentiated 3T3-L1 cells, as suggested by increased phosphorylation of PIK3R1 by immunoprecipitated CDK4 (Figure 5A). Similar results were observed when eWAT from insulin-treated mice was used (Supplemental Figure 3A). Interestingly, CDK4 knockdown (Figure 5B) or treatment of 3T3-L1 adipocytes with PD0332991 (Supplemental Figure 3B) abrogated the effects of insulin on PIK3R1 phosphorylation. Furthermore, association of CDK4 with its regulatory subunit CCND3 was dependent on the insulin signaling pathway, since AKT inhibition abolished this association (Figure 5C).

Next, we addressed how CDK4 could participate in the insulin-signaling pathway in adipocytes. Since the insulin signaling cascade is dependent on the rapid activation of a series of tyrosine and serine/threonine protein kinases (STKs), we used a new technology developed by PamGene to determine differential global kinase activity in $Cdk4^{nc}$ and control mice in response to insulin. We used arrays that consisted of 140 immobilized serine/threonine-containing peptides that are targets of most known kinases (STK PamChips) (22). These chips were incubated with lysates prepared from eWAT from $Cdk4^{nc}$ or control mice injected with insulin. The same experiment was performed using lysates from cells treated with PD0332991 and stimulated with insulin. Peptides whose phosphorylation varied significantly between the control and $Cdk4^{nc}$-treated mice or between the control and PD0332991-treated samples (Supplemental Figure 3, C and D) were indicative of differential specific kinase activities. Putative upstream kinase analysis underscored significant differences in the AKT pathway (Figure 5D and Supplemental Figure 3, E and F). This suggested that CDK4 activity played a role upstream of AKT, as indicated in Figure 5E. Western blot analyses further proved that AKT activity, as measured by phosphorylation in Ser473 and Thr308, was decreased in $Cdk4^{nc}$ mice in response to insulin (Figure 5F). Similarly, chemical inhibition of CDK4 also attenuated AKT signaling in 3T3-L1 adipocytes (Supplemental Figure 3G). This further supports the hypothesis that CDK4 regulates insulin signaling upstream of AKT. Upon insulin stimulation, the intrinsic tyrosine kinase domain of the insulin receptor leads to receptor autophosphorylation at tyrosine residues. The subsequent recruitment and phosphorylation of insulin receptor substrate 1 (IRS1) and IRS2 are the pivotal events that, in turn, activate the downstream PI3K-PDK1-AKT axis to regulate lipogenesis and lipolysis in adipocytes (23). We therefore investigated whether CDK4 regulated the insulin-signaling pathway by facilitating the recruitment of IRS into PIK3R1, the PI3K subunit p85a. We found that *Cdk4* deletion greatly impaired the ability of IRS2 to bind with PIK3R1 in response to insulin stimulation (Figure 5, G and H). Furthermore, CDK4 was recruited to PIK3R1 (Figure 5I) and IRS2 (Figure 5J) complexes in adipocytes. However, we only detected an increase of interaction in response to insulin between PIK3R1 and CDK4.

IRS2 is a substrate of CDK4. Interestingly, in silico analysis highlighted the presence of CDK4 consensus phosphorylation sites in the p85A subunit of PI3K (PIK3R1), phosphoinositide-dependent kinase 1 (PDK1), IRS1, and IRS2 (Table 1). However, in vitro kinase assays showed no phosphorylation of PIK3R1, or PDPK1 by CDK4 (data not shown). In vitro kinase assays showed, however, that CDK4 could phosphorylate recombinant glutathione S–transferase–purified (GST-purified) IRS2 protein (Figure 6A). IRS2 contains 5 CDK4 consensus sites distributed along the protein (Ser388, Thr576, Ser980, Ser1004, and Ser1226) (Table 1 and Supplemental Figure 4A). Site-directed mutagenesis (serine to alanine) and protein truncation approaches helped us to map the CDK4 phosphorylation sites of IRS2 at Ser388 and Ser1226 (Figure 6, B and C). Interestingly, these 2 potential phosphorylation sites are highly conserved through evolution (Supplemental Figure 4B).

We next evaluated the functional relevance of IRS2[S388A] and IRS2[S1226A] mutants that cannot be phosphorylated by CDK4. Rescue of IRS2 activity in $Irs2^{-/-}$ preadipocytes with ectopic expression of WT IRS2 resulted in the restoration of insulin signaling as assessed by immunofluorescence staining of AKT phosphorylation (Figure 6, D and E). In contrast, IRS2[S388A] mutants, which cannot be phosphorylated by CDK4, could not restore insulin signaling in these cells (Figure 6, D and E). No significant phenotype was observed for IRS2[S1226A] mutants (data not shown). Moreover, IRS2[S388A] mutants were not recruited to PIK3R1 protein complexes upon insulin stimulation when ectopically expressed in 293T cells (Figure 6, F and G). This demonstrated that the phosphorylation of IRS2 on Ser388 by CDK4 is essential for its activity.

CDK4 regulates insulin signaling in vivo via IRS2[Ser388] phosphorylation. To determine the potential roles of CDK4 on IRS2 phosphorylation, we generated a phosphospecific antibody to Ser388 of IRS2 that we validated by in vitro CDK4 kinase assay (Supplemental Figure 5A). IRS2 Ser388 was highly phosphorylated in the adipose tissue of $Cdk4^{+/+}$ mice after 50 minutes of insulin stimulation (Figure 7, A and B). This phosphorylation was almost abrogated in the adipose tissue of insulin-treated $Cdk4^{nc}$ mice. Moreover, decreased IRS2 Ser388 phosphorylation resulted in impaired insulin signaling pathways, as demonstrated by reduced AKT phosphorylation (Figure 7, A and B). In sharp contrast, CDK4 hyperactivity, as observed in $Cdk4^{R24C/R24C}$ mice, resulted in a robust increase in IRS2 Ser388 phosphorylation (Figure 7, C and D). Consequently, AKT phosphorylation was also increased (Figure 7, C and D). Chemical inhibition of CDK4 also resulted in the abrogation of both IRS2 Ser388 and AKT phosphorylations (Figure 7, E and F). From these results, we can conclude that this

Figure 6. CDK4 phosphorylates IRS2. (**A**) CCND3-CDK4 complex directly phosphorylates full-length GST-IRS2 in vitro ($n = 3$). (**B**) In vitro phosphorylation of GST-IRS2 fragments (1–494aa, 495–744aa, 745–993aa, 994–1099aa, 1100–1321aa) by CCND3/CDK4. Left panel, SDS-PAGE stained with Coomassie blue for the loading control. Middle panels, autoradiography of the SDS-PAGE gels containing the different GST-IRS2 fragments, incubated with CCND3/CDK4. Right panel, RB1 recombinant protein was used as a positive control ($n = 3$). (**C**) Defective IRS2[S388A] and IRS2[S1226A] phosphorylation by CCND3-CDK4. Upper panel, autoradiography; lower panel, SDS-PAGE gel stained with Coomassie blue for the loading control. ($n = 2$). (**D**) Decrease in pAKT Ser473 phosphorylation in Flag-IRS2[S388A] electroporated *Irs2^{-/-}* cells upon insulin stimulation, compared with the WT Flag-IRS2–transfected cells ($n = 3$). Original magnification, ×400. (**E**) Quantification of pAKT Ser473 fluorescence intensity for untransfected, Flag-IRS2–transfected, and Flag-IRS IRS2[S388A] electroporated *Irs2^{-/-}* preadipocytes was performed with ImageJ software (http://imagej.nih.gov/ij/). At least 100 cells were quantified per condition. (**F**) Representative Western blot analysis showing impaired interaction between PIK3R1 and Flag-IRS2[S388A] mutant after insulin stimulation compared with cells transfected with Flag-IRS2 in 293T cells. (**G**) Quantification of the blot shown in **F**. A representative Western blot is shown. Data are expressed as mean ± SEM. Statistically significant differences were determined with 2-way ANOVA followed by Tukey's multiple comparisons test (**E–G**). *$P < 0.05$.
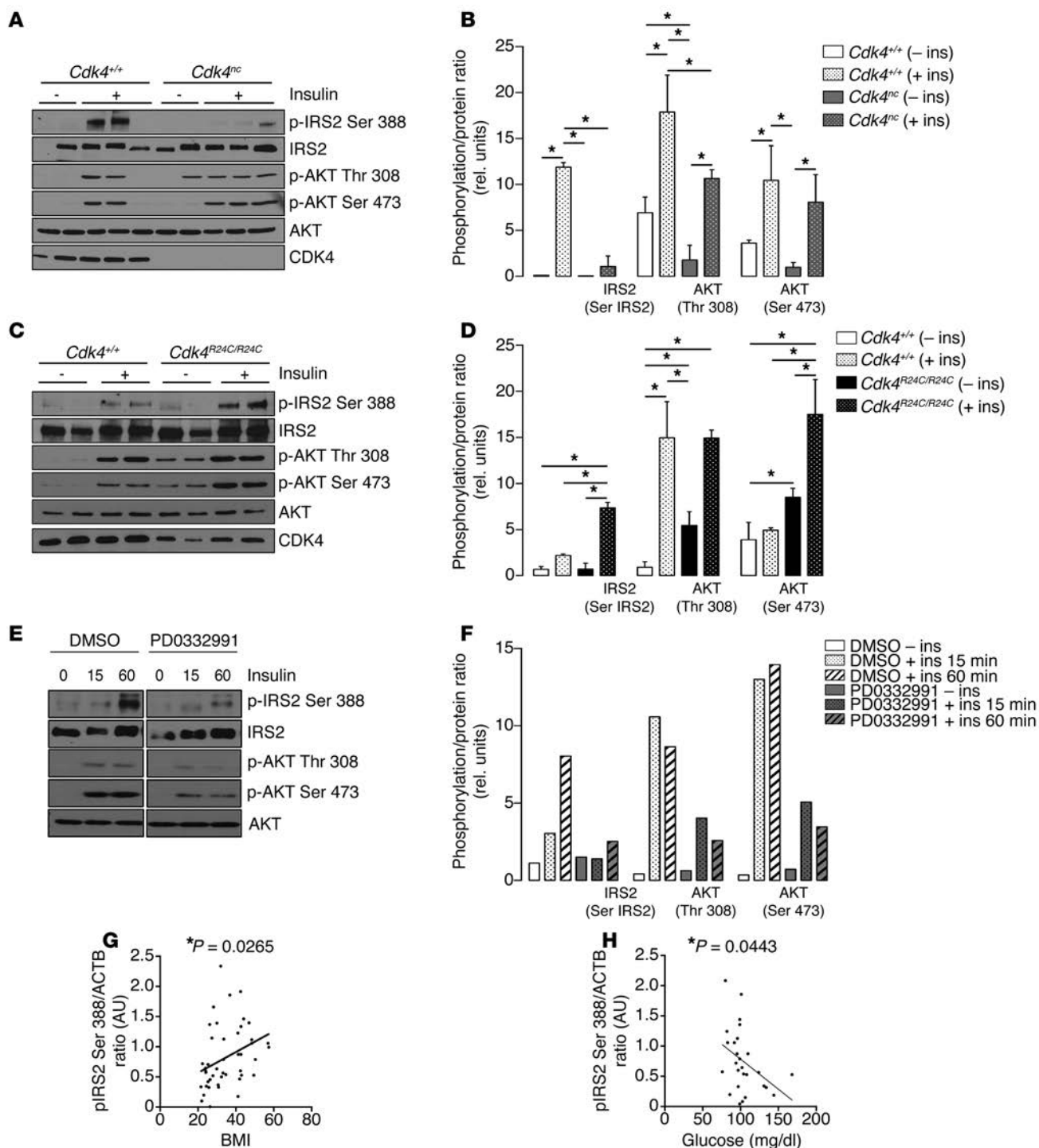
Figure 7. CDK4 phosphorylates in vivo the IRS2 protein at the Ser388. (**A**–**D**) Immunoblot analysis of IRS2 phosphorylation on Ser388 and AKT phosphorylation on Thr308 and Ser473 in control and *Cdk4^nc^* (*n* = 2 starved/5 insulin for *Cdk4^+/+^* and *n* = 2 starved/5 insulin for *Cdk4^nc^*) mice (**A**). (**B**) Quantification of the blot shown in **A** using ImageJ software. *Cdk4^R24C/R24C^* (*n* = 2 starved/3 insulin for both *Cdk4^+/+^* and *Cdk^R24C/R24C^*). (**C**) Mice were treated for 50 minutes with insulin. (**D**) Quantification of the blot shown in **C** using ImageJ software. (**E**) Immunoblot analysis of IRS2 phosphorylation on Ser388 and AKT phosphorylation on Thr308 and Ser473 in 3T3-L1 mature adipocytes during a time course insulin stimulation with or without PD0332991 (*n* = 1). (**F**) Quantification of the blot shown in **E** using ImageJ software. (**G**) Correlation between the pIRS2 Ser388/ACTB ratio in VAT and the BMI of the subjects (*n* = 45, Pearson's *r* = 0.3307, *P* < 0.05). (**H**) Correlation between the pIRS2 Ser388/ACTB ratio in VAT and the glycemia of the subjects (*n* = 27, Pearson's *r* = −0.3900, *P* < 0.05). Data are expressed as mean ± SEM. Statistically significant differences were determined with 2-way ANOVA followed by Tukey's multiple comparisons test (**B**–**D**). *P < 0.05.

newly identified site in IRS2, which is phosphorylated by CDK4, maintains the activation of the insulin signaling pathway. To further investigate the status of IRS2 Ser388 in type 2 diabetic mouse models, such as *db/db* mice, that are known to be hyperinsulinemic, we analyzed this phosphorylation in the basal state and upon insulin stimulation in adipose tissue. The *db/db* mice have a tendency toward an increased IRS2 Ser388 phosphorylation under basal conditions, compared with *db/+* mice ($P = 0.0511$) (Supplemental Figure 5B). However, insulin-resistant *db/db* mice did not show increased IRS2 Ser388 phosphorylation upon insulin stimulation (Supplemental Figure 5B). Most important was the finding that IRS2 Ser388 phosphorylation in human visceral WAT samples was positively correlated with the BMI of the subjects (Figure 7G and Supplemental Figure 5, C and D). Interestingly, we found a negative correlation between IRS2 Ser388 phosphorylation and fasting glucose in human subjects. This further advocates for a role of CDK4 in both adipose tissue biology and glucose homeostasis (Figure 7H and Supplemental Figure 5E).

Discussion

We showed throughout this study that the cell-cycle regulatory kinase CDK4 is a key regulator of adipocyte function. The participation of this kinase in the control of proliferation through the control of the activity of E2F transcription factors has been extensively studied (24). The results of our study provide 3 lines of evidence that CDK4 acts independently of E2F to regulate adipocyte function. First, we discovered a role of the cell-cycle kinase CDK4 in the control of the insulin-signaling pathway. CDK4, through phosphorylation of IRS2, maintains insulin action in adipocytes. This is consistent with the phenotypes of genetic CDK4 mouse models. Indeed, adipose tissue from *Cdk4^{nc}* mice has decreased lipogenesis as well as increased lipolysis. In contrast, mice that express hyperactive CDK4^{R24C} exhibit decreased lipolysis and increased lipogenesis in WAT. These findings place CDK4 at the initiation of the insulin-triggered adipocyte-signaling pathway.

We show in this study a function of CDK4, that of a mediator of insulin signaling. Indeed, we show that the effects of CDK4 in adipocytes are independent of E2F activity and, therefore, most likely independent of the control of the cell cycle. E2F1 is the most studied member of the E2F family. E2F1 has numerous metabolic functions, such as the participation in adipose tissue metabolism through the transcriptional regulation of the master adipogenic factor PPARγ during early stages of adipogenesis (16). Here, we demonstrate, by generation of *Cdk4^{R24C/R24} E2f1^{+/+}* and *Cdk4^{R24C/R24C} E2f1^{-/-}* mice, that CDK4 has E2F1-independent functions in mature adipose tissue. Indeed, the genetic deletion of E2F1 in the R24C background does not affect adiposity or adipocyte proliferation (Figure 1, I and J, and Supplemental Figure 1N).

Based on our results, we propose that CDK4 is integrated in the insulin-signaling pathway as follows. In response to insulin, the canonical cascade of events is elicited. This includes the sequential activation of IR, IRS1-2, PI3K, PDPK1, and AKT. AKT then activates CDK4 (because inhibition of AKT blocks CDK4 activation), which then phosphorylates IRS2, creating a positive feedback loop. The activation of CDK4 by AKT is likely an indirect event. Several studies previously reported that AKT phosphorylates and inhibits p21 and p27, which are both CDK4 inhibitors (25, 26).

Interestingly, IRS proteins are also involved in the activation of several growth factor receptor pathways other than the insulin receptor pathway, such as the IGF 1 receptor (IGF1R) pathway (27). The prooncogenic activities of IGF1R (26) are mediated by its downstream effectors, IRS1 and IRS2. IRS proteins transduce mitogenic, antiapoptotic, and antidifferentiation signals to the cell, mainly through the PI3K–AKT module (28). Although antioncogenic synergistic effects have been observed using either CDK4 and IGF1R inhibitors or CDK4 and PI3K inhibitors, no crosstalk between both pathways has been described (29–32). The CDK4/CDK6 inhibitor (PD0332991, palbociclib) has been approved for the treatment of breast cancer (33). Two other CDK4/CDK6 inhibitors, LY-2835219 (also known as abemaciclib) and LEE011 (also known as ribociclib), are also currently in advanced stages of clinical trials (34). Interestingly, it has previously been reported that a major enzyme of de novo lipogenesis, the fatty acid synthase (FASN), is increased in numerous cancers, including breast cancer (35). The activity of FASN is known to be stimulated by insulin through the PI3K/AKT pathway, and here, we demonstrate that CDK4 is a key effector of insulin, thus promoting de novo lipid synthesis. Based on our findings, we can speculate that CDK4, through phosphorylation and regulation of IRS activity, could simultaneously sustain de novo lipid synthesis and the oncogenic activity of the aforementioned pathways in transformed cells.

The second major finding of our study is the discovery of a residue in IRS2 that is phosphorylated by CDK4 in response to insulin. A large number of publications previously focused on the effects of IRS1 and IRS2 phosphorylation on the insulin-signaling pathway. Both positive and negative phosphorylation sites finely regulate IRS1 and IRS2 activity and are a paradigm of the flexibility of insulin and IGF signaling (36). The final serine/threonine phosphorylation state of IRS proteins is a consequence of the combined action of several kinases that are activated by different pathways in a spaciotemporal manner. Multiple site phosphorylation of these proteins by distinct kinases, such as JNK (37), GSK3 (38), ERK1, or mTOR (39), provides a large number of combinations of phosphorylating events that generate a very complex network (40). We show that CDK4 phosphorylates IRS2 at the new Ser388 site. Moreover, we show that this phosphorylation renders IRS2 more active. Our results add more complexity to the understanding of the physiology of the phosphorylation of the IRS proteins. Phosphorylation by CDK4 may also have an impact on the phosphorylation of IRS2 by other kinases; however, the relative contribution of CDK4 to the final activation or inhibition of IRS compared with other kinases and the identification of which serine/threonine residues are the most critical in regulating IRS function in response to insulin remain to be elucidated. Similarly, we still do not understand why CDK4 activates IRS2 whereas AKT inhibits it through a negative feedback loop. The same stimulus, insulin, triggers concomitantly inhibitory and stimulatory phosphorylations in IRS. The fine regulation of these positive versus negative phosphorylation events requires further investigation. Interestingly, we were able to observe the stimulation of IRS2 Ser388 phosphorylation with insulin not only in adipocytes, but also in other cell types, such as C2C12 myotubes and primary hepatocytes. IRS2 Ser388 phosphorylation could also be detected in Min6 cells, but was not so insulin responsive. As shown in Supplemental Figure 6, A–C, upon insulin stimulation, IRS2 Ser388 phosphoryla-

tion was stronger after 1 hour of treatment, which is in agreement with our findings in mature adipocytes. These results open interesting perspectives into the contribution of CDK4 to IRS2 Ser388 phosphorylation in other insulin-sensitive tissues; CDK4 could, for instance, participate in the control of de novo lipid synthesis in liver upon insulin stimulation.

RNAi-mediated depletion of CDK6, the CDK4 ortholog, suggests that this kinase is also able to phosphorylate IRS2 at Ser388 in mature adipocytes upon insulin stimulation, but to a lesser extent (Supplemental Figure 6D). The effects of CDK6 on IRS2 in other tissues remain to be studied.

Defects in insulin action and insulin secretion are both features of type 2 diabetes. In line with previous publications reporting that CDK4 regulates β cell growth (11) and insulin secretion in β cells (41), it would be interesting to explore the relative contribution of this IRS2 Ser388 phosphorylation in β cell function. The involvement of IRS2 in the pathogenesis of type 2 diabetes is highlighted by the phenotype of *Irs2*^{-/-} mice. Indeed, these animals develop type 2 diabetes with impaired peripheral insulin signaling and pancreatic β cell function without compensation by IRS1 (42).

Third, the importance of our findings goes beyond the control of adipocyte biology in normal physiology. Here, we also report a significant ($P = 0.0362$) correlation between CCND3 expression and BMI in human subjects. Our model is further supported by the observed increase in the phosphorylation of the Ser388 of IRS2 in human obese subjects (BMI > 27). Insulin resistance is a major feature in various metabolic disorders, such as obesity and type 2 diabetes. We show here an inverse correlation of IRS2 Ser388 levels in VAT with the blood glucose levels from the subjects (Figure 7H). This strongly supports the notion that this phosphorylation participates in glucose homeostasis in humans.

In conclusion, our results demonstrate that CDK4 is a regulator of adipocyte insulin signaling. By combining experimental data from cellular and mouse models and data obtained using human samples, our study provides insights into the complex pathogenesis of obesity and insulin resistance.

Methods

Materials. All experiments with the CDK4 inhibitor (PD0332991, Azasynth Co.) were done using 1 μM of PD0332991 in mature 3T3-L1 adipocytes. All chemicals, unless stated otherwise, were purchased from Sigma-Aldrich. Actrapid human recombinant insulin was purchased from Novo Nordisk Pharma SA. AKT inhibitor (catalog 124017) was purchased from Calbiochem and used at 10 μM for 30 minutes. ^{14}C-acetate, and γ-^{33}P-ATP were purchased from PerkinElmer.

Animals. The generation of *Cdk4*[nc] and *Cdk4*[R24C/R24C] mice has been previously described (11, 13). The 8- to 12-week-old male db/+ and db/db as well as C57BL/6J (B6) mice were obtained from Janvier. *E2f1*^{+/+} and *E2f1*^{-/-} mice (B6;129S4-E2f1tm1 Meg/J) were purchased from The Jackson Laboratory. *Cdk4*[flox/flox] mice were generated for this study in collaboration with Cyagen Biosciences. The targeting vector included a Neo resistance cassette flanked by FRT sites as well as CRE-dependent lox P sites in introns 1 and 8 (Supplemental Figure 1I).

C57BL/6 embryonic stem cells were used for gene targeting, and the positive cells were bred into albino B6 female mice. This strategy allowed us to have a pure B6 background. *Cdk4*[flox/+] mice were then crossed with mice expressing Flp recombinase (B6.Cg-Tg[Pgk1-

FLPo]10Sykr/J) in order to remove the Neo resistance cassette. With one subsequent cross with B6 animals, the Flp transgene was removed and the obtained *Cdk4*[flox/+] mice were then intercrossed in order to generate the *Cdk4*[flox/flox] mice used in this study.

Animals were maintained in a temperature-controlled animal facility with a 12-hour light/12-hour dark cycle and had access to food and water according to the Swiss Animal Protection Ordinance (OPAn). Only male animals were used in this study. For the GTT, mice were starved for 16 hours and then injected i.p. with glucose (2 g/kg). Tail vein blood glucose was measured at the indicated times. For the insulin tolerance test (ITT), 6-hour–fasted mice were injected i.p. with 0.75 U/kg insulin and tail vein blood glucose was then measured at the indicated times. For the in vivo insulin-stimulation assay, mice were fasted overnight and injected in the portal vein or i.p. with 0.75 U/kg insulin or an equal volume of saline. After 3 or 50 minutes, the mice were sacrificed via cervical dislocation. For insulin level measurements, tail vein blood was collected under fed conditions 2 hours after the beginning of the 12-hour dark cycle.

Plasmid constructs and mutagenesis. pDONR-IRS2 was subcloned from pBS mouse IRS-2 (Addgene plasmid catalog 11372) (43) and generated using the pDONR221 vector of Gateway Cloning Technology (Invitrogen). Flag-IRS2 and GST-IRS2 were obtained using the pDEST pCMV14-3XFlag and pGEX-2T vectors of Gateway Cloning Technology starting from the above-described pDONR-IRS2 constructs. A similar strategy was used to obtain the truncated versions of GST-IRS2. The Flag-PIK3R1 and Flag-PDPK1 plasmids were obtained from the Montpellier Genomic Collection (MGC). pDONR-hRB 379–928aa was subcloned from pCMV human RB1 and generated using the pDONR221 vector of Gateway Cloning Technology. pGEX-2T hRB 379–928aa was obtained using the pDEST pGEX-2T from Gateway Cloning Technology. The different serine-to-alanine mutants of GST-IRS2 were generated using a QuikChange Site-Directed Mutagenesis Kit (Stratagene).

Cell culture. 3T3-L1 and 293T were obtained from ATCC. *Irs2*^{-/-} cells were cultured in DMEM with 10% FBS (PAA Laboratories) in 5% CO_2 in an incubator set at 37°C. Two days after reaching confluence, 3T3-L1 cells were differentiated with DMEM, 10% FBS, 0.5 mM 3-isobutyl-1methylxanthine (IBMX), 1.7 μM insulin, 1 μM dexamethasone, and 1 μM rosiglitazone for 2 days. From day 3 onward, the cells were incubated with DMEM, 10% FBS, and 10 μg/ml insulin, and the medium was changed every 2 days until day 8 of differentiation. 3T3-L1 mature adipocytes were maintained in medium containing FBS only. For insulin (100 nM) or isoproterenol (100 nM) treatments, fully differentiated 3T3-L1 adipocytes were incubated in serum-free DMEM containing 0.2% fatty acid–free BSA. Primary hepatocytes were obtained from B6 mice. Mouse hepatocytes were harvested and cultured as previously described (44). Min6 cells were provided by Christian Widmann (Department of Physiology, Université de Lausanne, Lausanne). They were maintained as previously described (45) and incubated in DMEM supplemented with 15% FBS and 5 mM glucose overnight. The day after, cells were incubated in serum-free DMEM containing 0.1% fatty acid–free BSA for 6 hours. C2C12 myoblasts were obtained from ATCC and were cultured in low-glucose DMEM with 10% FBS in 5% CO_2 in an incubator set at 37°C. For myotube differentiation, C2C12 myoblasts were seeded in 6-cm plates. When the cells reached 95% confluency, the culture medium was switched to DMEM containing 2% horse serum. The medium was changed every 2 days until day 5 of

differentiation. C2C12 myotubes were incubated in α-MEM overnight to induce starvation. Primary hepatocytes, Min6 cells, and C2C12 myotubes were stimulated with insulin (100 nM).

Proteins extraction, coimmunoprecipitation assays, and immunoblot analyses. For endogenous immunoprecipitation experiments between CDK4 and IRS2, mature 3T3-L1 adipocytes were lysed in a buffer containing 0.3% CHAPS, 40 mM Hepes, pH 7.5, 120 mM NaCl, 1 mM EDTA, 10 mM pyrophosphate, 10 mM glycerophosphate, and protease inhibitor cocktail. Lysates were precleared with protein A/G–agarose beads (Life Technologies) and 4 μg of control antibody (HA antibody) for 1 hour. After this step, anti-CDK4 antibodies or HA antibodies were added to the precleared lysates overnight to immunoprecipitate CDK4 or for the control immunoprecipitation, respectively. For endogenous immunoprecipitation experiments, mature 3T3-L1 adipocytes or eWAT from mice was lysed in a buffer containing 20 mM Tris, pH 7.5, 150 mM NaCl, 1 mM EDTA, 1% Triton X-100, 1 mM Na_3VO_4, 1 mM β-glycerophosphate, 50 mM NaF, and protease inhibitor cocktail. Whole protein extracts were precleared with protein A/G–agarose beads (Life Technologies) for 1 hour, and anti-CDK4 antibody (Santa Cruz Biotechnology Inc., sc-260AC) and negative control (Rabbit IgG) (Santa Cruz Biotechnology Inc., sc-2345) were added to immunoprecipitate CDK4 overnight at 4°C. For IRS2 and PIK3R1 immunoprecipitation experiments from mature adipocytes and mice, whole protein extracts were precleared with protein A/G–agarose beads (Life Technologies) and 4 μg of control antibody (HA antibody) for 1 hour. Then anti-IRS2 anti-PIK3R1 antibody and negative control (HA antibody) were added to the precleared lysates for immunoprecipitation overnight at 4°C. Immunoprecipitation experiments in 293T cells were performed using the same buffer as above. Anti-CDK4 antibody (Santa Cruz Biotechnology Inc., sc-601) and negative control (rabbit IgG) (Santa Cruz Biotechnology Inc., sc-2027) were used for the immunoprecipitation. Flag-PIK3R1, Flag-PDKP1, and Flag-IRS2 were transfected with Lipofectamine 2000 (Invitrogen) and immunoprecipitated with Flag beads (Sigma-Aldrich A2220). Proteins were extracted with the same lysis buffer described above and subjected to SDS-PAGE electrophoresis. Protein extractions from the different tissues (eWAT, BAT, brain, muscle, heart, kidney, lung, spleen, and liver) were prepared using M-PER mammalian extraction buffer (Thermo Scientific) containing 1:100 Halt phosphatase inhibitor cocktail (Thermo Scientific) and 1:100 Halt protease inhibitor cocktail, EDTA-free (Thermo Scientific). All the tissues were snap-frozen and then ground with Liquid N2 before lysis. The following antibodies were used for Western blot analysis: anti-CCND1 (NeoMarkers Rb-010-P0), anti-CCND3 (clone sc-6283), anti-CDK4 (clone sc-260), anti-HSL (clone sc-25843), anti-HA (clone sc-805), anti-IRS2 (clone sc-8299) (Santa Cruz Biotechnology Inc.); anti-CCND2 (clone ab3085), anti-CDK4 (clone DSC-35), anti-Ki67 (clone ab15580) (Abcam); anti–LMNA (clone 2032), anti–pHSL Ser573 (clone 4139), anti–RB1 Ser780 (clone 9307), anti–pAKT Thr308 (clone 4056), anti–pAKT Ser473 (clone 4060), anti-AKT (clone 9272), anti-CDK6 (clone DCS83) (Cell Signaling Technology); anti-Flag (clone F3165), anti-actin (clone A2066), anti-tubulin (clone T6199) (Sigma-Aldrich); anti-PI3K3R1 (clone 06-195) (Upstate); and anti-IRS2 (Millipore MABS15). The phosphospecific antibody against IRS2 Ser388 was synthesized and purchased from GenScript.

Kinase assays. 3T3-L1 mature adipocytes were incubated overnight in serum-free DMEM containing 0.2% fatty acid–free BSA and either stimulated with insulin (100 nM) or left untreated with lysates

of these cells used to immunoprecipitate CDK4, as described above. Additionally, CDK4 was immunoprecipitated from eWAT collected from mice that had fasted for 16 hours and were injected i.p. with insulin (0.75 U/kg) for 30 minutes. Kinase assays were performed using immunoprecipitated CDK4 and 500 ng of recombinant RB1 protein (Santa Cruz Biotechnology Inc.) as a substrate in kinase buffer (25 mM Tris/HCl, pH 7.5, 150 mM NaCl, 10 mM $MgCl_2$, 1 mM DTT, 5 mM $Na_4P_2O_7$, 50 mM NaF, 1 mM vanadate, and protease inhibitor cocktail) with 40 μM ATP and 8 μCi γ-[33P]ATP for 30 minutes at 30°C. Recombinant CDK4/CCND3 (ProQinase) was used as positive control. Boiling the samples for 5 minutes in the presence of denaturing sample buffer stopped the reaction. Samples were subsequently subjected to SDS-PAGE, and the gels were then dried in a gel dryer for 1 hour and exposed to an x-ray film at –80°C.

When using GST-purified proteins as substrates, kinase assays were performed using 500 ng of recombinant RB1 protein (Santa Cruz Biotechnology Inc.) as a positive control and recombinant CDK4/CCND3 kinase (ProQinase) and incubated in kinase buffer (described above) supplemented with 40 μM ATP and 8 μCi γ-[33P]ATP for 30 minutes at 30°C.

PamChip peptide microarrays for kinome analysis following insulin stimulation. For kinome analysis, STK microarrays were purchased from PamGene International BV. Each array contained 140 phosphorylatable peptides as well as 4 control peptides. Sample incubation, detection, and analysis were performed in a PamStation 12 according to the manufacturer's instructions. Briefly, extracts from *Cdk4+/+* and *Cdk4nc* mice or mature 3T3-L1 adipocytes were made using M-PER mammalian extraction buffer (Thermo Scientific) containing 1:50 Halt phosphatase inhibitor cocktail (Thermo Scientific) and 1:50 Halt protease inhibitor cocktail, EDTA-free (Thermo Scientific), for 20 minutes on ice. The lysates were then centrifuged at 15,871 *g* for 20 minutes to remove all debris. The supernatant was aliquoted, snap-frozen in liquid nitrogen, and stored at –80°C until further processing. Prior to incubation with the kinase reaction mix, the arrays were blocked with 2% BSA in water for 30 cycles and washed 3 times with PK assay buffer. Kinase reactions were performed for 1 hour with 5 μg of total extract for the mouse experiment or 2.5 μg of total extract for the mature adipocyte and 400 μM ATP at 30°C. Phosphorylated peptides were detected with an anti-rabbit–FITC antibody that recognizes a pool of anti–phospho serine/threonine antibodies. The instrument contains a 12-bit CCD camera suitable for imaging of FITC-labeled arrays. The images obtained from the phosphorylated arrays were quantified using the BioNavigator software (PamGene International BV), and the list of peptides whose phosphorylation was significantly different between control (3 minutes of insulin treated in *Cdk4+/+* mice or 5 minutes of insulin stimulation in cells starved in the presence of DMSO) and test (3 minutes of insulin treated in *Cdk4nc* mice or 5 minutes of insulin stimulation in cells starved in the presence of PD0332991) conditions was uploaded to GeneGo for pathway analysis. The list of the significantly different peptides is shown in Supplemental Figure 3, C and D. The BioNavigator software was used to perform the upstream STK analysis that is shown in Figure 4D.

Statistics. All statistics are described in the figure legends. The results were expressed as mean ± SEM. Pearson's correlation coefficient was calculated to test for correlation between 2 parameters. Comparisons between 2 groups were performed with an unpaired

2-tailed Student's *t* test, and multiple group comparisons were performed by 1-way ANOVA followed by Tukey's test and 2-way ANOVA followed by Tukey's test. $P < 0.05$ was considered significant.

Study approval. All animal care and treatment procedures were performed in accordance with Swiss guidelines and were approved by the Canton of Vaud SCAV (authorization VD 2627.b). For human samples, the protocol concerning the use of biopsy from patients was approved in agreement with Spanish regulations, either by the Ethics and Research Committee of Virgen de la Victoria Clinical University Hospital or by the Institutional Ethics Committee of the Joan XXIII University Hospital. All patients provided written informed consent.

Supplemental data. Additional methods information is available in Supplemental Experimental Procedures. The sequences of the primers used for RT-qPCR are available in Supplemental Table 1.

Author contributions

LF designed the project. SL, ICLM, PDD, XE, JCA, CC, AG, QL, LMC, BD, JSA, EB, SH, AA, and PD designed and carried out the experiments. The design and execution of the PamGene experiment was done by ICLM. VJ and FB provided the AAV8 vectors. LZ performed the tail-vein injections. CRK provided pBS mouse IRS-2 and *Irs2*^{-/-} cells. JV and FJT provided human VAT samples. SL, ICLM, and LF wrote the manuscript.

1. Saltiel AR, Kahn CR. Insulin signalling and the regulation of glucose and lipid metabolism. *Nature*. 2001;414(6865):799–806.
2. White MF. Insulin signaling in health and disease. *Science*. 2003;302(5651):1710–1711.
3. Rask-Madsen C, Kahn CR. Tissue-specific insulin signaling, metabolic syndrome, and cardiovascular disease. *Arterioscler Thromb Vasc Biol*. 2012;32(9):2052–2059.
4. Vazquez-Vela ME, Torres N, Tovar AR. White adipose tissue as endocrine organ and its role in obesity. *Arch Med Res*. 2008;39(8):715–728.
5. Koch L, et al. Central insulin action regulates peripheral glucose and fat metabolism in mice. *J Clin Invest*. 2008;118(6):2132–2147.
6. Abel ED, et al. Adipose-selective targeting of the GLUT4 gene impairs insulin action in muscle and liver. *Nature*. 2001;409(6821):729–733.
7. Choi YH, et al. Alterations in regulation of energy homeostasis in cyclic nucleotide phosphodiesterase 3B-null mice. *J Clin Invest*. 2006;116(12):3240–3251.
8. Matsushime H, et al. Identification and properties of an atypical catalytic subunit (p34PSK-J3/cdk4) for mammalian D type G1 cyclins. *Cell*. 1992;71(2):323–334.
9. Connell-Crowley L, Harper JW, Goodrich DW. Cyclin D1/Cdk4 regulates retinoblastoma protein-mediated cell cycle arrest by site-specific phosphorylation. *Mol Biol Cell*. 1997;8(2):287–301.
10. Malumbres M, Barbacid M. Cell cycle, CDKs and cancer: a changing paradigm. *Nat Rev Cancer*. 2009;9(3):153–166.
11. Rane SG, et al. Loss of Cdk4 expression causes insulin-deficient diabetes and Cdk4 activation results in beta-islet cell hyperplasia. *Nat Genet*. 1999;22(1):44–52.
12. Serrano M, Hannon GJ, Beach D. A new regulatory motif in cell-cycle control causing specific inhibition of cyclin D/CDK4. *Nature*. 1993;366(6456):704–707.

13. Martin J, et al. Genetic rescue of Cdk4 null mice restores pancreatic beta-cell proliferation but not homeostatic cell number. *Oncogene*. 2003;22(34):5261–5269.
14. Abella A, et al. Cdk4 promotes adipogenesis through PPARgamma activation. *Cell Metab*. 2005;2(4):239–249.
15. Sarruf DA, Iankova I, Abella A, Assou S, Miard S, Fajas L. Cyclin D3 promotes adipogenesis through activation of peroxisome proliferator-activated receptor gamma. *Mol Cell Biol*. 2005;25(22):9985–9995.
16. Fajas L, Landsberg RL, Huss-Garcia Y, Sardet C, Lees JA, Auwerx J. E2Fs regulate adipocyte differentiation. *Dev Cell*. 2002;3(1):39–49.
17. Jimenez V, et al. In vivo adeno-associated viral vector-mediated genetic engineering of white and brown adipose tissue in adult mice. *Diabetes*. 2013;62(12):4012–4022.
18. Sotillo R, et al. Wide spectrum of tumors in knock-in mice carrying a Cdk4 protein insensitive to INK4 inhibitors. *EMBO J*. 2001;20(23):6637–6647.
19. Rodriguez-Diez E, et al. Cdk4 and Cdk6 cooperate in counteracting the INK4 family of inhibitors during murine leukemogenesis. *Blood*. 2014;124(15):2380–2390.
20. Zechner R, et al. FAT SIGNALS — lipases and lipolysis in lipid metabolism and signaling. *Cell Metab*. 2012;15(3):279–291.
21. Fry DW, et al. Specific inhibition of cyclin-dependent kinase 4/6 by PD 0332991 and associated antitumor activity in human tumor xenografts. *Mol Cancer Ther*. 2004;3(11):1427–1438.
22. Hilhorst R, Houkes L, Mommersteeg M, Musch J, van den Berg A, Ruijtenbeek R. Peptide microarrays for profiling of serine/threonine kinase activity of recombinant kinases and lysates of cells and tissue samples. *Methods Mol Biol*. 2013;977:259–271.
23. Thirone AC, Huang C, Klip A. Tissue-specific

roles of IRS proteins in insulin signaling and glucose transport. *Trends Endocrinol Metab*. 2006;17(2):72–78.
24. Malumbres M, Barbacid M. Mammalian cyclin-dependent kinases. *Trends Biochem Sci*. 2005;30(11):630–641.
25. Viglietto G, et al. Cytoplasmic relocalization and inhibition of the cyclin-dependent kinase inhibitor p27(Kip1) by PKB/Akt-mediated phosphorylation in breast cancer. *Nat Med*. 2002;8(10):1136–1144.
26. Zhou BP, Liao Y, Xia W, Spohn B, Lee MH, Hung MC. Cytoplasmic localization of p21Cip1/WAF1 by Akt-induced phosphorylation in HER-2/neu-overexpressing cells. *Nat Cell Biol*. 2001;3(3):245–252.
27. Reuveni H, et al. Therapeutic destruction of insulin receptor substrates for cancer treatment. *Cancer Res*. 2013;73(14):4383–4394.
28. Baserga R. The insulin receptor substrate-1: a biomarker for cancer? *Exp Cell Res*. 2009;315(5):727–732.
29. Heilmann AM, et al. CDK4/6 and IGF1 receptor inhibitors synergize to suppress the growth of p16INK4A-deficient pancreatic cancers. *Cancer Res*. 2014;74(14):3947–3958.
30. Vora SR, et al. CDK 4/6 inhibitors sensitize PIK3CA mutant breast cancer to PI3K inhibitors. *Cancer Cell*. 2014;26(1):136–149.
31. Muranen T, Meric-Bernstam F, Mills GB. Promising rationally derived combination therapy with PI3K and CDK4/6 inhibitors. *Cancer Cell*. 2014;26(1):7–9.
32. Miller ML, et al. Drug synergy screen and network modeling in dedifferentiated liposarcoma identifies CDK4 and IGF1R as synergistic drug targets. *Sci Signal*. 2013;6(294):ra85.
33. Turner NC, et al. Palbociclib in hormone-receptor-positive advanced breast cancer. *N Engl J Med*. 2015;373(3):209–219.
34. Asghar U, Witkiewicz AK, Turner NC, Knudsen

ES. The history and future of targeting cyclin-dependent kinases in cancer therapy. *Nat Rev Drug Discov*. 2015;14(2):130–146.

35. Menendez JA, Lupu R. Fatty acid synthase and the lipogenic phenotype in cancer pathogenesis. *Nat Rev Cancer*. 2007;7(10):763–777.

36. Copps KD, White MF. Regulation of insulin sensitivity by serine/threonine phosphorylation of insulin receptor substrate proteins IRS1 and IRS2. *Diabetologia*. 2012;55(10):2565–2582.

37. Solinas G, Naugler W, Galimi F, Lee MS, Karin M. Saturated fatty acids inhibit induction of insulin gene transcription by JNK-mediated phosphorylation of insulin-receptor substrates. *Proc Natl Acad Sci U S A*. 2006;103(44):16454–16459.

38. Sharfi H, Eldar-Finkelman H. Sequential phosphorylation of insulin receptor substrate-2 by glycogen synthase kinase-3 and c-Jun NH2-terminal kinase plays a role in hepatic insulin signaling. *Am J Physiol Endocrinol Metab*. 2008;294(2):E307–E315.

39. Fritsche L, et al. Insulin-induced serine phosphorylation of IRS-2 via ERK1/2 and mTOR: studies on the function of Ser675 and Ser907. *Am J Physiol Endocrinol Metab*. 2011;300(5):E824–E836.

40. Boura-Halfon S, Zick Y. Phosphorylation of IRS proteins, insulin action, and insulin resistance. *Am J Physiol Endocrinol Metab*. 2009;296(4):E581–E591.

41. Blanchet E, et al. E2F transcription factor-1 regulates oxidative metabolism. *Nat Cell Biol*. 2011;13(9):1146–1152.

42. Withers DJ, et al. Disruption of IRS-2 causes type 2 diabetes in mice. *Nature*. 1998;391(6670):900–904.

43. Tsuruzoe K, Emkey R, Kriauciunas KM, Ueki K, Kahn CR. Insulin receptor substrate 3 (IRS-3) and IRS-4 impair IRS-1- and IRS-2-mediated signaling. *Mol Cell Biol*. 2001;21(1):26–38.

44. Benhamed F, et al. The lipogenic transcription factor ChREBP dissociates hepatic steatosis from insulin resistance in mice and humans. *J Clin Invest*. 2012;122(6):2176–2194.

45. Annicotte JS, et al. The CDK4-pRB-E2F1 pathway controls insulin secretion. *Nat Cell Biol*. 2009;11(8):1017–1023.

References

Abella, A., Dubus, P., Malumbres, M., Rane, S. G., Kiyokawa, H., Sicard, A., . . . Fajas, L. (2005). Cdk4 promotes adipogenesis through PPARgamma activation. *Cell Metab, 2*(4), 239-249. doi: 10.1016/j.cmet.2005.09.003

Aguilar, V., & Fajas, L. (2010). Cycling through metabolism. *EMBO Mol Med, 2*(9), 338-348. doi: 10.1002/emmm.201000089

Alayev, A., & Holz, M. K. (2013). mTOR signaling for biological control and cancer. *J Cell Physiol, 228*(8), 1658-1664. doi: 10.1002/jcp.24351

Annicotte, J. S., Blanchet, E., Chavey, C., Iankova, I., Costes, S., Assou, S., . . . Fajas, L. (2009). The CDK4-pRB-E2F1 pathway controls insulin secretion. *Nat Cell Biol, 11*(8), 1017-1023. doi: 10.1038/ncb1915

Bar-Peled, L., & Sabatini, D. M. (2014). Regulation of mTORC1 by amino acids. *Trends Cell Biol, 24*(7), 400-406. doi: 10.1016/j.tcb.2014.03.003

Barnum, K. J., & O'Connell, M. J. (2014). Cell cycle regulation by checkpoints. *Methods Mol Biol, 1170*, 29-40. doi: 10.1007/978-1-4939-0888-2_2

Bockstaele, L., Coulonval, K., Kooken, H., Paternot, S., & Roger, P. P. (2006). Regulation of CDK4. *Cell Div, 1*, 25. doi: 10.1186/1747-1028-1-25

Brugarolas, J., Lei, K., Hurley, R. L., Manning, B. D., Reiling, J. H., Hafen, E., . . . Kaelin, W. G., Jr. (2004). Regulation of mTOR function in response to hypoxia by REDD1 and the TSC1/TSC2 tumor suppressor complex. *Genes Dev, 18*(23), 2893-2904. doi: 10.1101/gad.1256804

Buytaert, E., Dewaele, M., & Agostinis, P. (2007). Molecular effectors of multiple cell death pathways initiated by photodynamic therapy. *Biochim Biophys Acta, 1776*(1), 86-107. doi: 10.1016/j.bbcan.2007.07.001

Canepa, E. T., Scassa, M. E., Ceruti, J. M., Marazita, M. C., Carcagno, A. L., Sirkin, P. F., & Ogara, M. F. (2007). INK4 proteins, a family of mammalian CDK inhibitors with novel biological functions. *IUBMB Life, 59*(7), 419-426. doi: 10.1080/15216540701488358

Carroll, B., Maetzel, D., Maddocks, O. D., Otten, G., Ratcliff, M., Smith, G. R., . . . Korolchuk, V. I. (2016). Control of TSC2-Rheb signaling axis by arginine regulates mTORC1 activity. *Elife, 5*. doi: 10.7554/eLife.11058

Chow, Y. H., Zhu, X. D., Liu, L., Schwartz, B. R., Huang, X. Z., Harlan, J. M., & Schnapp, L. M. (2010). Role of Cdk4 in lymphocyte function and allergen response. *Cell Cycle, 9*(24), 4922-4930. doi: 10.4161/cc.9.24.14209

Chung, J., Kuo, C. J., Crabtree, G. R., & Blenis, J. (1992). Rapamycin-FKBP specifically blocks growth-dependent activation of and signaling by the 70 kd S6 protein kinases. *Cell, 69*(7), 1227-1236.

Cunningham, J. T., Rodgers, J. T., Arlow, D. H., Vazquez, F., Mootha, V. K., & Puigserver, P. (2007). mTOR controls mitochondrial oxidative function through a YY1-PGC-1alpha transcriptional complex. *Nature, 450*(7170), 736-740. doi: 10.1038/nature06322

De Duve, C., Pressman, B. C., Gianetto, R., Wattiaux, R., & Appelmans, F. (1955). Tissue fractionation studies. 6. Intracellular distribution patterns of enzymes in rat-liver tissue. *Biochem J, 60*(4), 604-617.

Dehay, B., Martinez-Vicente, M., Caldwell, G. A., Caldwell, K. A., Yue, Z., Cookson, M. R., . . . Bezard, E. (2013). Lysosomal impairment in Parkinson's disease. *Mov Disord, 28*(6), 725-732. doi: 10.1002/mds.25462

Demetriades, C., Doumpas, N., & Teleman, A. A. (2014). Regulation of TORC1 in response to amino acid starvation via lysosomal recruitment of TSC2. *Cell, 156*(4), 786-799. doi: 10.1016/j.cell.2014.01.024

Dibble, C. C., & Cantley, L. C. (2015). Regulation of mTORC1 by PI3K signaling. *Trends Cell Biol, 25*(9), 545-555. doi: 10.1016/j.tcb.2015.06.002

Dickinson, L. A., Edgar, A. J., Ehley, J., & Gottesfeld, J. M. (2002). Cyclin L is an RS domain protein involved in pre-mRNA splicing. *J Biol Chem, 277*(28), 25465-25473. doi: 10.1074/jbc.M202266200

Draetta, G., & Beach, D. (1989). The mammalian cdc2 protein kinase: mechanisms of regulation during the cell cycle. *J Cell Sci Suppl, 12*, 21-27.

Duronio, R. J., & Xiong, Y. (2013). Signaling pathways that control cell proliferation. *Cold Spring Harb Perspect Biol, 5*(3), a008904. doi: 10.1101/cshperspect.a008904

Duvel, K., Yecies, J. L., Menon, S., Raman, P., Lipovsky, A. I., Souza, A. L., . . . Manning, B. D. (2010). Activation of a metabolic gene regulatory network downstream of mTOR complex 1. *Mol Cell, 39*(2), 171-183. doi: 10.1016/j.molcel.2010.06.022

Dwivedi, R. S., Kaur, G., Srivastava, R. C., & Krishna Murti, C. R. (1985). Metabolic activity of lysosomes in tin-intoxicated regenerating rat liver. *Toxicol Lett, 28*(2-3), 133-138.

Egan, D., Kim, J., Shaw, R. J., & Guan, K. L. (2011). The autophagy initiating kinase ULK1 is regulated via opposing phosphorylation by AMPK and mTOR. *Autophagy, 7*(6), 643-644.

Fan, S. J., Snell, C., Turley, H., Li, J. L., McCormick, R., Perera, S. M., . . . Goberdhan, D. C. (2016). PAT4 levels control amino-acid sensitivity of rapamycin-resistant mTORC1 from the Golgi and affect clinical outcome in colorectal cancer. *Oncogene, 35*(23), 3004-3015. doi: 10.1038/onc.2015.363

Fang, Y., Tan, J., & Zhang, Q. (2015). Signaling pathways and mechanisms of hypoxia-induced autophagy in the animal cells. *Cell Biol Int, 39*(8), 891-898. doi: 10.1002/cbin.10463

Fisher, R. P. (2005). Secrets of a double agent: CDK7 in cell-cycle control and transcription. *J Cell Sci, 118*(Pt 22), 5171-5180. doi: 10.1242/jcs.02718

Franco, J., Balaji, U., Freinkman, E., Witkiewicz, A. K., & Knudsen, E. S. (2016). Metabolic Reprogramming of Pancreatic Cancer Mediated by CDK4/6 Inhibition Elicits Unique Vulnerabilities. *Cell Rep, 14*(5), 979-990. doi: 10.1016/j.celrep.2015.12.094

Friedl, P., & Wolf, K. (2003). Tumour-cell invasion and migration: diversity and escape mechanisms. *Nat Rev Cancer, 3*(5), 362-374. doi: 10.1038/nrc1075

Friedl, P., & Wolf, K. (2008). Tube travel: the role of proteases in individual and collective cancer cell invasion. *Cancer Res, 68*(18), 7247-7249. doi: 10.1158/0008-5472.CAN-08-0784

Furuta, K., Ikeda, M., Nakayama, Y., Nakamura, K., Tanaka, M., Hamasaki, N., . . . August, J. T. (2001). Expression of lysosome-associated membrane proteins in human colorectal neoplasms and inflammatory diseases. *Am J Pathol, 159*(2), 449-455. doi: 10.1016/S0002-9440(10)61716-6

Glick, D., Barth, S., & Macleod, K. F. (2010). Autophagy: cellular and molecular mechanisms. *J Pathol, 221*(1), 3-12. doi: 10.1002/path.2697

Goel, S., Wang, Q., Watt, A. C., Tolaney, S. M., Dillon, D. A., Li, W., . . . Zhao, J. J. (2016). Overcoming Therapeutic Resistance in HER2-Positive Breast Cancers

with CDK4/6 Inhibitors. *Cancer Cell, 29*(3), 255-269. doi: 10.1016/j.ccell.2016.02.006

Gotink, K. J., Broxterman, H. J., Labots, M., de Haas, R. R., Dekker, H., Honeywell, R. J., . . . Verheul, H. M. (2011). Lysosomal sequestration of sunitinib: a novel mechanism of drug resistance. *Clin Cancer Res, 17*(23), 7337-7346. doi: 10.1158/1078-0432.CCR-11-1667

Guertin, D. A., & Sabatini, D. M. (2007). Defining the role of mTOR in cancer. *Cancer Cell, 12*(1), 9-22. doi: 10.1016/j.ccr.2007.05.008

Guo, J. Y., & White, E. (2016). Autophagy, Metabolism, and Cancer. *Cold Spring Harb Symp Quant Biol, 81*, 73-78. doi: 10.1101/sqb.2016.81.030981

Gwinn, D. M., Shackelford, D. B., Egan, D. F., Mihaylova, M. M., Mery, A., Vasquez, D. S., . . . Shaw, R. J. (2008). AMPK phosphorylation of raptor mediates a metabolic checkpoint. *Mol Cell, 30*(2), 214-226. doi: 10.1016/j.molcel.2008.03.003

Hamalisto, S., & Jaattela, M. (2016). Lysosomes in cancer-living on the edge (of the cell). *Curr Opin Cell Biol, 39*, 69-76. doi: 10.1016/j.ceb.2016.02.009

Hanks, S. K. (1987). Homology probing: identification of cDNA clones encoding members of the protein-serine kinase family. *Proc Natl Acad Sci U S A, 84*(2), 388-392.

Hardie, D. G. (2007). AMP-activated/SNF1 protein kinases: conserved guardians of cellular energy. *Nat Rev Mol Cell Biol, 8*(10), 774-785. doi: 10.1038/nrm2249

Harrington, L. S., Findlay, G. M., & Lamb, R. F. (2005). Restraining PI3K: mTOR signalling goes back to the membrane. *Trends Biochem Sci, 30*(1), 35-42. doi: 10.1016/j.tibs.2004.11.003

Hawley, S. A., Ross, F. A., Gowans, G. J., Tibarewal, P., Leslie, N. R., & Hardie, D. G. (2014). Phosphorylation by Akt within the ST loop of AMPK-alpha1 down-regulates its activation in tumour cells. *Biochem J, 459*(2), 275-287. doi: 10.1042/BJ20131344

Hu, D., Mayeda, A., Trembley, J. H., Lahti, J. M., & Kidd, V. J. (2003). CDK11 complexes promote pre-mRNA splicing. *J Biol Chem, 278*(10), 8623-8629. doi: 10.1074/jbc.M210057200

Iams, W. T., Sosman, J. A., & Chandra, S. (2017). Novel Targeted Therapies for Metastatic Melanoma. *Cancer J, 23*(1), 54-58. doi: 10.1097/PPO.0000000000000242

Inoki, K., Li, Y., Xu, T., & Guan, K. L. (2003). Rheb GTPase is a direct target of TSC2 GAP activity and regulates mTOR signaling. *Genes Dev, 17*(15), 1829-1834. doi: 10.1101/gad.1110003

Jaattela, M. (2004). Multiple cell death pathways as regulators of tumour initiation and progression. *Oncogene, 23*(16), 2746-2756. doi: 10.1038/sj.onc.1207513

Jacinto, E., Loewith, R., Schmidt, A., Lin, S., Ruegg, M. A., Hall, A., & Hall, M. N. (2004). Mammalian TOR complex 2 controls the actin cytoskeleton and is rapamycin insensitive. *Nat Cell Biol, 6*(11), 1122-1128. doi: 10.1038/ncb1183

Jayapal, S. R., Wang, C. Q., Bisteau, X., Caldez, M. J., Lim, S., Tergaonkar, V., . . . Kaldis, P. (2015). Hematopoiesis specific loss of Cdk2 and Cdk4 results in increased erythrocyte size and delayed platelet recovery following stress. *Haematologica, 100*(4), 431-438. doi: 10.3324/haematol.2014.106468

Jewell, J. L., Kim, Y. C., Russell, R. C., Yu, F. X., Park, H. W., Plouffe, S. W., . . . Guan, K. L. (2015). Metabolism. Differential regulation of mTORC1 by leucine and glutamine. *Science, 347*(6218), 194-198. doi: 10.1126/science.1259472

Kim, J., & Kim, E. (2016). Rag GTPase in amino acid signaling. *Amino Acids, 48*(4), 915-928. doi: 10.1007/s00726-016-2171-x

Kirkegaard, T., & Jaattela, M. (2009). Lysosomal involvement in cell death and cancer. *Biochim Biophys Acta, 1793*(4), 746-754. doi: 10.1016/j.bbamcr.2008.09.008

Klein, M. E., Kovatcheva, M., Davis, L. E., Tap, W. D., & Koff, A. (2018). CDK4/6 Inhibitors: The Mechanism of Action May Not Be as Simple as Once Thought. *Cancer Cell, 34*(1), 9-20. doi: 10.1016/j.ccell.2018.03.023

Knudsen, E. S., Kumarasamy, V., Ruiz, A., Sivinski, J., Chung, S., Grant, A., . . . Witkiewicz, A. K. (2019). Cell cycle plasticity driven by MTOR signaling: integral resistance to CDK4/6 inhibition in patient-derived models of pancreatic cancer. *Oncogene*. doi: 10.1038/s41388-018-0650-0

Koff, A., Giordano, A., Desai, D., Yamashita, K., Harper, J. W., Elledge, S., . . . Roberts, J. M. (1992). Formation and activation of a cyclin E-cdk2 complex during the G1 phase of the human cell cycle. *Science, 257*(5077), 1689-1694.

Kroemer, G., & Levine, B. (2008). Autophagic cell death: the story of a misnomer. *Nat Rev Mol Cell Biol, 9*(12), 1004-1010. doi: 10.1038/nrm2529

Lagarrigue, S., Lopez-Mejia, I. C., Denechaud, P. D., Escote, X., Castillo-Armengol, J., Jimenez, V., . . . Fajas, L. (2016). CDK4 is an essential insulin effector in adipocytes. *J Clin Invest, 126*(1), 335-348. doi: 10.1172/JCI81480

Lantsov, D., Meirmanov, S., Nakashima, M., Kondo, H., Saenko, V., Naruke, Y., . . . Yamashita, Sh. (2005). Cyclin D1 overexpression in thyroid papillary microcarcinoma: its association with tumour size and aberrant beta-catenin expression. *Histopathology, 47*(3), 248-256. doi: 10.1111/j.1365-2559.2005.02218.x

Laplante, M., & Sabatini, D. M. (2009). mTOR signaling at a glance. *J Cell Sci, 122*(Pt 20), 3589-3594. doi: 10.1242/jcs.051011

Laplante, M., & Sabatini, D. M. (2012). mTOR signaling in growth control and disease. *Cell, 149*(2), 274-293. doi: 10.1016/j.cell.2012.03.017

Laplante, M., & Sabatini, D. M. (2013). Regulation of mTORC1 and its impact on gene expression at a glance. *J Cell Sci, 126*(Pt 8), 1713-1719. doi: 10.1242/jcs.125773

Lee, D. F., Kuo, H. P., Chen, C. T., Hsu, J. M., Chou, C. K., Wei, Y., . . . Hung, M. C. (2007). IKK beta suppression of TSC1 links inflammation and tumor angiogenesis via the mTOR pathway. *Cell, 130*(3), 440-455. doi: 10.1016/j.cell.2007.05.058

Lee, Y., Dominy, J. E., Choi, Y. J., Jurczak, M., Tolliday, N., Camporez, J. P., . . . Puigserver, P. (2014). Cyclin D1-Cdk4 controls glucose metabolism independently of cell cycle progression. *Nature, 510*(7506), 547-551. doi: 10.1038/nature13267

Leman, E. S., Magheli, A., Yong, K. M., Netto, G., Hinz, S., & Getzenberg, R. H. (2009). Identification of nuclear structural protein alterations associated with seminomas. *J Cell Biochem, 108*(6), 1274-1279. doi: 10.1002/jcb.22357

Lohka, M. J., Hayes, M. K., & Maller, J. L. (1988). Purification of maturation-promoting factor, an intracellular regulator of early mitotic events. *Proc Natl Acad Sci U S A, 85*(9), 3009-3013.

Lopez-Mejia, I. C., & Fajas, L. (2015). Cell cycle regulation of mitochondrial function. *Curr Opin Cell Biol, 33*, 19-25. doi: 10.1016/j.ceb.2014.10.006

Lopez-Mejia, I. C., Lagarrigue, S., Giralt, A., Martinez-Carreres, L., Zanou, N., Denechaud, P. D., . . . Fajas, L. (2017). CDK4 Phosphorylates AMPKalpha2

to Inhibit Its Activity and Repress Fatty Acid Oxidation. *Mol Cell, 68*(2), 336-349 e336. doi: 10.1016/j.molcel.2017.09.034

Lopez-Otin, C., & Matrisian, L. M. (2007). Emerging roles of proteases in tumour suppression. *Nat Rev Cancer, 7*(10), 800-808. doi: 10.1038/nrc2228

Loyer, P., Trembley, J. H., Grenet, J. A., Busson, A., Corlu, A., Zhao, W., . . . Lahti, J. M. (2008). Characterization of cyclin L1 and L2 interactions with CDK11 and splicing factors: influence of cyclin L isoforms on splice site selection. *J Biol Chem, 283*(12), 7721-7732. doi: 10.1074/jbc.M708188200

Malumbres, M., & Barbacid, M. (2005). Mammalian cyclin-dependent kinases. *Trends Biochem Sci, 30*(11), 630-641. doi: 10.1016/j.tibs.2005.09.005

Malumbres, M., & Barbacid, M. (2009). Cell cycle, CDKs and cancer: a changing paradigm. *Nat Rev Cancer, 9*(3), 153-166. doi: 10.1038/nrc2602

Manning, B. D., & Cantley, L. C. (2007). AKT/PKB signaling: navigating downstream. *Cell, 129*(7), 1261-1274. doi: 10.1016/j.cell.2007.06.009

Martinez-Carreres, L., Nasrallah, A., & Fajas, L. (2017). Cancer: Linking Powerhouses to Suicidal Bags. *Front Oncol, 7*, 204. doi: 10.3389/fonc.2017.00204

Matsushime, H., Ewen, M. E., Strom, D. K., Kato, J. Y., Hanks, S. K., Roussel, M. F., & Sherr, C. J. (1992). Identification and properties of an atypical catalytic subunit (p34PSK-J3/cdk4) for mammalian D type G1 cyclins. *Cell, 71*(2), 323-334.

McBrayer, M., & Nixon, R. A. (2013). Lysosome and calcium dysregulation in Alzheimer's disease: partners in crime. *Biochem Soc Trans, 41*(6), 1495-1502. doi: 10.1042/BST20130201

Mejia-Guerrero, S., Quejada, M., Gokgoz, N., Gill, M., Parkes, R. K., Wunder, J. S., & Andrulis, I. L. (2010). Characterization of the 12q15 MDM2 and 12q13-14 CDK4 amplicons and clinical correlations in osteosarcoma. *Genes Chromosomes Cancer, 49*(6), 518-525. doi: 10.1002/gcc.20761

Meng, D., Frank, A. R., & Jewell, J. L. (2018). mTOR signaling in stem and progenitor cells. *Development, 145*(1). doi: 10.1242/dev.152595

Mettus, R. V., & Rane, S. G. (2003). Characterization of the abnormal pancreatic development, reduced growth and infertility in Cdk4 mutant mice. *Oncogene, 22*(52), 8413-8421. doi: 10.1038/sj.onc.1206888

Meyer, C. A., Jacobs, H. W., Datar, S. A., Du, W., Edgar, B. A., & Lehner, C. F. (2000). Drosophila Cdk4 is required for normal growth and is dispensable for cell cycle progression. *EMBO J, 19*(17), 4533-4542. doi: 10.1093/emboj/19.17.4533

Meyerson, M., & Harlow, E. (1994). Identification of G1 kinase activity for cdk6, a novel cyclin D partner. *Mol Cell Biol, 14*(3), 2077-2086.

Mizushima, N. (2007). Autophagy: process and function. *Genes Dev, 21*(22), 2861-2873. doi: 10.1101/gad.1599207

Mohamed, M. M., & Sloane, B. F. (2006). Cysteine cathepsins: multifunctional enzymes in cancer. *Nat Rev Cancer, 6*(10), 764-775. doi: 10.1038/nrc1949

Morgan, A. J., Platt, F. M., Lloyd-Evans, E., & Galione, A. (2011). Molecular mechanisms of endolysosomal Ca2+ signalling in health and disease. *Biochem J, 439*(3), 349-374. doi: 10.1042/BJ20110949

Muntean, A. G., Pang, L., Poncz, M., Dowdy, S. F., Blobel, G. A., & Crispino, J. D. (2007). Cyclin D-Cdk4 is regulated by GATA-1 and required for megakaryocyte growth and polyploidization. *Blood, 109*(12), 5199-5207. doi: 10.1182/blood-2006-11-059378

Neganova, I., & Lako, M. (2008). G1 to S phase cell cycle transition in somatic and embryonic stem cells. *J Anat, 213*(1), 30-44. doi: 10.1111/j.1469-7580.2008.00931.x

Nurse, P. (2000). A long twentieth century of the cell cycle and beyond. *Cell, 100*(1), 71-78.

Ohtsubo, M., Theodoras, A. M., Schumacher, J., Roberts, J. M., & Pagano, M. (1995). Human cyclin E, a nuclear protein essential for the G1-to-S phase transition. *Mol Cell Biol, 15*(5), 2612-2624.

Olmez, I., Brenneman, B., Xiao, A., Serbulea, V., Benamar, M., Zhang, Y., . . . Purow, B. (2017). Combined CDK4/6 and mTOR Inhibition Is Synergistic against Glioblastoma via Multiple Mechanisms. *Clin Cancer Res, 23*(22), 6958-6968. doi: 10.1158/1078-0432.CCR-17-0803

Olmez, I., Zhang, Y., Manigat, L., Benamar, M., Brenneman, B., Nakano, I., . . . Purow, B. (2018). Combined c-Met/Trk Inhibition Overcomes Resistance to CDK4/6 Inhibitors in Glioblastoma. *Cancer Res, 78*(15), 4360-4369. doi: 10.1158/0008-5472.CAN-17-3124

Onyenwoke, R. U., & Brenman, J. E. (2015). Lysosomal Storage Diseases-Regulating Neurodegeneration. *J Exp Neurosci, 9*(Suppl 2), 81-91. doi: 10.4137/JEN.S25475

Pastores, G. M., & Maegawa, G. H. (2013). Clinical neurogenetics: neuropathic lysosomal storage disorders. *Neurol Clin, 31*(4), 1051-1071. doi: 10.1016/j.ncl.2013.04.007

Pernas, S., Tolaney, S. M., Winer, E. P., & Goel, S. (2018). CDK4/6 inhibition in breast cancer: current practice and future directions. *Ther Adv Med Oncol, 10*, 1758835918786451. doi: 10.1177/1758835918786451

Petit, C. S., Roczniak-Ferguson, A., & Ferguson, S. M. (2013). Recruitment of folliculin to lysosomes supports the amino acid-dependent activation of Rag GTPases. *J Cell Biol, 202*(7), 1107-1122. doi: 10.1083/jcb.201307084

Piao, S., & Amaravadi, R. K. (2016). Targeting the lysosome in cancer. *Ann N Y Acad Sci, 1371*(1), 45-54. doi: 10.1111/nyas.12953

Pines, J., & Hunter, T. (1992). Cyclins A and B1 in the human cell cycle. *Ciba Found Symp, 170*, 187-196; discussion 196-204.

Platt, F. M., Boland, B., & van der Spoel, A. C. (2012). The cell biology of disease: lysosomal storage disorders: the cellular impact of lysosomal dysfunction. *J Cell Biol, 199*(5), 723-734. doi: 10.1083/jcb.201208152

Polk, A., Kolmos, I. L., Kumler, I., & Nielsen, D. L. (2016). Specific CDK4/6 inhibition in breast cancer: a systematic review of current clinical evidence. *ESMO Open, 1*(6), e000093. doi: 10.1136/esmoopen-2016-000093

Populo, H., Lopes, J. M., & Soares, P. (2012). The mTOR signalling pathway in human cancer. *Int J Mol Sci, 13*(2), 1886-1918. doi: 10.3390/ijms13021886

Rane, S. G., Cosenza, S. C., Mettus, R. V., & Reddy, E. P. (2002). Germ line transmission of the Cdk4(R24C) mutation facilitates tumorigenesis and escape from cellular senescence. *Mol Cell Biol, 22*(2), 644-656.

Rane, S. G., Dubus, P., Mettus, R. V., Galbreath, E. J., Boden, G., Reddy, E. P., & Barbacid, M. (1999). Loss of Cdk4 expression causes insulin-deficient diabetes and Cdk4 activation results in beta-islet cell hyperplasia. *Nat Genet, 22*(1), 44-52. doi: 10.1038/8751

Richter, J. D., & Sonenberg, N. (2005). Regulation of cap-dependent translation by eIF4E inhibitory proteins. *Nature, 433*(7025), 477-480. doi: 10.1038/nature03205

Romero-Pozuelo, J., Demetriades, C., Schroeder, P., & Teleman, A. A. (2017). CycD/Cdk4 and Discontinuities in Dpp Signaling Activate TORC1 in the Drosophila Wing Disc. *Dev Cell, 42*(4), 376-387 e375. doi: 10.1016/j.devcel.2017.07.019

Rubinsztein, D. C., Bento, C. F., & Deretic, V. (2015). Therapeutic targeting of autophagy in neurodegenerative and infectious diseases. *J Exp Med, 212*(7), 979-990. doi: 10.1084/jem.20150956

Sabatini, D. M. (2017). Twenty-five years of mTOR: Uncovering the link from nutrients to growth. *Proc Natl Acad Sci U S A, 114*(45), 11818-11825. doi: 10.1073/pnas.1716173114

Sabir, M., Baig, R. M., Mahjabeen, I., & Kayani, M. A. (2012). Novel germline CDK4 mutations in patients with head and neck cancer. *Hered Cancer Clin Pract, 10*(1), 11. doi: 10.1186/1897-4287-10-11

Sagne, C., Agulhon, C., Ravassard, P., Darmon, M., Hamon, M., El Mestikawy, S., . . . Giros, B. (2001). Identification and characterization of a lysosomal transporter for small neutral amino acids. *Proc Natl Acad Sci U S A, 98*(13), 7206-7211. doi: 10.1073/pnas.121183498

Salazar-Roa, M., & Malumbres, M. (2017). Fueling the Cell Division Cycle. *Trends Cell Biol, 27*(1), 69-81. doi: 10.1016/j.tcb.2016.08.009

Sancak, Y., Peterson, T. R., Shaul, Y. D., Lindquist, R. A., Thoreen, C. C., Bar-Peled, L., & Sabatini, D. M. (2008). The Rag GTPases bind raptor and mediate amino acid signaling to mTORC1. *Science, 320*(5882), 1496-1501. doi: 10.1126/science.1157535

Settembre, C., Fraldi, A., Medina, D. L., & Ballabio, A. (2013). Signals from the lysosome: a control centre for cellular clearance and energy metabolism. *Nat Rev Mol Cell Biol, 14*(5), 283-296. doi: 10.1038/nrm3565

Sharma, J., di Ronza, A., Lotfi, P., & Sardiello, M. (2018). Lysosomes and Brain Health. *Annu Rev Neurosci, 41*, 255-276. doi: 10.1146/annurev-neuro-080317-061804

Sherr, C. J., & Roberts, J. M. (2004). Living with or without cyclins and cyclin-dependent kinases. *Genes Dev, 18*(22), 2699-2711. doi: 10.1101/gad.1256504

Shimobayashi, M., & Hall, M. N. (2016). Multiple amino acid sensing inputs to mTORC1. *Cell Res, 26*(1), 7-20. doi: 10.1038/cr.2015.146

Solaki, M., & Ewald, J. C. (2018). Fueling the Cycle: CDKs in Carbon and Energy Metabolism. *Front Cell Dev Biol, 6*, 93. doi: 10.3389/fcell.2018.00093

Steffan, J. J., Dykes, S. S., Coleman, D. T., Adams, L. K., Rogers, D., Carroll, J. L., . . . Cardelli, J. A. (2014). Supporting a role for the GTPase Rab7 in prostate cancer progression. *PLoS One, 9*(2), e87882. doi: 10.1371/journal.pone.0087882

Towers, C. G., & Thorburn, A. (2017). Targeting the Lysosome for Cancer Therapy. *Cancer Discov, 7*(11), 1218-1220. doi: 10.1158/2159-8290.CD-17-0996

Trembley, J. H., Tatsumi, S., Sakashita, E., Loyer, P., Slaughter, C. A., Suzuki, H., . . . Mayeda, A. (2005). Activation of pre-mRNA splicing by human RNPS1 is regulated by CK2 phosphorylation. *Mol Cell Biol, 25*(4), 1446-1457. doi: 10.1128/MCB.25.4.1446-1457.2005

Tsutsui, T., Hesabi, B., Moons, D. S., Pandolfi, P. P., Hansel, K. S., Koff, A., & Kiyokawa, H. (1999). Targeted disruption of CDK4 delays cell cycle entry with enhanced p27(Kip1) activity. *Mol Cell Biol, 19*(10), 7011-7019.

Wang, S., Tsun, Z. Y., Wolfson, R. L., Shen, K., Wyant, G. A., Plovanich, M. E., . . . Sabatini, D. M. (2015). Metabolism. Lysosomal amino acid transporter

SLC38A9 signals arginine sufficiency to mTORC1. *Science, 347*(6218), 188-194. doi: 10.1126/science.1257132

Wikman, H., Nymark, P., Vayrynen, A., Jarmalaite, S., Kallioniemi, A., Salmenkivi, K., . . . Anttila, S. (2005). CDK4 is a probable target gene in a novel amplicon at 12q13.3-q14.1 in lung cancer. *Genes Chromosomes Cancer, 42*(2), 193-199. doi: 10.1002/gcc.20122

Wouters, B. G., & Koritzinsky, M. (2008). Hypoxia signalling through mTOR and the unfolded protein response in cancer. *Nat Rev Cancer, 8*(11), 851-864. doi: 10.1038/nrc2501

Xie, J., Wang, X., & Proud, C. G. (2016). mTOR inhibitors in cancer therapy. *F1000Res, 5*. doi: 10.12688/f1000research.9207.1

Xu, H., Yu, S., Liu, Q., Yuan, X., Mani, S., Pestell, R. G., & Wu, K. (2017). Recent advances of highly selective CDK4/6 inhibitors in breast cancer. *J Hematol Oncol, 10*(1), 97. doi: 10.1186/s13045-017-0467-2

Yang, S., Wang, X., Contino, G., Liesa, M., Sahin, E., Ying, H., . . . Kimmelman, A. C. (2011). Pancreatic cancers require autophagy for tumor growth. *Genes Dev, 25*(7), 717-729. doi: 10.1101/gad.2016111

Yang, Y. P., Liang, Z. Q., Gu, Z. L., & Qin, Z. H. (2005). Molecular mechanism and regulation of autophagy. *Acta Pharmacol Sin, 26*(12), 1421-1434. doi: 10.1111/j.1745-7254.2005.00235.x

Yang, Z., & Klionsky, D. J. (2009). An overview of the molecular mechanism of autophagy. *Curr Top Microbiol Immunol, 335*, 1-32. doi: 10.1007/978-3-642-00302-8_1

Yonekawa, T., & Thorburn, A. (2013). Autophagy and cell death. *Essays Biochem, 55*, 105-117. doi: 10.1042/bse0550105

Yoshida, A., & Diehl, J. A. (2015). CDK4/6 inhibitor: from quiescence to senescence. *Oncoscience, 2*(11), 896-897. doi: 10.18632/oncoscience.256

Yu, J. H., Zhong, X. Y., Zhang, W. G., Wang, Z. D., Dong, Q., Tai, S., . . . Cui, Y. F. (2012). CDK10 functions as a tumor suppressor gene and regulates survivability of biliary tract cancer cells. *Oncol Rep, 27*(4), 1266-1276. doi: 10.3892/or.2011.1617

Zachari, M., & Ganley, I. G. (2017). The mammalian ULK1 complex and autophagy initiation. *Essays Biochem, 61*(6), 585-596. doi: 10.1042/EBC20170021

Zhang, H. H., Huang, J., Duvel, K., Boback, B., Wu, S., Squillace, R. M., . . . Manning, B. D. (2009). Insulin stimulates adipogenesis through the Akt-TSC2-mTORC1 pathway. *PLoS One, 4*(7), e6189. doi: 10.1371/journal.pone.0006189

Zhang, J., Zhou, L., Zhao, S., Dicker, D. T., & El-Deiry, W. S. (2017). The CDK4/6 inhibitor palbociclib synergizes with irinotecan to promote colorectal cancer cell death under hypoxia. *Cell Cycle, 16*(12), 1193-1200. doi: 10.1080/15384101.2017.1320005

Zheng, L., Zhang, W., Zhou, Y., Li, F., Wei, H., & Peng, J. (2016). Recent Advances in Understanding Amino Acid Sensing Mechanisms that Regulate mTORC1. *Int J Mol Sci, 17*(10). doi: 10.3390/ijms17101636

Zhong, X. Y., Xu, X. X., Yu, J. H., Jiang, G. X., Yu, Y., Tai, S., . . . Cui, Y. F. (2012). Clinical and biological significance of Cdk10 in hepatocellular carcinoma. *Gene, 498*(1), 68-74. doi: 10.1016/j.gene.2012.01.022

Zoncu, R., Bar-Peled, L., Efeyan, A., Wang, S., Sancak, Y., & Sabatini, D. M. (2011). mTORC1 senses lysosomal amino acids through an inside-out mechanism that

requires the vacuolar H(+)-ATPase. *Science, 334*(6056), 678-683. doi: 10.1126/science.1207056